TU Delft

Delft University of Technology

Document Version
Final published version

Citation (APA)
Damianakis, N. (2026). *Grid Impact and Power Control of Low-Carbon Technologies in Future Distribution Grids: converting the problem to its solution*. [Dissertation (TU Delft), Delft University of Technology]. https://doi.org/10.4233/uuid:52e26da9-a501-41b7-bfe3-2ba000eac31f

Important note
To cite this publication, please use the final published version (if applicable).
Please check the document version above.

Copyright
In case the licence states “Dutch Copyright Act (Article 25fa)”, this publication was made available Green Open Access via the TU Delft Institutional Repository pursuant to Dutch Copyright Act (Article 25fa, the Taverne amendment). This provision does not affect copyright ownership.
Unless copyright is transferred by contract or statute, it remains with the copyright holder.

Sharing and reuse
Other than for strictly personal use, it is not permitted to download, forward or distribute the text or part of it, without the consent of the author(s) and/or copyright holder(s), unless the work is under an open content license such as Creative Commons.

Takedown policy
Please contact us and provide details if you believe this document breaches copyrights.
We will remove access to the work immediately and investigate your claim.

*This work is downloaded from Delft University of Technology.*

# Grid Impact & Power Control of Low-Carbon Technologies in Future Distribution Grids

converting the problem to its solution

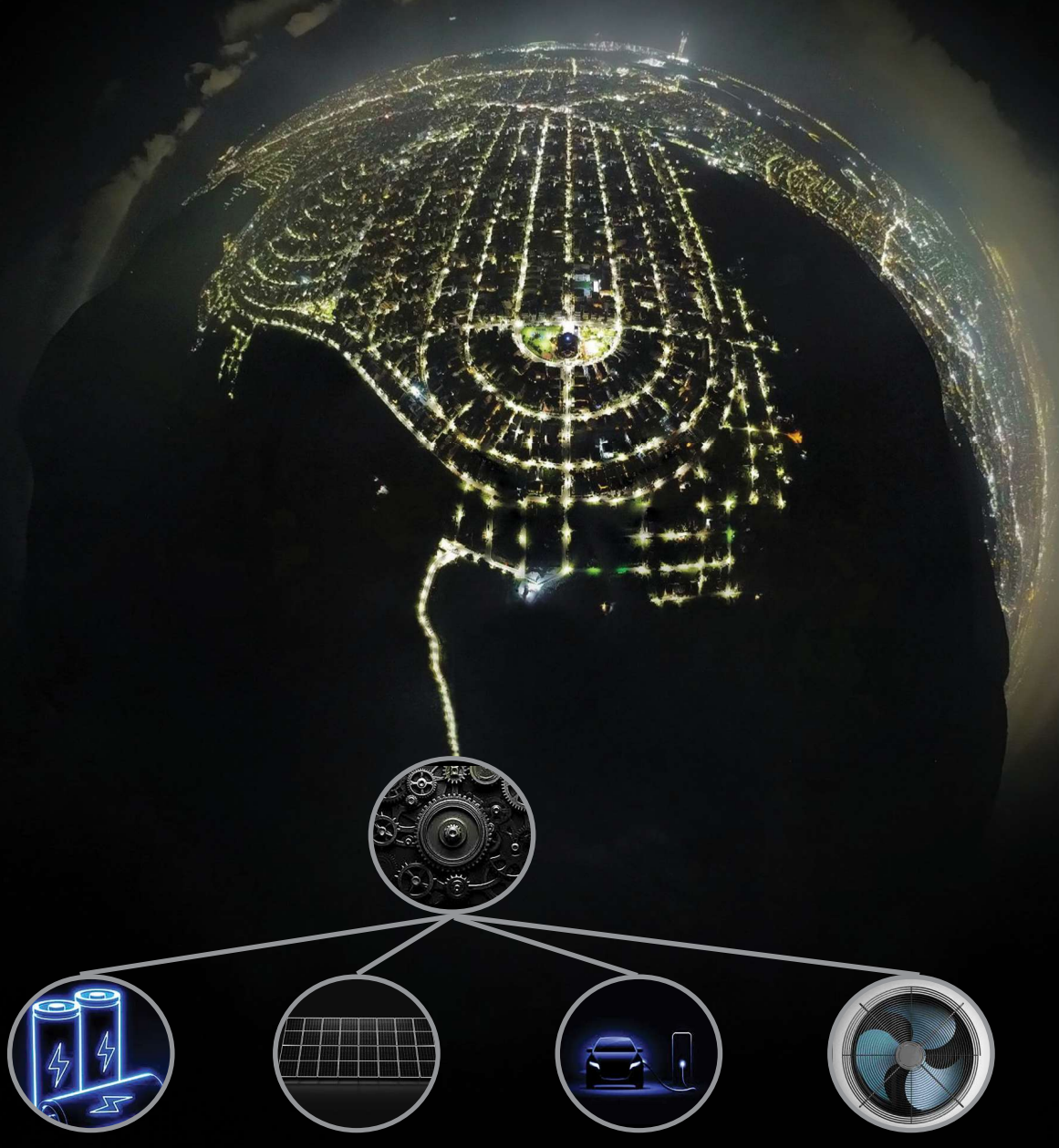

Nikolaos Damianakis

# Grid Impact & Power Control of Low-Carbon Technologies in Future Distribution Grids

converting the problem to its solution

# Grid Impact & Power Control of Low-Carbon Technologies in Future Distribution Grids

converting the problem to its solution

**Dissertation**

for the purpose of obtaining the degree of doctor
at Delft University of Technology
by the authority of the Rector Magnificus, Prof. dr. ir. H. Bijl,
chair of the Board for Doctorates,
to be defended publicly on
Thursday 19 February 2026 at 17:30

by

**Nikolaos DAMIANAKIS**

This dissertation has been approved by the promotors.

Composition of the doctoral committee:

| | |
|---|---|
| Rector Magnificus | chairperson |
| Prof. dr. ir. P. Bauer | Delft University of Technology, *promotor* |
| Dr. ir. G.R. Chandra Mouli | Delft University of Technology, *copromotor* |

*Independent members:*

| | |
|---|---|
| Prof. dr. ir. A.H.M. Smets | Delft University of Technology |
| Dr. Dipl.-Ing. J.L. Rueda Torres | Delft University of Technology |
| Prof. dr. W.G.J.H.M. van Sark | Utrecht University, Netherlands |
| Dr. R.A. Mastromauro | University of Florence, Italy |
| Dr. P.H. Nguyen | Eindhoven University of Technology, Netherlands |
| Prof. dr. ir. M. Popov | Delft University of Technology, reserve member |

*Keywords:* low-carbon technologies, grid impact, power control systems, distribution grids, electric vehicles, heat pumps, battery energy storage

*Printed by:* Gildeprint

*Cover by:* Panajot Sinjari, Nikolaos Damianakis

This Ph.D. project is funded by the Dutch Research Council (NWO) as part of the ongoing research project New Energy Outlook for the Netherlands (NEON) with project number 17628 of the research program Crossover.

Copyright © 2026 by N. Damianakis

ISBN 978-94-6384-911-1

An electronic copy of this dissertation is available at
https://repository.tudelft.nl/.

"Να δημιουργείς και δημιουργώντας να δημιουργείσαι
και να μην είσαι τίποτα άλλο από τη δημιουργία σου"
Αριστοτέλης *384-322* π.Χ.

*dedicated to the love of the ones who are here*
*and the remembrance of the ones who left*

*in memory of my best friend Ares*

"Έχω ένα όνειρο τρελό
και για αυτό μ' αγαπάνε...

# Contents

**Summary** xi

**Nomenclature** xiii

**1 Introduction** 1
- 1.1 Motivation . . . 1
- 1.2 Research Goal Statement and Research Questions . . . 3
  - 1.2.1 Research Goal Statement . . . 3
  - 1.2.2 Research Questions . . . 3
- 1.3 Challenges . . . 5
- 1.4 Contributions . . . 6
- 1.5 Thesis Outline . . . 8

**2 Literature Review** 9
- 2.1 Carbon Emissions and LCTs . . . 11
- 2.2 Contributions . . . 11
- 2.3 Combined Impact of PVs, EVs, and HPs . . . 12
  - 2.3.1 Impact of PVs and EVs . . . 12
  - 2.3.2 Impact of PVs and HPs . . . 15
  - 2.3.3 Impact of PVs, EVs, and HPs . . . 16
- 2.4 Analysis and Discussion of Grid Impact of LCTs . . . 21
  - 2.4.1 Introduction . . . 21
  - 2.4.2 General Key Insights . . . 23
  - 2.4.3 Grid Impact Analysis . . . 24
  - 2.4.4 Limitations of Grid Impact Analysis . . . 28
  - 2.4.5 Conclusions of Impact Analysis & Proposed Solutions . . . 31
- 2.5 Solution 1: Energy Storage Systems (ESS) . . . 31
  - 2.5.1 Categories of ESS . . . 31
  - 2.5.2 Lithium-ion Batteries (LIB) . . . 33
  - 2.5.3 LIB Degradation . . . 34
- 2.6 Solution 2: Power Control Systems (PCS) . . . 37
  - 2.6.1 Definition . . . 37
  - 2.6.2 Ancillary Services by PCSs: aFRR reserves provision . . . 39

**3 Grid Impact of Balanced Grid Integration of LCTs** 43
- 3.1 Motivation . . . 45
- 3.2 Contributions . . . 45
- 3.3 Data Description & Models of LCTs . . . 47
  - 3.3.1 Data Description . . . 47

3.3.2 EV model . . . 48
3.3.3 HP & Building models . . . 50
3.3.4 Solar Irradiation . . . 54
3.3.5 PV model . . . 55
3.3.6 Seasonal Analysis of LCTs . . . 57
3.4 Description of Set-Up & Case Studies . . . 58
3.4.1 Investigated Distribution Grids . . . 58
3.4.2 Case Studies . . . 59
3.4.3 LCT Grid Distribution . . . 61
3.4.4 Simulation Set-Up . . . 61
3.5 Results . . . 62
3.5.1 Results Overview . . . 63
3.5.2 Transformer Overloading . . . 63
3.5.3 Lines Overloading . . . 66
3.5.4 Nodes Voltage Deviation: Under-/Over- voltage . . . 68
3.5.5 Comparison of Grid Impact Issues . . . 69
3.5.6 Bottom-up & Top-down Approaches Comparison . . . 70
3.6 Discussion of Results . . . 72
3.6.1 Summary of Findings . . . 72
3.6.2 Recommendations . . . 75
3.7 Conclusion and Future Work . . . 76

**4 Grid Impact of Unbalanced Grid Integration of LCTs 77**
4.1 Motivation . . . 79
4.2 Contributions . . . 79
4.3 Methodology . . . 81
4.3.1 Voltage Unbalance Factor (VUF) . . . 81
4.3.2 Load & LCT Phase Connections . . . 82
4.4 Case Studies & Simulation Setup . . . 83
4.5 Results . . . 84
4.5.1 Phase Connections: Unbalance Factor (UF) 1 . . . 84
4.5.2 LCT Grid Locations: Unbalance Factor 2 . . . 87
4.5.3 Seasons: Unbalance Factor 3 . . . 90
4.5.4 LCT Consumption & Power Levels: Unbalance Factor 4 . . . 92
4.5.5 Evaluation of LCT Consumption and Power Levels Variation as Phase Unbalance Mitigation Measures . . . 94
4.6 Discussion of Results . . . 95
4.6.1 Summary of Findings . . . 95
4.6.2 Critical Voltage Unbalance results & Recommendations . . . 99
4.6.3 Limitations . . . 101
4.7 Conclusion and Future Work . . . 101

**5 Power Control of LCTs and Energy Arbitrage 103**
5.1 Motivation . . . 105
5.2 Contributions . . . 107
5.3 Power Control Concept . . . 108

5.4 Power Control Modeling . . . 112
5.4.1 Battery Energy Storage & EV Constraints . . . 112
5.4.2 Building Constraints . . . 114
5.4.3 Node Constraints . . . 117
5.4.4 Battery Degradation . . . 118
5.4.5 Objective Function . . . 121
5.4.6 Optimization Overview . . . 121
5.5 Case Studies & Scenarios . . . 124
5.5.1 Small (3-node) & Large (13-node) LV Grids . . . 124
5.5.2 Data Input . . . 126
5.5.3 Overall Case Studies . . . 126
5.5.4 Simulation Setup & Utilized Software . . . 127
5.5.5 Limitations . . . 127
5.6 Results . . . 128
5.6.1 Small Grid Scenario . . . 129
5.6.2 Large Grid Scenario . . . 134
5.7 Discussion and Validation . . . 137
5.7.1 Summary of Findings . . . 137
5.7.2 Comparison with existing power control works . . . 138
5.7.3 Validation . . . 139
5.8 Conclusions & Future Work . . . 144

**6 Power Control of LCTs and Ancillary Services Provision: Part 1 147**
6.1 Motivation & Contributions . . . 149
6.2 Power Control Concept . . . 151
6.3 Power Control Modeling . . . 151
6.3.1 EV & BESS Constraints . . . 151
6.3.2 Building Constraints . . . 153
6.3.3 Imbalance Market Constraints . . . 153
6.3.4 Node Constraints . . . 155
6.3.5 Objective Function . . . 156
6.4 Data Input, Case Studies & Limitations . . . 157
6.4.1 Data Input & Simulation Setup . . . 157
6.4.2 Case Studies & Scenarios . . . 158
6.4.3 Limitations . . . 160
6.5 Results & Discussion . . . 160
6.5.1 Power Flow Analysis . . . 160
6.5.2 Energy and Cost Analysis . . . 163
6.5.3 aFRR Provision Analysis . . . 167
6.5.4 Large Grid Scenario Results . . . 169
6.5.5 Discussion of Results . . . 172
6.6 Conclusions . . . 173

**7 Power Control of LCTs and Ancillary Services Provision: Part 2 175**
7.1 Motivation & Contributions . . . 177
7.1.1 Optimal BESS allocation . . . 177

7.1.2 PCS & Implicit/Explicit Demand Response (DR) . . . . . 178
7.1.3 Contributions . . . . . 178
7.2 Power Control System & Ancillary Services Concepts . . . . . 180
7.2.1 Concept of Power Control System . . . . . 180
7.2.2 Concept of Ancillary Services Provision Studies . . . . . 181
7.3 Power Control Modeling . . . . . 182
7.3.1 BESS/EV Operational Constraints . . . . . 182
7.3.2 Building Constraints . . . . . 183
7.3.3 aFRR Market Constraints . . . . . 183
7.3.4 BESS Optimal Allocation Constraints . . . . . 184
7.3.5 Node Constraints . . . . . 185
7.3.6 Objection Function . . . . . 186
7.4 Data Description, Simulation Setup, Case Studies & Scenarios . . . . 187
7.4.1 Data input . . . . . 187
7.4.2 Studies, Cases, and Scenarios . . . . . 190
7.4.3 Simulation Setup and Used Software . . . . . 191
7.4.4 Limitations . . . . . 191
7.5 Results . . . . . 191
7.5.1 Study 1: Direct Load Control . . . . . 191
7.5.2 Study 2: aFRR Energy Provision with optimal BESS allocation 195
7.6 Discussion & Validation . . . . . 201
7.6.1 DLC . . . . . 201
7.6.2 Optimal BESS installation and allocation . . . . . 202
7.6.3 aFRR provision with the use of different assets . . . . . 203
7.6.4 Validation . . . . . 203
7.7 Conclusions . . . . . 205

**8 Conclusion** **207**

**Acknowledgements** **235**

**Curriculum Vitæ** **237**

**List of Publications** **239**
1 Publications Related to the Thesis . . . . . 239
1.1 Journal Publications . . . . . 239
1.2 Conference Publications . . . . . 239
2 Publications Collaborative Projects . . . . . 240
2.1 Journal Publications . . . . . 240
2.2 Conference Publications . . . . . 240

# Summary

European and global goals have been set concerning the reduction of carbon emissions over the next decades. In this regard, the residential and mobility sectors constitute two of the main contributors to carbon emissions. For that reason, renewable energy sources such as photovoltaics (PVs), and electric mobility and heating with electric vehicles (EVs) and heat pumps (HPs) will play a major role in the energy transition. However, on the one hand, these low-carbon technologies (LCTs) do not come without various side effects for the future distribution grids. On the other hand, their co-integration with energy storage systems (ESS) into power control systems (PCSs) can not only reduce these side effects but also offer various ancillary services.

**Part 1: Grid Impact Review of LCTs and Introduction to Mitigation Solutions**
The Ph.D. thesis begins with a review of all the important findings concerning the various grid impact issues that can appear due to the combined grid integration of PVs, EVs, and HPs. Moreover, a qualitative analysis of the impact level of the most investigated grid issues and quantitative comparisons is incorporated between the different grid types and LCTs. Then, the thesis continues with an introduction to the various ESS categories, focusing on lithium-ion batteries (LIBs), the definition of PCS, and frequency regulation provision, which are the main mitigation solutions and ancillary services considered in this work.

**Part 2: Grid Impact of LCTs in distribution grids**
In continuation, the grid impact is firstly investigated in terms of overloading and voltage deviations in various distribution grids due to the balanced grid integration of PVs, EVs, and HPs. Several influencing factors have been considered, such as different LCT combinations, penetration levels, grid types (rural, suburban, urban), intra-week and seasonal effects, and existing loading conditions. The major objectives are the identification of the most severe LCT, grid impact issue, seasonal effect, and vulnerable distributional area, considering the physical models of the LCTs. While the investigation followed a bottom-up approach, using detailed physical models, aggregated national data has also been acquired, which is often used by top-down approaches. The investigation has been repeated following a top-down approach to reveal the influence of the utilized approach and for cross-validation. Secondly, the grid impact investigation proceeded with the use of the same distribution grids for the voltage unbalance quantification due to unbalanced grid integration of PVs, EVs, and HPs under the same combined increasing penetration levels. The identification of the most severe LCT and vulnerable distributional area has also been the focus of this grid impact investigation part. The effect of four main unbalance influencing factors has been addressed; namely, the LCT phase connections, grid distributions,

the seasonal effect, and the power and consumption levels. Finally, the use of one power-based (average EV charging), and consumption-based (lower thermal comfort) has been evaluated as potential mitigation methods for phase unbalance.

**Part 3: Power Control of LCTs for Energy Arbitrage**

After the grid impact investigation, this Ph.D. thesis proceeded with the analysis of the benefits of the co-integration of PVs, EVs, and HPs, with and without battery ESS (BESS) in PCSs. Firstly, a two-level mixed integer quadratic programming (MIQP) power control model for day-ahead and real-time scheduling of LCTs has been developed, aiming for energy arbitrage and maximum cost savings without grid violations. The contribution of load flexibility, such as vehicle-to-grid (V2G) use, and BESS is compared, considering the effect of different grid types (residential, commercial, mixed), grid sizes, seasons, and battery degradation. In this regard, a physics-guided semi-empirical battery degradation model has been linearized and incorporated, which accounts for both calendar and cyclic aging, and considers various degradation-influencing factors, such as time, temperature, C-rate, and throughput.

**Part 4: Power Control of LCTs for Ancillary Services Provision**

Secondly, the thesis enhanced the previously developed PCS of PVs, EVs, HPs, and BESS to provide ancillary services while simultaneously performing energy arbitrage without grid violations. The ancillary service considered is the provision of automated frequency restoration reserves (aFRR), where the day-ahead level has been used to offer aFRR to the wholesale market and the real-time level to deploy them in real-time. The individual and combined contribution of load flexibility (V2G) and BESS has also been compared here, providing aFRR reserves either with the use of the one asset or the other or both. The results have been evaluated under various influencing conditions, such as different seasons, grid types (residential, commercial, and mixed), small and large grid size levels, and energy/reserve prices. This investigation has been conducted using fixed BESS capacities at the considered nodes. Finally, the MIQP PCS has been improved to provide aFRR reserves comparing the same LCT synergies, however, simultaneously optimally allocating BESS capacity at the nodes of the distribution grid. The effect of the same influencing factors has been analyzed with the addition of the distribution line losses and the BESS investment cost, which are highly important for the optimal BESS allocation. Finally, the potential of the PCS for explicit demand response strategies, such as direct load control, has been investigated with and without the use of BESS while performing energy arbitrage (implicit demand response), which can be used for other ancillary purposes, such as congestion management.

# Nomenclature

| | |
|---|---|
| **(AS)HP** | Air-sourced Heat Pump |
| **aFRR** | Automated Frequency Restoration Reserves |
| **AOI** | Angle of Incidence |
| **(B/T/H)ESS** | (Battery/Thermal/Hybrid) Energy Storage System |
| **BRP** | Balancing Responsible Party |
| **BSP** | Balancing Service Provider |
| **CAES** | Compressed Air Energy Storage |
| **CAPEX** | Capital Expenditure |
| **CC-CV** | Constant Current - Constant Voltage |
| **CHP** | Combined Heat and Power |
| **CI/CD** | Consumption Increase/Decrease |
| **CL** | Capacity Loss |
| **COP** | Coefficient of Performance |
| **CPP** | Critical Peak Pricing |
| **CT** | Capacity Tariff |
| **CvaR** | Conditional Value at Risk |
| **DA(M)** | Day-ahead (Market) |
| **DER** | Distribution Energy Resource |
| **DF** | Distribution Feeder |
| **DG** | Distribution Grid |
| **DHW** | Domestic Hot Water |
| **DLC** | Direct Load Control |
| **DMP** | Duration-magnitude Product |
| **DOD** | Depth of Discharge |
| **DR** | Demand Response |
| **DSM** | Demand Side Management |
| **EMC** | Energy Management Controller |
| **EoL** | End of Life |
| **FBES** | Flow Battery Energy Storage |
| **FCR** | Frequency Containment Reserves |
| **FES** | Flywheel Energy Storage |
| **(H/B/D)EMS** | (Home/Building/District) Energy Management System |
| **HH** | Household |
| **ICE** | Internal Combustion Engine |
| **ISP** | Imbalance Settlement Period |
| **LAM** | Loss of Active Material |
| **LCT** | Low-carbon Technology |

| | |
|---|---|
| **LFC** | Load-Frequency Control |
| **LFP** | Lithium Iron Phosphate |
| **LIB** | Lithium-ion Battery |
| **LLI** | Loss of Lithium Inventory |
| **LP** | Lithium Plating |
| **LV** | Low Voltage |
| **MCS** | Monte-carlo Simulation |
| **MIL/QP** | Mixed-integer Linear/Quadratic Programming |
| **MPC** | Model Predictive Control |
| **MPP** | Maximum-power Point |
| **NOCT** | Normal Operation Conditions Temperature |
| **O-C / S-C** | Open-circuit / Short-circuit |
| **O/L** | Overloading |
| **O&M** | Operational & Maintenance |
| **OH** | Overhead |
| **OV/UV** | Overvoltage/Undervoltage |
| **(P)EV** | (Plug-in) Electric Vehicle |
| **PCS** | Power Control System |
| **PDF** | Probability Distribution Function |
| **PF** | Power Factor |
| **PHES** | Pumped Hydro Energy Storage |
| **PWL** | Piecewise Linear |
| **PV** | Photovoltaic |
| **RES** | Renewable Energy Source |
| **RHO** | Receding Horizon Optimization |
| **RMSE** | Root Mean Squared Error |
| **RPF** | Reverse Power Flow |
| **RT** | Real-time |
| **RTP** | Real-time Pricing |
| **(S.)B-U** | (Stochastic) Bottom-up |
| **SC** | Smart Charging |
| **SEI** | Solid Electrolyte Interphase |
| **SH/C** | Space-heating/cooling |
| **SMES** | Superconducting Magentic Energy Storage |
| **SOC** | State of Charge |
| **STC** | Standard Test Conditions |
| **(T/D)SO** | (Transmission/Distribution) System Operator |
| **T-D** | Top-down |
| **T/F** | Transformer |
| **TC** | Thermal Comfort |
| **TMD** | Transition Metal Dissolution |
| **TOU** | Time of Use |
| **UF** | Unbalance Factor |
| **V2G** | Vehicle-to-Grid |
| **VUF** | Voltage Unbalance Factor |

# 1 Introduction

## 1.1. Motivation

Due to the ever-growing environmental impact and depletion of fossil fuels, 197 nations have pledged to decrease greenhouse gas emissions and keep global warming below 1.5°C until 2050 during the “Paris Agreement” in 2015 [1]. In this regard, the residential and mobility sectors constitute two of the main contributors. For example, residential heating is mostly produced by gas-fired boilers in most European countries, e.g., in 84.2% of UK households. Moreover, 99% of the passenger vehicles in the UK in 2017 were conventional internal combustion engine (ICE)-powered vehicles [2]. An analysis of 27 European countries (EU-27) found that the residential sector accounts for 24-26.7% of the total annual energy use in 2010, which is mainly fossil-fueled [3]. It also contributed to 70% of the total carbon emissions in 2011 in [4]. Moreover, an analysis, published by Eurostat in [5], shows that the transportation sectors and buildings are responsible for 26.2% and 13.8% of the total gas emissions in Europe, respectively. Finally, heating and mobility sectors were reported to be jointly responsible for 60% of all carbon emissions in [6]. Hence, the electrification of heating and transportation with electric vehicles (EVs) and heat pumps (HPs), as well as renewable energy sources (RESs), e.g., photovoltaic (PVs), are cornerstones of the energy transition success. All of the above fall under the category of "low-carbon technologies (LCTs)" whose adoption in Europe has an exponential rate during the last decades, as seen in Figure 1.1.

However, LCTs do not come without the side effect of major grid impact. For example, increased power peaks [1] and load consumption [3] were seen due to energy demand electrification, leading inevitably to grid capacity reduction and congestion in distribution grids (DGs) [6]. Moreover, power quality issues, such as over-/under-voltage deviations, were reported in [10], while vastly uncertain and rapidly changing PV power caused voltage fluctuations or light flickering in [11]. Additionally, cables and transformers overloading were seen in [12], which could also lead to even more important hazards such as blackouts. Finally, an increase in phase and voltage imbalance was observed due to the connection of single-phase generators (e.g., PVs) or electric loads (e.g., EVs) in distribution grids [13], [14].

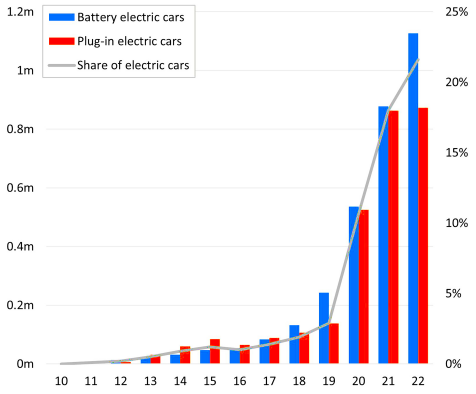


(a) New EV registrations, EU-27 [7].

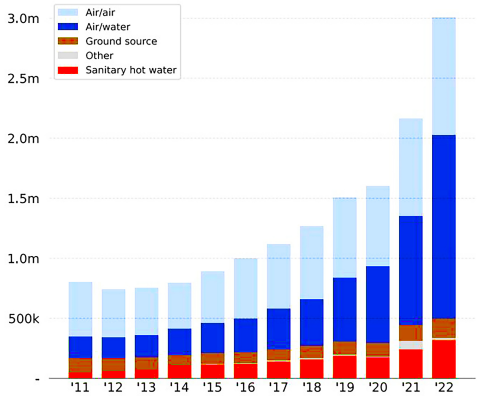


(b) Sales development of HPs, EU [8].

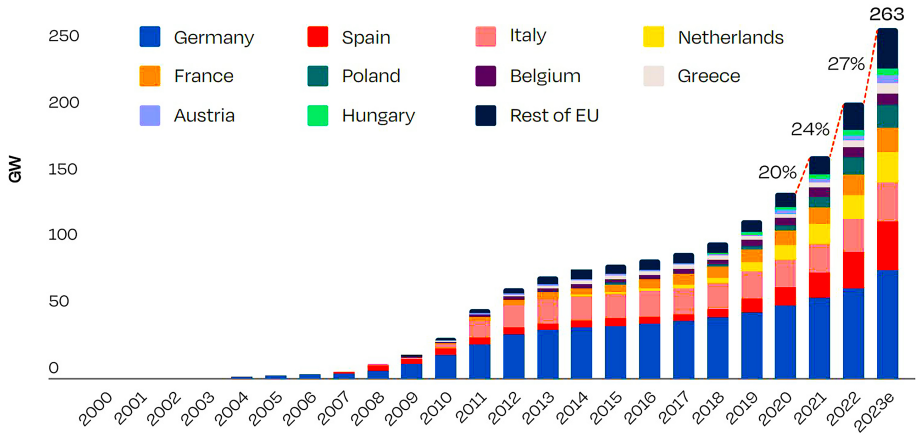


(c) EU cumulative solar PV installed capacity 2000-2023 [9].

Figure 1.1: Trends of Low-Carbon Technologies in Europe

All of the above constitute important issues, which prove that successful 100% integration of LCTs cannot be achieved unless the above challenges are managed.

Therefore, on the one hand, power control of PVs, flexible loads such as EVs and HPs, and (battery) energy storage systems ((B)ESS) in energy management systems (EMSs) (in the sense of power flows' management) will become necessary in future low voltage (LV) DGs with the aim of energy arbitrage with minimum cost, PV self-consumption increase and avoiding grid violations [15], [16]. Demand side management (DSM) concepts have emerged to assist in the power scheduling of EMSs performing load shifting, load shedding, etc. [17]. On the other hand, ancillary services such as frequency regulation or congestion management can be provided to the power grid [18], [19]. In this regard, the vehicle-to-grid (V2G) capability of the EVs can also provide significant support, transforming the EVs into mobile ESS [20].

Such EMSs have been developed on a home level, e.g., home energy management systems (HEMSs) [21], or grid level, usually using aggregators [16].

It must be noted that in this Ph.D. thesis, the terms "power control systems (PCSs)" and EMSs are used interchangeably. Although most existing works prefer the term "EMS", according to the author's opinion, the term "PCS" is more suitable since such systems mainly control power directly, and as a consequence, energy. Moreover, power control refers to the management of the power flows of the generation, consumption, and energy storage units.

## 1.2. Research Goal Statement and Research Questions

### 1.2.1. Research Goal Statement

A graphical abstract of this Ph.D. dissertation is depicted in Figure 1.2, while the research goal statement is defined as follows:

"What is the grid impact of integrating Renewable Energy Sources, Electrified Mobility & Heating in future distribution grids, and how can their power be controlled together with Energy Storage Systems to minimize the cost, the grid impact, and to provide ancillary services?"

### 1.2.2. Research Questions

*Q1: What is the grid impact on component overloading and voltage deviations due to the balanced grid integration of uncontrolled electrified mobility, heating, and distributed generation in distribution grids* **(Chapter 3)**?

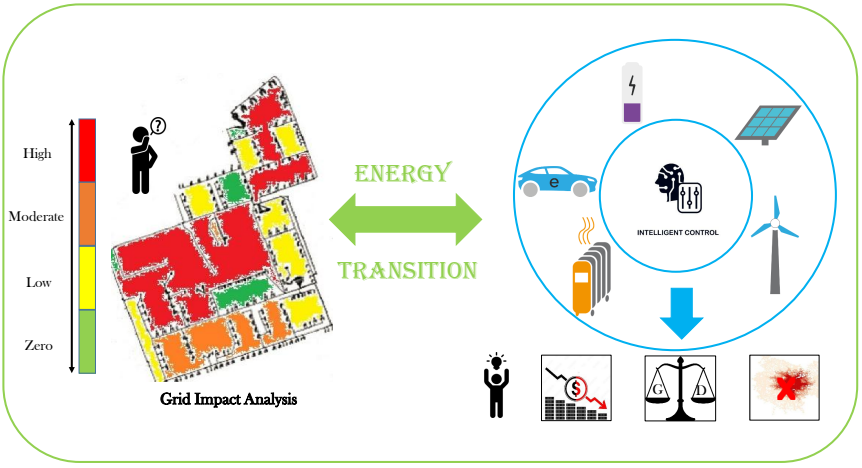


Figure 1.2: Graphical abstract of the Ph.D. Dissertation

The gradual combined increasing grid penetrations of electric vehicles, heat pumps, and distributed energy resources (DERs), such as PVs, until 2050, are going to induce several grid impact issues, such as transformer and distribution line overloading and voltage deviations, that need to be quantified. Moreover, due to the variety of distribution grids and the different LCT adoption rates, the "heaviest" LCT combination and the most affected distributional area currently and in the future need to be identified. It is also important to quantify the influence of the existing grid loading, spatial, intra-week, and seasonal effects on the level of the forthcoming grid impact issues. Finally, grid impact assessment studies follow different approaches and data generation methods that can also have a significant effect on the respective results and findings.

*Q2: What is the grid impact on phase unbalance due to the unbalanced grid integration of uncontrolled electrified mobility, heating, and distributed generation in distribution grids* **(Chapter 4)**?

Grid impact assessment studies often consider balanced LCT penetrations, ignoring the fact that most small-scale LCTs are still single-phase connected and the deteriorating effect on the grid phase balance. The induced voltage unbalance by increasing penetrations of different combinations of PVs, EVs, and HPs in different distributional areas needs to be quantified. Furthermore, several influencing factors should also be investigated here, which can again be the existing grid loading, spatial, intra-week, and seasonal effects, but also the LCT phase connections, grid distributions, and power levels. Finally, the potential of voltage unbalance mitigation without the use of additional mitigation assets and grid reinvestments, e.g., by varying the LCT power and consumption levels, should be assessed.

*Q3: How can power control of energy storage systems (ESS) and flexible loads, such as electric vehicles (EVs) and heat pumps (HPs), contribute to energy arbitrage without grid violation* **(Chapter 5)**?

Power control systems can be designed to perform energy arbitrage with maximum cost savings and without violating the grid limits, either exploiting the flexibility of loads, such as V2G-capable EVs and HPs, alone or with their synergy with energy storage systems, e.g., BESS. However, flexible loads are prone to uncertainties, and their performance on energy arbitrage without the use of BESS needs to be evaluated. Additionally, the level at which flexible loads can substitute a BESS needs to be identified either in small grids with a number of buildings and EV chargers or in large grids comprising hundreds of loads. Moreover, it is important to assess the performance of the synergy of flexible loads and BESS during different seasons and in different grid types that affect the behavior of the comprised loads (e.g., residential, commercial, etc). Finally, battery degradation can have a seriously detrimental effect on the power control and its total cost due to the overuse of the available assets. However, accurate battery degradation models are highly nonlinear. It is important to linearize and integrate a physics-guided battery degradation model into power control with a low computational burden and high accuracy.

*Q4: While performing energy arbitrage, how can the power of energy storage systems (ESS) and flexible loads, such as electric vehicles (EVs) and heat pumps (HPs), be controlled to provide grid ancillary services* **(Chapters 6 and 7)**?

Apart from energy arbitrage, power control systems can exploit the flexibility of loads and energy storage to provide various ancillary services to the main grid. System-wide ancillary services, such as frequency regulation (e.g., provision of automatic frequency restoration reserves aFRR), can be provided when the PCS participates in the wholesale reserve market; however, the scheduling of the aFRR reserves provision day-ahead and their deployment in real-time can be challenging due to uncertainties, especially if a BESS is not used. Moreover, PCSs usually deploy implicit (price-based tariffs) or explicit (direct load control, DLC) demand response strategies to provide ancillary services. It is interesting to evaluate the combination of both strategies, such as real-time pricing (RTP) and DLC in PCSs for simultaneous energy arbitrage and congestion management. Furthermore, the potential of flexible loads to substitute ESS in PCS concerning ancillary services provision, such as aFRR reserves provision and DLC needs to be evaluated, while the influence of different seasons, grid types and sizes, and energy-reserve prices needs to be assessed. Finally, it is important to investigate how the location and sizing of BESS capacity can be optimized in distribution grids by performing energy arbitrage and/or providing ancillary services and how the optimal BESS capacity allocation is affected by power losses, energy prices, and seasons.

## 1.3. Challenges

The first main challenge of this Ph.D. research, for both the grid impact analysis of Research Questions 1 & 2 (Part 1) and the optimization methods of Research Questions 3 & 4 (Part 2), has been the investigation of a suitable balance between high accuracy and low computational burden. A detailed LCT modeling has been intended to maintain a high accuracy level. However, all chapters constitute grid-level studies that need to be solved in a reasonable computational time. Especially for the optimization methods, the co-optimization of PV generation, EV charging, V2G, HP heating, and BESS use in PCS frameworks that can be scalable in high grid sizes has induced great challenges when integrating detailed LCT modeling. A representative example is the accurate integration of the highly non-linear battery degradation in quadratic optimization. The second main challenge of this research has been the investigation and quantification of the impact of several influencing factors on the answer to all Research Questions 1-4, such as different seasons, grid types and sizes, LCT combinations/synergies, penetration levels, grid distributions, etc. More in particular, all these factors affect the results not only individually but also co-dependently. For example, LCT behaviors deviate depending on the grid type, but also on the investigated season. Moreover, the comparison between ESS and flexible loads changes not only according to the season but also to the size of the grid and the number of loads. For that reason, a vast number of case studies and scenarios have been investigated in the analysis of all chapters for the testing of the models to perform fair comparisons and strengthen each chapter's findings.

## 1.4. Contributions

The contributions of this thesis are summarized below. Moreover, the related chapter and publication for each contribution are also listed.

1. A comprehensive review of grid impact issues provoked by the integration of different combinations of PVs, EVs, and HPs in LV DGs, investigating the effect of various characteristics such as penetration levels, seasons, grid types, uncertainty management techniques, and followed approaches. Moreover, the grid impact level of the most investigated grid issues has been analyzed, and different grid types and LCTs have been compared concerning their violation levels. Finally, an introduction to mitigation solutions such as PCSs and BESS is provided, focusing on the role of lithium-ion batteries (LIBs), their main degradation mechanisms, influencing factors, and interrelations that cause the non-linear LIB capacity fading **(Chapter 2)**. The publications related to this contribution are the following:

- **J1:** N. Damianakis, G. R. C. Mouli and P. Bauer. 'Grid impact of photovoltaics, electric vehicles and heat pumps on distribution grids — An overview'. In: *Applied Energy* 380 (2025), p. 125000. ISSN: 0306-2619
- **J2:** P. Lozano Ruiz, N. Damianakis and G. Ram Chandra Mouli. 'Physics-Based and Data-Driven Modeling of Degradation Mechanisms for Lithium-Ion Batteries—A Review'. In: *IEEE Access* 13 (2025), pp. 21164–21189

2. A grid impact assessment study regarding component overloading and voltage deviations caused by balanced grid integration of uncontrolled operation of PVs, EVs, and HPs. Different real-world LV DGs and detailed LCT models have been used, while the effects of different grid types, LCT combinations, penetration levels, existing loading conditions, seasons, and followed approaches have been analyzed **(Chapter 3)**. The publications related to this contribution are the following:

- **C1:** N. Damianakis, G. C. R. Mouli and P. Bauer. 'Risk-averse Estimation of Electric Heat Pump Power Consumption'. In: *2023 IEEE 17th International Conference on Compatibility, Power Electronics and Power Engineering (CPE-POWERENG)*. 2023, pp. 1–6
- **J3:** N. Damianakis, G. R. C. Mouli, P. Bauer and Y. Yu. 'Assessing the grid impact of Electric Vehicles, Heat Pumps & PV generation in Dutch LV distribution grids'. In: *Applied Energy* 352 (2023), p. 121878. ISSN: 0306-2619

3. A grid impact assessment study regarding the phase unbalance caused by unbalanced grid integration of uncontrolled operation of PVs, EVs, and HPs on different types of real-world LV DGs under different combinations and penetration levels. The influence of four main unbalance factors, namely LCT phase connections and grid distributions, seasons, and LCT power and consumption levels, has been analyzed, the latter of which has been evaluated as a mitigation measure **(Chapter 4)**. The publication related to this contribution is the following:

- **J4:** Y. Wesseling, N. Damianakis, G. Ram Chandra Mouli and P. Bauer. 'Grid Impact of Unbalanced Phase Integration of PV Generation, Electrified Mobility, and Heating in LV Distribution Grids'. In: *IEEE Access* 13 (2025), pp. 56887–56907

4. A two-stage power control method for day-ahead (DA) and real-time (RT) scheduling of PVs, V2G-capable EVs, HPs, and BESS for energy arbitrage under uncertainties without grid violations. The contribution of flexible loads and BESS to energy arbitrage has been compared while considering the influence of different seasons, grid types and sizes, and battery degradation. A physics-guided semi-empirical degradation model has been linearized and integrated into the power control, maintaining high accuracy **(Chapter 5)**. The publications related to this contribution are the following:

- **C2:** N. Damianakis, G. R. C. Mouli, Y. Yu and P. Bauer. 'Coordinated Power Control of PV Generation, Electric Mobility and Electric Heating in Different Grids'. In: *2024 IEEE 10th International Power Electronics and Motion Control Conference (IPEMC2024-ECCE Asia)*. 2024, pp. 2082–2087
- **C3:** N. Damianakis, Y. Yu, G. R. C. Mouli and P. Bauer. 'Impact of Uncertainties and Price of Robustness in receding-horizon EV Smart-Charging'. In: *2024 IEEE 21st International Power Electronics and Motion Control Conference (PEMC)*. 2024, pp. 1–6
- **J5:** N. Damianakis, G. R. C. Mouli and P. Bauer. 'Power Control of PV Generation, Electric Mobility, Electric Heating and Battery Energy Storage'. In: *Applied Energy* (2025). Under Review

5. A two-stage power control method of PVs, V2G-capable EVs, HPs, and BESS for bidding aFRR reserves in the wholesale market DA and deploying them in RT under uncertainties while respecting the customers' comfort and grid limits. The contribution of flexible loads and BESS to aFRR reserves provision has been compared while considering the influence of different seasons, grid types and sizes, and energy-reserve prices **(Chapter 6)**. The publication related is the following:

- **J6:** S. Warmerdam, N. Damianakis and G. R. C. Mouli. 'Power Control of PV Generation, Flexible Loads, and Battery Energy Storage for Frequency Reserves Provision'. In: *Sustainable Energy, Grids and Networks* (2025). Under Review

6. A two-stage power control method of PVs, V2G-capable EVs, HPs, and BESS that exploits implicit (RTP) and explicit (DLC) demand response (DR) strategies for simultaneous energy arbitrage and congestion management in different distribution grids and seasons. Moreover, an optimal sizing and location method for BESS integration into power control of flexible loads while respecting the customers' comfort and grid limits is introduced under the influence of ancillary services provision (e.g., aFRR reserves), distribution line losses, grid type, energy/reserve prices, seasons, and different BESS-loads synergies. **(Chapter 7)**. The publication related to this contribution is the following:

- **J7:** N. Damianakis, K. Kuresoo and G. R. C. Mouli. 'Battery Storage Integration in Power Systems of PVs, and Flexible Loads for Frequency Reserves Provision and Direct Load Control'. In: *Journal of Energy Storage* (2025). Under Review

## 1.5. Thesis Outline

The outline of this thesis and the interrelations of the thesis chapters are depicted in Figure 1.3. Chapter 2 integrates the literature review of the thesis, which comprises, firstly, an overview of the various grid impact issues that are caused by grid integration of LCTs such as PVs, EVs, and HPs. Secondly, it comprises an overview of PCSs and BESS, especially LIBs and LIB degradation mechanisms with their causes and interrelations. Chapters 3 and 4 integrate two grid impact assessment studies for balanced and unbalanced integration of PVs, EVs, and HPs, respectively, considering effects, such as grid types, LCT combinations, and penetration levels, seasons, etc. Moreover, Chapters 5 and 6 comprise PCS methods of flexible loads and BESS for energy arbitrage without and with ancillary services provision, such as frequency regulation, respectively. Chapter 7 develops a PCS method that combines implicit and explicit DR strategies for energy arbitrage and DLC, while an optimal BESS capacity allocation is also proposed for grids controlled by such PCSs. The influence of grid sizes and types, seasons, energy-reserve prices, distribution line losses, battery degradation, and BESS-load synergies has been investigated on the performance of the PCS methods. Finally, Chapter 8 concludes the Ph.D. thesis.

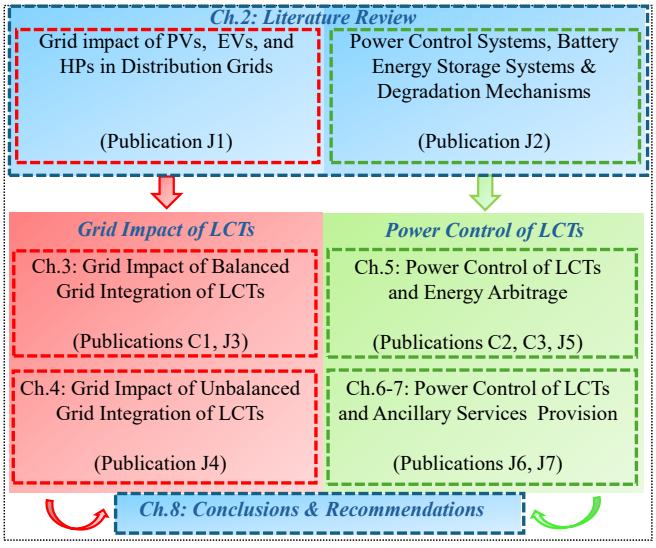


Figure 1.3: Thesis Outline and interrelations of thesis chapters.

# 2

# Literature Review

*Summary*

As explained in Chapter 1, PVs, EVs, and HPs will play a major role in the energy transition; however, these LCTs do not come without various side effects for the future distribution grids. This chapter begins with a review, analysis, and summary of all the important findings concerning the various grid impact issues that can appear due to the grid integration of these 3 LCTs. Moreover, the chapter incorporates a qualitative analysis of the impact level of the most investigated grid issues and quantitative comparisons between the different grid types and LCTs. This Ph.D. thesis employs power control of LCTs and BESS to provide solutions for the customers (e.g., energy arbitrage) as well as for the system operator (ancillary services). The chapter continues with an introduction to the various ESS categories and applications, giving more focus on the different chemistries, characteristics, applications, and degradation causes of LIBs. Finally, the chapter proceeds with the definition of PCSs and frequency regulation provision, which is the main ancillary service investigated in this Ph.D. thesis, defining the different market parties, types, and operation of balancing markets.

*Outline*

The chapter is categorized as follows: Section 2.1 starts with this chapter's motivation, with an introduction to LCTs and carbon emissions of various sectors, while the contributions are comprised in 2.2. Section 2.3 comprises the existing knowledge about the various grid impact issues of combined integration of PVs, EVs, and HPs, while Section 2.4 comprises this chapter's discussion concerning evaluations of the grid impact issues, LCTs, DG types, mitigation strategies, etc., and related limitations and conclusions. Finally, the chapter concludes with an introduction to ESS and LIBs (categories, characteristics, degradation, etc.) in Section 2.5 and to PCSs and ancillary services in Section 2.6, which are the main solutions investigated in this Ph.D. thesis.

This chapter is based on parts of:

N. Damianakis, G. R. C. Mouli and P. Bauer. 'Grid impact of photovoltaics, electric vehicles and heat pumps on distribution grids — An overview'. In: *Applied Energy* 380 (2025), p. 125000. ISSN: 0306-2619

P. Lozano Ruiz, N. Damianakis and G. Ram Chandra Mouli. 'Physics-Based and Data-Driven Modeling of Degradation Mechanisms for Lithium-Ion Batteries—A Review'. In: *IEEE Access* 13 (2025), pp. 21164–21189

## 2.1. Carbon Emissions and LCTs

As explained in Chapter 1, the residential and mobility sectors are two of the major reasons for the current carbon emissions, accounting for 26.2% and 13.8% of the total European emissions, respectively, as depicted in Figure 2.1. LCTs, such as PVs, EVs, and HPs, responsible for their electrification, have raised concerns about the huge forthcoming grid impact that will be provoked at higher grid penetrations. Multiple works have been published regarding the individual and combined impact of the future integration of EVs, PVs, and HPs. These works highly differ regarding the investigated grid cases and seasons, LCT combinations, and penetration levels, proposed mitigation solutions, consideration of uncertainties, etc. However, a comprehensive review incorporating and comparing insights about the grid impact of combinations of PVs, EVs, and HPs is still missing from the existing literature.

## 2.2. Contributions

This review chapter summarizes the state-of-the-art knowledge about the various grid impact issues caused by grid integration of PVs, EVs, and HPs. It incorporates important research characteristics, such as different penetration levels and combinations, seasons, DGs, and DG types, uncertainty management techniques, and followed approaches. Moreover, the chapter provides a qualitative analysis of the impact level inflicted by the different LCT combinations and quantitatively compares the different LCTs and DG types regarding the most investigated grid impact issues. In continuation, it summarizes the investigated mitigation solutions and correlates them with the various grid issues. Finally, it provides a general introduction to ESS, PCSs, and ancillary services, which are the mitigation solutions that will be extensively investigated in this Ph.D. research. In this regard, the contributions of this review chapter can be summarized as follows:

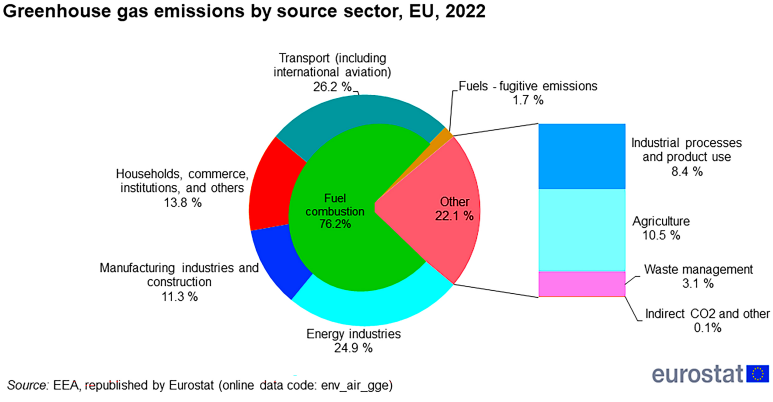


Figure 2.1: Greenhouse gas emissions by source sector, EU, 2022 (Eurostat [5]).

- Investigates the various grid impact issues from grid integration of PVs, EVs, and HPs, considering the studied penetration levels and combinations, seasons, DGs, and DG types, uncertainty management techniques, and followed approaches. While such investigations exist individually for each technology (e.g., PVs or EVs), a combined analysis that shows the interactions of these 3 LCTs regarding the grid impact issues when integrated in combination is still missing from the literature.
- Performs qualitative analysis of the level of the inflicted grid impact by different LCT combinations and quantitatively compares it with respect to different DG types and LCTs. The interrelated effect of the characteristics of different DG types with different LCT integrations on the level of the various grid issues has not yet been investigated in earlier review works.
- Analyzes the various investigated mitigation effects and solutions for each combined LCT integration in grid impact assessment studies, and correlates them with the appropriate grid impact issues. This analysis is realized for the first time for PVs, EVs, and HPs together and their combined grid integration.
- Provides a general introduction to ESS, PCSs, and ancillary services that will be investigated in this Ph.D. thesis for grid impact mitigation.

## 2.3. Combined Impact of PVs, EVs, and HPs

Section 2.3 is devoted to the combined impact of the investigated technologies, which is categorized into the following pairs: PVs-EVs, PVs-HPs, and PVs-EVs-HPs. These pairs were selected because their combined grid impact is thoroughly investigated in Chapters 3 and 4. For more information, the reader is referred to the related publication [22].

### 2.3.1. Impact of PVs and EVs

The authors in [32] utilized the Phoenix metropolitan area in Arizona to study the co-adoption of EVs and PVs by analyzing the consumption and peak demand behaviors. It was found that while EV owners consumed, on average, approximately 0.4kWh additional hourly energy demand compared to the non-EV owners, the hourly demand on the grid was decreased by 1.1kWh when PVs were added. Similarly, co-adopting PVs and EVs could reduce the system's peak-hour demand.

Furthermore, the net power profile of the distribution transformers and, hence, their loading conditions have been used as metrics for the grid impact assessment of residential PVs and EVs on a DG in Austin in [33]. Reverse flows due to PV feed-in have been observed through the transformers in the morning and in the afternoon, while demand peaks due to EV charging were seen during breakfast and dinner time. While no significant transformer voltage swells or sags were seen, PV generation was found to have a higher impact than EV charging. The impact of EV chargers and PV modules on the net load of distribution transformers has also

been studied in the data-driven forecasting model in [34] to assess asymmetric changes in transformer load patterns. The proposed forecasting method, which used a diffusion pattern generator for the EV-PV uptake scenarios, predicted a future transformer net load that could reach up to 100% higher final value of other methods utilized in the literature. Moreover, a stochastic model for addressing the coincidence between plug-in EV (PEV) charging and PV generation (hence, PV self-consumption) was also developed in [35], where single and aggregated households (HHs) with or without PEVs were investigated. Firstly, it was found that PEV charging increases the yearly HH consumption by 37%. Secondly, the introduction of PEV charging could be a benefit for PV self-consumption, but mostly in aggregated HH-level scenarios.

Additionally, authors in [14] studied the phase imbalance caused by single-phase technologies such as PVs and EVs under increasing LCT penetrations in the form of total imbalance cost. Distinguishing the total cost in energy losses and capacity wastes, it was found that when LCT penetrations reached 70%, the cost of energy losses surpassed the cost of reinforcement regarding the urban UK networks. A Croatian LV network has also been used in [13] for unbalance investigation with the Voltage Unbalance Factor (VUF). Unbalance during Summer was found to be more severe, reaching up to 19% when all LCTs were connected in one phase. Unbalance was also found to exceed the maximum 2% threshold for 20% of the time, even from 20% LCT penetrations, while it was always present in the network due to single-phase HH load connections.

In addition, current and voltage harmonic distortions have been assessed by the authors in [36] on the standard IEEE LV 123-node distribution feeder, where current harmonics were found to be more severe than voltage harmonics. Moreover, while both distortions were increased by higher PV injections (current distortions increased up to 18%), they were both decreased with EV charging (current distortions decreased to 7%). However, the mitigation results have been more seen at the proximity of the substation, while combined penetrations still provoked high harmonics at the end of the feeder. The impact of EV charging uncertainty on power quality, such as harmonic levels and unbalance, was also studied in [37], where the different EV charging locations, power modes, and presence of PVs and other non-linear loads were incorporated. Charging locations were found to have a more significant impact on unbalance and voltage harmonics than power modes, while injections by the $3^{rd}$ harmonic were higher than those of the $5^{th}$ and $7^{th}$.

The power quality issues of unbalance and harmonics have also been analyzed in the rural and suburban grids of [38]. The most important insight was the significance of the distribution line type on the unbalance and harmonics results. For example, the rural grid's overhead (OH) lines were severely violated regarding both issues, even from low combined penetrations (10% EVs, 50% PVs). On the contrary, unbalance and harmonics in the cable lines of both rural and suburban grids did not exceed the predefined thresholds even at the extreme 100% LCT penetrations. Furthermore, 21 distribution grids from 3 different countries (Austria, Germany, and the Netherlands) have been investigated in [39] regarding overloading and voltage deviations. While most of the simulated grids showed minor violations, suburban

grids could become highly vulnerable in the future. The various countries were also encapsulated, showing that Germany had the highest adequacy for high EV charging accommodation compared to Austria and the Netherlands, with moderate PV penetration. The same issues have been investigated in the Maltese LV network of [40] using as a metric the percentage of consumers with grid violations under increasing penetration levels. Voltage violations were first observed from 40% combined or individual penetrations of PVs and EVs, while feeder overloading was not seen even in extreme integration scenarios. Nevertheless, the percentage of consumers with voltage violations was reduced by 15% under 70% combined penetrations, also showing in this work the potential of violation mitigation during combined PV generation and EV charging.

On the contrary, the analysis of voltage and consumption profiles in [41] in an LV Swedish distribution grid showed that EV integration hardly provoked grid voltage decrease (a maximum of 0.01 p.u. voltage decrease was observed under 10% EV penetration level). Moreover, in this work, EV integration did not notably contribute to the minimization of PV curtailment, and hence, mitigation by combined EV-PV integration was not seen. Moreover, analyzing the consumption results for different seasons, a 9.3% and 17.1% consumption increase was observed for Winter and Summer, respectively. The authors in [42] also incorporated system losses apart from voltage profiles, overloading, and unbalance as impact metrics in their investigation. They have found that, on the one hand, increasing PV generation decreased energy losses; however, on the other hand, it also simultaneously increased reverse power flow. Additionally, while increased EV penetration could moderate this reverse power flow, it also provoked asymmetrical loading even from a low number of EVs, increased the neutral voltage as well, and overloaded the distribution lines, especially those close to the MV/LV transformer. The investigated issues in [42] and the neutral losses were incorporated in the study of [43]. In this work, EVs were more closely connected with component overloading, whereas PVs were more connected with feeder overvoltage. An interesting insight was that while system losses increased linearly with increasing LCT penetrations, neutral losses showed an exponential increase.

Finally, the impact of PV-EV integration on smart grid operation was assessed in [44], considering the Mueller community in Austin-Texas, constituting a residential smart grid of 735 households. Transformers' voltage profiles and capacities, as well as cable losses and unbalance, were analyzed before and after adding 178 PVs and 100 EVs. While the local PV generation created reverse power flows of 12kW at the transformers, it generally decreased the cable losses while the active power demand of the smart grid was also decreased by 66%. However, the smart grid's reactive power was still provided by the main grid. Due to the relatively high simultaneity factor of these two LCTs, their high technology maturity and social acceptance, and the emergence of DSM techniques, such as smart-charging (SC), the co-adoption of PVs and EVs has been studied extensively. As can be seen in Figure 2.2, while their individual grid integration can provoke several issues in future distribution grids, their co-adoption and co-integration in EMSs can provide several benefits and suppression of their individual negative impacts.

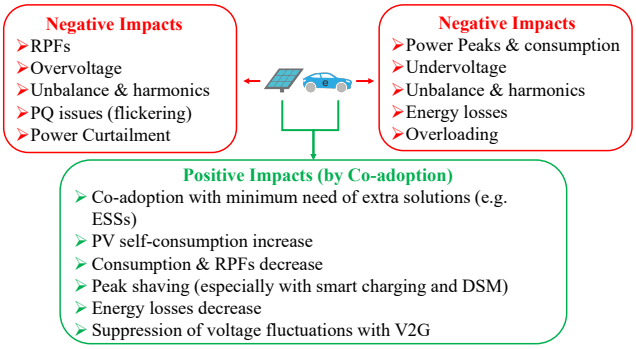


Figure 2.2: Summary of negative impacts of PVs & EVs and benefits from co-adoption.

### 2.3.2. Impact of PVs and HPs

Load profiles were analyzed in [45] for a Dutch all-electric neighborhood in Meerstad comprising 200 HHs. With the introduction of electric heating and distributed generation, the net consumption was found to be 1.75 times higher than in the reference case, while the required capacity should be increased by 300% (peak demand reached 5.1kW from 1.7kW per HH). Additionally, voltage fluctuations and transformer overloading were analyzed in [46] for a real LV urbanized area. This study investigated different types of buildings, such as apartments, townhouses, semi-detached houses, etc. While low PV-HP penetrations did not have a notable grid impact, the transformer reached a loading of 240% and 190% under 100% LCT penetration during Summer and Winter, respectively. Furthermore, the impact of PVs, HPs, and combined-heat-and-power devices (CHPs) on a German grid's power and voltage profiles has been quantified in [47]. Moreover, this work highlighted the importance of using pseudo-measurements for quantifying this impact to increase accuracy. Results showed that the usual state estimation methods could be proven highly optimistic about the final impact on the power grid.

The authors in [48] used voltage deviations, transformer capacity, and load profiles analysis to address the effect of weather conditions on the grid impact in rural and urban grids in Belgium. The importance of considering weather uncertainty in grid impact studies with PVs-HPs was highlighted since an extremely cold Winter day could result in 10% higher transformer overloading and 2.5% higher voltage violations. The diversity and the effect of the ambient temperature on the peak load inflicted by residential heat pumps have also been considered in the analysis of [49]. According to their findings, an ambient temperature deviation of 4° could nearly double the peak load, while a 72% peak load increase was noted from 20% HP penetration when the ambient temperature reached -4°. Additionally, high reverse power flows were seen even from 25% PV penetration, while overvoltage violation reached 14V at 30% PV penetration. Additionally, grid losses were incorporated along with the previous metrics for quantifying the impact of home energy systems

with electric heating and PV generation on the power grid in [50]. However, in the German suburban area investigated in this work, which comprises 36 HHs, no violations of any kind were observed.

Unbalance was incorporated with the other grid impact metrics in [51] to calculate needed grid reinforcements in real urban and rural grids. No unbalance was observed for the urban grid, while unbalance was noted only with HP integration for the rural grid, starting from 40% HP penetration. An interesting insight was also that grid reinforcements could lead to significantly higher costs than the costs inflicted by energy losses. A comparison between urban and rural grids under increasing combined PV-HP penetrations was also performed in [4], where the rural feeders were also found to be more vulnerable to overloading and voltage violations than the urban ones. Regarding this work, overloading was deemed a more crucial issue than undervoltage, appearing from lower LCT penetrations. Metamodeling techniques have been used in the probabilistic work in [52] to assist reliable high-level gid impact assessment in rural and urban distribution feeders. Rural feeders were also found to be more prone to intolerable undervoltage violations in this work. More specifically, voltage levels below 200V were noted even from 15% HP penetration or fewer than 15 buildings, while the related values of urban feeders were approximately 30% HP penetration and 25 buildings. Similar results were also observed for the PV generation.

Finally, the significance of Belgian building specifications on the PV-HP grid impact has been quantified in [53], finding strong correlations of voltage profiles, transformer peak loads, and distribution losses with characteristics such as total volume, heat load, electricity demand, conductivity factors, etc. Overall, the key insights for this LCT combination can be summarized as follows:

- PVs and HPs: similar impact on voltage deviations and unbalance.
- PVs are more correlated with overvoltage and reverse power flows (RPFs), while HPs are correlated with undervoltage and overloading.
- Rural grids: most vulnerable for combined integration.
- High influence of weather conditions (e.g., ambient temperature) for grid impact.
- ESS, such as BESS and/or thermal energy storage systems (TESS): important for their co-adoption due to low simultaneity factor.

### 2.3.3. Impact of PVs, EVs, and HPs

Load profiles and their strong seasonal dependence have been studied in the yearly assessment of [54], but on a German HH level. When HPs were introduced in the place of gas boilers, the household's electric consumption and peak demand were increased by 3.6 and 4.2 times, respectively, while the introduction of EVs had the greatest impact on peak demand (4.7 times higher power peak and 13 times more peak hours). While PV generation succeeded in decreasing total consumption by

85%, it had a minimum impact on decreasing power peaks. On the contrary, the authors in the data-driven approach of [55] focused their research on analyzing load profiles of EVs, PVs, and HPs for different urban scales (neighborhoods until municipalities), aiming to understand the spatial effect on different profile characteristics. According to their results, all urban areas could be clustered into "residential", "business", and "mixed" regarding their load profile behavior under LCT integration.

Additionally, the authors have realized a system-wide analysis in [56], which analyzed Winter and Summer load flows and voltage profiles for the MV Irish distribution network comprising 20 different network areas. The main goal of this work has been the discussion of various scenario modeling techniques and the identification of the effect that the changing landscape of the Irish distribution had on constraint identification and load flow analysis. Moreover, energy losses, together with power factors (PF) behavior, voltage fluctuations, and unbalance, were the main grid impact metrics in [57], where PV generation, EV consumption, and HP consumption have been sequentially added to the base load demand. It was generally found that separate integration could be, in principle, tolerated; however, unbalance could notably deteriorate with EV integration, while PV integration caused mainly a decrease in PFs.

Component overloading was added in the probabilistic approach in [58], which was conducted in 128 real-world LV distribution feeders (DFs). In this study, PVs were linked highly with voltage violations (64% of the DFs) while HP consumption was linked with overloading incidents (57% of the DFs). However, the number of customers in the DFs also played an important role since DFs with fewer than 25 customers did not encounter any violations. Lines overloading was also studied in [59], intending to estimate the lifetime of main and distribution cables used in distribution grids under combined and individual LCT penetrations. Individually, HPs did not seem to have such a high impact on cables' end-of-life (EoL), such as EVs. However, they could reduce cable EoL up to 30% by 2028 when they were studied in combination. Another important contribution of this work was the utilization of detailed cable models that could incorporate temperature dependencies, which were necessary to assess the thermal loading impact on cables' EoL. The same metrics were utilized in the study of [60] in three future penetration case studies for a DG in Brescia, where home and public chargers were considered. In this study, MV/LV transformer overloading was mostly correlated with EV consumption due to the high-rated charging power of the EV chargers. However, PVs were found to be the most responsible for grid reinforcement, especially at high-level PV penetration.

Furthermore, a spatial analysis of available grid capacity and expected costs was performed in [6], which, however, was focused on the high deployment of PVs, EVs, and HPs in a Swiss DG comprising thousands of HHs. Whereas the results were highly dependent on the penetration scenarios, rural grids generally needed the highest reinforcements due to weaker infrastructure. In addition, the most spread cost values were noted for the HP penetration scenarios, while massive deployment scenarios were found to be more cost-effective than scenarios of current deployment (20-30%). In [61], the authors investigated two different Dutch DGs (1 older and 1

newer), analyzing components' overloading and voltage violations. According to their findings, older DGs are insufficient for future LCT penetrations; however, the newer ones are relatively robust. Transformer overloading was found to be a more critical issue than line overloading, which was more critical than voltage deviations.

Moreover, component overloading and voltage deviations were also utilized as grid impact metrics in [12], while unbalance was also incorporated in [62]. However, in both studies, only the individual LCT impact was analyzed. In [62], EV consumption was mostly correlated with component overloading and undervoltage, while PV generation and HP consumption provoked mainly overvoltage incidents and power quality issues such as harmonics and frequency fluctuations. In [12], a probabilistic framework was developed to investigate 25 different UK LV networks with 128 LV DFs in total. It was found that the longest DFs, which served the most customers, were affected the most. While voltage violations began from 30% PV penetration, EVs and HPs were highly connected with transformer and feeder overloading. In general, the smaller DFs were not notably affected under any scenario. In addition, in [63], the authors took a step further to perform a large-scale simulation investigating thousands of grids and not only analyzed component overloading and voltage deviations but also calculated the costs for the needed grid reinforcement. This study highlighted the importance of the right coincidence factor selection according to different grid case studies.

Additionally, in the yearly assessment of [64], the authors analyzed, apart from load profiles and carbon emissions, the various inter-effects between the operations of different LCTs in scenarios comprising PVs, HPs, EVS, and CHPs for a Swedish county. They found that PV rooftops could reduce the imported power in the investigated area; however, together with HP consumption, they reduced the operation of CHPs. EV and HP consumption also increased significantly the consumption of the region, even from low penetrations (30% HP penetration). Individual LCT scenarios for different penetrations have been applied in analyzing power profiles, overloading, and voltage deviations of [65] for suburban and urban grids in Munich. EVs and HPs were found to produce power peaks of similar magnitude. The share of the grid load remained similar in all scenarios regarding the urban area, which was also significantly lower than the suburban grid load. Considering the different scenarios, the suburban grid load encountered large changes even from low penetrations. While the grids were found to be generally robust for hosting future LCT penetrations, a double energy consumption and a slight line overloading were observed for the suburban area in extreme scenarios.

All of the above studies remained on a grid impact analysis level; however, there are also numerous studies that investigated mitigation solutions. Load profiles and their seasonal dependence were analyzed in [66] in different grid case studies (rural, suburban, urban). The highest consumption was noted during Winter and, especially, in December, while the evening power peaks during weekdays were shifted closer to 12:00 during weekends. The impact of different tariff utilization was also proven, showing that, in contrast with the flat tariffs, peak demands were mostly observed during the morning for the customers with a multi-rate tariff. Moreover, apart from the load profile analysis and the resulting costs, authors in [67] applied

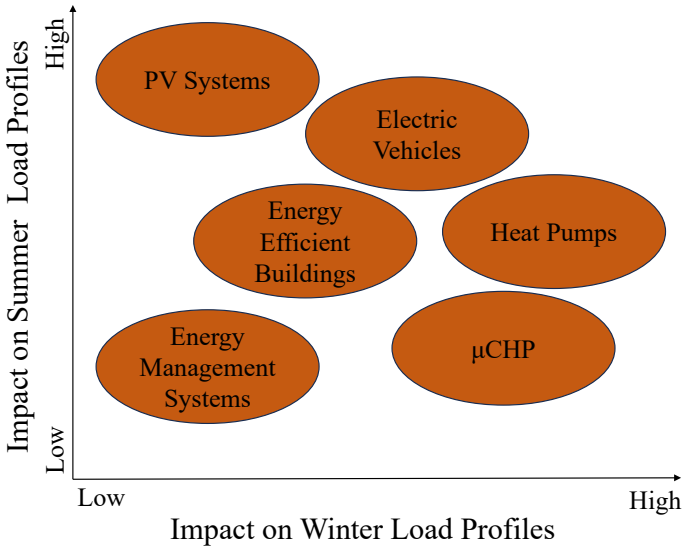


Figure 2.3: Comparison of the impact on load profiles of different LCTs and mitigation solutions. Adapted by [3].

different coordinated strategies to reduce power peaks and cost operations such as different tariffs, use of solar and/or battery optimization, and full coordinated control. The investigation was conducted in 5 different HHs for 3 EV-PV-HP penetrations. According to the authors in [3], without a coordination technique, Summer load profiles were more affected by the simultaneity factor between EV consumption and PV generation. On the contrary, Winter load profiles mainly depended on the penetration level of the HPs in the DG. Their comparison about the impact of the different LCTs and mitigation solutions on Winter and Summer load profiles is depicted in Figure 2.3.

A clustering method has been applied in [68] to link grid impact issues and potential mitigation solutions with grid case study characteristics. Their results showed that residential transformer loading was heavily dependent on EV charging, for which the use of energy storage has been found to be the most effective strategy. In contrast, using PV generation was more effective in mitigating violations in commercial and industrial transformers. Another data-driven approach in [69] analyzed temporal voltage violations of different LCTs throughout the day. PVs had the highest impact, which occurred during the morning. However, EVs and HPs combined provoked violations of similar magnitude during the evening. Consequently, taking into account various sensitivity factors by historical data analysis, the authors proposed different mitigation solutions such as the use of the flexibility of DERs, the use of transformers with tap changers, etc.

Energy losses were added to the load profile analysis as a metric in the nationalized Swiss study in [1]. In this study, the effects of different parameters

of the operations of LCTs on different grid impact issues were analyzed. Some examples were that the flow temperature of the HPs could play a major role in total national energy savings and power peaks, while PV production was highly responsible for incidents of power surplus or deficit. A probabilistic framework was also developed with Monte-Carlo Simulation (MCS) in [70] to analyze the impact of these LCTs and micro-CHPs on cable investments, studying power peaks and component overloading. Different individual and combined mitigation strategies were introduced, from which the highest investment reduction (54%) was noted with a combination of DSM and smart charging.

Furthermore, the LCT hosting capacity (the maximum allowed LCT penetration) of different DGs has also been assessed in [71] under combined PV-HP-EV penetrations by analysis of thermal and voltage violations. With the presence of PVs, the investigated DGs could generally accommodate 24.2% HP penetration without any violations. A maximum of 30% EV penetration could also be achieved if no SC were implemented. However, with the employment of SC techniques, the EV penetration that could be assessed was greatly increased (more than double in some grids). Different types of grids were utilized in [72] to show the impact of full grid electrification and the importance of BESS for its mitigation and maximum PV self-consumption. While no voltage violations were found in rural or suburban grids, much PV curtailment was realized (reaching up to 54% of the total generation) at noon to avoid lines and transformer overloading. With the use of BESS and EV-HP coordinated control, self-sufficiency and self-consumption were greatly increased, reaching, in some examples, 72% and 40% from 34% and 19%, respectively. The use of PV-BESS for impact mitigation was also considered in the developed stochastic bottom-up framework in [73], which analyzed load profiles of future grid conditions due to different LCT integration (PVs, EVs, HPs, CHPs). The peak load for a German neighborhood comprising 1550 HHs was increased by 1.3MW, which was mainly caused by HP integration and was further increased by a factor of 1.8 when the buildings were not well insulated.

Different cable capacities along with individual PV-HP-EV penetrations were considered in [74] for calculating the non-supplied amount of energy and needed grid investments for a typical German urban LV grid. According to the results, a 120kW capacity cable was needed to facilitate all delivered energy to the prosumers without LCT penetration. While a 200kW cable capacity was sufficient for power and energy delivery when the prosumers were equipped with PVs and HPs, there was still an amount of 0.16MWh of unsupplied energy when they were equipped with EVs. Finally, a combined technical, environmental, and economic network impact analysis can be found in [75], which studied carbon emissions, consumption, and peak demands as well as costs for different penetration scenarios of EVs, HPs, and ESS combined with PVs. While the impact of EVs and HPs on the load profiles was found to be of a similar magnitude, HPs contributed to a higher emissions reduction than EVs. However, in contrast with EVs, they also greatly increased the multi-energy system's cost, reaching a value of 60% when they replaced the CHPs in the buildings of the DGs.

## 2.4. Analysis and Discussion of Grid Impact of LCTs

### 2.4.1. Introduction

Table 2.1 summarizes all the works regarding the grid impact of the combined integration of PVs, EVs, and HPs with the related investigated features: areas, sectors, issues, penetrations, approaches followed, seasons, uncertainty management methods, solutions, and mitigation. According to each feature, the explanation of the abbreviations is as follows:

- Areas: Hypoth. for hypothetical, Synthet. for synthetic, LV for low-voltage, MV for medium-voltage, DG for distribution grids, HH for households, and ES for energy systems.
- Sector: Res for residential, Com for commercial, Ind for industrial, Rur for rural, Sub for suburban, Urb for Urban, and Unspec. for unspecified.
- Metrics: LP for load profiles, V for voltage, TF for transformer, C for cable, TFC for transformer and cable, OL for overloading, H for harmonics, Host for LCT hosting capacity, and U for unbalance.
- Penetrations: C for combined, I for individual.
- Approach: B-U for bottom-up, S.B-U for stochastic bottom-up, T-D for top-down, and R-B for rule-based.
- Time: Wint. for Winter, Sum. for Summer, Apr. for April, Aut. for Autumn, and Spr. for Spring.
- Uncertainties: SBA for scenario-based approach, SLP for synthetic load profiles, MCS for Monte Carlo simulation, PDF for probability density function, Stoch. Prof. for stochastic profiles, S.A. for sensitivity analysis, Cluster. for clustering, RS for random sampling.
- Solutions: DSM for demand side management, LS for load shedding, ESS for energy storage systems, Cap. for capacity (of lines/transformers), BES for battery energy storage, Insul for insulation, SC for smart-charging, DER for distributed energy resources, TCTFs for tap-change transformers, Ctrl for control.
- Mitigation: PS for peak shaving, DS for demand shaving, Decr for Decrease, Incr for Increase, Curtail for Curtailment.

Concerning the different approaches that can be followed for the generation of the LCT profiles in grid impact assessment studies, the two main categories are the bottom-up (B-U) and top-down (T-D) approaches. B-U approaches usually generate the LCT profiles by modeling the LCTs and their physical operation and then scaling them up to the size level of the study. Their main advantages are the interpretation of the physical laws, expandability, modifiability, and low need for input data. However, their outcome depends highly on the case study characteristics

Table 2.1: Summary of Research Papers on Combined Grid Impact of PVs, EVs, and HPs

| Ref | Area(s) | Sector | Metrics | Penetrations | Approach | Time | Uncertainties | Solutions | Mitigation |
|---|---|---|---|---|---|---|---|---|---|
| [1] | Swiss Grid | Res-Com-Ind | LP | Multiple C | Data-driven | Yearly | Regression | DSM, LS, ESS | PS-DS |
| [3] | Hypoth. DG | Res | LP, V | Multiple C&I | B-U&T-D | Wint.-Sum. | SBA, SLPs | TF Cap. Incr | PS |
| [6] | Swiss DG | Res-Com Rur-Sub-Urb | LP, TF OL C OL | Multiple C&I | B-U | Unspec. | MCS Regression | BES | Load Reduction |
| [12] | 25 UK DGs | Res | LP, V TFC OL | Multiple I | B-U Meters | Sum. PVs Wint. EVs | MCS | No | No |
| [73] | German DG | Res | LP | Multiple C | S.B-U | Yearly | No | BES, TES, Insul | PS-DS |
| [54] | German HH | Res | LP | Fixed I | S.B-U | Yearly | PDFs | No | DS with PV |
| [60] | Brescia MVDG | Unspec. | LP, TF OL | Fixed C&I | T-D Meters | Apr. Workday & Sunday | No | No | No |
| [70] | Dutch DG | Res | TFC OL | Multiple C | T-D | Yearly | MCS | DSM, SC, ES | PS |
| [61] | Dutch DGs Old & New | Res. | TFC OL V, H | Fixed C | T-D | Yearly | No | SC, PV Cap. HP power | OL&H Decr by PV-HP |
| [57] | Adapt DG | Res | V,U,PF,L | Fixed C&I | B-U | Daily Avg. | Stoch. Prof. | No | U Decr by PV |
| [56] | Irish MVDG | Rur-Urb | V, TFC OL | Multiple C | Meters | Wint.-Sum. | SBA | No | No |
| [71] | 5 UK DGs | Res. | V, Host TFC OL | Multiple C | B-U Meters | Wint. | No | SC | Host Incr by SC |
| [66] | UK DG | Res-Com-Ind Rur-Urb-Sub | LP | Multiple I | Meters | Yearly | No | Smart Tariffs | PS |
| [63] | 7114 Aust DGs | Rur-Sub | V, TFC OL | Fixed C | T-D | Unspec | MCS | Reinforcement | No |
| [65] | 5 Synthet DGs | Res Sub-Urb | LP | Multiple C | B-U | Yearly | No | No | No |
| [22] | 6 Dutch DGs | Rur-Sub-Urb | V, TFC OL | Multiple C&I | B-U&T-D | Wint.-Sum. | MCS, RS | No | OL,UV Decr: PV-EV |
| [59] | 2 Feeders | Res | Lifetime | Multiple C&I | B-U&T-D | Unspec | S.A | No | No |
| [58] | 25 DGs Comp-based | Res | V, TFC OL L, U | Multiple I | B-U & Meters | PV Sum. HP/EV Wint. | MCS, RS & S.A | No | No |
| [74] | Typical DG | Urb | Energy Loss | Fixed C | R-B&B-U | Wint. | No | Higher C Rating | Loss Reduction |
| [69] | 6 Euro DGs | Urb, semi-Urb | V, U | Fixed C | Data-driven | Unspec | Regression | DER Ctrl, TCTFs | OV-UV Reduction |
| [75] | Synthet MG Manchster Univ. | Res | LP, Host V, TFC OL | Multiple C&I | B-U & Meters | Unspec | No | No | ESSs |
| [67] | 5 UK HHs | Res | LP | Fixed C | Real LCTs | Yearly | No | Ctrl Strategies | Demand,Cost Decr |
| [68] | Swiss ES | Unspec | LP | Multiple I | S.B-U & Meters | Yearly | Stat. Analysis & S.A | Ctrl Strategy | Demand Decr: HPs Mismatch Decr: EVs |
| [64] | Real-DG TFs | Res | TF LP | Multiple C&I | Data-driven | Yearly | SBA&Cluster. | ESSs | PS by ESS & PV |
| [72] | 5 Synthet DGs | Rur-Sub | V, TFC OL Curtail | Fixed C | B-U | Sum., Wint. Aut., Spr. | No | BES Ctrl Strategy | PV Host Incr: BES Curtail Decr: Ctrl |
| [55] | 15k Dutch DGs | Various Levels | LP | Fixed C | Data-driven | Unspec | Cluster. | No | No |

and conditions, while uncertainty management must be added by other means, such as stochastic profile generation using probability distribution functions (PDFs) (S.B-U). On the contrary, T-D approaches usually handle generalized national-level data and scale it down to the size level of the study. Their main advantage is the lower dependence on the case conditions and uncertainties because the data has already been processed using data analysis methods; however, they often need accessibility to large-scale data for the generation of the profiles. Using real measurements by installed meters at HHs is a subcategory of the B-U approaches since they use the profiles of a low number of LCTs and scale them up to the needed study level. However, they don't use LCT models and have been accounted for as a separate category [73].

Solutions and mitigation have been distinguished because solutions mean the authors used extra means to reduce the grid impact, such as ESS, DSM, etc. On the contrary, mitigation can also occur by inverse operations of different LCTs (e.g., PVs and EVs) without the use of any extra solutions.

### 2.4.2. General Key Insights

The most important general key insights from Table 2.1 are summarized below:

- 80% of the works used real-world grid case studies.
- 57% focused only on the residential sector.
- 60% utilized multiple LCT penetrations to identify the grid impact. However, only very few works used both combined and individual penetrations to identify the overall inflicted impact and compare the contribution of each LCT.
- The approaches used can be mainly categorized as B-U, T-D, and measurements from real meters, while some works incorporated a combination of them, e.g., for the different LCTs.
- 68% followed a yearly assessment or used the extreme seasons, Summer and Winter. Since Summer is a more hazardous season for PV generation and Winter is more hazardous for EV and HP consumption, they are combined in one case study in some works.
- Mitigation effects such as peak shaving and loading/loss reduction have been observed by combined LCTs integration or using mitigation solutions such as DSM, use of BESS, control strategies, etc.
- Some works have incorporated uncertainty management techniques such as MCS, regression, clustering, etc, but without addressing all uncertainties that were present in the investigations.

### 2.4.3. Grid Impact Analysis

#### Correlation of LCT Combinations with Grid Impact Metrics

In Figure 2.4, the percentage of PV-HP, EV-HP, PV-EV, and PV-EV-HP works related to different grid impact metric investigations is depicted. Most works have used as metrics the grid supply and demand power profiles for all combinations, observing energy consumption and power peaks (more than 80% of the PV-EV works), and they haven't proceeded in investigating directly the impact on the power grid. Voltage and overloading of transformer (T/F) and distribution lines represent the next most investigated impact metric, reaching 60%, 50%, and 40% for HP-EV works, respectively. On the contrary, unbalance and losses have been studied much less until now, while analysis of harmonics, power factors, lifetime, and LCT hosting capacities is still missing from the literature for most of the LCT combinations.

#### Assessment of Grid Impact issues by LCT Combinations

Focusing on the four most important grid impact issues: voltage deviations, T/F and cable overloading, and unbalance, Figure 2.5 summarizes a qualitative comparison of the works from the different LCT combinations. The results of the works are categorized as low, medium, and high, mainly using the magnitude of violation as a metric: $< 10\%$, $< 50\%$, and $> 50\%$, respectively. However, it must be noted that each work uses its own metric of violation, and thus, it was necessary to use our own metric to categorize the works as low-, medium-, and high-impact. The two main methods used in the literature are either the magnitude of violation on a specific component (e.g., % overloading of a T/F) or the percentage of violated components in the distribution network (e.g., % overloaded distribution lines or components). Additionally, some works utilize a combination of the above two methods to conclude about the level of grid impact of the investigated LCT or LCT combination. Finally, the remarks and conclusions of each work about the level of the impact on the investigated grid and its conditions have also been taken into account for the qualitative comparison of Figure 2.5.

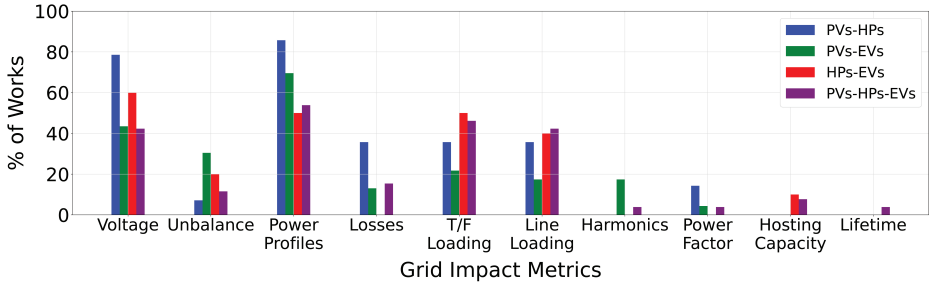


Figure 2.4: Percentage of PV-HP, PV-EV, HP-EV works related to grid impact metric investigation.

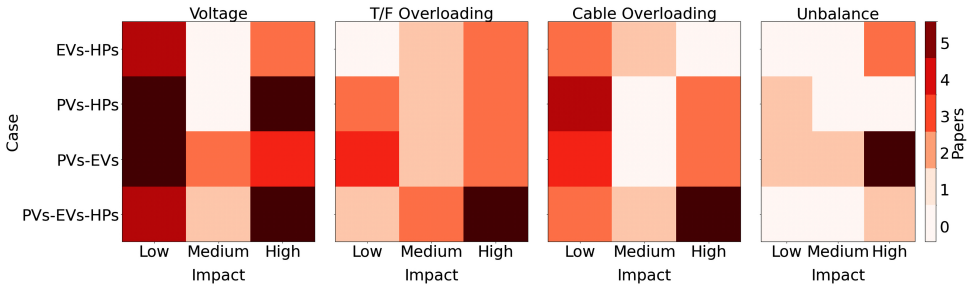


Figure 2.5: Summary of impact assessment for all LCT combinations concerning Voltage, T/F & Cable Overloading and Unbalance.

Moreover, Figure 2.5 depicts the number of works investigating each grid issue to show the comparison's trustworthiness level. As can be observed, most works that integrated all PVs, EVs, and HPs found a high impact level for voltage and overloading. However, impact mitigation was observed for PV-HP and PV-EV combinations, especially for the voltage deviations. For example, the coincidence of EV charging or HP heating/cooling with PV generation reduced the grid impact of both LCTs. These observations were more seen for the PV-EV combination because of the higher simultaneous operation, e.g. HP heating occurs more in the evening when there is no PV generation. On the contrary, the PV-EV combination showed a higher impact regarding phase unbalance than the PV-HP because of the simultaneous power injections and withdrawals from different phases, which can occur more frequently for PVs and EVs. Additionally, EV-HP and PV-EV-HP combinations were both found to inflict a high unbalance impact. However, it must be noted that only a few works have studied phase unbalance and incorporated all 3 LCTs in the analysis.

Finally, in several cases, it has been observed that the majority of the works are concentrated in the low or high-impact levels. On the one hand, this can be justified by the fact that grid impact assessment works usually use either one fixed moderate LCT penetration level to study the current or near future situation, or multiple penetrations, focusing on the 100% penetration level to study the totally sustainable future. Consequently, results are more likely to fall into the low or high-impact categories, respectively. On the other hand, this observation is mostly made for the PV-integrated case studies and for the voltage and cable overloading grid issues. Voltage and cable overloading represent local grid issues, for which most of the studies utilize as a metric the maximum violation (lowest/highest voltage or highest cable overloading) that occurred in the investigated network. As already explained, simultaneous PV generation with consumption of EVs, HPs, or EVs-HPs has resulted in several studies on mitigation phenomena that have the highest influence on local grid components, such as nodes and distribution lines. However, the success of these mitigation events also depends on the conditions of each study, such as the LCT modeling, the considered simultaneity factors, the setup of scenarios, etc., and are not always present in the studies.

### Grid Type and LCT Comparison for different Grid Issues

Figures 2.6 and 2.7 depict quantitative comparisons between the different grid types (rural, suburban, and urban) and LCTs concerning voltage, cable, and T/F overloading, and unbalance, respectively. Regarding the grid comparison, the rural grids suffered the most from voltage deviations in most works. This is justified by the fact that the rural grids have, in general, longer line lengths (and hence, higher line impedances) than the urban and suburban grids, and the loads cause higher voltage drops. Rural grids were also found to be the most vulnerable to phase unbalance compared to the two other types of grids. This is also due to the higher voltage deviations, which jeopardize further voltage and current unbalance. On the contrary, suburban grids were found to be more vulnerable to cable and T/F overloading because of the higher population that usually lives in the city suburbs. Additionally, for the above reason, the work in [22] represents an exception where the suburban grids were found to be the most vulnerable regarding all 3 grid issues since the Dutch suburbs are usually extremely populated areas.

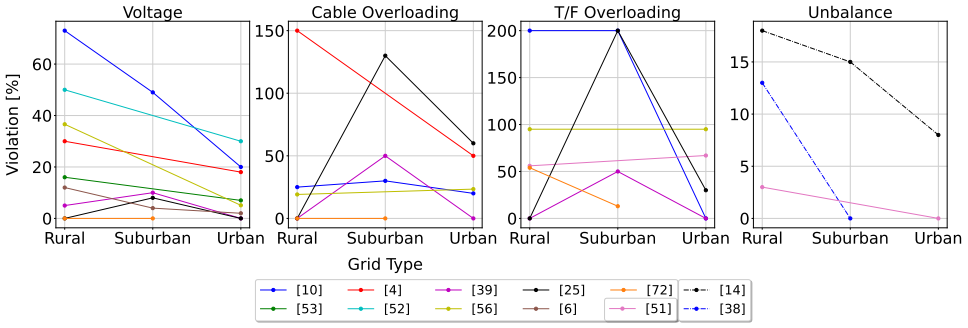


Figure 2.6: Summary of impact assessment for rural, suburban, and urban grids concerning Voltage, T/F & Cable Overloading, and Unbalance.

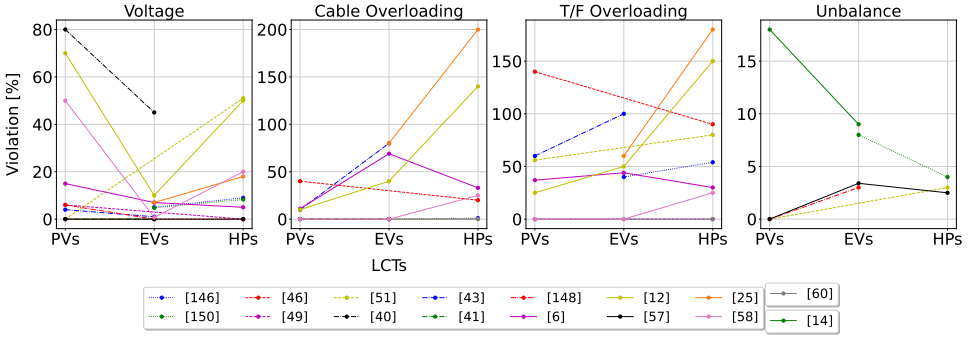


Figure 2.7: Summary of impact assessment for PVs, EVs, and HPs concerning Voltage, T/F & Cable Overloading, and Unbalance.

Considering the LCT comparison in Figure 2.7, PVs were mostly correlated with voltage deviations and less with cable and T/F overloading. This can be justified because all grids usually have an existing loading, which cancels out a fragment of the PV production. On the contrary, EVs and HPs were mostly associated with cable and T/F overloading. In most studies, HPs caused higher overloading and voltage issues than EVs due to the higher number of HPs than EV chargers under the same penetrations. This is because the correlation of HPs (and PVs) with the penetration is straightforward. A penetration level of 100% means that all buildings are equipped with an HP or a PV. However, the method by which the number of EVs or EV chargers per penetration level is calculated in each study varies and depends on the assumptions of the authors and the conditions of the study, e.g., statistics for each investigated country. For example, some works assume that every building is equipped with an EV charger at 100% penetration levels. However, other works define the 100% penetration as the number of passenger cars that are replaced by EVs. If, according to the country's statistical data, there is an average number of passenger cars per number of people, which can be, e.g., different for rural and urban regions, then the total number of EVs is calculated in that way and distributed to the grid home or public chargers. As a consequence, the number of EVs that are added at each penetration level at each study is always lower than or equal to the number of HPs and/or PVs.

Moreover, HP operation is more frequent since the buildings need to be heated and cooled regularly during Winter and Summer, respectively, while EVs are usually charged around 3 times per week due to their large range. However, there are some studies that contradict these findings. For example, in [51], HPs caused up to 50% voltage violations compared to 0% violation by PVs. This was justified because the study was conducted on a radial Belgian rural DF where significant undervoltage events occurred, especially at the end of the DF, during the cold Winter days when HP consumption was at its highest. Moreover, PVs and EVs were found to be more hazardous than HPs for overloading in [46] and [6], respectively. For the study in [46], this was possibly due to the use of large-scale PV systems in the PV integration case, which caused high-level PV power flows in the LV network. Regarding the work in [6], the study was focused on a Swiss DG of 170000 HHs that comprises both residential and public zones. In the extreme scenarios, HPs were assumed to equip 100% of only the residential buildings, while, on the contrary, all passenger cars were replaced with EVs being charged in residential and public chargers.

Concerning phase unbalance, there are contradictions about which LCT is the most hazardous for grid unbalance. Most works agreed that EVs could highly jeopardize grid unbalance if they are charged by one phase, since they are charged with higher power ratings. This is true for EVs with charging ratings up to 7.4kW, which are charged single-phase and withdraw up to 32A. However, the authors in [14] found an 80% higher violation of phase unbalance by PV phase injections than by EV withdrawals. Nevertheless, such comparisons between LCTs and grid case studies regarding grid unbalance have been performed in only a few works, and more investigation should be conducted to strengthen these insights.

It must be noted that these contradictions have been expected because these

comparisons are highly grid case-dependent, and it is difficult to extract a conclusion that can be generalized across all the grid impact assessment works. Moreover, as explained, every work has its own metric of violation (% magnitude of T/F overloading or % overloaded T/F in the DG). This is why there is a significant difference between different works for the same grid impact metric. While this is less significant for the qualitative analysis of Figure 2.5, where the conclusions can also be used for the categorization, high precision gains more importance in quantitative comparisons. Hence, it is recommended that the results shown in Figures 2.6 and 2.7 should not provide insights by comparisons between different works, but only by comparisons between different grids and LCTs within the same work, where the setup and input parameters are the same.

#### Mitigation Strategies to Grid Impact Issues

The correlation of different mitigation strategies with various investigated grid impact issues is summarized in Table 2.2, where ESS, DSM, LS, EV SC, OLTC, APF, SOP, and O/L denote energy storage systems, demand-side management, load shedding, EV smart-charging, on-load tap charging, active power filters, soft-open points, and overloading, respectively. ESS, DSM, and LS are mostly used for peak and excessive consumption reduction and mitigation of overloading and voltage violations. Varying the LCT power levels, such as with EV SC or variable-speed HP operation, can also assist with the aforementioned issues and unbalance, but not with consumption reduction. On the contrary, consumption reduction can be better achieved with higher building insulation, lower HP flow temperature, and increased LCT efficiencies. OLTC transformers have been used to mitigate voltage violations, while active power filters can assist with overloading and harmonics presence. Finally, SOP power electronic devices are often utilized for undervoltage-overvoltage, unbalance, and thermal overloading mitigation.

### 2.4.4. Limitations of Grid Impact Analysis

Overall, the grid integration of PVs, EVs, and HPs has been extensively studied in the literature. The positive and negative impacts of all LCTs and LCT combinations investigated in this chapter are summarized in Table 2.3. The right side of Table 2.3 (green color) belongs to the positive impacts, while the left side (red color) belongs to the negative ones. It must be noted that the positive and negative impacts of PV-EV-HP grid integration are omitted because they are a combination of the positive and negative impacts of the partial combinations (PVs-EVs, PVs-HPs, PVs-EVs-HPs), respectively. However, there are still certain aspects regarding LCT grid integration that need to be further investigated.

As already seen in the previous section, while many of the findings of the existing grid impact assessment studies are in agreement and can be generalized, others are contradictory because they depend heavily on the conditions considered in each study. One such aspect is the comparison of the different types of DGs (e.g., rural, suburban, urban, etc.) concerning the grid integration of PVs, EVs, and HPs and various grid issues. Observing Table 2.1, only the works in [6, 22, 56,

Table 2.2: Correlation of Mitigation Strategies with Grid Impact Issues.

| Mitigation Strategies | Power Peaks | Excessive Cons/tion | Voltage Issues | Thermal O/L | Harmonics | Unbalance | Losses - Efficiency | Fault Limit |
|---|---|---|---|---|---|---|---|---|
| ESS | ✓ | ✓ | ✓ | ✓ | | | | |
| DSM | ✓ | ✓ | ✓ | ✓ | | | ✓ | |
| LS | ✓ | ✓ | ✓ | ✓ | | ✓ | | |
| EV SC | ✓ | | ✓ | ✓ | | ✓ | | |
| smart-tariffs | ✓ | | ✓ | ✓ | | | | |
| LCT var. power | ✓ | | ✓ | ✓ | ✓ | ✓ | | |
| TF Cap. Increase | ✓ | | | ✓ | | | | |
| OLTC | | | ✓ | | | | | |
| LCT efficiency | | ✓ | | | | | ✓ | |
| HP flow Temp. | | ✓ | | | | | | |
| Building Insulation | | ✓ | | | | | ✓ | |
| Cable Rating increase | | | | ✓ | | | ✓ | |
| APF | | | | ✓ | ✓ | | | |
| SOP | | | ✓ | ✓ | | ✓ | | ✓ |
| Reinforcement | ✓ | ✓ | ✓ | ✓ | ✓ | ✓ | ✓ | ✓ |

63, 66, 69] have conducted such a comparative analysis utilizing real-world DGs. Moreover, most studies utilize only one DG for their investigation, except for [22, 63, 69]. However, the grid impact analysis in multiple DGs is important for the generalization of the findings. Finally, the analysis of the seasonal effect on the different LCT integrations in different grid types has only been accounted for in [22]. The profiles of different LCTs highly differ during different seasons, greatly affecting both their individual grid integration and their interaction during combined integration [56, 72]. The knowledge about the vulnerability of each DG type to the integration of each LCT/ LCT combination, considering the weather and seasonal dependency, is critical for the analysis regarding the available LCT hosting capacity and needed reinforcement for the successful deployment of the various LCTs.

Furthermore, while the grid impact of PV-EV integration and the benefits from their co-adoption have been extensively studied, a smaller number of works were found for the other combinations, and most of them remained on load profile analysis, overloading, and voltage deviations. There is no grid impact study that assessed phase unbalance in the PV-HP category, while only 3 unbalance assessment works were found in the PV-EV-HP category, which, however, did not thoroughly take into account the interdependencies between the grid specifications, seasonal effects, and various LCTs. Moreover, harmonic distortion has mostly been assessed in the PV-EV integration. However, power quality issues, such as phase unbalance and harmonic distortion, are highly expected in the future DGs with high LCT penetration levels. Additionally, PF and energy losses assessment is still missing

Table 2.3: Positive and Negative Impacts of Grid Integration of various LCTs and LCT Combinations.

| | | POSITIVE IMPACTS | | |
|---|---|---|---|---|
| | | **PVs** | **EVs** | **HPs** |
| **NEGATIVE IMPACTS** | **PVs** | Grid Resilience<br>Self Sufficiency<br>DL Losses decrease<br>Lower Utility Generation<br>Lower Generation Costs<br><br>Overvoltage<br>Unbalance<br>RPFs<br>Voltage Flicker<br>Harmonic Distortion<br>Power losses (shading) | Co-adoption with minimum need of extra solutions (ESS)<br><br>PV self-consumption increase<br><br>RPFs & Energy losses decrease<br><br>Peak Shaving<br>(esp. with SC or DSM)<br><br>Mitigation of:<br>unbalance, overloading<br>& voltage deviations<br><br>Voltage Fluctuations suppresion by varying PV output with V2G<br><br>Frequency regulation & Congestion Management<br><br>LCT hosting capacity increase<br><br>Unbalance control<br>(same LCT phase-connection) | PV self-consumption increase<br><br>RPFs and Energy losses decrease<br><br>Peak Shaving<br>(DSM/TES needed)<br><br>Solar-powered TES<br><br>Mitigation of:<br>unbalance, overloading<br>& voltage deviations<br>with extra solutions<br><br>Frequency regulation & Congestion Management<br><br>LCT hosting capacity increase<br><br>Unbalance control<br>(same LCT phase-connection) |
| | **EVs** | High risk of:<br>overloading,<br>voltage deviations,<br>harmonic distortion,<br>unbalance,<br>PV curtailment<br>(without proper control strategies) | Frequency Regulation<br>Voltage Control<br>PF Improvement<br>Congestion Management<br>Energy Storage (V2G)<br><br>Undervoltage<br>Unbalance<br>Overloading<br>Harmonic Distortion<br>Power Losses | Frequency Regulation<br><br>Unbalance Control with phase-changing chargers<br><br>Use of V2G for heating flexibility<br><br>Congestion Management<br>(use of V2G or TES) |
| | **HPs** | Extra solutions needed<br>(e.g. ESS)<br><br>High risk of:<br>overloading,<br>voltage deviations,<br>harmonic distortion,<br>unbalance,<br>PV curtailment | Most hazardous co-adoption:<br>consumption & peak demand<br>can be increased >100%<br><br>Critical grid issues:<br>voltage deviations,<br>overloading and unbalance<br><br>Necessary extra<br>mitigation solutions<br>(e.g. SC, DSM, ESSs, etc) | Voltage Control<br>Frequency Regulation<br>RES integration<br>Congestion Management<br><br>Undervoltage<br>Unbalance<br>Overloading<br>Power peaks<br>Excess Consumption |

from the literature for the EV-HP integration and can be critical for the combined integration of these technologies when local PV generation is not present to reduce the distribution losses. Furthermore, most studies have assessed grid impact issues; however, only a few of them have taken a step further and found the final grid impact results, calculating the available LCT hosting capacity and needed grid reinvestments, such as [63, 71, 75]. Finally, many studies chose to generate the LCT profiles using a specific approach, e.g., T-D, B-U, real measurements, etc. Only a limited number of them used the advantages of multiple approaches, such as [58, 59, 74]; however, no reviewed work proceeded in comparing the influence of T-D and B-U approaches on the results. All of the above represent important limitations of the existing grid impact assessment literature, on most of which this Ph.D. thesis aims to shed light in Chapters 3 and 4.

### 2.4.5. Conclusions of Impact Analysis & Proposed Solutions

In conclusion, a literature review assessment has been conducted in this chapter regarding the grid impact of PVs, EVs, and HPs in LV DGs. Various investigated issues have been summarized for different LCT combinations, while research characteristics have also been incorporated, such as penetration levels, seasons, grid types, uncertainty management techniques, and followed approaches. The grid impact level of the most investigated grid issues has been analyzed, while different grid types and LCTs have also been compared concerning their violation levels. Finally, mitigation solutions have been summarized and correlated with respective grid issues. Results have shown that mitigation effects can be observed for PV-EV and PV-HP combinations, especially for voltage violations without extra solutions. Moreover, rural grids were found to be more vulnerable to voltage deviations and unbalance, while suburban grids were more associated with T/F and line overloading. While power profiles, voltage deviations, and component overloading have been extensively analyzed, other grid issues, such as unbalance, losses, and harmonics, are still inefficiently investigated. Additionally, comparisons between different grids, seasons, approaches, and LCTs for various grid issues are especially important and recommended for future research so that the grid operators are prepared for the forthcoming risks of energy transition to the distribution grids.

Several solutions have been investigated in the literature regarding grid impact mitigation. This Ph.D. thesis investigates individually and in combination two of the already discussed measures: a) the deployment of PCSs exploiting RES generation (e.g., PVs) and flexible loads, such as HPs and EVs with V2G capabilities [76], and b) the use of ESSs in such PCSs [77], focusing on energy arbitrage and ancillary services provision. The thesis proceeds with a short introduction to these solutions.

## 2.5. Solution 1: Energy Storage Systems (ESS)

### 2.5.1. Categories of ESS

The main ESS categories are categorized below, and their volumetric power and energy density are compared in Figure 2.8 [78], [79], [80], [81].

1. Mechanical Energy Storage, such as Pumped Hydro Energy Storage (PHES), Compressed Air Energy Storage (CAES), and Flywheel Energy Storage (FES): designed for bulk power management, demonstrate the lowest volumetric power and energy density, but are the most mature and durable ESS.

2. Electrical Energy Storage, such as capacitors, supercapacitors, and superconducting magnetic energy storage (SMES): designed for rapid grid power injections, demonstrate high power density but low energy density.

3. Chemical Energy Storage, such as hydrogen and ammonia, combined with fuel cells, achieves the highest energy and power density, but their adoption is limited due to low economic viability and maturity.

4. Thermal Energy Storage, using either the bulk mass of material (sensible heat) or the heat from phase change (latent heat).

5. Electrochemical Energy Storage, such as BES and flow-BES (FBES): occupy a middle ground on the density plot, from which LIBs achieve relatively high energy and power density.

BESS can be deployed from residential to utility-scale, and are highly suitable for energy management and ancillary services, such as voltage support, RES fluctuations mitigation, emergency backup power, peak-shaving, load following, PV integration, EV SC, etc. ([79]). Some of the main reasons are the high scalability due to modularity, fast response times (e.g. of milliseconds for LIBs), high efficiency (up to 97% round-trip), compact size and low maintenance, remote monitoring, and high cycle life (up to 15000 cycles in LIBs) with a reasonable lifetime 10-15 years [82–84].

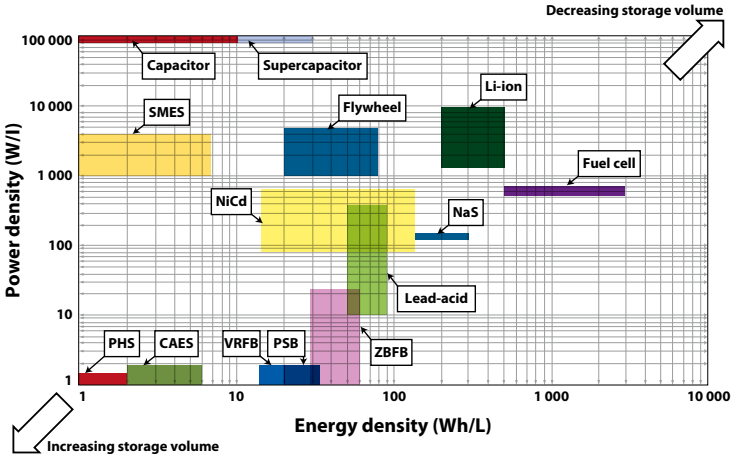


Source: Luo *et al.*, 2015.
Note: SMES = superconducting magnetic energy storage; NiCd = nickel cadmium; NaS = sodium sulphur; PHS = pumped hydro storage; CAES = compressed air energy storage; VRFB = vanadium redox flow battery; PSB= polysulfide bromine flow battery; ZBFB = zinc bromine flow battery.

Figure 2.8: Volumetric power and energy density of different ESS [79].

### 2.5.2. Lithium-ion Batteries (LIB)

LIBs are considered the preferred choice for future automotive and grid applications, outperforming other battery technologies (e.g. lead-acid, Ni-Cd, Ni-MH) 2.5x times regarding energy density and 5x times regarding power density, reaching up to 250Wh/kg and 2000W/kg, respectively, while providing the highest efficiency (up to 98%), and relatively high cycle life (up to 6000 cycles). Their main limitations constitute their limited lifetime (5-15 years) and high cost [80, 85]. The electrochemical operation of a LIB is depicted in Figure 2.9, where the negative electrode consists of graphitic carbon, the positive of a lithium-intercalation compound, and a nonaqueous electrolyte that separates the electrodes and facilitates the transport of lithium ions between them [86].

Lithium-ion batteries have different chemistries for the anode and cathode, which give different technical characteristics to each chemistry. The anode material is usually graphite or lithium titanate oxide (LTO), while cathode materials vary more. The most common cathode materials are metal oxides like lithium manganese oxide (LMO), lithium cobalt oxide (LCO), lithium nickel cobalt aluminium oxide (NCA), lithium nickel manganese cobalt oxide (NMC), and lithium iron phosphate (LFP). The electrolyte between two electrodes is usually a mixture of lithium salts, such as LiPF6, and an organic solvent to allow for ion transfer [87]. The comparison of those different chemistries is depicted in Figure 2.10, where it can be seen that LFP stands out as the most suitable candidate for grid applications, because:

a) Safety: The iron phosphate-based cathode material is more stable compared to the other chemistries [86]; b) Lifetime: LFP has a relatively higher cycle life compared to other LIB chemistries [88] and has the lowest calendar degradation at the same conditions [89]; c) Cost: LFP is less expensive compared to NMC [90]; d) Performance: LFP maintains consistent performance even under varying temperatures and depth of discharge (DOD) [88]; e) Specific Power: LFP has the highest specific power among all LIB chemistries [87].

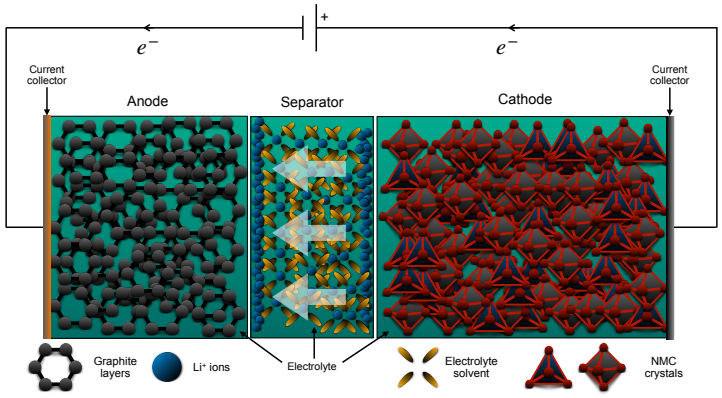


Figure 2.9: Schematic of a generic Li-ion cell during charging.

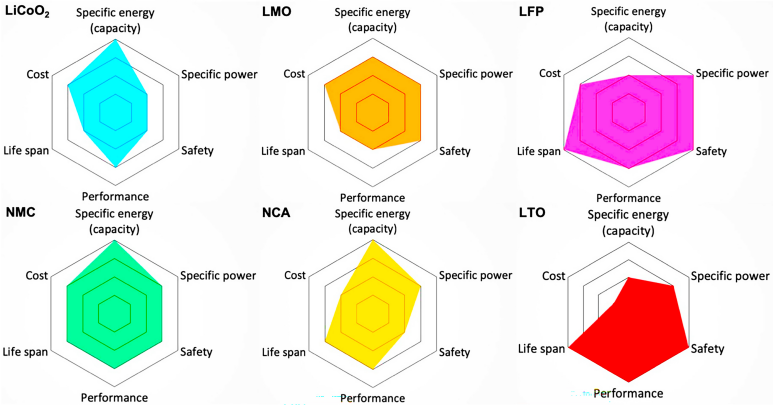


Figure 2.10: Comparison of different types of LIB chemistries [87].

### 2.5.3. LIB Degradation

#### Introduction

Over their lifetime, LIBs lose capacity through two mechanisms: on the one hand, cells undergo calendar aging while being stored as a result of side reactions resulting from the thermodynamic instability of materials; on the other hand, repeatedly charging and discharging the cell induces kinetical effects such as volume variations or concentration gradients in a process known as cyclic aging [91]. Degradation causes and mechanisms of LIBs have been assessed several times in the literature [92, 93]. Each degradation mechanism is associated with one or more of the following degradation causes: time, C-rate, charge throughput, cut-off voltage, temperature, state-of-charge (SOC), and DOD. In turn, each degradation mechanism leads to one or more of the following aging modes: Loss of Lithium Inventory (LLI), Loss of Active Material (LAM), and Conductivity Loss (CL). Cell capacity decreases due to LLI and LAM, while cell power fades as a consequence of LAM and CL [94]. Although all aging modes take place throughout the entire life of LIBs, their event rates differ depending on the stage of their lifespan and the operating and storage conditions the cells are subjected to [93].

From all the complex interplay of different LIB degradation mechanisms, the increased thickening of the solid electrolyte interphase (SEI) formation is generally accepted as the most dominant mechanism, especially during the first cycles [95, 96]. Yet, after prolonged cycling, lithium plating (LP) becomes more relevant based on the large amounts of metallic lithium at the anode surface detected in aged cells [91, 97]. Moreover, other aging mechanisms are the mechanical stress on electrode materials (node structural degradation) [98] and transition metal dissolution (TMD) from the cathode and deposition in the anode [99]. The Ph.D. thesis proceeds with a short introduction to the two main degradation mechanisms (SEI and LP), with their causes and influencing factors; for more information concerning the LIB degradation mechanisms, their causes and interactions, and different modeling techniques, the reader is referred to the related publication [23].

### SEI formation and growth

The SEI is a multi-layered structure that is both ion-conductive and electron-insulating, limiting additional electrolyte reduction at the anode while permitting reversible ion intercalation into it [100]. Due to its porous nature, after the formation cycle, a small amount of electrolyte can still diffuse across the SEI layer and be reduced on the electrode surface, resulting in uninterrupted thickening of the SEI and continuous LLI, consequently causing capacity fade [96, 101]. Figure 2.11 depicts how the SEI is formed by the interaction of lithium ions with electrolyte solvents and electrons when they are transported through the electrolyte and intercalate into graphite during charging.

Causes of thickened SEI formation are: a) high temperatures, which cause the SEI to break down or dissolve, leading to subsequent restructuring of the damaged SEI and dissolution of SEI products [92]; b) high C-rates that cause increased ohmic heating, and raise the temperature, subsequently leading to SEI thickening [102]; c) increased SOCs, which due to the potential imbalance at the anode/electrolyte interface, favor the occurrence of electrolyte reduction reactions [94]; d) higher cut-off voltages, because they lead to easier electrolyte oxidation by the cathode's higher potential forming SEI on the anode [103]; and e) anode volume changes, which hasten the loss of lithium and cause structural disorder sunsequently modifying the electrocatalytic properties and affecting the SEI thickness [104].

### Lithium Plating (LP)

LP is a major source of LLI and LAM on the anode [105]. LP occurs when the current of lithium ions in the electrolyte exceeds the intercalation current or the transport rate inside graphite because of overpotential sources, leading to partial deposition of lithium metal on the anode surface due to the electrode potential drop [106]. Therefore, instead of intercalating into the anode crystal structure, lithium ions are reduced to metallic lithium, which deposits between the active material and the SEI, causing clogging of anode pores and potentially forming dendrites [97]. As shown in Figure 2.12, the lithium ion concentration is larger towards the graphite surface since upon charging and discharging, they gradually intercalate from the core to the interface and deintercalate from the interface to the core, respectively; then, a secondary SEI layer is formed upon cycling around the plated lithium. The deposited metallic lithium and the clogging of pores reduce the anode surface area [107], while the developed dendrites are more prone to lose electrical contact with the anode and form floating fragments in the electrolyte (dead lithium) [108].

Causes of LP are: a) low temperatures, which hinder the lithium ions diffusion into graphite [109], requiring higher activation energy for charge transfer [110], leading to slower kinetics and greater anode polarization; b) high C-rates and c) cut-off voltages, since overcharging induces the accumulation of lithium ions at the anode-electrolyte interface which subsequently results in metallic lithium deposition on the anode surface if the amount of lithium ions transferred from the cathode cannot be accommodated [108].

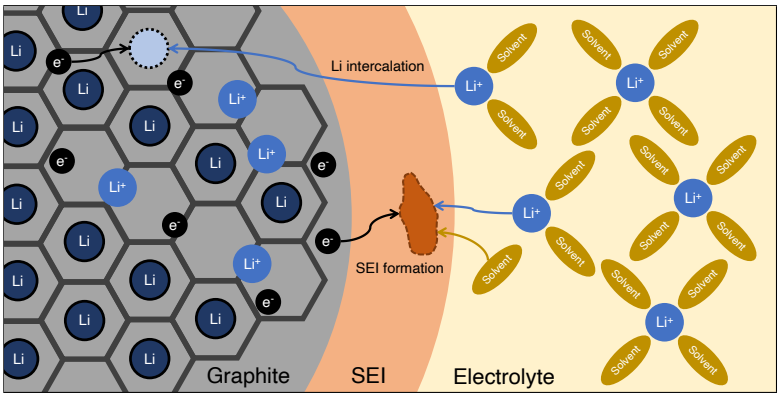


Figure 2.11: SEI Formation by interaction of lithium ($Li^+$) ions with electrolyte solvents and electrons during charging [101].

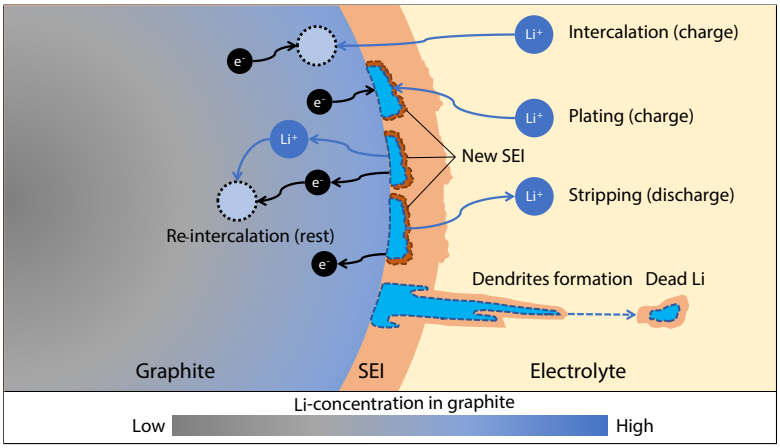


Figure 2.12: Lithium plating mechanism and its long-term consequences (dead lithium (Li) and formation of dendrites). Based on [111], [112], [113].

### Other degradation mechanisms & interaction

While the chapter will not proceed to a detailed explanation of the other degradation mechanisms and their interactions (refer to publication [23]), Figure 2.13 summarizes the main degradation mechanisms that lead to LAM and LLI and their causes, based on the work in [93]. As depicted, most mechanisms lead to LAM, while SEI formation and lithium plating cause both LAM and LLI. Moreover, the C-rate (current load) can be defined as the most hazardous cause, since it influences most of the mechanisms. Cell voltage, which is directly related to the SOC, and temperature follow since they affect both SEI formation and LP; low cell voltage and temperature ranges increase LP, while high ranges accelerate SEI formation and other mechanisms. Finally, time and mechanical stress are also important.

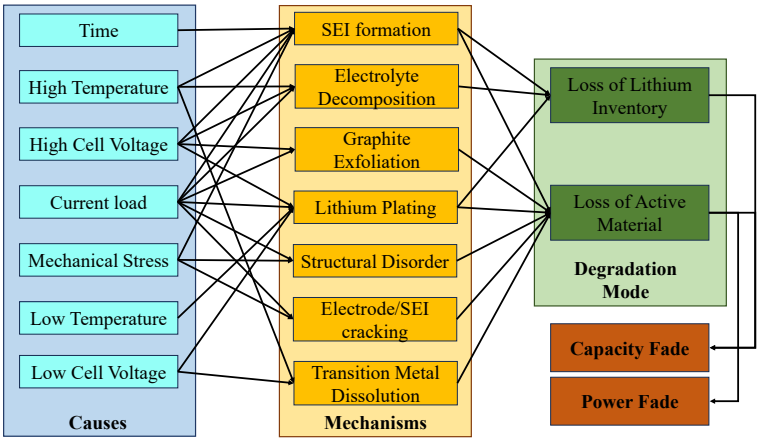


Figure 2.13: Summary of degradation modes, mechanisms, and causes that lead to capacity and power fade of LIBs [93].

## 2.6. Solution 2: Power Control Systems (PCS)

### 2.6.1. Definition

As already explained, PCSs/EMSs can be developed to provide benefits both for the customers and the system operator (SO). From the perspective of the customers, PCSs can provide benefits, such as energy arbitrage, supply-demand mismatch decrease and PV self-consumption increase, avoiding grid violations [15], [16], [114] and respecting the thermal and charging comfort of the consumers [115], [116], [117]. From the perspective of the SO, ancillary services can be provided to the power grid. Such services can be peak shaving [116], congestion management [19], provision of frequency containment reserves (FCR) [20], aFRR [118], etc. All of the above fall under the category of DSM or DR strategies. DR strategies can be distinguished into two main categories: Firstly, implicit DR strategies are based on dynamic energy prices and network tariffs, such as time-of-use (TOU), capacity tariff (CT), critical-peak-price (CPP), RTP, etc. Secondly, explicit DR strategies comprise mechanisms that use demand-side flexibility as a dispatchable resource, such as load reduction, increase, or shedding under incentives or contracts; such DR strategies are also called "Direct Load Control (DLC)" [119]. Finally, several uncertainties are present in power control, which can affect the objectives of the PCSs, such as the intermittent supply of PV power, weather conditions, energy prices, EV driving patterns, etc. [120], [121]. Therefore, PCSs, specialized in dealing with uncertainties, have been developed following stochastic, robust, and model-predictive control (MPC) approaches, such as in [122–124].

The PCS/EMS is fed with all required data, such as weather, grid limit, LCT operational data, etc, and efficiently organizes the energy sharing/trading and power flows across all accessible assets with the commands of the energy management controller (EMC). Measuring voltage, current, and power with the use of smart

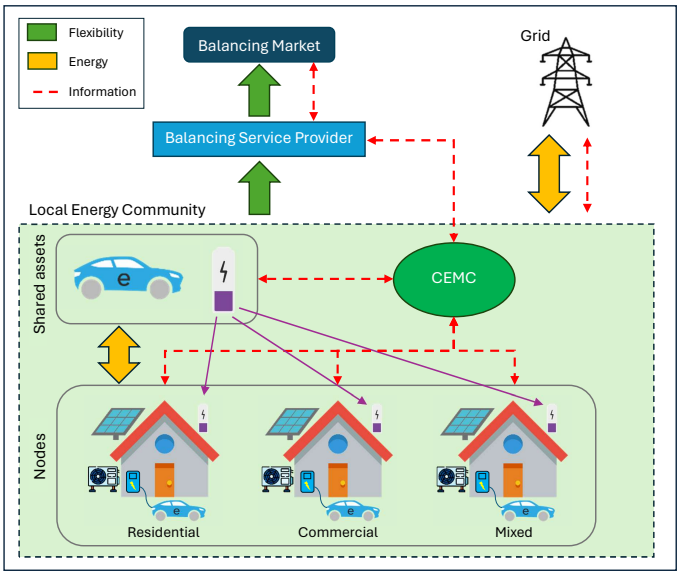


Figure 2.14: A community PCS/EMS participating in energy/flexibility markets.

meters is the key to a well-functioning PCS [125], [126]. The control architecture of a PCS can be centralized, decentralized, or hierarchical. The centralized architecture uses a central controller to manage the energy flows. The central controller collects data from all the nodes connected to the system, and can be an energy utility company or an aggregator. Centralized PCSs have the advantage that they can find global optimal solutions. However, a centralized PCS needs significant computational power to control the system effectively. The decentralized architecture uses distributed processing systems at each node, allowing autonomous control capability and node-to-node communication. The decentralized PCS has good expandability and more flexible operation, and it avoids single-point failure; however, it does not guarantee a global optimum. The hierarchical architecture divides the control into multiple levels, each with a different control objective. The data flows only vertically between the levels, not between the units at the same level [125].

PCSs/EMSs can be designed on a home-level (HEMS) or on a community-grid level. For grid-level PCSs, one of the important stakeholders is the aggregator, especially if ancillary services are provided, e.g., with participation in the balancing market. The aggregator acts as a community EMC (CEMC) and is a legal entity that facilitates the opportunity to harness the flexibility of small assets by pooling them together and giving them access to the ancillary service markets. For the balancing markets, the aggregator takes the role of the balancing service provider (BSP) [125]. Figure 2.14 depicts such a community PCS/EMS that participates in energy and flexibility markets with the use of the CEMC for the communication of all shared assets, such as buildings, EVs, and BESS, which this Ph.D. thesis intends to develop in Chapters 5-7.

### 2.6.2. Ancillary Services by PCSs: aFRR reserves provision

Ancillary services provision is becoming increasingly important due to emerging grid challenges, such as grid congestion, frequency imbalance, etc. This has already been seen in the Netherlands, where some grid areas can no longer accept new connections [127]. Thus, PCSs need to be able to provide ancillary services, such as congestion management and frequency regulation. This section includes a small explanation of the balancing markets, especially of the aFRR market, to provide the necessary theoretical background for Chapters 6 and 7 of the Ph.D. thesis.

#### Market Parties

There are three main types of energy market roles: Balancing Responsible Parties (BRPs), Balancing Service Providers (BSPs), and the Transmission System Operator (TSO) ([128]), which can be briefly explained as follows.

A BRP collects a portfolio of suppliers and users and is financially responsible for any imbalance present in the portfolio. Since every supplier, user, or trader of energy can cause an imbalance on the grid, each party is bound to a BRP. The BRP can keep its portfolio in balance by buying and selling energy from and to other market parties. The BRP communicates these transactions to the local network operator, who, in turn, passes them on to the national TSO. The sum of these transactions is called an energy program, or "E-program", and is a daily process ([129]). The difference between the nomination by Tennet (E-program) and the allocation (measured values by the metering company) is measured in blocks of 15 minutes, which is called an imbalance settlement period (ISP) ([130]).

When there is an imbalance between supply and demand, the TSO calls upon BSPs to help restore the grid balance. The BSP is the entity that offers balancing power in the form of a power bid against a certain price, independent from any portfolio ([131]). In the aFRR market, bids are placed per ISP and must be available for the full period ([130]). These bids are ranked from lowest to highest price, and are accepted and called according to the grid imbalance through a merit order (explained further later in the section). This merit order is closed on a minute-to-minute basis ([132]). The BSP gets remunerated by the TSO against the balancing energy price for the energy delivered during the ISP ([132]).

#### Balancing Markets

Europe has three distinct balancing markets: frequency containment reserves (FCR), automatic frequency restoration reserves (aFRR), and manual frequency restoration reserves directly activated (mFRRda). Each market has its own characteristics and purpose. FCR is the so-called "first line of defense" and is activated first in response to a frequency deviation. For FCR, the TSOs across Europe collaboratively ensure that there is enough primary power reserve available (Rancilio *et al.* [133]). This joint responsibility is governed by the European Network of Transmission System Operators for Electricity (ENTSO-E) ([134]). When, for example, a power plant in the Netherlands suddenly shuts down, Tennet measures the frequency deviation and concludes that FCR power is needed in its area. At this point, all European FCR

assets could potentially be automatically activated through the ENTSO-E. If the frequency deviation persists, local aFRR assets will be activated after 30 seconds to restore the full European FCR capacity as soon as possible ([135]). Lastly, mFRRda (previously "emergency power incident reserve") is activated during larger and longer duration imbalances and can support the net frequency for hours ([136]).

In the FCR market (TenneT [137]), the daily auctions are divided into 4-hour blocks. If a participant bids a certain capacity, it means that they are committing to provide that capacity for the duration of the 4-hour block if their bid is accepted. Full activation of the contracted FCR lasting 15 minutes (or proportionally longer) is possible when the deviation is less than 200 mHz (TenneT [135]).

The aFRR is a market where BSPs offer balancing power to help maintain or restore the balance of the power grid (TenneT [130]). When the frequency of the grid deviates from the standard (usually 50 or 60 Hz), aFRR is automatically requested by Tennet and activated by the BSP to restore the frequency to its normal level ([130]). Tennet ensures the availability of the required minimum amount of aFRR by entering into contracts with BSPs. Under these contracts, the BSPs commit to offering at least the agreed volume of aFRR energy in their bids. The contracted aFRR power must be continuously available throughout the contract period, enabling Tennet to correct frequency deviations within 15 minutes. Additionally, prequalified BSPs can voluntarily offer their available aFRR capacity in what are known as "free bids." It is important to note that contracted aFRR bids do not receive priority over voluntary bids; the merit order list is established solely based on the price of the bids ([130]).

Finally, mFRRda is a contract from 00:00 - 00:00 and cannot be changed during the day. The contract duration is in principle one calendar day and runs from 00:00 - 00:00. In special situations (e.g., solar eclipse), Tennet may decide to organize an additional auction for a shorter period. Within this contract period, the BSP must keep the contracted power available so that it can supply this power in case of activation.

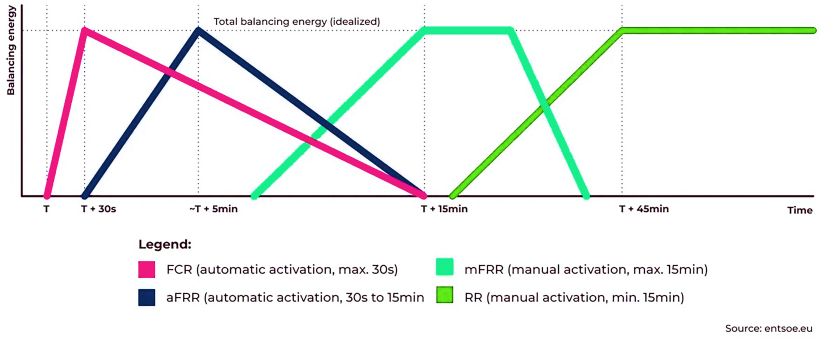


Figure 2.15: Timeline and hierarchy of FCR, aFRR, mFRRda markets. Adopted by ENTSO-E platform [1].

### Balancing Capacity Acquisition and Activation

Tennet buys balancing capacity to make sure that the supply and demand of energy can always be brought into equilibrium. As explained, there are three main balancing products: FCR, aFRR, and mFRRda. BSPs that are contracted for FCR activate their power automatically based on the grid frequency. When aFRR power is needed, Tennet automatically requests BSPs to activate their power. BSPs must then respond with the requested power within a certain time frame. mFRR is manually activated by Tennet during long-term imbalances. BSPs that participate in FCR are paid a certain amount to have the agreed-upon capacity on standby and do not receive any extra remuneration for actual activation. Figure 2.15 shows an overview of this balancing process in time.

To activate aFRR energy bids, Tennet sends aFRR activation volumes, also known as 'delta setpoints', to the BSPs that have submitted these energy bids ([130]). Delta setpoints indicate the demanded aFRR volume, and the total amount of aFRR energy bids activated by the load frequency control (LFC) is determined by the balance of the (national) power grid. When there are no significant frequency deviations in the Dutch grid, energy bids are activated according to the merit order approach; the necessary adjustment is determined based on the observed system imbalance and activated from the lowest to the highest price, as depicted in Figure 2.16 for a visualization.

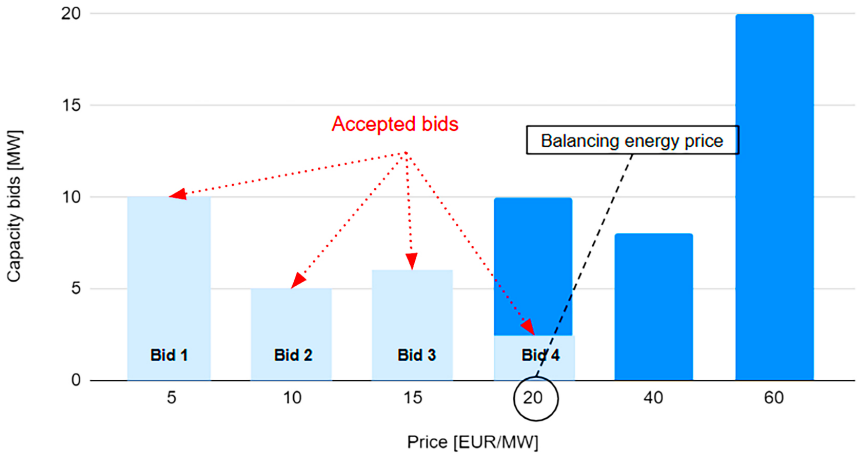


Figure 2.16: Regular merit order request example: Bids 1-3 are accepted for their full amount, and bid 4 receives a partial activation request, and sets the balancing energy price.

# 3

# Grid Impact of Balanced Grid Integration of LCTs

*Summary*

After the review of the existing knowledge about the grid impact of LCTs in distribution grids, this chapter investigates the grid impact in terms of overloading and nodal voltage deviations in different distribution grids due to increasing penetrations of PVs, EVs, and HPs. The major objectives are the identification of the most severe LCT, grid impact issue, seasonal effect, and vulnerable distributional area, considering the physical models of the LCTs. It is concluded that Winter is the most hazardous for the future grid impact, characterized by nearly 3 times higher overloading and 2.5 times higher voltage deviations during high HP penetrations, while suburban areas are the most vulnerable. Moreover, while HPs seem to have, in general, a greater impact compared to EVs, EVs cause more prolonged violations. While this chapter follows a bottom-up approach, using detailed physical models, aggregated national data has also been acquired, which is often used by top-down approaches. Different grid impact issues have been compared for the two approaches in terms of magnitude and duration. While bottom-up approaches generate more pessimistic results regarding the magnitude of the violations, results about the duration of the violations can be contradictory.

*Outline*

The chapter is categorized as follows: Sections 3.1 and 3.2 include the motivation and the contributions of the chapter. Section 3.3 comprises the methodology of the chapter, focusing on the modeling of the PVs, EVs, HPs, and the data utilized for the generation of the LCT profiles, which are also used for the next chapter. Section 3.4 contains the description of the utilized distribution grids, LCT grid distribution, simulation set-up, and the chapter's case studies, while Section 3.5 comprises the results of the chapter regarding the comparison and evaluation of grid impact issues by different LCT combinations in different distribution grids. In continuation, Section 3.6 integrates the discussion, which summarizes the findings and recommendations of the chapter. Finally, Section 3.7 concludes the chapter.

This chapter is based on parts of:

N. Damianakis, G. C. R. Mouli and P. Bauer. 'Risk-averse Estimation of Electric Heat Pump Power Consumption'. In: *2023 IEEE 17th International Conference on Compatibility, Power Electronics and Power Engineering (CPE-POWERENG)*. 2023, pp. 1–6

N. Damianakis, G. R. C. Mouli, P. Bauer and Y. Yu. 'Assessing the grid impact of Electric Vehicles, Heat Pumps & PV generation in Dutch LV distribution grids'. In: *Applied Energy* 352 (2023), p. 121878. ISSN: 0306-2619

Y. Wesseling, N. Damianakis, G. Ram Chandra Mouli and P. Bauer. 'Grid Impact of Unbalanced Phase Integration of PV Generation, Electrified Mobility, and Heating in LV Distribution Grids'. In: *IEEE Access* 13 (2025), pp. 56887–56907

## 3.1. Motivation

As seen in Chapter 2, grid impact assessment studies of different combinations of PVs, EVs, and HPs already exist in the literature. However, concerning the studies that integrate all three technologies, many works have analyzed only one aspect of the overall future grid impact, especially load profiles. Moreover, most works either use only one standard/adapted or a real LV network for their investigation, leaving out the effect of the different grid case studies on the grid impact assessment results. For example, only in [12] & [71], 25 and 5 UK LV networks were used to study the impact of different future LCT penetrations on load profiles, voltage violations, and overloading. Moreover, most studies do not distinguish their grids into different categories (grid areas), in order to observe how characteristics from different grid areas affect the grid impact results. For example, different sectors of interest (e.g., residential or commercial) and different population areas (e.g., rural-suburban-urban) were investigated only in [66], [63], and [65]. Finally, most works, apart from [3], [6], [57], and [54], constitute T-D approaches, using aggregated high-scale data extrapolated to the needed level. On the contrary, B-U approaches use physical models to generate the data needed. As explained, B-U approaches aim to consider the component-side point of view and their physical operation models, aiming for higher validity of results. Moreover, for that reason, they can be highly extendable and modifiable to incorporate different technologies or characteristics of different case studies (e.g., different regions, seasons, etc) [73]. However, from the B-U approaches, only authors in [3] consider detailed models of the LCTs and not simple regression formulas.

A comparison of the investigation characteristics for every existing work that studies all 3 LCTs (PVs, HPs, EVs) is summarized in Table 3.1. In Table 3.1, the following abbreviations stand for:

- For Grids: HH for Household, DG for Distribution Grid, Rur for Rural, Suburb for Suburban, Urb for Urban.
- For Impact Issues: LP for Load Profiles (Energy Consumption, Peak Power Demand), O/L for Overloading, V for Voltage Deviations, U for Unbalance, PF for Power Factor, EL for Energy Losses, H for Harmonics.
- For Penetrations: Mult for Multiple, C for Combined, I for Individual.
- T-D for Top-down, B-U for Bottom-up, simp for simplistic.

## 3.2. Contributions

Considering all of the above, a B-U investigation is needed that aims to investigate the future grid impact by different individual and combined penetrations of PVs, EVs & HPs, considering multiple grid impact issues and metrics. Hence, insights will be provided about the overall future grid impact, the contribution of each LCT according to each penetration, and the severity of the different issues that should be expected. Moreover, the use of real-world grids with different characteristics is needed so that

Table 3.1: Characteristics of existing grid-impact assessment works with PVs-EVs-HPs consideration.

| Ref | Grids (Type & No.) | Impact Issues | Penetrations (C - I) | LCT Comp. | T-D | B-U |
|---|---|---|---|---|---|---|
| [54] | German HH | LP | 1 (I) | ✓ | | ✓(simp) |
| [1] | Switzerland | LP | Mult (C&I) | ✓ | ✓ | |
| [3] | 1 adapted LV DG | LP | Mult (C&I) | ✓ | | ✓ |
| [60] | 1 Brescia MV DG | O/L | 1 (C&I) | ✓ | ✓ | |
| [70] | 1 Dutch LV DG | O/L | Mult (C) | | ✓ | |
| [6] | 1 Swiss LV DG | O/L, V | Mult (C&I) | | | ✓(simp) |
| [61] | 2 Dutch LV DGs | O/L, V | 1 (C) | | ✓ | |
| [57] | 1 adapted LV DG | V, U PF, EL | 1 (C&I) | ✓ | | ✓(simp) |
| [62] | 1 UK LV DG | O/L, V U, H | 1 (I) | ✓ | ✓ | |
| [56] | 1 Irish DG | LP, V | Mult (C) | | ✓ | |
| [12] | 25 UK LV DGs (residential) | LP, O/L V | Mult (I) | ✓ | ✓ | |
| [71] | 5 UK LV DGs | LP, O/L V | Mult (C) | | ✓ | |
| [66] | UK DGs (rur-sub-urb) | LP | 1 (C&I) | ✓ | ✓ | |
| [63] | LV DGs (rur-sub-urb) | O/L, V | 1 (C) | | ✓ | |
| [65] | 2 Munich DGs (sub-urb) | LP | Mult (I) | ✓ | PVs EVs | HPs |
| **Ch.3** | 6 Dutch LV DGs (rur-sub-urb) | LP, O/L V | Mult (C&I) | ✓ | ✓ | ✓ |

the effect of the different grid case study specifications (rural, suburban, urban) is considered on the future grid impact. This has not yet been done with the use of a B-U approach. Following a detailed B-U approach, the physical models and the realistic operation of the integrated components will be thoroughly considered, as well as the different effects that affect them. For example, the use of different weather data has a direct impact on the coefficient of performance (COP) and power consumption of the HPs, and therefore, the seasonal effect can be taken into account. However, it must be noted that the T-D approaches have the strength of providing high accuracy with low modeling complexity if a lot of historical data is available. In contrast, the validity of the B-U approaches is subject to the right selection of appropriate parameters of the utilized models [73], [138]. Therefore, the analysis has been repeated, following a T-D approach, so that, firstly, the two approaches are cross-validated, and secondly, important insights are drawn about the impact of the approach on the results, which has not yet been investigated in grid impact studies. Hence, this chapter's contributions can be summarized as:

- Analysis of the grid impact in different real Dutch LV residential & commercial DGs (urban, suburban, and rural), considering in detail the characteristics of the LCT physical models (bottom-up approach).

- Use of multiple metrics to assess several grid impact issues (node voltage deviations and overloading of network components) of individual and combined integration of PVs, HPs, and EVs, considering spatial, intra-week, and seasonal effects, penetration levels, and existing loading conditions. Hence, the bottom-up grid impact assessment is consistent and thorough with respect to other bottom-up existing works.

- Compares the results mentioned above, generated by physical models (bottom-up), with related results by aggregated data utilization from open-source data sources (top-down) in order to cross-validate the two main grid impact assessment approaches. According to the author's knowledge, this has not yet been done in grid impact studies.

## 3.3. Data Description & Models of LCTs

In this section, firstly, the utilized data is analyzed, and secondly, the 3 LCT models are explained. In this Ph.D. thesis, special focus has been placed on the character of the models that should be used for this B-U approach. Black-box models are usually suitable for data-driven approaches that have a lot of historical data available. However, they lack of interpretability of results and the various effects that can have an impact on them. On the contrary, white-box models are fundamentally based on the conservation of mass and energy, and, therefore, they are especially suited for B-U approaches, because they are able to consider various details of the models. However, this comes at the cost of high computational expense, especially for grid-level studies that comprise hundreds of loads [139]. Hence, the use of grey-box modeling has been decided for the scope of this thesis, which provides a trade-off between accuracy and computational expense, that suits best a grid-level B-U approach.

### 3.3.1. Data Description

The following data have been used as inputs for the developed models of the B-U approach and/or for the extraction of the T-D results:

1) Dutch electricity distribution consumption profiles of the year 2021 for the already existing electric demand of residential and commercial buildings have been acquired from the MFFBAS database[1]: used in both B-U and T-D approaches.

2) Probabilistic distributions of EVs, in terms of arrival and departure times, connection times & requested amounts of energy, have been acquired by the Elaad NL open database[2]: used in both B-U (EV model) and T-D approaches. The EV model, however, also comprises more features, explained in Section 3.3.2.

3) Weather data (wind speed, ambient temperature, irradiance components, solar elevation & solar orientation profiles) have been acquired from the Meteonorm

[1] https://www.mffbas.nl/documenten/
[2] https://platform.elaad.io/analyses/index.php

database[3]: used in B-U as input for the HP, irradiation, and PV models (Sections 3.3.3, 3.3.4 and 3.3.5).

4) Heating data (Space/water heating and COP profiles of various types of Heat Pumps), scaled to total yearly consumption, have been acquired from the When2heat database[4]: used for the T-D approach results.

5) PV power distribution profiles scaled to rated power have been acquired from the Royal Dutch Meteorological Institute (IKNMI)[5]: used for the T-D approach results.

6) The Dimplex LIK 8MER reversible HP module and Panasonic HIT PV module for the specifications of the HP and PV models, respectively.

### 3.3.2. EV model

Using MCS, 200 weekly profiles are created for 3 different charger locations (Home, Semi-Public, and Public) and randomly distributed to the chargers in the grid simulation. The EV pool comprises the "Kona, I3, I-Pace, and Model 3" EVs with rated power of 11kW, the "Model X, Model S" EVs of 16kW, and the "Zoe" EV of 22kW. It is assumed that all AC chargers can provide the maximum power of 22kW. The Home Chargers, in comparison with Semi-public and Public chargers, are typically characterized by lower EV frequency and higher requested amounts of energy (see Figure 3.1). Intra-week effects (weekdays and weekends) have also been taken into account regarding the charging times. For example, an EV is charged 3 times during weekdays and once during weekends at a Home Charger.

The Constant-Current - Constant-Voltage (CC-CV) EV charging regions have been considered, utilizing linear approximations, as dictated by (3.1)-(3.3). The maximum charging current in CC and CV regions, $I^{n,j,t}_{cc_{max,ch}}$ and $I^{n,j,t}_{cv_{max,ch}}$ in (3.1)

[3]https://meteonorm.com/
[4]https://data.open-power-system-data.org/when2heat/
[5]https://www.knmi.nl/

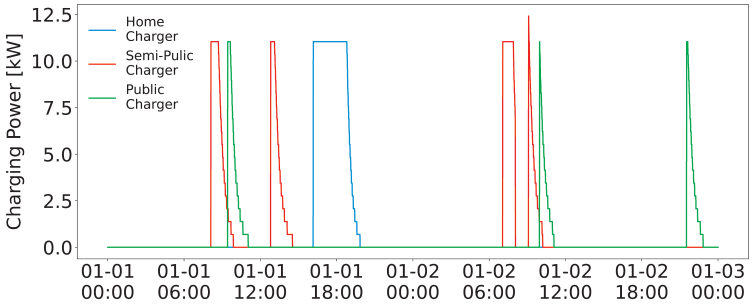


Figure 3.1: Typical EV Charging Profiles of Home, Semi-Public & Public Chargers (2 days duration).

and (3.2) respectively, depend on the maximum EV charging current $I_{ch_{max}}^{n,j}$ and instantaneous EV SOC $S^{n,j,t}$, where $[T_a^{n,j}, T_d^{n,j}]$ the EV parking period (arrival-to-departure time). Since the EV model is uncontrolled, (3.3) forces the charging current $I_{ch}^{n,j,t}$ to be equal to the maximum allowed current in each region. Adopting the parameters $\alpha = 10$, $\beta = 9$, $k = 16$, and $\gamma = 10$ from [39], the turning SOC point equals to $S_{n,j}^{CV} = 90\%$. The CC-CV charging model is depicted in Figure 3.2, where $p_{n,j}^{CCO}$ and $p_{n,j}^{max}$ are the charging power at 0% SOC and maximum charging power at 90% SOC, respectively.

$$I_{cc_{max,ch}}^{n,j,t} = \left(\frac{S^{n,j,t}}{k} + \frac{\alpha k - \beta}{\alpha k}\right) I_{ch_{max}}^{n,j} \quad \forall t \in [T_a^{n,j}, T_d^{n,j}]: \alpha = 10, \beta = 9, k = 16 \tag{3.1}$$

$$I_{cv_{max,ch}}^{n,j,t} = -\gamma I_r^{n,j,t} S^{n,j,t} + \gamma I_r^{n,j,t} \quad \forall t \in [T_a^{n,j}, T_d^{n,j}]: \gamma = 10 \tag{3.2}$$

$$I_{ch}^{n,j,t} = min(I_{cc_{max,ch}}^{n,j,t}, I_{cv_{max,ch}}^{n,j,t}) \tag{3.3}$$

This model has also considered a 30% higher consumption for EV charging during the Winter period in order to also encapsulate the seasonal effect. The reason for this consideration is twofold. Firstly, it has been found by data analysis from 7500 EVs, that EV consumption is higher during the Summer than in Winter, due to a number of reasons, e.g lower average temperature change to achieve thermal comfort inside the EV, capability of pre-cooling while plugged in, higher tire pressure, battery operation closer to their comfort zone, etc. [140]. Secondly, the particular investigation takes place in the Netherlands, which is characterized by

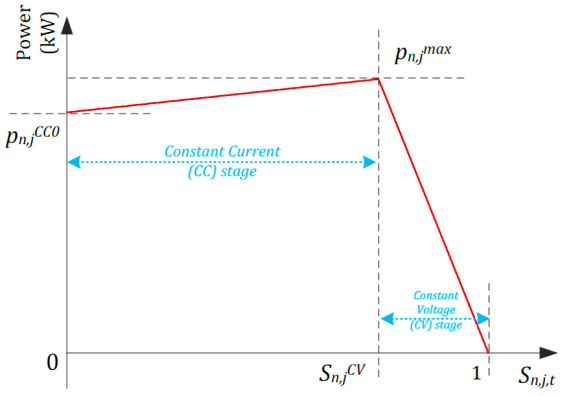


Figure 3.2: Linear approximations of the CC-CV EV charging regions.

more moderate Summers than Winters. This difference, regarding the deviation between the ambient and the EV interior temperature, has a direct impact on the cooling and heating COPs and hence, on the power consumption (see Section 3.3.3). The 30% increase has been integrated into the arrival SOC of the EVs at the chargers and the related requested energy $E_{req}$ in (3.4), assuming that the EV drivers will still request the same SOC upon departure.

$$\begin{aligned} S_{ar}^{win} &= 1.3 S_{ar}^{sum} - 0.3 S_{dep} \\ \& \; E_{req}^{win} &= (S_{dep} - S_{ar}^{win}) B_{ev} \end{aligned} \tag{3.4}$$

Where: $S_{ar}^{win}$ & $E_{req}^{win}$ the arrival SOC and requested energy during winter, respectively, $S_{ar}^{sum}$ the arrival SOC during summer, $B_{ev}$ the battery capacity of every EV and $S_{dep}$ its departure SOC.

### 3.3.3. HP & Building models

A power consumption and building temperature model has been designed, inspired by [2, 141]. This section comprises the main modeling features and results of the model; for further information, the reader is referred to the publication [24]. The model considers space-heating/cooling (SH/C) with floor-heating and domestic hot water (DHW) by air-sourced HPs (ASHPs). It is fed with building occupancy profiles, HP specifications (heating and cooling outputs, water flow rates, SH/SC/DHW supply temperatures), building specifications (materials, dimensions, parameters), and weather data (irradiation). The model extracts the HP consumption, keeping the space temperature on the desired levels (21°, 23°) when the buildings are occupied. Residential buildings are usually occupied throughout the day except during 08:00-14:00 on weekdays, while commercial buildings are occupied during 08:00-21:00 on weekdays and 09:00-18:00 on weekends. 200 randomized HP residential and commercial consumption profiles have been created with HP-rated power $P_{hp}^{r} = 3kW$, inserting a maximum of 15' uncertainty level at the occupation times of the buildings with the use of normal distribution. The concept of the simulator is depicted in Figure 3.3. Every time instant, the algorithm is fed by the input datasets. If the building is occupied, the HP is turned ON whenever the building temperature deviates from the desired temperature interval. When the water tank needs to be heated (twice per day), the DHW is given priority. In any other case, the HP is turned OFF.

$$T_b^{t+\Delta t} = \frac{Q_{hp}^t + Q_{ir}^t - Q_{los}^t}{C_b + V_b C_{air} \rho_{air}} \Delta t + T_b^t \tag{3.5}$$

$$Q_{los}^t = Q_{cond}^t + Q_{vent}^t \tag{3.6}$$

$$Q_{cond}^t = \sum_{surf}^{surfaces} (d_{surf} U_{surf} A_{surf})(T_b^t - T_a^t) \tag{3.7}$$

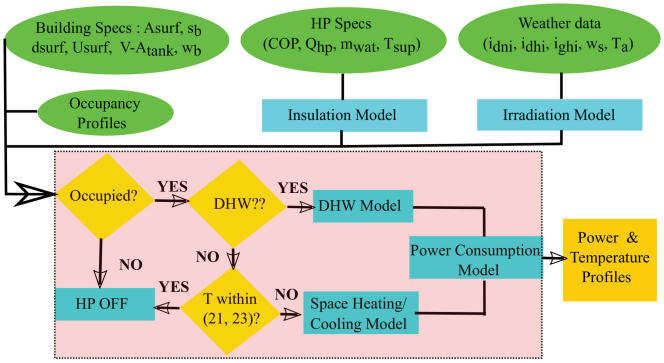


Figure 3.3: Concept of HP Power Consumption Model.

$$Q^t_{vent} = C_{air}\ \rho_{air}\ r_b(T^t_b - T^t_a) \tag{3.8}$$

$$Q^t_{ir} = G^t_{inc}\ w_b\ s_b \tag{3.9}$$

Equation (3.5) dictates the temperature of the building $T_b$ at every timestep $\Delta t$, which depends on the total gains of the building (HP output $Q_{hp}$ and heat from incident solar irradiation $Q_{ir}$), the total building losses $Q_{los}$ (conductive losses $Q_{cond}$ and ventilation losses $Q_{vent}$ indicated in (3.6) [142]. Moreover, it depends on the total heating capacity: the building capacity $C_b = 4.755\ kWh/K$ (a typical building value has been derived by [143]), and the capacity of the air volume inside the building, equal to $V_b = 585\ m^3$, where $C_{air}$ and $\rho_{air}$ represent the air's specific heat capacity and density, respectively. The conductive and ventilation losses, and incident irradiation heat gains are modeled in (3.7)-(3.9) [142], respectively, where $A_{surf}$, $d_{surf}$ & $U_{surf}$ the area, thickness, and conductivity of every surface, $T_b$ & $T_a$ the building and ambient temperatures, $r_b$ the air change rate of the building assumed $0.35h^{-1}$, $G_{inc}$ the incident irradiation on the building, $w_b = 0.3$ the building's wall-to-window ratio and $s_b = 0.2$ the solar heat gain coefficient of the windows. $s_b$ represents the heat proportion entering the building windows, considering the heat transfer by both conductivity and emissivity. It must be noted that only the solar heat transferred through the windows is taken into account, whereas the solar heat transferred through the building's walls has been ignored. The heat generation by household electric appliances and the people inside the buildings has also been ignored.

$$P^t_{hp} = \frac{Q^t_{hp}}{c^t_{p_{hp}}} \tag{3.10}$$

$$c^t_{p_{hp}} = 7.90471e^{-0.024(T^t_{ret} - T^t_a)} \tag{3.11}$$

$$T^t_{ret} = T_{sup} - \frac{Q^t_{hp}}{\dot{m}_{wat} C_{wat}} \tag{3.12}$$

The HP power consumption is calculated by (3.10), which dictates its relation to the HP output and COP [2]. The COP $c_{p_{hp}}$ and return water temperature $T_{ret}$ are modeled in (3.11) and (3.12), where $\dot{m}_{wat}$: the flow water rate and $T_{sup}$ the supply water temperature, which is set at 35°, 50°and 18°for floor-heating, DHW and floor-cooling, respectively.

DHW is assumed to be realized twice daily for the residential sector, once in the morning at 06:00 a.m. and once in the evening at 19:00, and once per day for the commercial sector at 10:00 a.m. The DHW system integrates a DHW tank, which is used to heat and store hot water. Moreover, it must be noted that the HP cannot simultaneously heat space and water. Therefore, DHW is given priority at these specific time intervals of the day. The DHW tank temperature dynamics are dictated based on the heat gains (HP output $Q_{hp}$), conductive losses $Q_{loss}$, and stored water capacity. The DHW temperature and the conductive losses are dictated by (3.13) & (3.14), where $C_{wat}$ & $\rho_{wat}$ are the water specific heat capacity and density, respectively and $U_{tank} = 0.598 W/m^2K$ is the tank conductivity.

$$T^{t+\Delta t}_{tank} = \frac{\dot{Q}^t_{hp} - \dot{Q}^t_{los}}{V_{tank}\, C_{wat}\, \rho_{wat}} \Delta t + T^t_{tank} \tag{3.13}$$

$$\dot{Q}^t_{loss} = U_{tank} A_{tank} (T^t_{tank} - T^t_a) \tag{3.14}$$

In Figure 3.4, the HP consumption and the building temperature are depicted during heating mode (winter day) and cooling mode (summer day). The space temperature is always within the desired levels (21°- 23°), except for the time

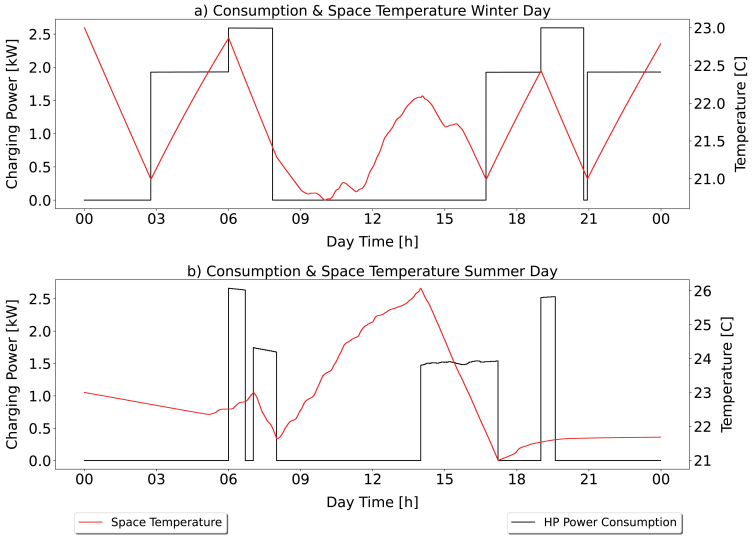


Figure 3.4: Power Consumption & Space Temperature at Residential Buildings.

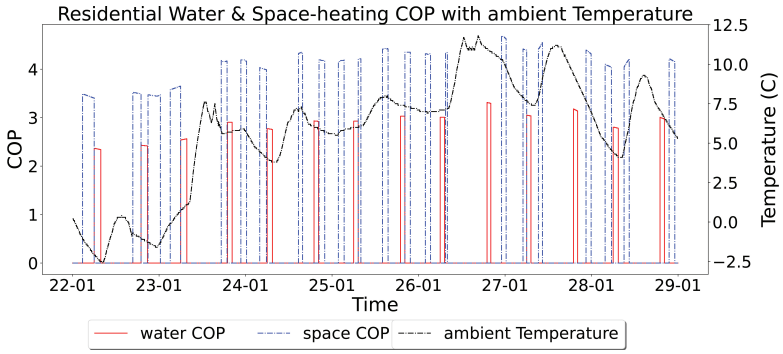


Figure 3.5: Winter Residential SH/DHW COPs & ambient Temperature.

period that the building is not occupied (from 08:00 until 14:00). The high and low power peaks represent the DHW and SH/SC modes, respectively. The SH and DHW COPs are plotted with the ambient temperature for the whole winter week in Figure 3.5. The SH COPs fluctuate between 3.4 and 4.4, while the DHW COPs fluctuate between 2.3 and 3.3. The increased SH COP has been expected, due to the higher heating temperature of the DHW, compared with the floor-heating temperature. Moreover, a relative increase in both COPs is observed with the increase in the ambient temperature. The consequences of the lower DHW COPS on the HP power consumption can be seen in Figure 3.6. While the HP consumption for space-heating deviates mostly around 2kWs, it can reach up to 3kWs when the DHW operation is on. However, the HP power consumption fluctuates less than the COP during variable ambient temperatures. This is due to the fact that both the COP and the heating capacity increase during higher ambient temperatures, both of which affect the HP power consumption.

Finally, Figure 3.7 visualizes the difference in the HP energy consumption in non-insulated and insulated buildings for commercial and residential buildings during Summer and Winter. It can be seen that both building types have a vastly increased

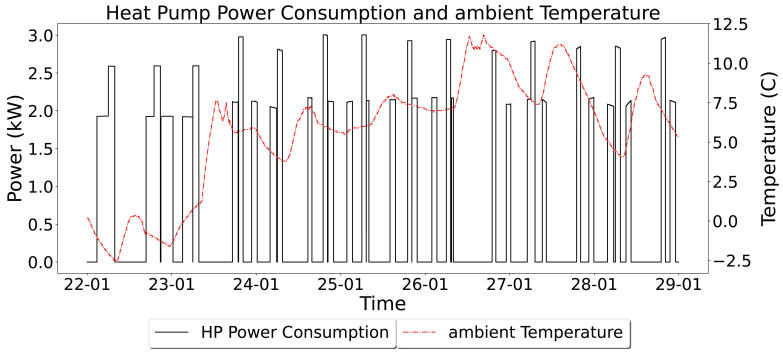


Figure 3.6: Winter Residential Consumption & ambient Temperature.

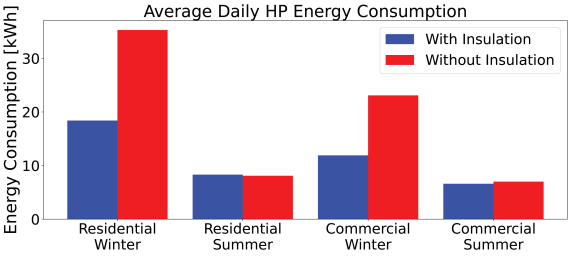


Figure 3.7: Daily Average HP Energy Consumption during Summer and Winter of insulated and non-insulated buildings.

Table 3.2: Parameters of HP & Building Models

| Parameters | Explanation | Value |
|---|---|---|
| $C_b$ | Building Thermal Capacity | $4.755kWh/K$ |
| $V_b$ | Building Volume | $585m^3$ |
| $w_b$ | Building Window-to-wall Ratio | 0.3 |
| $s_b$ | Building Solar Heat Gain Coefficient | 0.2 |
| $r_b$ | Building Air-change Rate | $0.35h^{-1}$ |
| $U_{tank}$ | Tank Conductivity | $0.598W/m^2K$ |
| $C_{air}$ | Air Specific Capacity | $0.279Wh/kgK$ |
| $\rho_{air}$ | Air Density | $1.225kg/m^3$ |
| $\dot{m}_{wat}$ | HP Flow Water Rate | $0.8kg/s$ |
| $C_{wat}$ | Water Specific Capacity | $1.16Wh/kgK$ |
| $\rho_{wat}$ | Water Density | $993kg/m^3$ |
| $P^r_{hp}$ | HP Rated Power | $3kW$ |

consumption during Winter, which can reach up to 100% and 350% with and without insulation, respectively. Moreover, residential buildings are characterized by higher consumption than commercial buildings during both seasons (19kWh and 10kWh compared to 11kWh and 6kWh for Winter and Summer, respectively. The parameters of the utilized HP and building models are summarized in Table 3.2.

### 3.3.4. Solar Irradiation

The total incident irradiation on the building is the sum of the incident irradiation on the four walls and the two roof surfaces. The walls are simulated as surfaces with tilt angle 90°and orientations 0°, 90°, 180°, 270° facing North, East, South, and West, respectively. The two roof surfaces are simulated as two surfaces with 45° tilt angle and 0° & 180°orientation.

$$G^t_{inc} = G^t_{dir} + G^t_{dif} + G^t_{alb} \tag{3.15}$$

$$G^t_{dir} = I^t_{DNI} cos(a^t_i) A_{surf}, \ where: \tag{3.16}$$

$$G^t_{dif} = I^t_{DHI}\frac{1+cos(\theta_{surf})}{2}A_{surf} \tag{3.17}$$

$$G^t_{alb} = I^t_{GHI}c_{alb}(1-\frac{1+cos(\theta_{surf})}{2})A_{surf} \tag{3.18}$$

$$cos(a^t_i) = sin(\theta_{surf})cos(\theta^t_s)cos(O_{surf}-O^t_s) + cos(\theta_{surf})sin(\theta^t_s) \tag{3.19}$$

For every surface (for both buildings and PV modules), the incident irradiation is dictated by (3.15) - (3.19) [144]. Equation (3.15) dictates that the total incident irradiation $G_{inc}$ at every time moment integrates the direct irradiation $G_{dir}$, diffuse irradiation $G_{diff}$, and albedo irradiation $G_{alb}$. The 3 types of irradiation are modeled by (3.16)-(3.18) respectively, where $a_i$ the angle of solar incidence (AOI), $c_{alb}$ the albedo coefficient and $I_{DNI}$, $I_{DHI}$ & $I_{GHI}$ the direct normal, diffuse horizontal, and global horizontal irradiances, respectively, expressed in $W/m^2$. The albedo coefficient represents the proportion of irradiance reflected by the surrounding environment and has been assumed to be an average of 0.175 for the concrete sidewalks and asphalt (0.225 & 0.125, respectively). Equation (3.19) models the AOI $a_i$, where $\theta_{surf}$ & $O_{surf}$ the title angle and orientation (azimuth) of the surface and $\theta_s(t)$ & $O_s(t)$ the momentary solar elevation angle and orientation. It must be noted that the "Isotropic Sky Model" has been utilized for the calculation of diffuse irradiation, and potential shading by other buildings has been neglected.

### 3.3.5. PV model

Equations (3.20)-(3.26) dictate the PV model, based on [144].

$$T^t_M = T^t_a + \frac{G^t_{inc}}{G_{noct}}(T_{noct}-20)\frac{9.5}{5.7+3.8s_w}(1-\frac{\eta_{stc}}{a_f}) \tag{3.20}$$

$$P^{T_M,G^{stc}}_{MPP} = P^{stc}_{MPP} + c_{P_{MPP}}(T_M - T_a) \tag{3.21}$$

$$\eta^{T_M,G_{stc}} = \frac{P^{T_M,G_{stc}}_{MPP}}{A_M G^{stc}} \tag{3.22}$$

$$P^{25^oC,G^{inc}}_{MPP} = f_f V^{25^oC,G^{stc}}_{OC} I^{25^oC,G^{stc}}_{SC} \tag{3.23}$$

$$\eta^{25^oC,G_{inc}} = \frac{P^{25^oC,G^{inc}}_{MPP}}{A_M G_{inc}} \tag{3.24}$$

$$\eta^{real}_{pv} = \eta^{25^oC,G_{inc}}[1+\frac{c_\eta}{\eta^{stc}}(T_M - 25^oC] \tag{3.25}$$

$$P^t_{pv} = \eta^{real}_{pv} A_M G_{inc} \eta^{inv} \tag{3.26}$$

The temperature of the PV model $T_M$ depends on the ambient temperature $T_a$, the wind speed $s_w$, the incident irradiance $G_{inc}$, consisting of the direct, diffuse, and albedo components, the irradiance and temperature under normal operating conditions (NOCT) $G_{noct}$ & $T_{noct}$, the absorptivity factor $af$, the efficiency under standard test conditions (STC) $\eta_{stc}$ and is estimated by (3.20). The effect of the module temperature on the PV power $P_{MPP}^{T_M,G^{stc}}$ and efficiency $\eta^{T_M,G_{stc}}$ is dictated by (3.21) & (3.22), where $G_{stc}$ the irradiance under STC, $A_M$ the module area and $c_{P_{MPP}}$ the power temperature coefficient. Equations (3.23) & (3.24) dictate the related effect of irradiance on the power of the maximum power point (MPP) $P_{MPP}^{25^oC,G^{inc}}$ and the module efficiency $\eta^{25^oC,G_{inc}}$, where $f_f$ the module fill factor and $V_{OC}^{25^oC,G^{stc}}$ & $I_{SC}^{25^oC,G^{stc}}$: the open-circuit (O-C) voltage and short-circuit (S-C) current of the module under different incident irradiance. The real module efficiency $\eta_{pv}^{real}$, dependent on both incident irradiance and module temperature, and the final PV generation $P_{pv}$ are modeled in (3.25) & (3.26), respectively, where $\eta^{inv}$ is the efficiency of the inverter and $c_\eta$ is the power temperature coefficient.

Using MCS, 90 Summer and Winter PV generation profiles have been created using a tilt angle from 10° to 50° with a step of 10° and using an orientation from 0° to 340° with a step of 20°. The profiles are created to represent the various roof orientations in a distribution grid and are, therefore, randomly distributed to the buildings in the grid simulation. All PV rooftops comprise 12 PV panels operating at MPP power, which all have a rated power $P_{PV}^r = 3kW$.

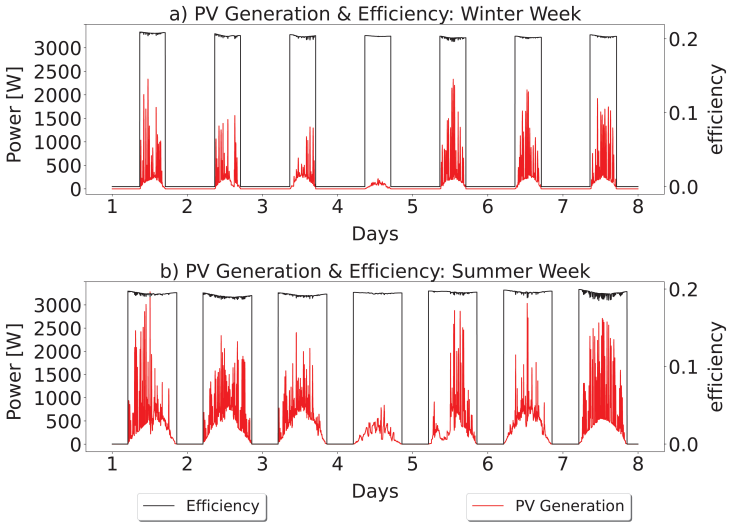


Figure 3.8: PV Rooftop 3kW-rated Power & efficiency for a) Winter & b) Summer (tilt angle = 30°, azimuth = 180°).

Table 3.3: Parameters of PV Model.

| Parameters | Explanation | Value |
|---|---|---|
| $G_{noct}$ | Irradiance (NOCT) | $800W/m^2$ |
| $T_{noct}$ | Temperature (NOCT) | $44^oC$ |
| $\eta_{stc}$ | Efficiency (STC) | 0.1943 |
| $\alpha_f$ | Absorptivity Factor | 0.9 |
| $P_{MPP}^{stc}$ | MPP PV Power (STC) | $245W$ |
| $c_{P_{MPP}}$ | Power Temp. Coefficient | $-0.29\%/^oC$ |
| $G^{stc}$ | Irradiance (STC) | $1000W/m^2$ |
| $f_f$ | Fill Factor | 0.7888 |
| $A_M$ | Module Area | $1.26m^2$ |
| $\eta^{inv}$ | PV Inverter Efficiency | 0.95 |
| $V_{OC}^{25^oC,G^{stc}}$ | O-C Voltage ($25^oC$, $G^{stc}$) | $53V$ |
| $I_{SC}^{25^oC,G^{stc}}$ | S-C Current ($25^oC$, $G^{stc}$) | $5.86A$ |

Figure 3.8 depicts the weekly PV rooftop generation profile and module efficiency during Winter and Summer seasons for the case of 30° tilt angle and 180° azimuth. The parameters of the utilized PV model are summarized in Table 3.3.

### 3.3.6. Seasonal Analysis of LCTs

Due to the important influence of LCT seasonal interrelations on the grid impact results of Chapters 3 and 4, a seasonal LCT operational analysis is summarized in this section, derived by the publication [26]. In Figure 3.9, daily power profiles for PVs, HPs, and EVs during Winter (upper row) and Summer (lower row) are summarized so that the seasonal differences of the LCTs are further clarified. Concerning PVs, PV power is generated between [09:00 and 16:00], with the highest power peak of 2.5kW occurring at 12:00. In contrast, PV generation lasts longer during Summer (more specifically between [05:00, 20:00]), having higher power peaks that reach up to 3.2kW. A weekly average PV rooftop generation is approximately 132kWh during Winter and 281kWh during Summer (113% higher).

Moreover, regarding the ON-OFF HPs, the high pulses belong to DHW while the low pulses to space heating and cooling in Winter and Summer, respectively. During Winter, as already seen, building heating is performed with approximately 2kW HP power, while building cooling needs only 1.5-1.6kW power. This is justified by the more moderate difference between the ambient and building temperatures, since the building temperature is maintained between [21°C), 23°C)], and the ambient temperature deviates between [20°C), 30°C)] and [-5°C), 10°C)] during Summer and Winter, respectively. Furthermore, building cooling in Summer occurs mostly in the afternoon and endures approximately 4h, while building heating in Winter occurs at night and in the evening and lasts approximately 8h (100% longer than cooling). The seasonal difference in DHW power consumption is lower due to the high supply

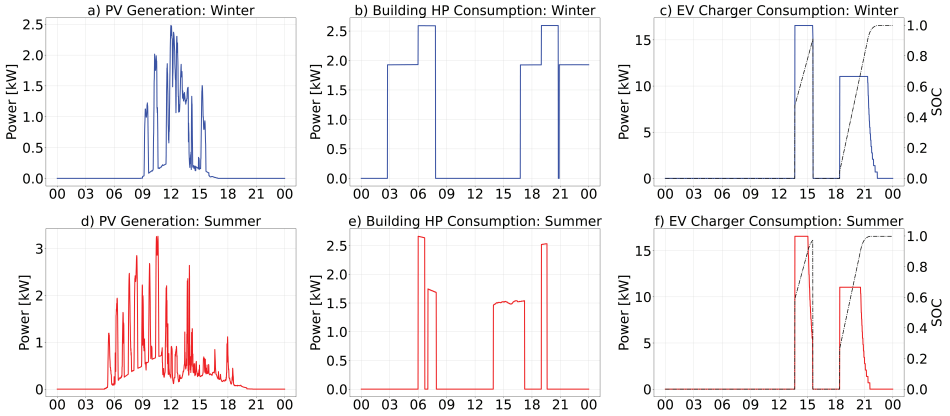


Figure 3.9: Daily Power Profiles for PVs, HPs, and EVs during Winter [a), b), c)] and Summer [d), e), f)].

temperature for DHW (50°C); however, the time needed for water heating in Winter is considerably higher. A weekly average HP energy consumption is approximately 286kWh during Summer and 645kWh during Winter (126% higher). Finally, it can be seen that HP consumption for cooling is more likely to overlap with PV rooftop generation during Summer than HP consumption for heating during Winter.

Finally, the 30% higher EV consumption (hence, requested energy) during Winter due to cabin heating is visible in Figure 3.9 c), since the EVs arrive with a lower SOC than in Figure 3.9 f). While the power levels remain unchanged, since the EVs are charged with the rated charging power in uncontrolled charging, the total charging duration can considerably increase (e.g., 30-45' longer).

## 3.4. Description of Set-Up & Case Studies

This section contains the description of the distribution grids, LCT grid distribution, the simulation set-up, and the definition of the chapter's case studies and scenarios.

### 3.4.1. Investigated Distribution Grids

As already mentioned, real DGs have been used for the investigations of this Ph.D. thesis. In this regard, six LV DGs have been acquired from Enexis Groep[6], two from each of the urban, suburban, and rural areas, that comprise both residential and commercial buildings. The rationality behind this selection is, firstly, to investigate different grid topologies and, secondly, to study representative light-loaded and heavy-loaded DGs. The spatial visualizations of the six LV DGs are depicted in Figure 3.10.

[6]https://www.enexisgroep.nl/

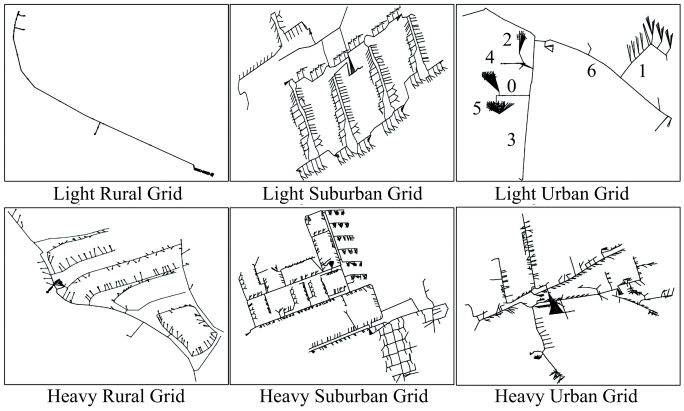


Figure 3.10: 6 Dutch LV Distribution Grids, provided by Enexis Groep.

Table 3.4: Characteristics of Distribution Grids.

| Distribution Grids | Nodes | Buildings | Homes | Yearly Consumption |
|---|---|---|---|---|
| Rural (light-loaded) | 23 | 3 | 0 | 97,954MWh |
| Rural (heavy-loaded) | 373 | 138 | 133 | 486,782MWh |
| Suburban (light-loaded) | 1742 | 809 | 772 | 2353,034MWh |
| Suburban (heavy-loaded) | 1920 | 885 | 809 | 2830,574MWh |
| Urban (light-loaded) | 1334 | 349 | 269 | 1680,223MWh |
| Urban (heavy-loaded) | 1322 | 876 | 680 | 2745,560MWh |

Moreover, Table 3.4 summarizes the basic grid characteristics: Nodes, Buildings, and Homes (residential buildings) with their yearly consumption, while Figure 3.11 depicts the existing loading of the six LV grids without LCT penetration during Winter and Summer weeks so that the seasonal grid loading variations can also be shown. It can be seen that the Winter base load is always higher than the respective Summer load. Moreover, comparing the same grid types, the load power peaks can be considerably higher in the heavier-loaded grids, which can reach up to 6x and 1.5x times higher in the rural and urban grids, respectively.

### 3.4.2. Case Studies

The main objective is the thorough identification and quantification of the future grid impact, encapsulating the effects of different DGs, LCT conditions, LCT penetrations, seasons, and approaches. In this regard, Table 3.5 summarizes the developed case studies for the grid impact evaluation.

With the use of the aforementioned case studies, the chapter intends to identify quantitatively:

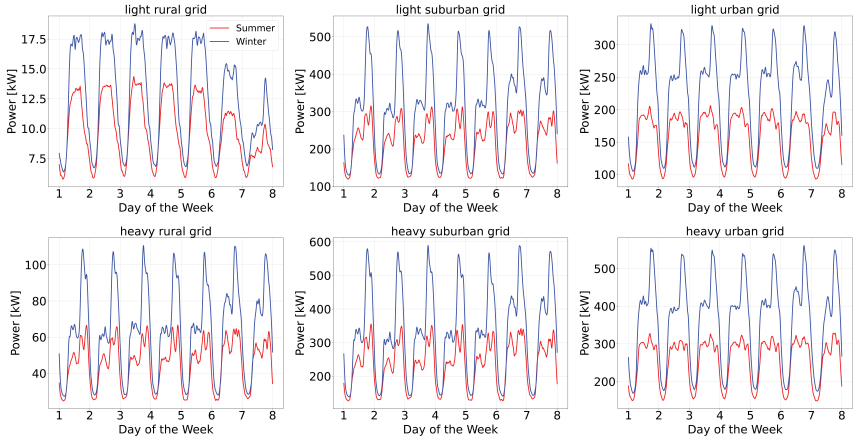


Figure 3.11: Existing loading profiles of the six LV DGs during Summer and Winter.

Table 3.5: Case Studies for Grid Impact Evaluation.

| **Case Studies** | | | | |
|---|---|---|---|---|
| Grids | LCT Conditions | LCT penetrations | Seasons | Approaches |
| 2 Rural (light & heavy) | PVs-EVs | 0 % | Summer | bottom-up |
| 2 Suburban (light & heavy) | PVs-HPs | 50 % | Winter | top-down |
| 2 Urban (light & heavy) | PVs-EVs-HPs | 80 % | | |
| | | 100 % | | |

- the most vulnerable distributional area according to each grid impact metric.
- the most crucial grid impact issue.
- the most "heavy" LCT considering different penetrations.
- the most "heavy" season.
- the total future grid impact of all LCTs integration.

However, the author acknowledges that grid impact assessment studies are highly dependent on the investigated grid specifications and case study characteristics. Therefore, the results should not be straightforwardly generalized for all case studies that investigate different distribution grids. Nevertheless, since the investigated grids are provided as area-specific representatives by the Dutch grid operator "Enexis Groep", this chapter can provide valuable insights, especially for the Netherlands.

### 3.4.3. LCT Grid Distribution

With the use of the LCT pools generated from the LCT models in Sections 3.3.2-3.3.5 (B-U approach), or the LCT data of Section 3.3.1 (T-D approach), LCT profiles have been randomly selected with a uniform probability function, and distributed to the 6 LV DGs according to each penetration and combination case study. An example of the LCT grid distribution is shown in Figure 3.12 for the heavy rural grid. The LCT penetration level depends mainly on the number of buildings (existing loads). Figure 3.12 a. depicts the heavy rural grid with the existing loads without LCT penetration. A penetration of 50% means that half of the buildings comprise a PV rooftop, an HP module, and an EV charger (see Figure 3.12 d. where a part of the grid is depicted).

In continuation, 80% and 100% LCT penetration levels are depicted in Figures 3.12 e. and f. The LCT profiles have been increasingly added to the DGs under the increasing penetrations, meaning that all buildings that comprise, e.g., a PV rooftop at 50% penetration, will comprise a PV rooftop also at 80% penetration. Hence, every next penetration level comprises the LCTs of the previous level at the exact locations. Furthermore, a penetration of 100% means that all buildings comprise one of the 3 LCTs. Finally, PV systems and HPs have been distributed to the existing buildings, regardless of their type (residential or commercial). In contrast, home EV chargers have been distributed at residential buildings, while public and semi-public EV chargers have been distributed at commercial buildings. No LCT of the same type could be connected to the same node. Finally, LCT distributions in every case study are independent of one another, meaning that a building may own a PV rooftop and not an EV or an HP, and vice versa. The LCT grid distribution concept explained above is utilized for all grid simulations performed in Chapters 3 and 4.

### 3.4.4. Simulation Set-Up

The simulation time period has been selected to be 1 week in order to capture the intra-weekly effects. For example, the heating demand of buildings, as well as EV driving and consequently charging behavior, differ greatly during weekdays and weekends and must also be considered. According to the data used for EV charging, drivers tend to charge their EVs 3 times during the week and once during the weekend. Moreover, commercial buildings are less occupied during the weekends, while the opposite applies to residential buildings. Moreover, the timestep of the simulation has been set to be 1 minute. While this timestep can increase the computational expense of the simulation, it provides higher accuracy to the grid impact assessment results. This is particularly important for the consideration of the coincidence of the operation of the different LCTs [10]. Additionally, the durations of the simulations are maintained for every grid case study between 20' (light rural grid) and 90' (heavy suburban grid). These durations are appropriate for grid impact assessment studies, which serve scheduling purposes. Finally, the grid simulations have been performed in the DigSilent PowerFactory 2019 environment with the use of the AC-balanced Newton-Raphson load flow calculation method [145]. The grid simulations have been managed with the use of the Python 3.9 environment.

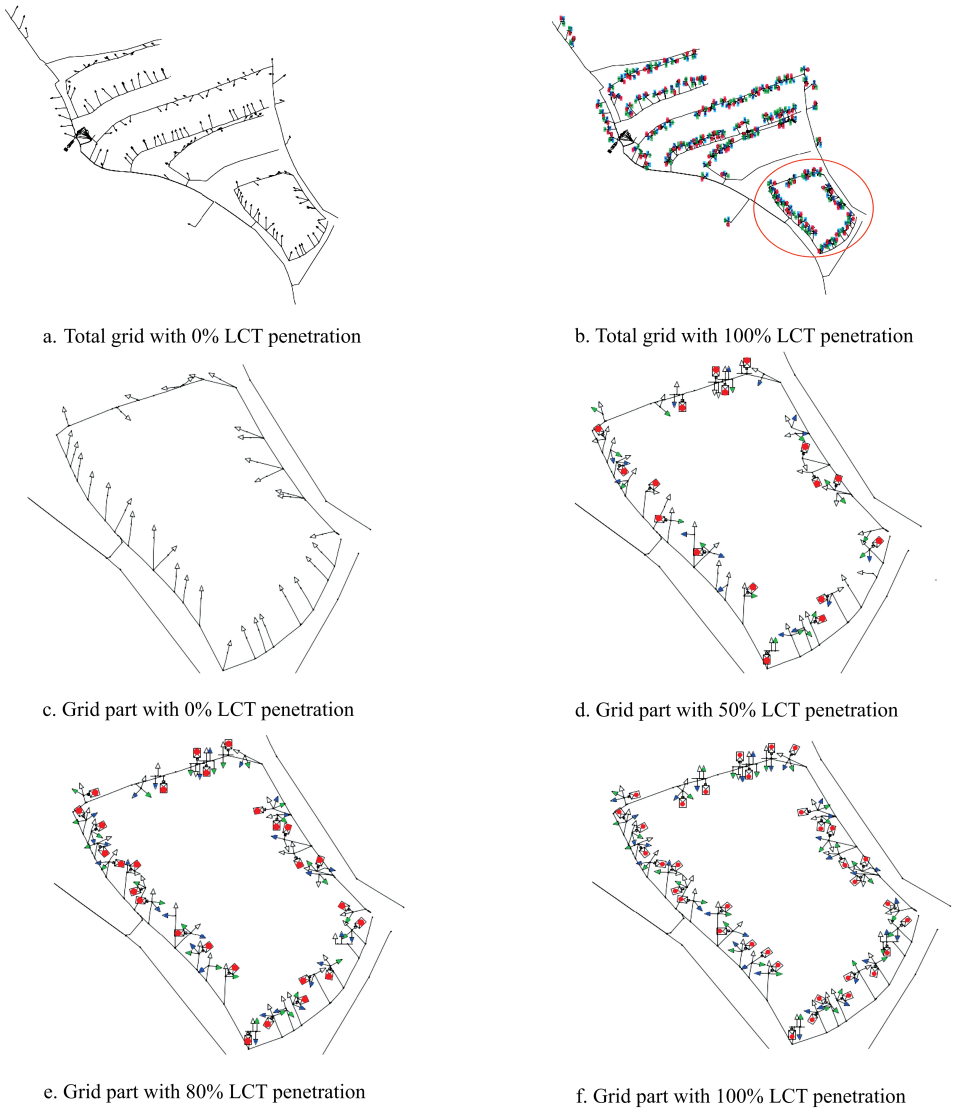

a. Total grid with 0% LCT penetration

b. Total grid with 100% LCT penetration

c. Grid part with 0% LCT penetration

d. Grid part with 50% LCT penetration

e. Grid part with 80% LCT penetration

f. Grid part with 100% LCT penetration

Figure 3.12: LCT grid integration in the heavy-loaded rural grid under 0, 50, 80, and 100% LCT penetrations: Red color (PVs), Blue color (EVs), Green color (HPs), Black color (existing loads).

## 3.5. Results

This section comprises this chapter's results concerning the LCT balanced grid integration under the case studies and scenarios summarized in Table 3.5 that belong to publication [25].

### 3.5.1. Results Overview

The grid impact is addressed in all case studies at the following grid components' issues:

- Transformer (T/F) Overloading (O/L) [%].
- Lines O/L [%].
- Nodes Voltage Deviations: under- (UV) and over-voltage (OV) [p.u].

The utilized grid impact metrics for every component are summarized as follows:

- Total (weekly) maximum issue magnitude.
- Total (weekly) issue duration of all violation incidents.
- Total (weekly) issue incidents.
- Magnitude & duration per issue incident.
- (Duration)x(Magnitude) called as Duration-Magnitude Product (DMP) per issue incident: New metric that intends to encapsulate both important aspects of the issue, also defined as "issue's violated area".
- Number of simultaneous issue locations within the grid (applies to the lines and the nodes).

### 3.5.2. Transformer Overloading

In Figure 3.13, the maximum T/F loading at each DG, for 0-100% penetrations of the 3 different LCT conditions and 2 seasons, is depicted. The light rural grid is the only distributional area with no violations in every case. On the contrary, the heavy rural grid's T/F is already overloaded from 50% penetration of combined PVs, HPs, and EVs. The suburban area has the most serious violations, especially the heavy grid, under both seasons and all LCT (loading) conditions, which can reach up to 800% T/F O/L. It is noteworthy that the Winter season always provokes greater violations than Summer, reaching up to double the value in the heavy suburban grid at 100% combined LCT penetrations. Furthermore, the HP loading condition is also at most grids heavier than the EV loading condition. For example, the EV loading condition does not overload the T/Fs of the Urban area, while HP loading can reach up to 3-4 times higher in the suburban areas.

Moreover, a T/F loading decrease is observed at the light suburban grid for EV loading from 50% to 80%, which means that the increased PV generation can cover the increased EV charging demand more efficiently. This phenomenon is not seen for HP loading. The behavior of the slopes is also very important. Saturation can be seen in the light rural grid for all cases from 80% to 100% penetration. We can conclude that for most of the cases at the other grids, the increase presents a rather linear behavior, apart from the exponential increase at the heavy suburban grid for combined 100% penetrations of LCTs.

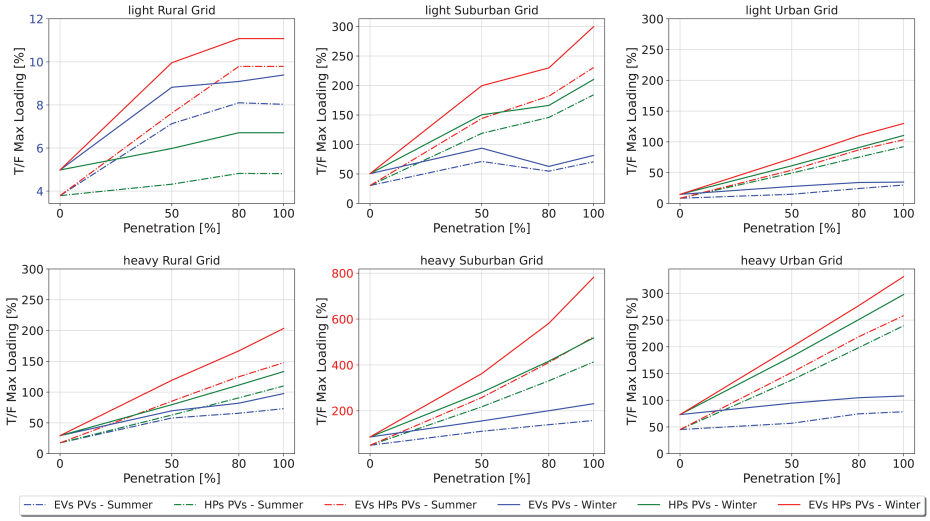


Figure 3.13: Total Transformer Maximum Loading per LCT penetration under different LCT conditions and seasons.

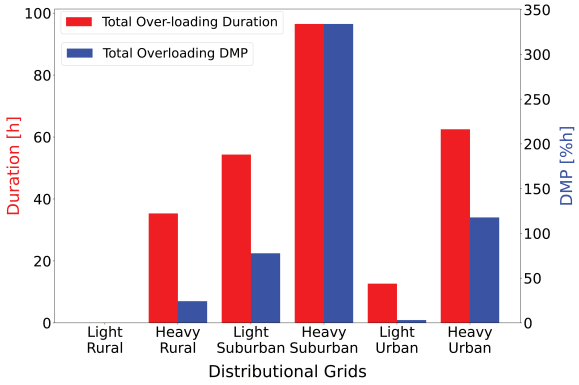


Figure 3.14: Total O/L Duration and DMP under combined PVs-EVs-HPs 100% penetration during Winter.

Figure 3.14 depicts the total O/L duration and DMP (violation area) for the 6 DGs, under 100% penetration of combined PVs-EVs-HPs during Winter. While both problems are crucial in the heavy Suburban area (reaching approximately 95h total violation duration and 330 [%h] DMP), comparing the other grids' respective results with this area, duration is of greater importance for the rest of the grids. However, apart from the light rural area, which is not violated, the transition from light-loaded

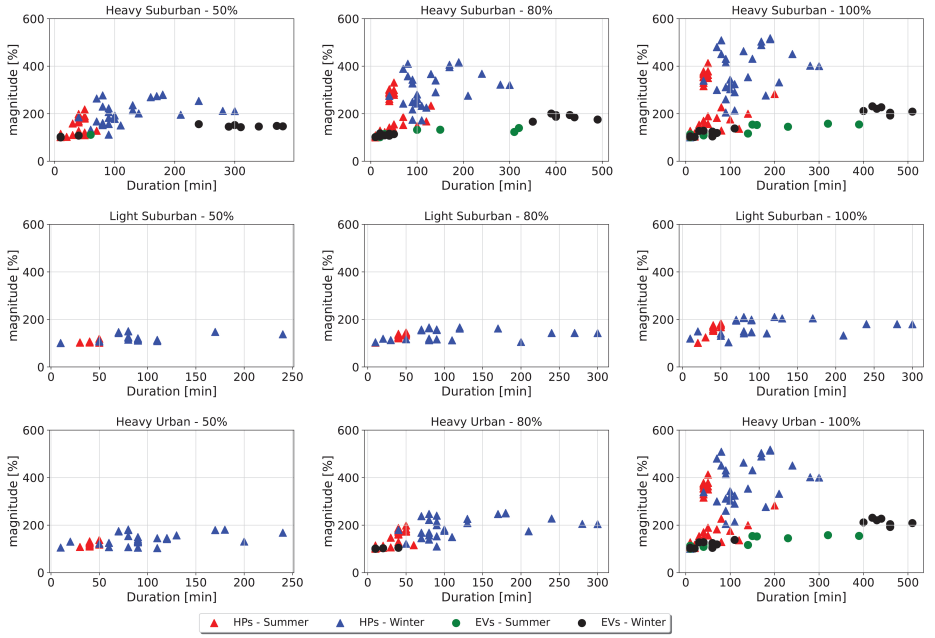


Figure 3.15: Duration and Magnitude of each O/L incident at the 3 most vulnerable DGs under HP & EV load conditions and 50, 80, 100% penetrations.

to heavy-loaded grids increases the DMP more than the total violation duration. Especially for the urban case, the duration increases 4.4 times, while the respective number for the DMP is approximately 38.5.

Finally, Figure 3.15 summarizes the comparison between EV and HP loading in the most vulnerable distribution grids. The magnitude and the duration of each T/F O/L incident are depicted (during both seasons) at 50, 80 & 100% penetrations. The higher grid impact of the Winter over the Summer season and of the HP over the EV loading can also be seen here. All Winter O/L incidents for both loading conditions are shifted to the upper and/or right direction in the plots (higher magnitude and/or higher duration), compared with the respective summer incidents, and are significantly more at all penetrations. Moreover, the heavy urban grid, with 80% penetration, and the light suburban grid are not affected by EV loading. In agreement with Figure 3.14, in the heavy grids, higher penetrations provoke more O/L incidents and prolonged durations rather than higher violation magnitudes. However, in the case of the light urban grid, the violation magnitudes are barely increased during higher penetrations, while there is a notable increase in violation times and durations, which can reach up to 300'. Hence, the significance of the duration in the lighter grids is also seen here.

Last but not least, it is important to mention that when O/L is caused by EV

loading, it is typically seen at the lower-right place in the plots (higher durations - lower magnitudes). On the contrary, violations by HP loading are typically seen at the left place in the plots and are characterized by higher magnitudes. For example, no HP violations surpass 300', while EV violations in heavy grids can reach up to 500'. This is an outcome of the use of real models of the LCTs in our work. EV charging endures for several hours. However, while rated EV charging power is much higher than HP power (at least 11kW as seen in Figure 3.1), people use their HPs more frequently than they charge their EVs. Hence, the fewer but long-lasting O/L times by EV loading are justified. The more frequent HP operation causes notably more O/L incidents. The simultaneous ON-OFF operation of the HPs in the DGs results in remarkably higher O/L magnitudes. However, the violations endure less because the HPs switch to the OFF stage as soon as the desired building temperatures are reached (typically in 30'), which is faster than the typical EV charging duration.

### 3.5.3. Lines Overloading

The maximum grid line loading (extracted from all the lines) is depicted in Figure 3.16 at the 6 grids for 50, 80, and 100% penetrations of combined PVs, EVs, and HPs. Moreover, the total number of overloaded lines, for 100% penetration at every time instant, can be seen as well. The selected results refer to the Winter season since its higher grid impact has already been seen in the previous subsection.

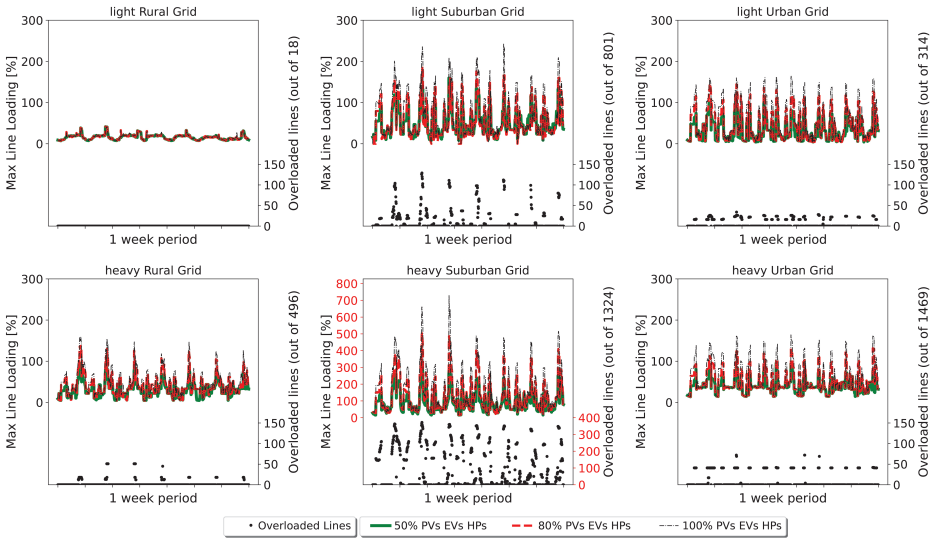


Figure 3.16: Max Line Loading (of all grid lines) under 50, 80 & 100% and Number of Overloaded Lines under 100% penetrations of combined PVs, EVs, HPs during the Winter season.

The heaviest grid impact on suburban grids is again seen in Figure 3.16. The light rural grid is again the only one that does not suffer from O/L, while O/L happens at the heavy rural grid from 80% and can reach up to 60 simultaneously overloaded lines. However, the suburban grids are both overloaded from 50% combined LCTs penetration, with the heavy suburban grid having lines exceeding 700% O/L and reaching approximately 400 overloaded lines (approximately the maximum 30.2% of the total lines). Furthermore, the O/L time incidents are vastly more in the suburban area. It is also very important to note the significance of the simultaneous violated locations at the grids. Similar O/L, in terms of violation times and magnitude, is seen at the light and heavy urban grids for all 3 penetrations. However, the number of simultaneously overloaded lines is double at the heavy grid (maximum 25 lines for the light urban grid, whereas over 60 lines for the heavy one).

A comparison of 100% EV and HP loading at the 3 heaviest grids is presented in Figure 3.17. The O/L DMP of all the grid lines is depicted in Figure 3.17(a), while the total O/L time is depicted in Figure 3.17(b). Most of our previous insights are also strengthened here. Regarding EV and HP loading conditions comparison, HPs also produce worse results regarding the line loading. For example, heavy urban and light suburban grids are minimally or not affected by EV loading, while HP loading overloads the same grids for 35h and 28h, respectively. Moreover, the heavy suburban grid's DMP can reach up to 12%h, which is considerably higher than the respective one by EV loading. The DMP median is close to 4.9%h, and the maximum is more than 6x the related maximum by EV loading, even though some outliers reaching up to 5.5%h can be seen. However, at the same grid, the O/L time of EV loading, in contrast with the respective DMP, can reach up to 48h, only 17.2% less than the O/L time by HP loading. This comes in agreement with Figure 3.15,

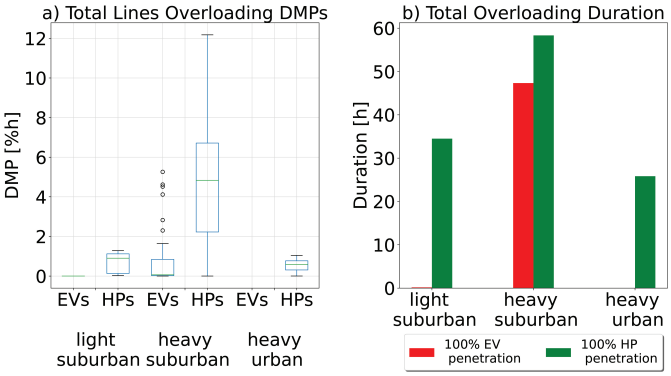


Figure 3.17: Total O/L DMP (a) & Duration (b) at the 3 most vulnerable DGs under 100% of EV & HP loading.

which suggests that EV loading inflicts long-lasting O/L durations, with however low magnitude. Finally, compared with the heavy suburban grid, the total violation duration of the other two grids is more comparable than the respective DMPs, reaching a maximum of only 2x lower. This also strengthens the insight that duration is more significant than the violation area in the lighter grids.

### 3.5.4. Nodes Voltage Deviation: Under-/Over- voltage

OV issues are more likely to appear during the Summer season due to increased PV generation, while UV issues are more severe during the Winter season when HP and EV consumptions are higher. Therefore, the minimum node voltage (of all the nodes) at every time instant for 50, 80, and 100% penetrations of combined LCTs at the 6 DGs during the Winter season is depicted in Figure 3.18. In addition, the maximum node voltage at 100% penetration during Summer is integrated. No OV is seen at any of the 6 investigated Dutch DGs since the maximum node voltage always stays below 1.1 p.u. Furthermore, no UV is seen in the investigated rural and urban areas since the minimum node voltage always stays above 0.9 p.u. However, suburban grids are severely affected by UV. The light suburban grid sees a voltage drop under 0.9 p.u., even from 50% penetration (once), while also once voltage drops under 0.85 p.u. at 100% penetration. Multiple UV incidents are observed in the heavy suburban grid at all 3 penetrations. Reaching up to 0.65 p.u. and 0.42 p.u. at 80% and 100% penetrations, respectively, combined LCTs penetrations vastly distort the node voltage profile at the heavy suburban grid.

The comparison of HP and EV loading regarding UV is summarized in Figure 3.19, which depicts the maximum UV magnitude and number of violated nodes at 50% and 100% penetrations for the heavy suburban grid. The greater grid impact

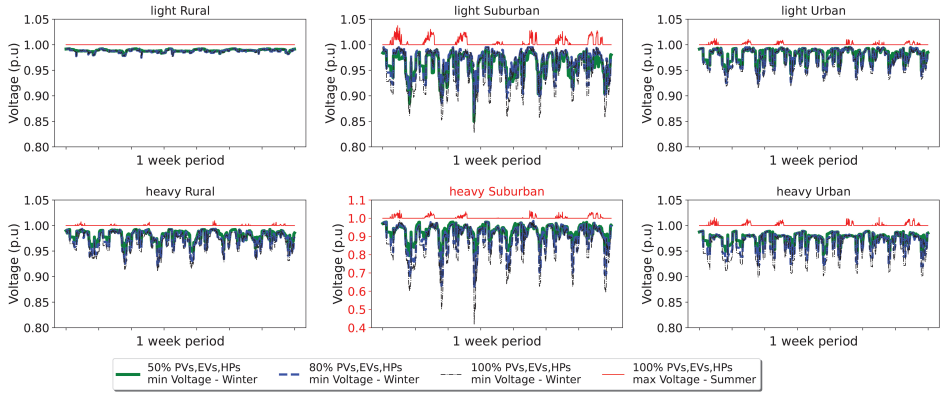


Figure 3.18: Min Node Voltage during Winter under 50, 80 & 100% and Max Node Voltage during Summer under 100% penetrations of combined PVs, EVs, HPs.

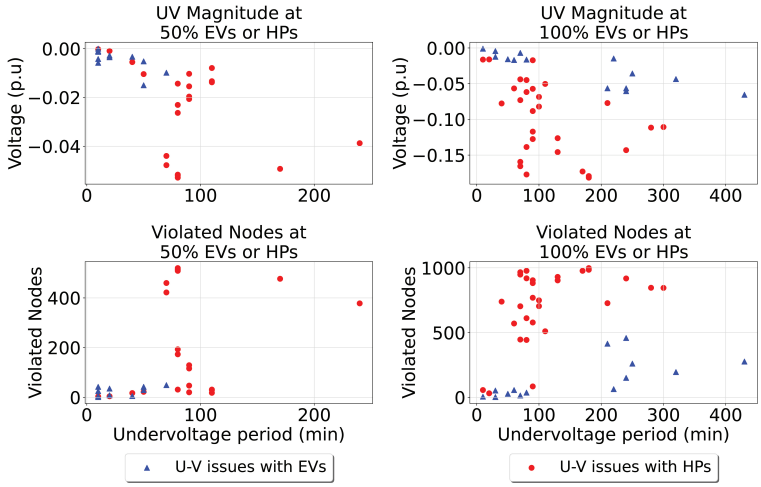


Figure 3.19: Max UV & violated nodes at heavy Suburban grid under 50 & 100% of EV and HP loading.

regarding voltage deviation of the HP loading can also be seen here. At both 50% & 100% loading, HP causes more times UV issues with higher magnitude. For example, 50% HP loading causes UV 21 times with a max drop of 0.058 below 0.9 p.u. and 590 violated nodes. The related values of 50% EV loading are 10 times, 0.018 p.u. max drop and 53 nodes. Additionally, the long-term low-magnitude grid impact characteristic of EV loading compared to HP loading can be seen at 100% loading, where multiple UV times can be seen with duration over 200' up to 400', but with 50% fewer max simultaneously violated nodes and 65% lower maximum voltage drop.

### 3.5.5. Comparison of Grid Impact Issues

In the previous subsections, useful insights have been derived by comparing directly different distributional areas, seasons, and EV-HP loading for every considered grid impact issue. This section is devoted to the comparison of these grid impact issues. In Figure 3.20, the magnitude and duration of the four important investigated grid impact issues are compared regarding the different distributional areas (DA comparison) and LCT integration (LCT comparison), and depending on the utilized grid impact metrics. The definitions "High (H)", "Medium (M)", "Low (L)", and "Zero (Z)" are defined as follows:

- Z: No impact.
- L: Violation occurs only in heavy grids and < 50% magnitude - 3% duration.

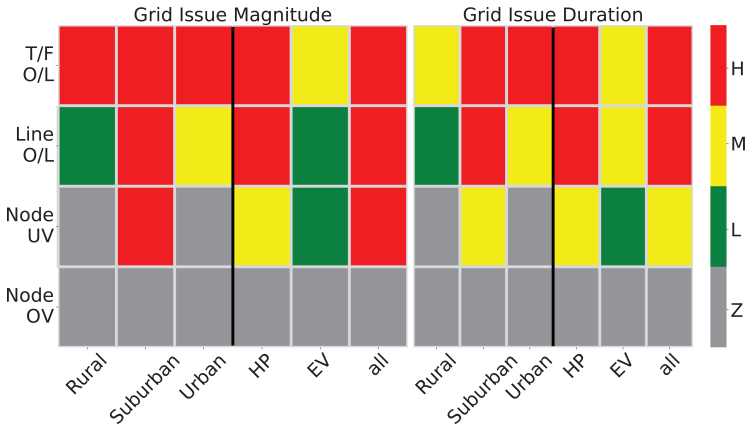


Figure 3.20: Grid Issues Evaluation (Magnitude & Duration).

- M: Violation occurs in heavy and light grids and < 100% violation - 25% duration.
- H: Violation occurs in heavy and light grids and > 100% violation - 25% duration.

Observing the 2 heatmaps, it is concluded that T/F O/L is the most crucial grid impact issue for the 6 assessed grid case studies in terms of both magnitude and duration, followed by lines O/L and, consequently, by node UV in both DA and LCT comparisons. No node OV has been observed in this work.

### 3.5.6. Bottom-up & Top-down Approaches Comparison

Table 3.6: Comparison of grid impact for B-U & T-D approaches during 100% penetration of PVs, EVs & HPs.

| | Transformer (Over-)Loading | | | | Lines Maximum (Over-)Loading | | | | Nodes (Under-)Voltage | | | |
|---|---|---|---|---|---|---|---|---|---|---|---|---|
| | bottom-up | | top-down | | bottom-up | | top-down | | bottom-up | | top-down | |
| | max% | Time% | max% | Time% | max% | Time% | max% | Time% | min p.u | Time% | min p.u | Time% |
| **Winter-rural** | 203.38 | 21 | 132.08 | 10.7 | 159.54 | 7 | 120.96 | 1.6 | 0.911 | 0 | 0.941 | 0 |
| **Winter-urban** | 331.35 | 37.2 | 191.79 | 53.9 | 164.03 | 18.4 | 102.36 | 0.1 | 0.899 | 0.3 | 0.936 | 0 |
| **Winter-suburban** | 781.63 | 57.4 | 395.19 | 83.3 | 728.54 | 51.3 | 306.72 | 69.2 | 0.42 | 44.6 | 0.763 | 48.6 |
| **Summer-rural** | 147.75 | 3.6 | 75.41 | 0 | 132.9 | 1.4 | 79.64 | 0 | 0.936 | 0 | 0.96 | 0 |
| **Summer-urban** | 258.25 | 13.4 | 155.56 | 6.3 | 124.87 | 4.66 | 88.62 | 0 | 0.923 | 0 | 0.962 | 0 |
| **Summer-suburban** | 521.66 | 31.3 | 252.51 | 31.7 | 413.72 | 22.7 | 179.98 | 19.8 | 0.675 | 14.6 | 0.859 | 4.8 |

The analysis in Sections 3.5.2 - 3.5.5 is conducted with the use of physical models from Sections 3.3.2 - 3.3.5 since this investigation constitutes a B-U approach. However, simulations under the same case studies have been performed with the use of aggregated data from Section 3.3.1 for all considered LCTs (T-D approach). The contribution of this subsection is the comparison and cross-validation of the two different approaches, mostly used in grid impact studies, which are summarized in

Table 3.6. In Table 3.6, the total violation magnitude and time in (%) are presented for the transformer loading, lines maximum loading, and node minimum voltage at the 3 different heavy-loaded DGs during Winter and Summer under 100% penetration of PVs, EVs & HPs for the two approaches.

It can be seen that when a B-U approach is used, the magnitude of all grid impact issues is greater for all distributional areas and seasons. Additionally, the highest differences between the two approaches can be seen in the suburban grid. For example, suburban grid lines are by approximately half overloaded in the T-D approach (57.9% and 56.5% reduction for Winter and Summer seasons, respectively). Moreover, a related 49.44% and 51.59% reduction of the T/F loading is also seen in the same grid for the two seasons. Considering that the suburban area is already found to be the most vulnerable one due to a high number of nodes and loads, it can be concluded that the vulnerability of an area enhances the difference between the two approaches. Similar observations can also be made for the nodes' UV issue. On the contrary, different seasons do not seem to have a consistent effect on the comparison of the approaches, since contradictory results can be seen. A higher reduction is seen for the rural area during Summer, while the opposite is seen for the urban area.

However, an interesting insight from this comparison is that the total violation duration does not always follow the same trend as the maximum magnitude. In 3 different scenarios (Urban area - Winter, Suburban - Summer & Suburban - Winter), the total violation duration of grid impact issues is found to be higher in the T-D approach. These observations are marked in red color in Table 3.6. Especially for the suburban area during Winter, this can be seen for all 3 grid impact issues. More specifically, the total duration of the transformer O/L rises by 45.1%, while the O/L duration of the lines rises by 34.9%, which corresponds to approximately 76h and 58.5h, respectively. Moreover, most of these observations belong to the transformer O/L issue.

The above contradiction regarding the violations' magnitude and duration can be justified if we consider the nature of the two approaches. Regarding the T-D

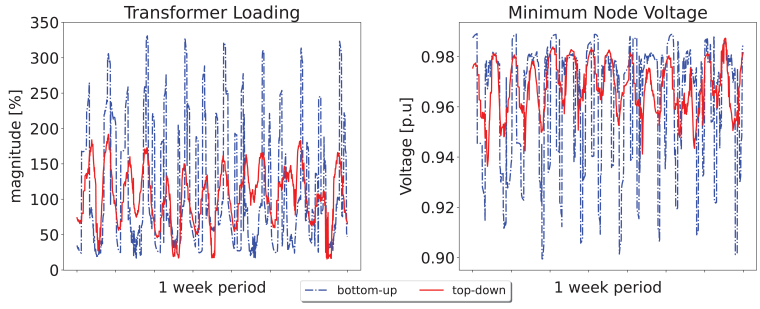


Figure 3.21: T/F Loading & Nodes Min Voltage for top-down and bottom-up approaches (heavy urban grid, 100% LCTs penetration, Winter).

approaches, the use of nationally aggregated data, extrapolated to the appropriate level, contains characteristics of different areas, which enhance sparsity and tend to average results over time. On the contrary, the use of physical models can better capture the effect of simultaneous components' operation and therefore produce higher peaks, spikes, and violations' magnitude. This can also be seen in Figure 3.21, which compares the T-D and B-U results for the transformer loading and nodes' minimum voltage at the heavy urban grid at 100% penetration of LCTs during Winter. In both cases, the B-U results are characterized by more spikes and higher slopes than the more dispersed top-down results, which occupy more area by width. Hence, this can lead to the disappearance of violation if a grid is lightly loaded. However, if a grid is heavily loaded enough, this can lead to higher violation durations. Furthermore, these cases belong mostly to the transformer loading because all of the investigated grids comprise an LV transformer, which handles all the power flow. Therefore, due to the aggregated power flow through the transformer, this can happen more easily for the particular grid impact issue.

However, observing Table 3.6, it must be noted that despite the differences between the two approaches, the main insights from the B-U analysis remain the same. The suburban grid remains the most vulnerable distributional area, the transformer O/L is the most critical grid impact issue, and the Winter season also provokes more significant violations than the Summer season. Therefore, the two approaches are also well cross-validated.

## 3.6. Discussion of Results

### 3.6.1. Summary of Findings

The most important chapter's findings are summarized below, divided into the following categories:

- I: findings that agree with the existing literature.
- II: findings that contradict the existing literature. Existing contradictions in the literature are also integrated here.
- III: new insights.

Regarding Category I, firstly, Winter is considered overall a heavier season than Summer, due to the higher heating and transportation load, in terms of all investigated grid impact issues, which comes in agreement with many works, such as [2] and [48]. On the one hand, this is justified by the higher EV consumption during Winter due to cabin heating and by the higher HP consumption due to lower COPs. On the other hand, it is justified by the low PV generation during Winter. Secondly, mitigation of grid impact issues during increasing combined EV-PV penetrations, such as in [11], has also been observed here in the light suburban grid from 50% to 80% penetration (see Figure 3.13). EV charging, especially at semi-public and public chargers, has a higher chance of time overlap with PV generation, and therefore, mitigation of issues at higher penetrations is expected in

some cases. Finally, as in [46], OV is also less likely to appear for the grids of this thesis in high PV penetrations due to simultaneously high EV and HP loading (Figure 3.18).

The contradictions of this chapter are integrated into Category II, which, at most times, refers to already contradicted findings in the literature. The impacts of HPs and EVs have already been compared in the literature. Increasing EV penetrations were found to cause higher T/F O/L in [60], [62]. EVs were also characterized by higher power peaks in [54]. On the contrary, higher voltage deviations were caused by HPs in [12], while higher T/F and lines O/L appeared in [146]. In this chapter's grid case studies, HPs are found to be a heavier LCT to be integrated into the grid in terms of total violation magnitude, duration, DMP, and number of incidents. This is justified, firstly, by the fact that the thermal comfort of the households was completely respected. Charging sessions are less frequent than the operation of the HPs to keep the temperature of the buildings at the desired level. Secondly, as already explained, the use of component models, which directly model their physical operation, produces denser and simultaneous consumption. On the contrary, T-D works, such as [54] and [60], used extrapolated aggregated data, which are usually more dispersed. This difference heavily affects the consumption results of the HPs, which continuously maintain the desired buildings' temperature.

Suburban and rural grids were found to be more vulnerable regarding voltage deviations and T/F loading in [10]. Line O/L also appeared from low EV penetrations in suburban grids in [42], while rural grids were more violated than urban ones in [6] and [4]. In this investigation, the Dutch suburban areas were vastly violated in all cases compared to the other two areas, while grid impact issues in Dutch rural areas appeared less frequently. The main reason for this contradiction comes directly from the difference in the grid loads. The utilized rural, suburban, and urban grids in this Ph.D. thesis are real LV grids from the Netherlands, where city suburbs are overpopulated (Table 3.4). On the contrary, the rural grids are typically characterized by a lower number of loads. As can be seen in Table 3.4, especially the light rural grid comprises only 3 commercial buildings. This directly decreases the chances and magnitude of violations in rural areas.

Another popular debate in the literature is about the most hazardous grid impact issue. In the grids of this investigation, OV was not seen, while UV was seen less frequently and mostly in the suburban area. On the contrary, O/L, especially of T/Fs, is the most crucial issue under all conditions regarding both duration and magnitude. Authors in [147] and [146] agreed with the superiority of T/F O/L. On the contrary, cable O/L appeared from lower penetrations in [4]. However, voltage issues were more severe than line O/L in [147] and [40]. The absence of OV is because consumption remains high also in Summer since the thermal and transportation comfort of the population is always respected (e.g., reversible HPs). Moreover, it is justified by the rather moderate Dutch Summers with respect to Dutch Winters. The significance of the T/F O/L was expected since all 6 used DGs are fed by an MV/LV T/F, which is burdened with all grid power exchange.

The explained points of category II are already well-known contradictions in the literature. In this chapter, efforts have been made to address them, considering

various effects that can considerably impact their results. Moreover, real grids have been used for this purpose. However, according to the author's point of view, the insights of these comparisons are highly dependent on the characteristics of the different case studies in the various works, such as grid locations, grid characteristics, consumers' behavior, etc. Therefore, they can be very grid-specific and can result in contradictions. For example, especially voltage deviations are highly subject to the parameters of the components of the different grid topologies, e.g., of the distribution lines. In this chapter, a higher level of O/L than of UV incidents is found in many cases, e.g., at heavy rural, light urban, and heavy urban DGs at 80% and 100% LCT penetrations. This is highly dependent on the specification of the Dutch DG case studies, the adequacy of reactive power in the networks, the PF of the loads, etc. Hence, the respective findings should only be carefully considered and not be effortlessly over-generalized for every investigated grid case study.

Finally, regarding category III, this chapter's new findings can be summarized as follows. Observing Figure 3.13, saturation is seen for the T/F (over)loading under increasing penetrations of LCTs in the light rural grid (least population). In contrast, exponential behavior is seen in the heavy suburban grid (the highest population), while linear behavior is observed in the rest of the DGs. Hence, the nature of grid nodes and loads directly affects the behavior of the slope of the T/F maximum loading curve. In Figure 3.13, we can also see that while increasing EV-PV penetrations can mitigate grid impact issues such as T/F overloading, this is not seen in HP-PV penetrations. The long-lasting (often several hours) and high-powered ($> 11kW$) EV charging sessions appear to favor more mitigation than the HP ON time period, which is typically shorter-term and with less power (max of 2-3kWs). Moreover, the HPs are less easily temporarily combined with PVs, because the PV generation is at its highest when the buildings are not occupied.

In several figures, such as Figures 3.14, 3.15, and 3.17, it can be seen that violation duration plays a more important role in the lighter grids than magnitude (in total). However, upon transition to the heavier DGs, the magnitude and the DMP of the violations increase vastly compared with the respective duration. The lower magnitude and DMP of the violations in the lighter DGs are justified by the lower number of integrated loads and LCTs. However, while the number of loads increases greatly in the heavier DGs, their time of operation does not change that much. For example, it has been assumed that in both DGs, people leave and return to their buildings or charge their EVs at home or at work during similar time periods. Therefore, this adds up to the loading of the LCTs, greatly increasing the total magnitude, but the impact on the total violation duration is considerably less.

Furthermore, in Figures 3.15, 3.17, and 3.19, specific violations (T/F O/L and node UV, respectively) by EVs are more likely to have a smaller magnitude and longer duration, in contrast with the HPs. This is also justified by the long-lasting EV charging sessions compared with the ON-OFF operation of the HPs. However, the number of violation incidents under HP integration increases vastly, and the total violation duration exceeds that of EV integration. Finally, according to the author's knowledge, a comparison of B-U and T-D approaches for grid impact studies has

not yet been conducted in the existing literature. B-U approaches have been found to produce violations of higher magnitude due to the simultaneous operation of the components. However, T-D approaches can produce violations with longer-term duration because they tend to average the results over time.

### 3.6.2. Recommendations

In light of this chapter's findings, this Ph.D. thesis takes the initiative to provide the following recommendations. While a yearly grid impact assessment is always highly recommended in grid impact studies, the investigation of worst-case scenarios during Winter should always be prioritized. Additionally, it is recommended that the distribution system operators (DSOs) carefully consider the already existing loading condition of the inspected grids, which can play a vital role in the increase of the grid impact by the LCTs. For example, Dutch suburban grids will probably require a higher level of grid investments and/or a higher level of power control for impact minimization, due to the fact that they are usually overpopulated. Moreover, the mitigation of grid impact issues by the PV-EV combination shows that there is more "room" for power control between these 2 LCTs with the aim of lower grid investments. On the contrary, an efficient PV-HPs combination is more difficult to achieve, and hence, the use of energy storage or of a higher energy storage size is more important in this case.

While this Ph.D. thesis realizes the importance of the investigated grid selection in the results, it is recommended that a high focus is placed on the future HP integration. The higher insulation and the improvement of the energy label of future buildings are highly recommended for the minimization of the grid impact by future electric heating. Similarly, T/F O/L is highly expected for LV DGs that are fed only by an MV/LV T/F, because the T/F handles all the power flow. However, due to the observed contradictions depending on the grid and case study selection, it is advised that all impact issues be investigated under individual or combined LCT integration. In that way, insights can be drawn concerning the connection of LCTs with impact issues for the inspected case, and hence, an appropriate issue weight factor is given for the needed grid investments.

Regarding the fact that the violation magnitude becomes more important in heavily loaded distribution grids, a high focus should be given to the selection of the appropriate simultaneity factor concerning the investigated grid. The simultaneity factor is grid-specific, and the already existing grid loading condition should be considered before its estimation in grid impact studies. Furthermore, as already explained, both T-D and B-U approaches have reverse advantages and disadvantages. Despite their difference, the main insights of this chapter remained similar with the use of both approaches. Therefore, it is advisable that both approaches are followed for every grid impact analysis so that the results are cross-validated.

Overall, this investigation shows that grid impact issues are expected even from 50 % of combined LCT penetrations. Hence, grid-specific power control of LCTs with or without energy storage, operated by the future DSOs, will be indispensable

for future LCT integration so that the needed level of future grid investments is decreased as much as possible.

## 3.7. Conclusion and Future Work

In this chapter, several grid impact issues are addressed in real LV Dutch DGs, caused by increasing LCT penetrations, such as PVs, EVs, and HPs. Despite the dependence of the results on the assumptions and specifications of the case studies, the findings of this chapter can provide grid operators, especially in the Netherlands, with valuable insights about the grid impact from future LCT integration and the various factors that affect it. Comparisons are made between different seasons, distributional areas, LCTs, and LCT penetrations, showing the greater hazards for the Winter season, the Dutch suburban grids, and HP integration. Winter is characterized by higher consumption in the heating and transportation sectors, while the Dutch suburban grids are vulnerable due to the higher number of grid loads. The more frequent use of HPs for heating/cooling provokes a higher grid impact overall, but the longer EV charging periods provoke more long-lasting violations. Detailed LCT physical models have been used in the analysis in order to follow a B-U approach, considering the physical layer of the component operation. The results have also been compared with results from aggregated data from databases, showing that B-U approaches present more pessimistic results than T-D approaches; however, the main insights remain similar. However, higher violation durations can be seen when a T-D approach is used, due to the higher sparsity of the results.

This chapter has introduced a level of uncertainty during the development of the physical models used. Examples of considered uncertainties are the randomization of the orientation of the PV modules, building occupation, distribution of LCTs in the distribution grids, as well as the use of MCS for the generation of the EV charging profiles. However, many more sources of uncertainty exist in grid impact studies, such as different properties of buildings and technologies, that should also be encapsulated. This is considered the main limitation of this chapter. Moreover, the chapter comprises only slow AC EV charging, whereas DC fast charging will also be a main feature of the future of electrified transportation.

# 4

# Grid Impact of Unbalanced Grid Integration of LCTs

*Summary*

Phase unbalance can lead to overheating, suboptimal capacity utilization, and power losses. In continuation of the previous chapter analyzing the grid impact inflicted by balanced LCT grid integration, this chapter analyzes the unbalance impact inflicted by the grid integration of PVs, HPs, and EVs under different combinations and penetration levels. The main novelty of this chapter is the use of different types of real-world distribution grids (rural, suburban, and urban) for the LCT unbalance impact comparison, while simultaneously considering the influence of several unbalance factors; LCT phase connections and grid distributions, the seasonal effect, and the power and consumption levels, the latter of which have been evaluated as mitigation strategies. The results showed that the combined integration of PVs, EVs, and HPs can cause high voltage unbalance, especially in grids with high existing loading. The seasonal effect was the most impactful unbalance factor, intensifying unbalance by the integration of PV-HP and PV-EV combinations during Winter and Summer, respectively. Furthermore, reductions in the power and consumption levels of the LCTs decreased the unbalance total violation duration in a range between 11% and 25% for all distribution grids. Reducing the LCT consumption levels also decreased the unbalance magnitude, which reached up to 15% for the urban grid under 100% HP and PV penetration. Finally, it was found that consumption duration enhances unbalance, such as the peak power levels, because it increases the simultaneity of technologies operating in different phases.

*Outline*

The chapter is categorized as follows. Sections 4.1 and 4.2 comprise the motivation and contributions of the chapter. Section 4.3 integrates the methodology of this chapter, focusing mostly on the voltage unbalance factor modeling, and LCT phase connections, since the modeling and analysis of LCTs and respective data used have already been described in the previous chapter. Section 4.4 includes the case studies and simulation setup. Sections 4.5 and 4.6 comprise the results and discussion, respectively, where the chapter's findings are compared with the existing knowledge and recommendations are given for critical unbalance situations. Finally, Section 4.7 comprises the conclusions and future work recommendations.

This chapter is based on:
Y. Wesseling, N. Damianakis, G. Ram Chandra Mouli and P. Bauer. 'Grid Impact of Unbalanced Phase Integration of PV Generation, Electrified Mobility, and Heating in LV Distribution Grids'. In: *IEEE Access* 13 (2025), pp. 56887–56907

## 4.1. Motivation

As seen in Chapter 2, the grid impact assessment studies of LCT grid integration that investigated load profiles, overloading, and voltage deviations are vastly more than those that studied phase unbalance. Regarding the combined impact of unbalanced LCT integration, the unbalance induced by combined PV-EV integration has been investigated the most. The impacts of EV charging and PV generation on phase unbalance were compared on an IEEE residential DF in [148], and on the Irish LV grids in [43]. The effect of EV charging location was investigated in [37] while different seasons and DG types were compared in [13] and [38], respectively, under increasing EV-PV penetration levels. Moreover, the total imbalance-induced cost was studied in [14], while the impact of unbalance on smart grid performance was evaluated in [44]. On the contrary, the studies of [149] and [150] studied the impact of unbalanced integration of EVs and HPs under various penetration levels, where the importance of newer buildings with higher energy labels was also proven. In addition, the effect of combined integration of PVs and HPs in different DG types was investigated in [51]. Few works have also focused on the impact of the combined integration of PV, EVs, and HPs on unbalance, such as [57], [58], and [69]. In [57], it was shown that the distribution network could tolerate integrating LCTs separately. However, the integration of EV chargers caused significant voltage unbalance due to the large variability in demand compared to HPs. Moreover, the significance of the number of customers in the DFs was shown in [58] while the importance of the customers' location in the grid was identified in [69]. However, none of these works investigated the effect of different types of DGs in combination with the seasonal effect and different power levels when all PVs, EVs, and HPs are integrated under different penetrations.

The existing LCT grid unbalance assessment works with their respective characteristics are summarized in Table 4.1, where:

- "Multi Pen/s" stands for if multiple penetrations were investigated.
- "Comp." stands for the comparisons made, such as between LCTs, grids, or seasons (seas).
- "LCT Grid Dis/tion Effect" and "LCT Power & Cons/tion Effect" denote if the effects of grid distribution and power/consumption levels of LCTs on phase unbalance were studied.
- "Mitig." denotes if any mitigation measure was used, such as DSM, BESS, 3-phase connection (3-ph.), SC, TOU and DR, transformer and cable capacities (T/F and cab. cap), and low temperature (low Temp.) for HPs.

## 4.2. Contributions

It can be seen that only a few phase unbalance assessment works have incorporated all PVs, EVs, and HPs in their study, while season comparison has

Table 4.1: Characteristics of existing grid unbalance assessment works with combined PV-EV-HP consideration.

| Ref | LCT | Multi Pen/s | Comp. | Real Grids | LCT Grid Dis/tion Effect | LCT Power & Cons/tion Effect | Mitig. |
|---|---|---|---|---|---|---|---|
| [44] | PV,EV | | | ✓ | | | |
| [148] | PV,EV | | LCT | | | | DSM |
| [43] | PV,EV | ✓ | | ✓ | | | BESS |
| [38] | PV,EV | ✓ | LCT, grid | | | | |
| [14] | PV,EV | ✓ | LCT, grid | ✓ | | | |
| [13] | PV,EV | ✓ | LCT, seas | ✓ | | | 3-ph., BESS |
| [37] | PV,EV | ✓ | LCT | | ✓ | ✓ | SC |
| [149] | EV,HP | ✓ | | | | | TOU,DR |
| [150] | EV,HP | ✓ | LCT | ✓ | ✓ | | |
| [51] | PV,HP | ✓ | LCT, grid | ✓ | ✓ | | T/F cap, 3-ph., cab. cap |
| [57] | all | | LCT | | | | |
| [69] | all | | LCT, grid | | | | |
| [58] | all | ✓ | LCT | ✓ | ✓ | ✓(EVs) | |
| **Ch.4** | all | ✓ | LCT, grid, seas | ✓ | ✓ | ✓ | EV SC, HP: low Temp. |

only been investigated in [13]. While works such as [51] and [58] have conducted analysis of several months, the phase unbalance was analyzed for the total duration, neglecting the seasonal interrelations of the investigated LCTs and their influence on the phase unbalance in different seasons. Additionally, on the one hand, the effect of the random LCT grid distribution on phase unbalance under multiple penetrations has only been studied in [37], [150], [51], and [58]. On the other hand, comparisons of different types of DGs (e.g., rural, suburban, urban, etc) have only been conducted in [14], [38], [51], and [69]. From these sets of works, only [58] and [69], respectively, comprise the integration of PVs, EVs, and HPs, while none of the existing works analyze them together utilizing real-world grid case studies. Furthermore, apart from different LCT phase connections and LCT grid distribution, adjusting the power and consumption levels of LCTs can have a significant impact on the induced phase unbalance and can potentially be used as an unbalance mitigation measure. From the existing works, only [37] and [58] have studied this effect as a mitigation measure, and only for EVs (SC use in [37]). Finally, most of the studies follow T-D approaches, missing the important benefits of B-U studies, which have already been explained in Chapter 3. Overall, this chapter's contributions are summarized as follows:

- A B-U study that analyzes and compares the phase unbalance inflicted by

EVs and HPs in PV-integrated grids under multiple penetrations, accounting simultaneously for the influence of the season. This kind of study has only been conducted in [13], which, however, comprised only a comparison of PVs and EVs, whereas [58] neglected the comparison of different seasons. On the one hand, different LCT pairs (PVs-EVs, PVs-HPs) inflict different unbalance on DGs due to different simultaneity and operation characteristics, such as duration and power levels. On the other hand, different seasons directly affect the different LCT profiles in B-U approaches, increasing and decreasing power peaks and consumption levels. The study of this combined effect is still missing from the existing literature.

- Investigates and compares the phase unbalance inflicted by LCT integration in different DG types (namely rural, suburban, and urban), utilizing six real-world (Dutch) DGs and considering the existing grid loading and the LCT grid distribution effect. Concerning works that comprise PVs, EVs, and HPs, the effect of LCT grid distribution on phase unbalance has only been investigated in [58], while a comparison of different DG types is still missing from the literature. The study of this combined comparison under the integration of different LCTs in real-world grids can provide significant insights about the most hazardous LCT depending on the type of the investigated DG and its characteristics, and the LCT distribution.
- Evaluates one power-based and one consumption-based mitigation method for EVs and HPs, respectively, analyzing the effect of different LCT power and consumption levels on phase unbalance. The effect of the LCT power and consumption level on phase unbalance has been accounted for only in [37] and [58] (see Table 4.1); however, only concerning the EV mode of operation, e.g., SC. Moreover, the authors in [37] did not consider HPs in their study, while in [58], it was not assessed as a potential phase unbalance mitigation measure.

## 4.3. Methodology

### 4.3.1. Voltage Unbalance Factor (VUF)

In this investigation, the VUF was chosen to quantify three-phase unbalance, which is defined as the ratio between the negative sequence voltage component $V_n$ and the positive sequence voltage component $V_p$, as shown in (4.1) where $V_{ab}, V_{bc}, V_{ca}$ the three phase-to-phase voltages of the three phases $a, b, c$ and $\alpha_p$ the phasor rotation operator [151]. This metric has been chosen, firstly, because it considers both the voltage magnitudes and the voltage angles and is defined as the true definition of voltage unbalance [151]. Secondly, it is the most commonly used metric in the literature, and its utilization for the highest accuracy in estimation is endorsed by multiple studies, such as in [150]. Finally, VUF is the metric used for VU limits definition for Dutch DSOs [152]. It must be noted that the legal phase unbalance limits considered in this work (e.g., 3% maximum VU) apply for the case of the Netherlands, defined in [152, 153].

$$\%\text{VUF} = \frac{V_n}{V_p} 100 \tag{4.1}$$

$$V_n = \frac{V_{ab} + \alpha_p^2 \cdot V_{bc} + \alpha_p \cdot V_{ca}}{3}$$

$$V_p = \frac{V_{ab} + \alpha_p \cdot V_{bc} + \alpha_p^2 \cdot V_{ca}}{3},$$

Where $\alpha_p = 120°$.

### 4.3.2. Load & LCT Phase Connections

The LCT models and respective data input, such as LCT module specifications, weather data, distribution grids, etc., used in Chapter 4 are the same as the ones used in Chapter 3 and are already explained in detail in Sections 3.3.1 - 3.3.5. Hence, for this chapter's unbalanced power flows, the chapter proceeds directly to the LCT phase connections' explanation. Two-phase connection types were considered according to each LCT specification: three-phase WYE connections and single-phase-to-neutral connections, which can be connected to any phase.

#### Phase Connection of Base Load

The phase connections of the base load depend on the building specifications, which were provided together with the DGs by the Enexis groep.

#### Phase Connection of Heat Pumps and PV Systems

Both HP and PV systems are distributed as single-phase components since both LCTs have a 3kW-rated power level, which is below the legal limit for single-phase components [153]. When an HP/PV system is assigned to a single-phase connected building, the LCT is connected to the same phase as the building. In the case of a three-phase connected building, the LCT is connected randomly to one phase.

#### Phase Connection of EV Chargers

Regarding the EV chargers, the number of EV charging phases depends on the rated power levels of the incoming EVs. A 7.4kW-rated power constitutes the maximum limit for single-phase EV charging, which relates to a maximum 32A phase current at a 230V node voltage. The charging of EVs that have a higher rated power (11-22kW) is realized using all three phases. It must be noted that most EV driving patterns have rated charging powers above 7.4kW (11kW, 16kW, or 22kW). Hence, to allow simulations with both single- and three-phase charging, the rated charging power of all 11kW-rated and 50% of the 16kW-rated EVs has been reduced to 7.4kW, increasing the charging time window and keeping the requested energy the same. The charging of the rest of the EVs (50% of the 16kW-rated and all 22kW-rated) was performed three-phase.

## 4.4. Case Studies & Simulation Setup

The case studies of this chapter have been summarized in Table 4.2. Such as in Chapter 3, the same 6 DGs have been utilized, one light- and one heavy-loaded grid per rural, suburban, and urban category, to account for the grid type and existing grid loading influences on phase unbalance. Moreover, the same three LCT combinations have been considered to study the interrelated unbalance impact of PV integration with EV, HP, and EV-HP integration in the DGs under 4 increasing penetrations (0, 50, 80, 100%). In addition, the same LCT grid distribution concept has been used, which is extensively explained in Section 3.4.3. Finally, 4 main unbalance factors are considered: the LCT phase connections, grid locations, Summer and Winter seasons, and LCT power and consumption (cons/tion) levels. The fourth unbalance factor has also been evaluated as a potential mitigation measure, utilizing average charging (power-based measure) and thermal comfort (TC) decrease (consumption-based measure) for EVs and HPs, respectively.

As in Chapter 3, the simulation period has been selected to be one week to capture the intra-weekly effects (different building occupancy, charging frequency, etc.), and the simulation timestep has been set at 1 minute to realize a trade-off between accuracy and computational time. The most computationally expensive simulations (for the heavy suburban grid) remained under 90 minutes, which is considered appropriate for grid scheduling unbalance studies. Moreover, 1-minute simulations can more accurately consider the coincidence factor of LCT operation [10]. Finally, the AC-unbalanced Newton-Raphson load flow calculation method was utilized for the unbalance analysis of all investigated DGs, LCT combinations, and penetration levels. The grid simulations were realized in the DigSilent PowerFactory 2019 environment, while the LCT integration management was performed in the Python 3.9 environment.

Table 4.2: Case Studies for LCT Impact on Phase Unbalance.

| **Case Studies** | | | | |
|---|---|---|---|---|
| Distribution Grids | LCT Comb/s | LCT Pen/s | LCT Unbalance Factors | Mitigation Measures |
| 2 Rural (light & heavy) | PVs-EVs | 0 % | 1.Phase connections | EVs: Avg. charging (power-based) |
| 2 Suburban (light & heavy) | PVs-HPs | 50 % | 2.Grid locations | HPs: TC decrease (cons/tion-based) |
| 2 Urban (light & heavy) | PVs-EVs -HPs | 80 % | 3.Seasons: (Winter/Summer) | |
| | | 100 % | 4.Power-Cons/tion levels **(for mitigation)** | |

## 4.5. Results

This section comprises this chapter's results concerning the LCT unbalanced grid integration under the case studies and scenarios summarized in Table 4.2 that belong to publication [26].

### 4.5.1. Phase Connections: Unbalance Factor (UF) 1

#### Introduction of Phase Connections

Firstly, the VU was studied by randomizing the LCT phase connections at their initial locations, which were obtained from [25], to compare the results with the related results of the balanced integrations and to be used as a base case study. A uniform probability function in a Python environment was used to randomly select the integrated LCT profiles from their respective families.

#### Phase Connections - Results (1): Unbalance Magnitude & Duration

Figure 4.1 depicts the maximum and average VUF in the 6 DGs for 0%, 50%, 80% & 100% LCT penetration levels and all LCT combinations after randomizing their phase connections. No phase unbalance is seen in the light rural grid under any circumstances. For the urban grids and the heavy rural grid, the maximum VUF is below 3%. The heavy suburban grid exceeds 3% for 80% and 100% LCT penetration even for the PV-HP scenario, reaching a maximum VUF of 7.5%, whereas in the light suburban grid, the VUF slightly overpasses the threshold of 3% at 50% and 100% combined penetration levels.

These observations show that VU depends heavily on the type of DG and the existing grid loading conditions summarized in Table 3.4, and it generally increases

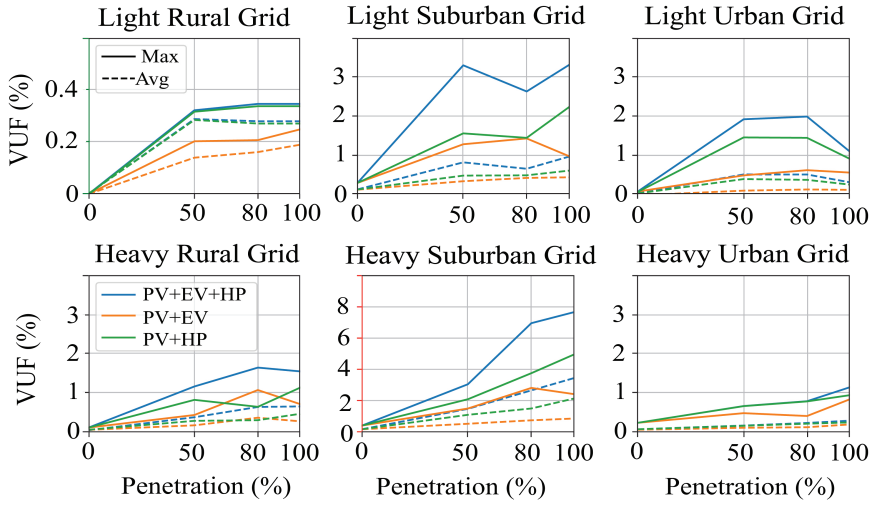


Figure 4.1: Maximum and average VUF in the 6 DGs for all LCT penetration levels and combinations in the initial locations.

with higher LCT penetrations. For example, the light-loaded rural grid maintains low VU for all levels of LCT penetration. Even for 100% penetration, the maximum VUF stays below 0.35%. However, the heavy rural grid reaches a maximum of 1.6% VUF at 100% combined LCT penetration, 5x higher than the light counterpart. Similar observations have been made for all depicted light and heavy suburban grid scenarios. Moreover, the significant influence of the existing grid loading can be seen not only by comparing the VU inflicted by the same LCT combinations on different DGs but also by comparing the combined PV-EV-HP integration with the partial PV-EV and PV-HP integrations in the same DG. It can be seen that in the suburban grids that are already characterized by higher existing loading than the rural and urban grids, the combined PV-EV-HP can increase the VUF by a factor up to 100% compared to the PV-EV and PV-HP integrations, which are not seen in the other types of grids.

However, a decrease in VU in increasing penetration levels can also be seen in several cases, e.g., from 50% to 80% penetration for the light suburban grid or from 80% to 100% for the light urban grid. This is justified because integrated LCTs at higher penetration levels can even out LCTs at lower levels if the extra load is added to a different phase (or extra generation is added to a phase with existing loads).

Regarding LCT comparison, the highest VUF was observed for the PV-EV-HP integration scenario, as expected for all DGs. However, for almost all DGs and LCT penetration levels, VU is higher for HP integration than for EV chargers. Especially for both the light rural and heavy urban grids, it can be seen that the VU in the PV-HP-EV integration scenario is very close to the VU in the PV-HP scenario. This can be justified, firstly, by the fact that HP operation lasts longer than the fewer EV charging events to continuously maintain the building's thermal comfort, as seen in Figure 3.9. Secondly, all HPs are single-phase LCTs due to low power rating, while multiple EV charging sessions are realized with $> 7.5kW$ charging power and use all 3 phases for EV charging.

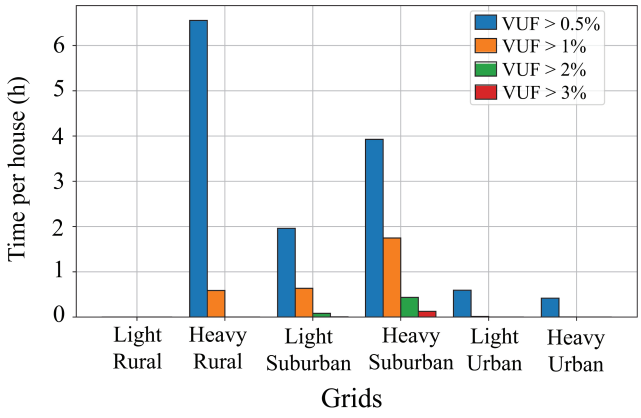


Figure 4.2: Duration of maximum VUF exceeding certain levels for 100% PV, EV & HP penetration.

As the Dutch electricity code obligates DSOs to maintain a VUF lower than 3% for 95% of the time at the point of common coupling [153], the duration of VU exceeding certain levels was investigated. The hourly duration of 0.5, 1, 2 & 3% VUF that every grid experiences for 100% combined LCT penetrations is depicted in Figure 4.2. The heavy-loaded grids experience more long-lasting VU than their lighter counterparts. While the light rural grid experiences no VU, the heavy rural grid is characterized by a $VUF > 0.5\%$ for more than 6 hours during the week. However, the VUF remains under 1%. The heaviest VUF of the heavy suburban grid is also seen here, which is the only grid exceeding 3%.

### Phase Connections - Results (2): Grid Comparison

In Figures 4.1 & 4.2, it is observed that in contrast with the rural and suburban grids, the light urban grid shows a slightly higher VU than the heavy one such concerning magnitude (more than double for 50% and 80% penetrations), as also concerning duration. Therefore, the investigation proceeded to grid analysis to justify this observation.

Figure 4.3 depicts the amount of energy consumption in the 6 DGs regarding the distance from the MV/LV T/F that connects the DG with the main grid. Moreover, Figure 4.4 visualizes the relative distance (0-1) at which 50% of the total feeder energy is consumed inside the radial DFs in the grids to show which DFs are more heavily loaded at their first or their second half. In this regard, nearly all consumption occurs at the furthest point of the loaded DFs of the light urban grid, apart from DFs 3 and 4, which are empty. This can also be seen for the light urban grid in Figure 3.10, which depicts the grids' spatial visualizations. In contrast, 50% of energy consumption occurs at around 60%-80% feeder length in most of the radial DFs of

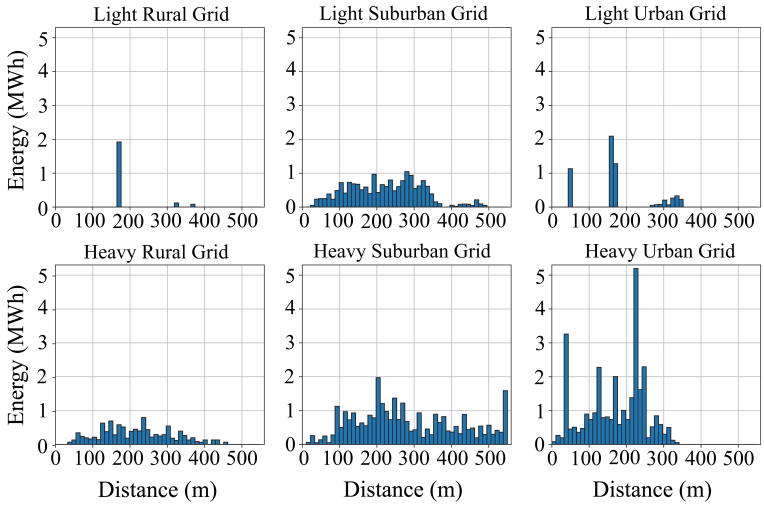


Figure 4.3: Energy Consumption amount at the distance from the MV/LV Transformer of the DGs.

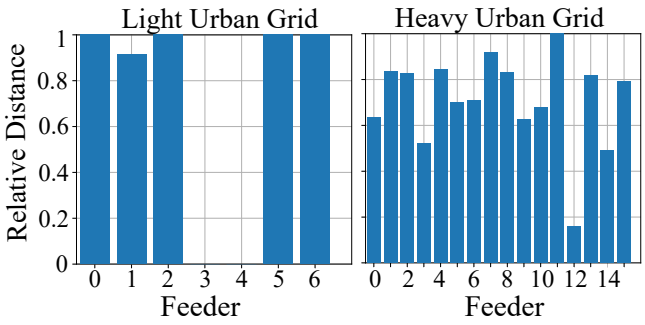


Figure 4.4: Relative feeder-length point where 50% energy consumption occurs at the two urban grids' radial DFs.

the heavy-loaded urban grid. Hence, consumption at longer distances from the T/F contributes to the increase of VU (heavy suburban grid). However, the distance inside the radial DFs has an equally significant effect.

Moreover, information about the percentage of loads situated at radial DFs is provided in Table 4.3 to strengthen the above conclusion. The rural and urban grids consist only of radial DFs, while the suburban grids service loads through a combination of meshed and radial DFs, as can also be seen in Figure 3.10. It is also seen here that 100% of the loads in the light urban grid are placed in radial DFs. The reasoning for the effect of distance on unbalance in the radial DFs comes from the fact that voltage deviations are more severe when higher consumption occurs at the end of the feeders due to the higher impedance in the distribution line. Additional randomly phase-connected loads that simultaneously draw power from different phases can provoke a higher VU at distant nodes, which are characterized by a higher voltage drop.

### 4.5.2. LCT Grid Locations: Unbalance Factor 2

#### Introduction & Contribution of LCT Grid Locations

Secondly, after the VU impact analysis of random LCT phase distribution, the work proceeded to study the effect of LCT grid distribution. In this regard, 10 different LCT distributions were simulated for each of the 0, 50 & 100% penetration levels in

Table 4.3: The load share per grid in radial feeders

| **Grid** | % **Loads in feeders** |
|---|---|
| Light Rural | 100% |
| Heavy Rural | 97.8% |
| Light Suburban | 19.5% |
| Heavy Suburban | 78.3% |
| Light Urban | 100% |
| Heavy Urban | 99.7% |

order to show the effect of the LCT locations, which have not yet been studied for different real-world grid case studies (rural, suburban, urban). For each of the 10 iterations, the LCTs were also here increasingly inserted in the DGs according to the increasing penetration levels, meaning that every next penetration level comprises the LCTs of the previous penetration level in their previous grid locations.

### LCT Grid Locations - Results

The maximum VUF results of the above iterations for all DGs and LCT combinations are presented in Figure 4.5. Similar to the results of the previous section, the light rural grid maintains the lowest VU, while the heavy suburban grid experiences the highest VU. Irrespective of the LCTs used, the median maximum VUF increases with increasing LCT penetration. Moreover, the VU in the PV-EV-HP scenarios is closer to the VU in the respective PV-HP scenarios in most grids. Hence, the previous observation that EV integration has a smaller impact on the VU than HP integration is also strengthened here and is independent of the LCT locations. In addition, the light urban DG suffers from an equal or slightly higher VU than the heavy urban grid despite its lower amount of loads, as also expected from the previous grid analysis. Finally, the already highly loaded suburban grids present a much higher VUF during combined PV-EV-HP integration (up to 300% increase compared to the other two partial combinations), an observation that was also made in Figure 4.1.

Furthermore, the VUF variance is higher in the light-loaded grids than in their heavy-loaded counterparts. This can be justified by the smaller amount of loads and LCTs in these DGs that affect the VUF results more significantly according to their location in the grid feeders. On the contrary, a random re-distribution of a vast amount of loads at the nodes of a DG changes more moderately the status quo of the grid situation. This can be seen especially for the light rural grid, which, with a median maximum VUF of 0.48% at 50% PV-EV-HP penetration, is characterized by a variance of approximately 0.2%. Hence, it can be concluded that the VUF of LCT grid distribution is less impactful than expected. This is justified by the fact that all the insights from Section 4.5.1 concerning the comparison of different DGs, LCT combinations, and penetrations remain the same, and the most notable impact has been on the variance of the VUF results regarding the grid type and loading.

Regarding further comparison between EV and HP integration, Figure 4.6 depicts the median VUF of the PV-EV and PV-HP 100% integration scenarios against the median VUF of the 100% PV-HP-EV integration scenario for all DGs. The interpretation of the figure is that the distance of the VUF markers of the one combination in the Y axis (e.g., PV-HP) from the dashed grey identity line depends on the influence of the other combination (e.g., PV-EV) and vice versa, as compared with the PV-EV-HP combination in the X axis. Hence, if the influence of the PV-EV integration were negligible, the markers of the PV-HP scenario would lie on the identity line. Therefore, the vertical distance to the identity line can be interpreted as the impact of the omitted LCT. For most of the grids, the PV-HP integration VUF markers are closer to the identity line, indicating that the impact of EVs on unbalance is notably lower. For the heavy suburban grid, the outliers suggest that they contribute greatly in combination.

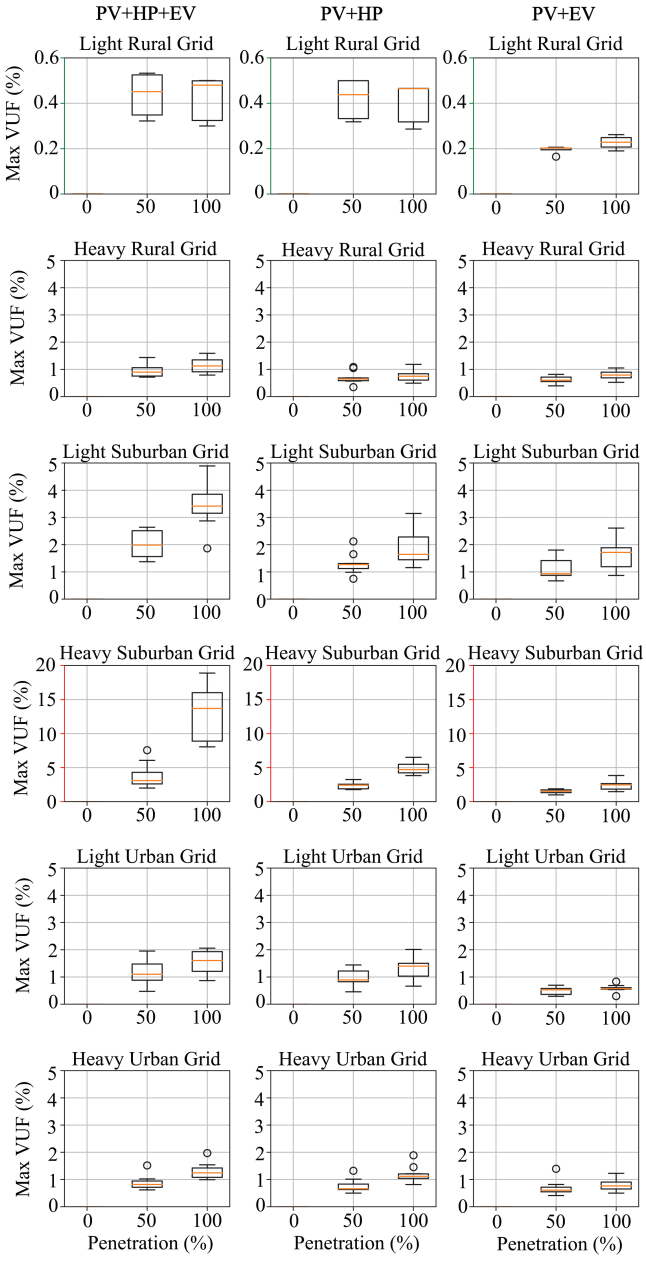


Figure 4.5: Maximum grid VUF for 10 iterations of randomized LCT locations for PV-HP/PV-EV/PV-HP-EV combinations under 0%, 50% & 100% penetrations.

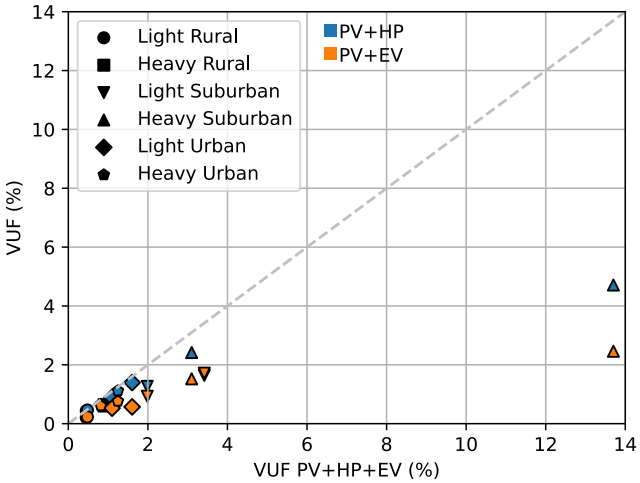


Figure 4.6: The median VUF of the different scenarios (PV-HP and PV-EV) plotted versus the median VUF of the scenario PV-HP-EV under 100% penetration.

### 4.5.3. Seasons: Unbalance Factor 3

#### Introduction & Contribution of Seasons

Thirdly, the focus has been placed on showing the effect of different seasons on the VU impact of LCT integration. As already shown in Section 4.2, a phase unbalance impact comparison due to the integration of different LCT combinations under different seasons, e.g., Summer and Winter, is still missing from the existing works that comprise PVs, EVs, and HPs. More specifically, this chapter has already conducted a comparative analysis of EVs and HPs in different PV-integrated grids during Winter in Sections 4.5.1 and 4.5.2. However, the seasonal effect has a strong influence on the profiles of all 3 LCTs since, on the one hand, the PV generation highly increases in Summer, and on the other hand, the EV and HP consumption highly increase in Winter. Hence, the Summer season can significantly alter the Winter findings by the comparative unbalance assessment due to the combined integration of PVs-EVs and PVs-HPs. For this case study, in order to avoid the effect of the LCT phase and grid distributions, the LCTs were distributed again back to their initial grid locations and phases for a fair comparison with the respective winter results in Figure 4.1.

#### Seasons - Results

Figure 4.7 shows the maximum and average VUF during a Summer week for the considered LCT combinations, penetration levels, and DGs. Regarding the combined PV-EV-HP integration scenarios, a slightly lower VU can be seen during Summer for most of the grids. For example, the maximum VUFs for the light and

heavy suburban and urban grids for the Winter season are 3.2, 7.8, 1.1 & 1.1%, respectively, while the respective numbers for the Summer season are 3, 6.2, 1 & 1%. However, the PV-EV integration produces similar or higher VU than PV-HP integration in most penetrations, apart from the light rural and urban grids. The reasoning behind this difference is twofold. Firstly, the HP consumption decreases significantly during Summer, especially for the Dutch grid case studies, which are characterized by a more moderate ambient temperature. This was also concluded in [24] and Chapter 3, for which the same LCT profiles were utilized. Hence, PV-HP integration scenarios result in lower unbalance than in the Winter season. EV consumption also decreases due to the lack of cabin heating. However, this decrease amounts to 30% while HP heating consumes approximately 50% more energy than HP cooling.

Secondly, PV generation is assumed to be integrated into all the simulated scenarios. PV generation coincides with a higher duration of EV charging than HP cooling because the buildings are mostly unoccupied when PV power is generated, since most of them are residential. Concerning balanced power flows, coincident LCT operation is mostly beneficial for better grid impact mitigation. However, it can become detrimental for unbalanced power flows if LCTs inject and withdraw power from different phases simultaneously, increasing phase unbalance. Therefore, considering also the higher PV generation during Summer (see Figure **??**), and hence higher phase power difference, PV-EV integration scenarios result in higher VU compared to Winter.

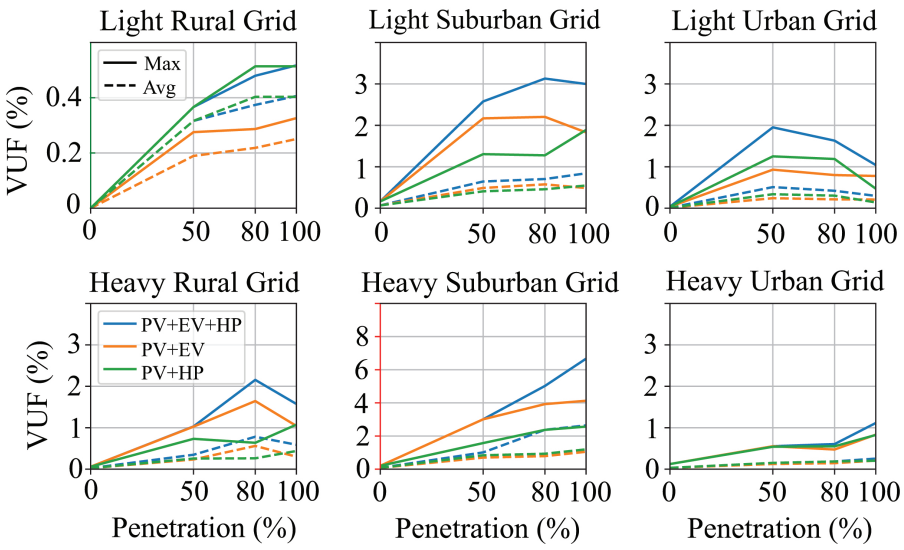


Figure 4.7: Maximum and average VUF for 0, 50, 80 & 100% penetration of PV-EV, PV-HP & PV-EV-HP LCT combinations during Summer.

### 4.5.4. LCT Consumption & Power Levels: Unbalance Factor 4

#### Introduction & Contribution of LCT Consumption & Power Levels

Finally, the LCT power and consumption levels have been studied as final VU factors for EV chargers and HPs, respectively. This part was realized for different LCT locations and 0%, 50% & 100% penetration levels, however, only for the Winter season. The maximum and mean VUF metrics were utilized for the VU analysis since they are correlated with the impact of the peak power and consumption on unbalance, respectively.

Averaged EV charging has been used to study the effect of power levels on VU inflicted by EV grid integration. In averaged charging, the power levels are decreased since the charging power is averaged over the parking time of each vehicle for all EV charger profiles while keeping the energy consumption the same [154]. This is shown in (4.2) where $P_{ch}, E_{req}, T_p$ are the charging power, requested energy, and parking time, respectively. It must be noted that the CV charging region was not considered in the average charging.

$$P^t_{ch} = E_{req}/T_p \tag{4.2}$$

On the contrary, the HP consumption levels have been lowered with a slight decrease in the building thermal comfort to study the effect of the LCT consumption levels on voltage unbalance inflicted by HP integration. This was realized by decreasing the desired temperature interval from [21°C, 23°C] to [20°C, 21°C] in the HP heating model presented in Section 3.3.3. Hence, new lower-consumption HP heating profiles were generated and distributed in the initial phases and locations of Section 4.5.1 for the Winter season to cancel out the effect of the other VU factors. While average EV charging affects the LCT power levels, decreasing the desired building temperature affects the LCT consumption levels. This is because while it decreases the total HP consumption needed to keep the thermal comfort of the buildings, the power levels are hardly changed since the utilized HPs are ON-OFF and not variable-speed. Moreover, since the VUF was tested for the Winter season, the desired temperatures have been decreased to reduce the heating consumption. To apply the concept during Summer, the desired temperatures should be increased to reduce the HP cooling consumption.

#### LCT Consumption & Power Levels - Results

This case study examines the effect of different power and consumption levels of the integrated LCTs on VU. This case ("Low Power Mode" in Figure 4.8) has been investigated only for Winter and three DGs: light- and heavy-loaded urban grids and the heavy-loaded suburban grid. Figure 4.8 depicts the VUF magnitude results of the "low power mode" on the right with the original results (named as "normal") on the left, which are taken from Figure 4.1. Moreover, Figure 4.9 shows the respective comparison concerning the duration of unbalance with VUF above certain levels at 100% PV-EV-HP penetration.

Varying power and consumption levels for EV charging and HP heating, respectively, have varying effects on the VUF violation magnitude and duration. On

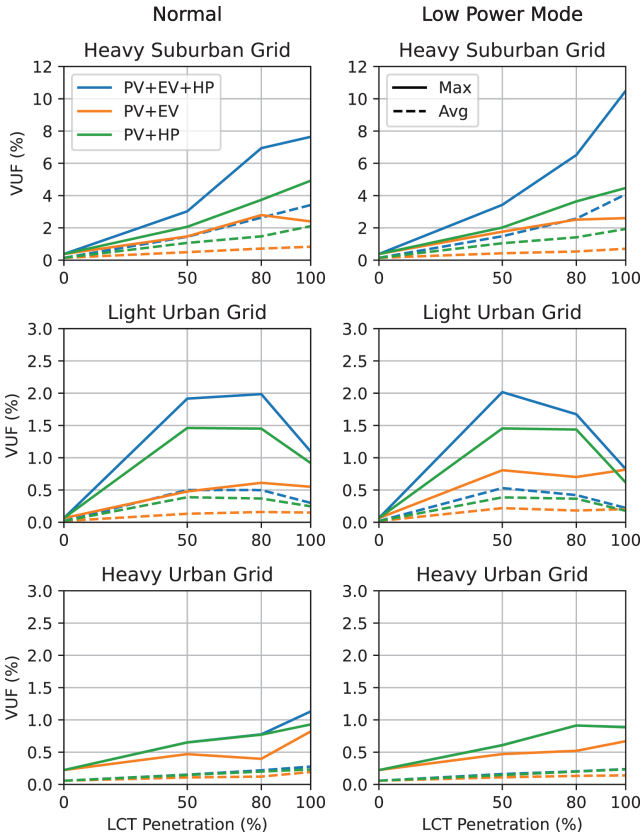


Figure 4.8: Average and maximum VUF comparison at low and original power modes for all LCT combinations and penetrations in 3 DGs.

the one hand, the duration of the unbalance is decreased for all DGs in a range between 11% and 25% regarding all VUF levels, as seen in Figure 4.9. On the other hand, Figure 4.8 shows that the effect on the VUF magnitude varies per combination. Concerning the PV-HP integration scenarios, a lower VUF can be seen (up to 15% decrease) regarding both maximum and average VUF when the HP consumption levels are decreased. However, concerning the PV-EV integration scenarios, an approximate 60% VUF increase is observed in the light urban grid (VUF reached 0.8% from 0.5%) while a 30% decrease is seen in the heavy urban grid, both at the 100% penetration level. Moreover, a VUF increase of 20% is observed for the combined PV-EV-HP scenario at 100% penetration level at the heavy suburban grid (VUF reached 10% from 8%).

As discussed, this case study has different effects on HP operation and EV charging. While energy consumption for HP heating is decreased due to lower thermal comfort, the effect on the power peaks of the ON-OFF HP operation is minimal. This is because while the ON HP duration is decreased, the power peak

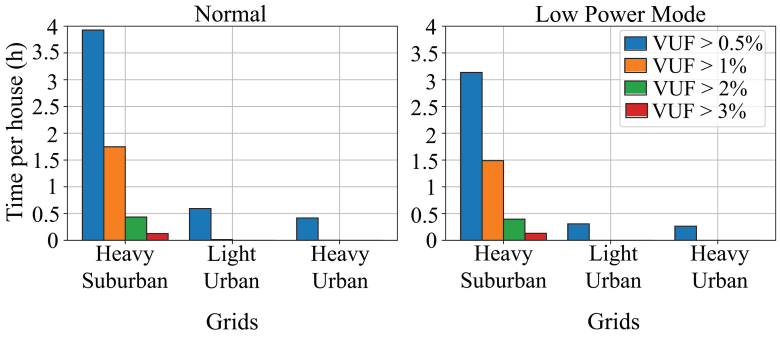


Figure 4.9: Comparison of the duration of the maximum VUF at low and original power modes for 100% PV-EV-HP penetration in 3 DGs.

itself remains the same since it depends on the COP and the ambient temperature. On the contrary, average EV charging results in the following opposite effects. While the power peaks of EV charging are reduced, the duration of the EV charging is increased since the EV is charged during the whole parking time, because the total amount of requested energy remains the same. Hence, on the one hand, simultaneous PV peak power injections and EV peak power withdrawals during uncontrolled charging (normal mode) can result either in a higher VUF if they occur on different phases or in a lower one if they occur on the same phase. On the other hand, the prolonged EV average charging (low power mode) can reduce the VUF due to reduced power peaks, but also increase the probability of a higher VUF in time due to increased simultaneous operation with the PVs. Therefore, it can result in contradictory observations. For example, a lower maximum VUF is observed at 80% penetration of the combined PV-EV-HP integration in the heavy suburban grid (6.1% instead of 7%) during the mitigation mode, whereas VUF increase is noted at 100% penetration (10.1% instead of 7.9%).

### 4.5.5. Evaluation of LCT Consumption and Power Levels Variation as Phase Unbalance Mitigation Measures

This investigation also evaluates varying the LCT consumption and power levels as a potential unbalance mitigation measure for HPs and EVs, respectively. The reasoning behind the investigation of such strategies is, firstly, their simplicity in implementation and, secondly, the potential for mitigation without the installation of further assets, such as ESS. Such unbalance mitigation measures were only investigated in [37]; however, only for EVs, since HP integration was not considered.

While simple, the two implemented control strategies managed to have some notable effects on VU mitigation. Firstly, the duration of VUF violation was decreased up to 25% for all investigated DGs, which is especially important for the heavy-loaded suburban grid, which suffers from the highest VU levels. Secondly, decreasing the LCT consumption levels could effectively decrease the VU up to

15%, although the mitigation measure was not effective enough to reduce the VUF of the heavy suburban grid below the 3% legal limit. Finally, decreasing the LCT power levels at the expense of consumption duration was found to have uncertain results concerning VU mitigation; while the VUF will be decreased during the previous charging window, it can be increased during the extended window when the operation of PVs and EVs overlaps in different phases. This is also the reason why the VUF magnitude could result in higher or lower; however, the duration of the violation is always decreased. Hence, it can be seen that while peak power levels are important for phase unbalance decrease, the consumption duration is also significant. A mitigation measure that affects both should be implemented only with the coordination of the phase connections of the LCTs. For example, the PVs and EVs must inject and withdraw power, respectively, to and from the same phase.

Overall, this chapter was mainly devoted to quantifying the VU impact of the grid integration of PVs, EVs, and HPs, addressing different combinations, penetration levels, and influencing factors. Additionally, the chapter proceeded to evaluate the fourth unbalance factor as a mitigation measure due to its simplicity and lack of need for additional assets and investments. It has effectively reduced the VU duration in all investigated cases and grids. Moreover, while it had some notable mitigation results in half of the investigated cases (PV-HP scenarios), its effectiveness was proven uncertain in all scenarios that included EVs. While the further investigation of phase unbalance mitigation is out of the scope of this chapter, more sophisticated power-control measures (such as SC and DSM), which can also alter the LCT phase connections in real-time, should be investigated to reach a final conclusion about the potential of phase unbalance mitigation without the need for additional assets (e.g., ESS) or grid reinforcements (e.g., higher cable area, etc.). In this regard, emerging phase-changing EV chargers, such as the Zaptec EV charger, can assist in the implementation of the power control strategies proposed above in practice.

## 4.6. Discussion of Results

### 4.6.1. Summary of Findings

Compared with the knowledge in the existing literature, the findings of this chapter have been distinguished into the following three categories:

I) Findings in agreement.
II) Contradictory findings.
III) New findings.

#### I) In agreement:

The significance of the phase unbalance impact due to LCT integration has also been shown in this work. Especially the unbalance impact increase due to combined LCT integration has been shown in multiple studies such as in [13], [38] for PVs and EVs, in [149], [150] for EVs and HPs, in [57], [58] for PVs, EVs, and HPs, etc.

For example, the authors in [13] showed that the VUF exceeded 2% even from 20% combined penetrations of PVs and EVs for 28% and 31% of the simulation

time during Winter and Summer, respectively, reaching a maximum value of 10% under 80% combined penetrations. Moreover, a higher VUF was found during Summer compared to Winter for all studied penetration levels, showing higher violations that could reach up to 40%. This comes in agreement with this chapter's observation about higher VU during Summer in the PV-EV scenarios. However, the authors in [13] did not include HPs in their investigation to show the HP contribution combined with the seasonal influences to VU. Furthermore, VU violations were investigated in [38] in rural and suburban grids during increasing combined EV and PV penetrations. While no violations were found for both grids, the suburban grids showed lower unbalance reserves for further EV and PV integration when cables were considered for distribution lines in both grids. However, the investigated networks, while developed in coordination with the German DSOs, did not constitute real DGs. Additionally, the authors in [150] found more pessimistic results, showing VUF violations even from 20% combined penetrations of EVs and HPs, which reached a maximum value of 12%. However, no PV integration and season comparison were performed in the study, neglecting the interrelations of the EVs and HPs with the PV generation, while simultaneously considering the impact of the seasonal effect.

In this investigation, the combined integration of PVs, EVs, and HPs provoked the highest VU compared to the other LCT combinations, as was also seen in [57]. Compared to the maximum predicted VUF of 4.1% under 100% combined penetration in [57], the VUF results for the Dutch suburban grids are even more pessimistic, reaching a value up to 8%. This is justified by the overpopulation that characterizes the Dutch suburban grids; in contrast, an adapted network was investigated in [57]. Furthermore, while seasonal comparisons were ignored in [57], the authors investigated the effect of the cable size, showing that a 30% cable size decrease can result in 10% higher VUF; however, only the 100% penetration level was investigated in the study. Furthermore, a higher amount of violations was also identified in [58] during the combined integration of all PVs, EVs, and HPs. However, the authors showed how balanced power flows underestimate violations concerning voltage deviations, loading utilization, and energy losses, without directly measuring the unbalance in the investigated grids. For example, it was shown that voltage violations begin only at 90% PV-EV-HP penetration levels during balanced power flows, while the respective penetration level was only 40% during the case of unbalanced power flows. Moreover, the effects of different seasons and distribution grid types on phase unbalance were not quantified.

Moreover, the strong effect of the existing grid loading was also proven in this chapter by comparing light- and heavy-loaded grids of the same type. This comes in agreement with the findings in [150], where two Scottish urban grids (one large- and one small-sized) were compared, predicting a 100% higher maximum unbalance for the first one. Furthermore, the general influence of the increasing penetration levels on the VU increase was also evident in this analysis since, in most cases, 100% LCT penetration had the most detrimental effect on unbalance, with 50% penetration level being the most important intermediate step for all studied LCT combinations. Such findings agree with the insights about the penetration level importance in the

studies of [13, 14, 37, 38, 43], [149, 150], [51], and [58] for combined integration of PVs-EVs, EV-HPs, PVs-HPs, and PVs-EVs-HPs, respectively.

Finally, the importance of the grid topology on VU was also proven in this study. It was seen that DGs that comprise a high number of radial feeders are more prone to VU due to higher voltage deviations by loads located at the feeders' ends (away from the T/F). This comes in agreement with similar observations made in [37], where the furthest point from the distribution T/F suffered from the highest unbalance. Furthermore, similar observations were made in [69], where the authors compared the contributions to voltage violations of PVs, EVs, and HPs, analyzing them both temporarily and spatially during unbalanced power flows. It was found that the customers located after the 40% feeder length caused the highest amount of violations.

### II) Contradictory findings:

Firstly, regarding grid comparison, suburban grids were found to be more vulnerable to VU, and they were the only DGs exceeding the legal limit of 3% VUF. On the contrary, LCT integration was less hazardous for rural and urban grids. This contradicts the findings in [14] where the authors calculated the phase residual current in urban, suburban, and rural grids of the UK, finding an average value of 100A, 60A, and 40A, respectively. Hence, while the UK suburban grids were found more prone to unbalance than the UK rural grids, the urban grids were found to be the most vulnerable. Moreover, the authors in [38] found the German rural grid more vulnerable to unbalance than the investigated suburban grid (even from 50% of combined PV-EV penetrations); however, only when they considered overhead distribution lines for the rural grid. In contrast, as explained before, better results were seen for the rural grid when cables were considered for the distribution lines of both grids. In this chapter's case studies, the higher vulnerability of the suburban grids is justified by their overpopulation in the Netherlands, which is multiple times higher than the Dutch rural and urban grids. Moreover, the studied heavily loaded rural grid in this investigation showed an x2 times higher VUF than the respective heavily loaded urban grid, which is in agreement with the comparison between rural and urban grids in [14] and [51]. The above comparisons between the findings of this analysis and the existing knowledge show the strong influence of the characteristics of the DGs of different countries, and hence, the results should not be generalized regarding grid-type comparisons. Therefore, a study investigating VU in the same grid types of different countries could provide more conclusive insights concerning this matter.

Secondly, regarding LCT comparison, the HP integration always provoked higher VU than the EV integration during Winter under all penetration levels. This finding contradicts with results in [150], where EV charging was found to be more hazardous for VU than HPs. More specifically, the VUF reached a value of 7% and 3% under a 100% penetration level of EVs and HPs, respectively. However, the authors did not consider the seasonal effect and PV integration in their study, neglecting the seasonal LCT interrelations. Moreover, similar insights were also drawn in the two investigated LV DFs in [57], finding a maximum VUF of 2.9% and 3.4% during

100% EV integration and 2% and 2.5% during 100% HP integration for the two DFs, respectively. However, while PVs were included in this study, their co-integration was not considered in the above comparisons. Moreover, only one developed network was investigated in [57], and concerning the seasonal influence, the authors used Summer PV profiles and Winter EV profiles to investigate the worst-case scenario. In contrast, in this study, the higher impact of HP integration on VU was justified by the fact that HP operation lasts longer than the fewer EV charging events, since this Ph.D. thesis modeled the HPs to continuously maintain the thermal comfort of the occupied buildings. Thus, this is also a direct effect of utilizing detailed models of the LCTs for the generation of their profiles (B-U studies) instead of using nationalized data (T-D studies) or more simplified formulas. Moreover, residential HPs are all single-phase connected in contrast with EV charging, which is performed single-phase only for rated power $< 7.4kW$. Finally, distinguishing Summer and Winter profiles for all LCTs, it was found that different seasons affect the inflicted unbalanced results differently by different LCT combinations; hence, while Winter is more hazardous for PV-HP integration, the opposite applies for Summer and PV-EV integration.

Thirdly, regarding season comparison, a slightly lower overall VU was seen during Summer compared to Winter for the combined PV-HP-EV integration cases. From the works in Table 4.1, only the work in [13] compared explicitly the unbalance results between Summer and Winter, and found the Summer season as the most hazardous for VU by LCT integration. However, the authors in [13] did not include HPs in their investigation, which were found in this investigation to have a crucial effect on the total provoked unbalance between different seasons. If the results in [13] are compared with the results from the PV-EV scenarios, investigating the same LCTs, the findings of the two studies come into agreement.

Finally, taking everything into account, it can be concluded that these findings are highly case-specific and dependent on the characteristics of the study and should not be generalized over works with highly different case conditions. Nevertheless, they are valuable for DSOs in the Netherlands and should be taken into consideration for other countries with similar influencing factors, such as grid characteristics and weather conditions.

### III) New findings:

The key new insights of this chapter are summarized as follows:

1) While the VUF generally increases during increasing LCT penetration levels, VU mitigation effects were observed for all LCT combinations in some penetration levels after 50% penetration. While this was seen in some works for the PV-EV combination ([148], [37]), it wasn't seen again for the PV-HP combination (e.g., in [51]) or the PV-HP-EV combination ([57], [58], [69]). In this study, these mitigation effects without the use of any measures were seen because integrated LCTs at higher penetration levels can even out LCTs at lower levels if the extra load is added to a different phase.

2) The main effect of the LCT distribution unbalance factor concerns the unbalance variance, which was higher in the light-loaded grids than in their

heavy-loaded grid counterparts. That means that the unbalance can deviate higher from the average value when LCT locations are altered in lighter-loaded grids; however, the insights from DG and LCT comparisons remained the same.

3) In balanced power flows, coincident operation of generators and loads (e.g., PVs and EVs) would most probably be beneficial for the mitigation of violations. On the contrary, coincident LCT operation can become detrimental to unbalanced power flows if LCTs inject and withdraw power from different phases simultaneously. This is the reason why the VU provoked by PV-EV integration was considerably increased during Summer, when PV generation is higher, while this was not observed for PV-HP integration; PVs and EVs overlap much more than PVs and HPs.

4) Concerning the unbalance factors' comparison, the seasonal effect was found to have a much stronger influence on the VU than the LCT grid distribution. While PV-HP integration caused a higher VUF than PV-EV integration during Winter at all penetration levels and DGs, PV-EV integration approximated and, in some levels, surpassed PV-HP integration during Summer (due to insight 3). On the contrary, LCT grid distribution, while increasing the unbalance variance, did not alter this study's main insights.

5) Consumption-based (thermal comfort decrease) and power-based (average charging) mitigation measures decreased the total duration of unbalance violations in a range between 11% and 25%.

6) Regarding the consumption-level effect, the utilization of thermal comfort decrease as a mitigation measure notably decreased the VUF (up to 15% decrease). Mitigation of unbalance was seen in some works by power-based measures. For example, the authors in [37] reduced the unbalance from 5% to 3.5% using EV SC. This work is the first study in which a consumption-based measure (heating consumption decreased by a decrease in thermal comfort) provided notable phase unbalance mitigation. However, it did not manage to reduce the VUF below 3% for the heavy-loaded suburban grid.

7) Average charging caused contradictory results (increase and decrease) concerning the magnitude of VU violations. This was justified by the fact that average charging reduces the charging power levels while simultaneously increasing the charging duration (it expands the duration during the whole parking period). Hence, according to insight 3, the simultaneity of EV charging with other LCT operations (e.g., PV generation) can be increased and provoke higher VU. Hence, more sophisticated power control strategies (such as phase-changing SC) should be investigated for unbalance mitigation.

8) From insights 3 and 7, it is concluded that the consumption duration is as important as peak power levels for unbalance. Hence, decreasing the peak power levels at the expense of duration (e.g., average charging) is not always effective.

### 4.6.2. Critical Voltage Unbalance results & Recommendations

From the above analysis, it is concluded that uncontrolled phase integration of LCTs such as PVs, EVs, and HPs in future DGs can cause major phase unbalance issues, and several critical situations have been identified.

1. Due to the high existing loading and overpopulation, suburban grids are highly vulnerable, especially at high combined penetrations of PVs, HPs, and EVs. It is important that, especially in heavily loaded grids, such as in suburban areas, the LCT phase connection planning is coordinated beforehand during the LCT grid installations.

2. A high number of loads at the end of radial feeders can highly jeopardize phase unbalance even in grids with lower loading, due to higher voltage deviations compared with the nodes closer to the distribution transformer. Hence, high loading at the end of radial feeders should be avoided if possible; otherwise, the installation of additional assets, such as ESS, could benefit high voltage deviations and, consequently, phase unbalance.

3. Simultaneous LCT operation can be critical for phase unbalance when LCTs operate in different phases. This was seen for EV integration during Summer due to higher overlap with PV generation (PV generation lasts longer during Summer), and it was also endorsed with the average EV charging results (average charging increases the duration of the EV charging). Hence, power-injecting and power-withdrawing LCTs whose operations overlap, such as PVs and EVs, respectively, should be considered to be connected at the same phase to reduce the impact on phase unbalance. Furthermore, emerging phase-changing chargers can assist in solving unbalance by managing the LCT phase connections in real time.

4. HP integration can critically affect phase unbalance, especially concerning heating during Winter seasons, when HP consumption levels are higher and are operated for a longer period during the day. Moreover, most residential HPs are single-phase devices. A first step in varying LCT power and consumption levels has been taken in this study, which resulted in mitigating effects; however, to a limited extent. More sophisticated power/consumption control and DSM solutions capable of utilizing different price mechanisms should be investigated further for potential unbalance mitigation without the use of additional installations and/or grid reinforcements. Additionally, the further adoption of LCT 3-phase connections can further reduce phase unbalance.

5. Moreover, grid investments and reinforcements (e.g., higher transformer capacities, larger cable cross-section areas, etc) are also recommended for unbalance mitigation if the less costly strategies are not adequate to keep voltage unbalance below the legal limit of 3%.

6. Finally, it was seen that different grid types, seasons, and weather conditions favor or deteriorate the inflicted unbalance of different integrated combinations of LCTs. In addition, the power injections and withdrawals by simultaneous LCT operation can magnify the unbalance issue further and are strongly dependent on the social adoption of LCTs and user behavior. Therefore, the developed mitigation solutions can highly differ and must be adapted to the needs of each DG and its characteristics, accounting simultaneously for a yearly analysis.

### 4.6.3. Limitations

Taking everything into consideration, this chapter's limitations can be summarized as follows:

Firstly, as in Chapter 3, the analysis has incorporated a level of uncertainty in the grid unbalance assessment with the use of MCS for the generation of different EV charging profiles, PV orientations, and building occupancy profiles. Moreover, the Meteonorm weather data are averaged over the duration of the last 10 years. However, there are a lot of other sources of uncertainty that were not considered in the analysis, such as LCT modules, building types, grid specifications, etc.

Secondly, on the one hand, the utilization of the Dutch DGs contributes to the unbalance analysis of different grid types and LCT distributions, considering real-world data and not synthesized test feeders. On the other hand, it decreases the level of generalization in some of the previously explained findings. The same also applies to the use of the Dutch weather conditions. Therefore, the contradictory findings in Section 4.6.1 regarding DG and LCT comparisons apply mostly to the country of the Netherlands and at a level for countries with similar grid characteristics and weather conditions. However, other findings in Section 4.6.1, such as the importance of the grid topology, comparisons between different unbalance factors, the importance of the seasonal effect, the mitigation potential of LCT power and consumption levels, etc, can be generalized for grid unbalance assessment studies and are independent of the study's grid and weather conditions.

Thirdly, as already discussed, the alteration of the LCT power and consumption levels has been investigated as a mitigation solution for the grid unbalance. However, only one power-level solution (average charging) and one consumption-level solution (decrease of buildings' thermal comfort) have been included in the study. Further solutions in this regard should be studied in order to conclude about the effectiveness of LCT power and consumption levels on their inflicted unbalance.

Finally, this investigation did not consider social acceptance factors in the analysis. For example, the LCT distribution was realized homogeneously, while in reality, people living in higher-income areas tend to adopt new technologies more easily, leading to a skewed distribution. Moreover, a household with a PV system is more likely to also own an EV and/or an HP; however, in this work, a building may own a PV rooftop and not an EV or an HP, and vice versa.

## 4.7. Conclusion and Future Work

This chapter has followed a B-U approach to evaluate the inflicted phase unbalance by the integration of PVs, EVs, and HPs on different types of Dutch LV DGs (rural, urban, and suburban) under different combinations and penetration levels. Focus has been placed on the quantification of the influence of 4 main unbalance factors on the interrelated unbalance inflicted by the different LCT combinations: the LCT phase connections and grid distributions, the seasonal effect, and the LCT power and consumption levels. The use of the latter as a mitigation measure has also been evaluated.

The Dutch suburban grids were found to be the most vulnerable concerning the

future phase unbalance. Moreover, the seasonal effect significantly enhanced the provoked unbalance by PV-HP and PV-EV integration during Winter and Summer, respectively. While LCT grid distribution showed a notable effect on the unbalance variance, it was less significant on the overall unbalance observations concerning grid and LCT comparisons. Regarding the mitigation strategies, the decrease in the LCT consumption level decreased the magnitude of the unbalance violation and, remarkably, its duration. Finally, it was found that the increase of consumption duration can be as detrimental to unbalance as the power levels, because it can increase the simultaneity factor of LCTs that operate in different phases.

In future work, a higher level of uncertainty in the analysis is recommended to study its impact on the unbalance results (e.g., different LCT and building properties, etc.). Furthermore, the use of more real-world rural, suburban, and urban DGs, preferably from a different country than the Netherlands, is proposed to ensure the generalization of results. Finally, it was seen that the effect of LCT power and consumption levels as mitigation can be contradictory. While further investigation of phase unbalance mitigation is out of the scope of this chapter, further power and consumption control strategies with the use of phase-changing devices (such as EV chargers) are recommended for future work to conclude about the effectiveness of mitigation measures without additional assets or reinforcements for phase unbalance.

# 5

# Power Control of LCTs and Energy Arbitrage

*Summary*

As explained in Chapter 2, power control of PVs, EVs, HPs, and BESS is important for energy arbitrage, avoiding grid violations. This chapter develops a two-level mixed integer quadratic programming (MIQP) power control model for day-ahead and real-time scheduling, where the contribution of flexible loads (e.g., V2G use) and BESS is compared, considering the effect of different grid types, grid sizes, seasons, and battery degradation. An empirical degradation model has been linearized and incorporated, including cyclic and calendar aging. Results showed that V2G is less used than the BESS in small grids due to higher power losses, especially when degradation is considered. However, BESS use decreases as the grid size increases, while PV self-consumption and the likelihood of V2G increase due to the higher number of loads. Moreover, the grid type also has a notable impact on the power control results since commercial grids need much less grid energy and use less V2G due to lower flexibility. On the contrary, they are capable of using the BESS for revenues more due to the higher power window. The seasonal effect also has a strong influence, since the available PV generation is preferred compared to BESS or V2G use. Finally, while degradation costs are much lower than the power control costs in smaller grids, affecting only the BESS power levels, they become more important in larger grids and can significantly alter the energy arbitrage decisions. Finally, the model has been compared and validated against other benchmark and control models, showing cost reductions of up to 5.81% and 30.6%, without and with BESS use, respectively.

*Outline*

The chapter is categorized as follows: The motivation and contributions are summarized in Sections 5.1 and 5.2. Sections 5.3 and 5.4 comprise the concept and modeling of power control, respectively, hence the modeling of the BESS/EVs, buildings, nodes, degradation, and objective function. Section 5.5 integrates the utilized case studies and scenarios, together with the explanation of the used grid scenarios and data input. Results are summarized in Section 5.6 while Section 5.7 integrates the summary of findings, comparison with existing works, and validation of the PCS and battery degradation models. Finally, Section 5.8 concludes the chapter.

This chapter is based on parts of:

N. Damianakis, G. R. C. Mouli, Y. Yu and P. Bauer. 'Coordinated Power Control of PV Generation, Electric Mobility and Electric Heating in Different Grids'. In: *2024 IEEE 10th International Power Electronics and Motion Control Conference (IPEMC2024-ECCE Asia)*. 2024, pp. 2082–2087

N. Damianakis, Y. Yu, G. R. C. Mouli and P. Bauer. 'Impact of Uncertainties and Price of Robustness in receding-horizon EV Smart-Charging'. In: *2024 IEEE 21st International Power Electronics and Motion Control Conference (PEMC)*. 2024, pp. 1–6

N. Damianakis, G. R. C. Mouli and P. Bauer. 'Power Control of PV Generation, Electric Mobility, Electric Heating and Battery Energy Storage'. In: *Applied Energy* (2025). Under Review

## 5.1. Motivation

As Chapter 2 initiated, several PCSs exist in the literature that exploit the flexibility of ESS and flexible loads (e.g., EVs and/or HPs), with various objectives, such as minimum cost, peak shaving, DR, voltage control, etc. The authors in [155] showed the potential of using BESS to cover PV generation intermittency; however, they did not consider the effect of residential loads that are present on the grid. Multiple residential loads were considered in [156], [157], and [117], where the sizes of PV and BESS were optimized in coordination to maximize self-sufficiency, relieve the grid, and leverage cost-effective tariff incentives. On the contrary, the use of different hybrid ESS (HESS) in EMSs is analyzed in [158] and [159] to show the benefits of using HESS for RES integration and high-frequency loads coverage. In addition, the enhanced overall performance and longer lifespan of HESS in EMSs of islanded microgrids with high RES penetration are studied in [160], [161], and [162]. However, the above works studied the effect of ESS flexibility in PCSs without considering flexible loads, such as EVs and HPs.

ESS, PVs, and EVs with V2G capability were integrated into the rule-based HEMS of [163] and tested under different price mechanisms. The benefits of the synergy between PV generation, EVs, and BESS were also compared to the individual integration of technologies for further cost decrease and grid resilience enhancement while simultaneously covering the base load demand in [164] and [165]. Furthermore, uncertainties present in power control, such as EV driving patterns, weather conditions, and energy prices, were effectively managed in the 2-stage stochastic dynamic approach in [122]. Stochastic approaches for power control of PVs, EVs, and ESS can also be found in the HEMSs of [166] and [167] and the smart EV charging stations of [168] and [169], using handling techniques such as Markov decision processes or the Conditional Value at Risk. A goal programming approach was followed in [170] for the energy management of a smart building equipped with PVs, EVs, and BESS, while different DR programs were implemented in the developed residential HEMS of [171], which achieved a reduction of electricity cost and peak-to-average ratio by 25.55% and 36.98%, respectively. Regarding grid-level studies, a district EMS (DEMS) that managed RES, ESS, and EVs was formulated in [172] and solved deterministically and stochastically to reveal the effect of uncertainties in power control. Voltage management was provided by the same LCTs in the multi-agent DG in [173], while the flexibility provided by regenerative braking energy combined with PVs and ESS was studied for the integrated rail system and EV parking lot in [174]. In [175] and [124], the authors also considered the effect of battery degradation, where centralized and decentralized strategies were compared concerning the EMS performance. Moreover, battery degradation was also accounted for in the studies of [176] and [177], which investigated the potential of the PV-EV-ESS cooperation for ancillary services provision. However, none of the above ESS-integrated studies exploited the flexibility of HPs.

Regarding HP integration in ESS-integrated studies, PVs, HPs, and ESS were combined in the building-level MPC studies of [178] and [179], and the deep-learning study of [180] for energy arbitrage, showing significant cost savings. Furthermore, [181] compared PV-BESS-gas boiler and PV-BESS-HP-TESS configurations in

smart buildings concerning total cost and uncertainty management. Different ESS control strategies for self-consumption increase were studied in [182], and a carbon and cost analysis was conducted in [183] for PV-HP-TESS-integrated EMSs. HPs and TESS/BESS were also coupled using DSM strategies for peak reduction and uncertainty management in the district-level studies of [184] and [185] and the grid-level study of [186], where different energy demands were considered for residential, commercial, and industrial areas. PVs were also integrated into the EMSs of [187] and of a virtual power plant comprising 67 dwellings in [114], while their contribution to ancillary services provision in multi-energy communities respecting the thermal comfort of the residents was shown in [188]. The synergy of thermal and electrical storage was also considered in [123] and [189], showing the benefits of their coupling in multi-carrier microgrids when scheduling under uncertainties. However, EVs were not accounted for in all of the above HP/ESS-integrated investigations.

EVs were also included in the multi-objective study in [190] where cost optimization and peak shaving were studied in combination. Multi-objective HEMS and building EMS (BEMS) were developed in [191] and [192], respectively, which control PVs, EVs, HPs, BESS, and non-flexible loads. Considered objectives were the total cost, thermal and habit discomfort, EV range anxiety discomfort, max PV self-consumption, etc. However, the battery degradation effect was ignored in these studies. On the contrary, an optimal trade-off between energy and battery degradation costs was searched in the MPC study in [116], but the seasonal effect was not considered. Finally, both seasonal and degradation effects, as well as uncertainty management, were incorporated in the 2-stage model in [193], showing that BESS and EV degradation costs are not negligible compared to the total energy cost. Finally, two building-level PV-EV-HP-BESS control works can be found in [194] and [195], respectively. The effect of the energy price and peak demand tariffs on the power control decision-making was studied in [194], while the authors in [195] showed the importance of adaptation of the MPC models according to deviations of uncertain variables from their forecasted values.

Nevertheless, while the studies in [116, 190–195] considered PVs, EVs, HPs, and ESS solutions, they are all HEMSs or BEMSs. Such an investigation was conducted in the multi-objective robust work in [196], where the cooperative optimization of three integrated energy systems was found via a Nash bargaining problem. However, consideration of V2G was left out of the study. A smart-grid analysis that comprised PV generation, HPs, EVs, and TESS can be found in [197], which showed that a coupled control system could effectively improve PV self-consumption by 77% and notably decrease cost. These findings are in agreement with [116], which showed a 34% decrease in electricity cost by integrating PV, EV, HPs, and a BESS into an HEMS, or with [198], which showed the significance of EV fleets for PV self-consumption increase. However, the degradation effect was ignored while the study remained on a microgrid level comprising 3 buildings. Additionally, a grid-level analysis was conducted in [199], which studied a robust EMS against uncertainties and various uncertainty budgets. However, effects such as the seasonal, degradation, and grid size effects were not incorporated.

Table 5.1: Characteristics & Contributions of Grid-level ESS-integrated Power Control Studies.

| Ref | PVs | EVs | V2G | HPs | Battery Degradation | ESSs vs Flexible Loads | Seasons | Grid Size | Grid Type |
|---|---|---|---|---|---|---|---|---|---|
| [184] | | | | ✓ | | | ✓ | | |
| [186] | | | | ✓ | | | ✓ | ✓ | ✓ |
| [189] | ✓ | | | ✓ | | | | | |
| [185] | ✓ | | | ✓ | | | ✓ | | |
| [187] | ✓ | | | ✓ | | | | | ✓ |
| [123] | ✓ | | | ✓ | ✓ | | | | |
| [188] | ✓ | | | ✓ | | ✓ | ✓ | | |
| [114] | ✓ | | | ✓ | | ✓ | ✓ | | |
| [173] | ✓ | ✓ | | | | | | | |
| [124] | ✓ | ✓ | | | ✓ | | | | |
| [174] | ✓ | ✓ | | | | ✓ | | | |
| [176] | ✓ | ✓ | | | ✓ | | | | |
| [172] | ✓ | ✓ | ✓ | | | | | | |
| [175] | ✓ | ✓ | ✓ | | ✓ | | | | |
| [177] | ✓ | ✓ | ✓ | | ✓ | | | | |
| [20] | ✓ | ✓ | ✓ | | ✓ | | ✓ | | |
| [196] | ✓ | ✓ | | ✓ | | | | ✓ | ✓ |
| [199] | ✓ | ✓ | ✓ | ✓ | | | | | |
| [197] | ✓ | ✓ | ✓ | ✓ | | | ✓ | | |
| **Ch.5** | ✓ | ✓ | ✓ | ✓ | ✓ | ✓ | ✓ | ✓ | ✓ |

## 5.2. Contributions

Table 5.1 summarizes the reviewed ESS-integrated power control studies. Because this work develops a grid-level PCS, and the grid size is very important to its findings, only grid-level studies are integrated in Table 5.1. Firstly, a grid-level power control work that comprises PVs, EVs, HPs, and ESS, and considers multiple influencing factors (e.g., different grid types, grid sizes, and seasons) for energy arbitrage without grid violations is missing. Secondly, comparing the flexibility of ESS and flexible loads (e.g., V2G-capable EVs) in a PCS has not been investigated in studies that consider all the above LCTs. Thirdly, the effect of battery degradation on power scheduling has not yet been investigated in such grid-level power control studies. However, the consideration of battery degradation is especially important in grid-level studies that perform energy arbitrage, since the accumulated degradation costs from the BESS and the multiple EV batteries can result in comparable numbers to the total power control cost. Therefore, a two-level mixed-integer quadratic programming (MIQP) model for both day-ahead and real-time scheduling of PVs, EVs, HPs, and BESS has been developed and tested under different seasons and grid scenarios. The contributions of the chapter can be summarized as follows:

- Develops a two-level MIQP power control of PV generation, EVs, HPs, and BESS, and investigates the contribution of BESS and flexible loads, such as V2G, to energy arbitrage without grid violations, which has not yet been investigated in earlier works.

- Applies the power control for day-ahead scheduling and real-time scheduling with uncertainty management, investigating the influence of different seasons, grid types (residential, commercial), small and large grid sizes, and battery degradation, which is still missing from the existing literature.
- Develops and integrates a linearized battery degradation model into the power control, which is based on a physics-guided semi-empirical battery degradation model that accounts for calendar and cyclic aging and considers various degradation influencing factors, such as time, temperature, C-rate, and throughput. The developed linearized battery degradation model is effectively incorporated into the power control, achieving high accuracy with significantly lower computational burden than the original highly non-linear semi-empirical model. According to the author's knowledge, this has not yet been done in the existing MI-Linear-P (MILP)/MIQP grid-level power control works.

To highlight more the contribution of this chapter, the integration of PVs, V2G-capable EVs, HPs, and BESS has not yet been investigated in multiple grid-level studies, because the greatest challenge is to encompass and optimize all the LCTs with reasonable accuracy and computational time, and provide proof that the PCS model can work effectively even when the testing grid size increases. In this work, the PCS managed to consider multiple modeling details that are often ignored in the literature and still remained MIQP to be solvable in a reasonable computational time. Moreover, its effectiveness is shown both in small grids comprising only a number of buildings and in larger grids comprising more than 100 buildings, proving its scalability. On top of that, co-optimization of detailed battery degradation and energy arbitrage in such large grids burdens even more the computational expense of such models. This chapter is the first study that has contributed to face this computational challenge, model, and solve such a power control problem. Furthermore, stationary BESS and flexible loads constitute competitive LCTS regarding their contribution to energy arbitrage. In such competition, the size of the grid, hence the number of the loads, plays a major role on the findings whether uncertain flexible loads can be comparable with stationary storage. The grid size also increases the importance of the degradation on power control, since the degradation of hundreds of loads is accumulated. Finally, the behavior of the loads is also heavily affected by the type of the grid (residential or commercial) and the season (higher PV generation or load consumption), and directly affects their performance compared to stationary storage. All of the above interrelations have not yet been investigated in existing works, and this study is the first one to provide insights by diving into the analysis of these correlations.

## 5.3. Power Control Concept

The PCS aims to exploit in both levels the flexibility of the flexible loads (HPs and V2G-capable EVs) and BESS to perform energy arbitrage, minimizing PV curtailment, satisfying the charging and thermal comfort of the customers, and avoiding grid violations. It is formulated as a decentralized node optimization; thus,

all grid nodes are optimized simultaneously and independently. In this chapter, a "node" means an aggregation of buildings equipped with PV rooftops and HPs, EV chargers, and a BESS (one BESS per node). EVs that are connected to the EV chargers participate in the power control after their SOC surpasses a predefined threshold; in this work, assumed to be 20%. It must be noted that it would be a very important limitation if the PCS were centralized. Hence, every further re-optimization trigger due to a larger set of EVs or buildings would substantially increase the computational expense. On the contrary, the developed PCS is decentralized and optimizes every node distributionally by initially setting their power limit setpoints (division of the grid capacity). In that way, the PCS is less affected by large grid sizes with thousands of loads, because every node has a limited number of EVs and buildings. Hence, the computational time is mostly dependent on the node with the highest number of loads.

The power control uses two optimization levels, which are described in Figure 5.1. The first level is used for DA scheduling, and it is a one-shot (single) optimization of the next day. It uses forecast data about the EV driving patterns (e.g., requested energy, arrival SOC, arrival and departure time, etc.) and the buildings' occupancy for the power control of the EVs and HPs, respectively. It is triggered at the start of the day (00:00), and besides providing an estimated power scheduling for the next day, it can be used in future work for other purposes, such as bidding in the wholesale reserve market for ancillary services provision, as will be seen in Chapters 6 and 7. The second level is used for RT power scheduling, and it is formulated as an MPC problem that uses receding horizon optimization (RHO) and triggers re-optimizations upon certain events. This level initially uses predicted data about the EV driving patterns and buildings' occupancy to control the horizon and replaces them with actual data when the EVs finally arrive, and the buildings are (dis-)occupied, respectively. Re-optimizations are triggered upon the events: start of the day (00:00), new/expected EV arrivals, EV participation in power control ($SOC > 20\%$), and new/expected building occupancy changes. Finally, Level 2 can

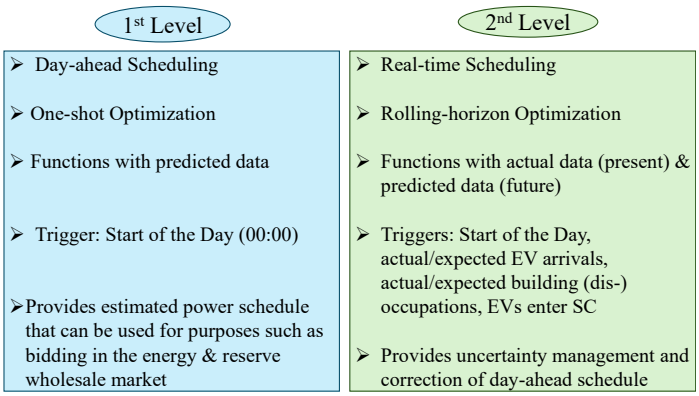


Figure 5.1: Characteristics of the optimization levels of the PCS.

also be used for ancillary services provision, such as deploying offered frequency regulation reserves or congestion management.

For a realistic PCS simulation, if historical data is not available for the estimated DA schedule, we assume a direct information feed between the customers and the PCS the day before. Triggering re-optimizations, the RHO of Level 2 provides uncertainty management and corrects forecast errors from the estimated DA schedule. The effectiveness of this concept has been demonstrated by inserting a level of uncertainty in all optimization triggers between the expected and the actual profiles using a normal distribution with 0' mean and 15' max deviation. The PCS has been successful in achieving its objectives (EV charging, building cooling/heating, PV curtailment minimization) at both levels. Hence, using a bi-level formulation can provide uncertainty management. To reason out the development of the PCS model as bi-level for uncertainty handling, the importance of uncertainties in power control, and the selection of the considered uncertainties (EV driving patterns), Figure 5.2 presents the impact of four different uncertainties on the power control performance. These results belong to the publication [28], which studies the initially developed single-level EV SC model, on which the PCS model of this Ph.D. thesis is based and has been enhanced with building thermal management, BESS use, etc. As can be seen for two EV charging nodes (Home and Public), PV generation and load demand uncertainties can be well handled by the PCS using only one level, because it is grid-connected and can always use the grid to increase the imported/exported power. However, forecast errors in EV driving patterns, such as arrival SOC and parking time, can be seriously detrimental to the power control performance, especially after 5% deviation, leaving the EV fleets uncharged upon their departure.

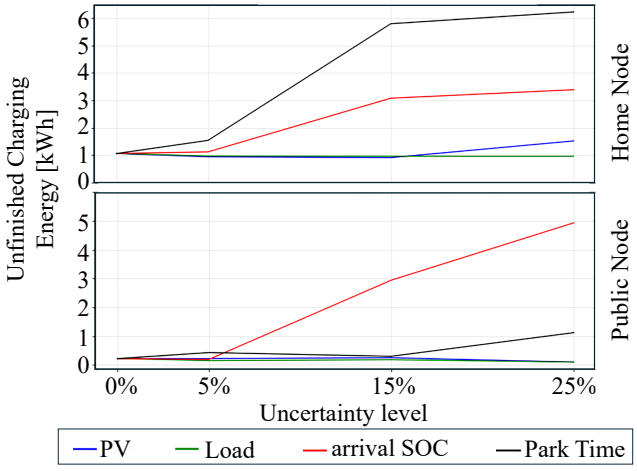


Figure 5.2: Impact of four different uncertainties in power control (EV SC); Publication [28].

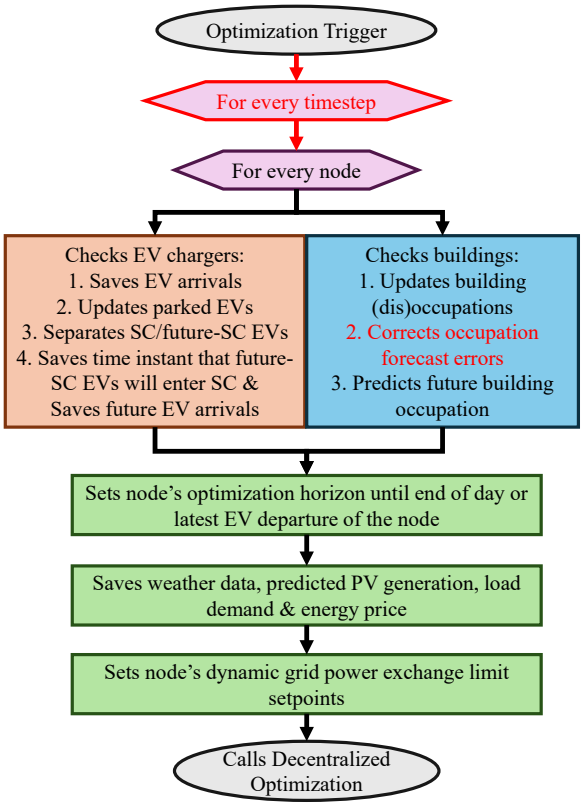


Figure 5.3: Flowchart of the PCS optimization levels.

The flowchart of the PCS model is depicted in Figure 5.3. All depicted control steps apply for both levels except for the red-colored ones that apply only for the RT scheduling (Level 2). Every node is checked at every timestep for optimization triggers. When an optimization is triggered, all EV chargers are checked for new EV arrivals, and the dynamic charging characteristics of every parked EV are updated. Additionally, the EVs that have $SOC > 20\%$ and participate immediately in the power control (SC EVs) are separated from the EVs that will participate in the future (future-SC EVs). Thereafter, the estimated control participation time of the future-SC EVs and the predicted future EV arrivals in the chargers are saved. Simultaneously, the current occupation of every building is checked, while the future dynamic building occupation is also stored. Afterward, the optimization horizon in both layers is set until the end of the day or the latest EV departure between the EVs still connected at the end of the day. The forecast data needed for the power control, such as weather data, PV generation, load demand, energy price, etc., during the optimization horizon, is saved, and the dynamic grid power exchange

limit setpoints are set for every node. All nodes share a total power capacity for grid power exchange, which is divided among the nodes according to the consumption level of their assets and is consequently used as a setpoint for imported and exported grid power. Finally, the decentralized optimization is called for the nodes with optimization triggers.

## 5.4. Power Control Modeling

The developed MIQP PCS model of this chapter, as described in publications [27] and [25], is categorized into BESS/EV, building, node, and degradation constraints. The model uses a timestep $\Delta t = 5'$ to maintain an efficient trade-off between accuracy and computational expense. The utilized indices $n, j, b, bes, t, T, ch, dis, init, end$ represent the node, charger, building, BESS, time instant, optimization horizon, charging, and discharging, initial, and final, respectively. All equations apply for $\forall t \in T$ unless stated otherwise.

### 5.4.1. Battery Energy Storage & EV Constraints

The EV and BESS constraints of the power control model are listed below, where the indices $a, d$ represent the arrival and departure, respectively. The constraints are formulated to be consistent with (3.1) - (3.4) of the EV model in Section 3.3.2. The BESS modeled represents an LFP battery.

$$P_{ch/dis}^{n,j/bes,t} = \Phi^{n,j} I_{ch/dis}^{n,j/bes,t} V^{n,t} \tag{5.1}$$

$$0 \leq P_{ch/dis}^{n,j/bes,t} \leq P_{ch/dis_{max}}^{n,j/bes} \;\&\; 0 \leq I_{ch/dis}^{n,j/bes,t} \leq I_{ch/dis_{max}}^{n,j/bes} \tag{5.2}$$

Equation (5.1) dictates the dynamic EV and BESS charging $P_{ch}^{n,j/bes,t}$ and discharging $P_{dis}^{n,j/bes,t}$ powers where $I_{ch}^{n,j/bes,t}$ and $I_{dis}^{n,j/bes,t}$ the instantaneous phase charging and discharging currents, $\Phi^{n,j} = 3$ the number of used phases, and $V^{n,t} = V_{nom}$ the node voltage assumed steady at the nominal 230V. The limits of charging and discharging power and current are dictated in (5.2), which depend on the rated LCT specifications, e.g., according to most commercial V2G chargers [1] (see Table 5.2).

$$B^{n,j/bes,t} = B_{init}^{n,j/bes} + \Delta t \sum_{t_{init}}^{t} (P_{ch}^{n,j/bes,t} - P_{dis}^{n,j/bes,t}) \tag{5.3}$$

$$\begin{aligned} S^{n,j/bes,t} &= B^{n,j/bes,t} / B_r^{n,j/bes} \\ S_{low}^{n,bes} &\leq S^{n,bes,t} \leq S_{high}^{n,bes} \end{aligned} \tag{5.4}$$

$$I_{ch}^{n,j,t}, I_{dis}^{n,j,t}, B^{n,j,t} = 0 \;\; \forall t \notin [T_a^{n,j}, T_d^{n,j}] \tag{5.5}$$

[1] https://fermataenergy.com/

The EV/BESS battery capacity dynamics $B^{n,j/bes,t}$ at every timestep $\Delta t$ are modeled in (5.3) where $B^{n,j/bes}_{init}$ the initial battery capacity, equal to the arrival $B^{n,j}_{a}$ for EVs and 50% for the BESS. The EV/BESS SOC dynamics $S^{n,j/bes,t}$ are modeled in (5.4), which depend on the dynamic and rated battery capacity $B^{n,j/bes}_{r}$ of the BESS and EVs. The BESS SOC is always limited in a selected interval $[S^{n,bes}_{low}, S^{n,bes}_{high}]$ to prevent accelerated aging at very low and very high SOCs. On the contrary, all variables turn to zero in (5.5) for the EVs outside of the EV parking time $[T^{n,j}_{a}, T^{n,j}_{d}]$.

$$P^{n,j/bes,t}_{ch} \leq \left(\frac{S^{n,j/bes,t}}{k} + \frac{\alpha k - \beta}{\alpha k}\right) P^{n,j/bes}_{ch_{max}} : \quad \alpha = 10, \beta = 9, k = 16 \tag{5.6}$$

$$\begin{aligned} I^{n,j/bes,t}_{cv_{max,ch}} &= -\gamma I^{n,j/bes,t}_{r} S^{n,j/bes,t} + \gamma I^{n,j/bes,t}_{r} \\ I^{n,j/bes,t}_{ch} &\leq I^{n,j/bes,t}_{cv_{max,ch}} : \ \gamma = 10 \end{aligned} \tag{5.7}$$

$$\begin{aligned} I^{n,j/bes,t}_{cv_{max,dis}} &= \gamma I^{n,j/bes,t}_{r} S^{n,j/bes,t} \\ I^{n,j/bes,t}_{dis} &\leq I^{n,j/bes,t}_{cv_{max,dis}} : \ \gamma = 10 \end{aligned} \tag{5.8}$$

Such as (3.1) - (3.3), (5.6) - (5.8) model a linear approximation of the CC-CV BESS/EV charging/discharging region. According to (5.6) - (5.7), the EVs and BESS are charged with linearly increasing power up to $SOC = 90\%$, where the charging power reaches its peak value, and consequently, the power decreases linearly to zero when SOC reaches 100%. The CV discharging region has also been considered in (5.8), according to which the power increases linearly to 100% when $SOC = [0\%, 10\%]$, and consequently the EVs and BESS provide maximum discharging power at $SOC = [10\%, 100\%]$. The variables $I^{n,j/bes,t}_{cv_{max,dis}}, I^{n,j/bes,t}_{cv_{max,ch}}$ are utilized to limit the EV and BESS discharging and charging power, respectively, during their respective SOC intervals, and they depend on the rated EV and BESS currents $I^{n,j/bes,t}_{r}$ and the dynamic SOCs $S^{n,j/bes,t}$. Parameters $\alpha, \beta, \gamma, k$ have been chosen as shown to create the slopes of the explained linear approximations, but can be moderated to create steeper or flatter slopes.

$$b^{n,j/bes,t}_{ch} + b^{n,j/bes,t}_{dis} \leq 1 \quad \forall t \in T \tag{5.9}$$

$$P^{n,j/bes,t}_{ch} \leq b^{n,j/bes,t}_{ch} P^{n,j/bes}_{ch_{max}} \quad \forall t \in T \tag{5.10}$$

$$P^{n,j/bes,t}_{dis} \leq b^{n,j/bes,t}_{dis} P^{n,j/bes}_{dis_{max}} \quad \forall t \in T \tag{5.11}$$

Equations (5.9) - (5.11) dictate that charging power $P_{ch}$ and discharging power $P_{dis}$ cannot be realized simultaneously. Binary variables $b^{n,j,t}_{ch}$ & $b^{n,j,t}_{v2g}$

are introduced and correlated to charging and discharging power, respectively, to activate only one mode at a time.

$$E_g^{n,j} = B_a^{n,j} + E_{req}^{n,j} - B_d^{n,j} \tag{5.12}$$

$$B_{end}^{n,bes} \geq \mu_{min}^{bes} B_{init}^{n,bes} \;\&\; B_{end}^{n,bes} \leq \mu_{max}^{bes} B_{init}^{n,bes} \tag{5.13}$$

Moreover, (5.12) dictates the EV unfinished charging gap $E_g^{n,j}$ which is calculated by subtraction of the departure capacity $B_d^{n,j}$ from the sum of the arrival capacity $B_a^{n,j}$ and the requested energy $E_{req}^{n,j}$. This gap induces penalty costs for the PCS to be paid to the EV owners and is incorporated in the cost minimization of the objective function. Finally, (5.13) forces the final stored BESS energy $B_{end}^{n,bes}$ to remain at similar levels with the initial stored energy $B_{init}^{n,bes}$ with an accuracy error that depends on the $\mu_{min}^{bes}, \mu_{max}^{bes} = 5\%$ capacity thresholds, to omit the influence of the initial BESS SOC because of the daily simulation period.

### 5.4.2. Building Constraints

The constraints of the PCS model concerning the PV generation and HP heating/cooling of the buildings are listed below, where: $surf, irr, sp, dhw, tank$ denote the surface, irradiation, space, DHW, and tank, respectively. All constraints apply for $\forall t \in T$. The building constraints are formulated to be consistent with (3.5)-(3.14) of HP and building models in Section 3.3.3. Moreover, the solar irradiation and PV power used in this section were generated using the irradiation model (3.15)-(3.19) of Section 3.3.4 and the PV model (3.20)-(3.26) of Section 3.3.5, respectively.

$$V_{tank} = V_{w_p} N_p f_{dhw} \tag{5.14}$$

$$A_{tank} = 2\pi R_{tank} H_{tank} + 2\pi R_{tank}^2 \tag{5.15}$$

$$T_{dhw}^{n,b,t} = T_{dhw_{init}}^{n,b} + \Delta t \sum_{t_{st}}^{t} \frac{(Q_{hp_{dhw}} - Q_{los_{dhw}})^{n,b,t}}{V_{tank} C_{wat} \rho_{wat}} \tag{5.16}$$

$$Q_{los_{dhw}}^{n,b,t} = U_{tank} A_{tank} (T_{dhw}^{n,b,t} - T_{sp}^{n,b,t}) \tag{5.17}$$

$$T_{dhw}^{n,b,t_{dhw}} = T_{dhw}^{des} \tag{5.18}$$

Regarding the DHW, the total volume $V_{tank}$ and surface area $A_{tank}$ of the DHW tank are modeled in (5.14) and (5.15) where $N_p, V_{w_p}, R_{tank}, H_{tank}$ the number of people in the building, the estimated water volume per person, the tank radius and the tank height, respectively. The DHW factor $f_{dhw}$ has been set at $1.25$ to provide a 25% extra tolerance for higher DHW use. The DHW temperature dynamics $T_{dhw}^{n,b,t}$ are dictated in (5.16), which depend on the heating gains from the HP operation

$Q_{hp_{dhw}}$ and heating losses $Q_{los_{dhw}}$ divided by the total thermal capacity of the tank water where $T^{n,b}_{dhw_{init}}$ the initial DHW tank temperature, $C_{wat}$ the water specific heating capacity and $\rho_{wat}$ the water density. The tank heating losses are modeled in (5.17) and depend on the difference between the tank temperature $T^{n,b,t}_{dhw}$ and the building temperature $T^{n,b,t}_{sp}$, where $U_{tank}$ the tank conductivity. Finally, (5.18) dictates that for every building b, the DHW tank temperature must reach the desired temperature $T^{des}_{dhw}$ at the desired time $t_{dhw}$, which has been set at 09:00 for commercial buildings, and 07:00 or 19:00 for residential buildings (see Table 5.3).

$$T^{n,b,t}_{sp} = T^{n,b}_{sp_{init}} + \Delta t \sum_{t_{st}}^{t} \frac{Q^{n,b,t}_{tot_{sp}}}{C_b + V_b C_{air} \rho_{air}} \tag{5.19}$$

$$Q^{n,b,t}_{tot_{sp}} = Q^{n,b,t}_{hp_{sp}} m^{n,b}_{hp} + Q^{n,b,t}_{irr} - Q^{n,b,t}_{los_{sp}} \tag{5.20}$$

$$Q^{n,b,t}_{los_{sp}} = (\sum_{sf} U_{sf} A_{sf} + C_{air}\ \rho_{air}\ r_b)(T^{n,b,t}_{sp} - T^{t}_{a}) \tag{5.21}$$

The building temperature dynamics $T^{n,b,t}_{sp}$ are modeled in (5.19), which depend on the initial building temperature $T^{n,b}_{sb_{init}}$ and the total space heating gains and losses $Q_{tot_{sp}}$ divided by the thermal capacity of the building mass $C_b$ and the capacity of the building air where $V_b$, $C_{air}$, and $\rho_{air}$ the building volume, the air-specific capacity and air density, respectively. Equation (5.20) denotes that $Q_{tot_{sp}}$ comprise the HP heating output $Q_{hp_{sp}}$, the heating gains from irradiation $Q_{irr}$ (calculated by (3.9) and (3.15)-(3.19)), and the total heating losses $Q_{los_{sp}}$ where $m_{hp}$ denotes the HP mode (+1/-1 for heating/cooling). The total heating losses $Q_{los_{sp}}$ depend on the conduction losses (first term) and ventilation losses (second term), which depend highly on the ambient temperature $T_a$ as shown in (5.21). The former also depends on the sum of the conductivity $U$ over the area $A$ of every building surface, while the latter also depends on the building air change rate $r_b$.

$$P^{n,b,t}_{hp_{dhw}} \leq b_{sp} P^{n,b}_{hp^{max}_{dhw}} \tag{5.22}$$

$$P^{n,b,t}_{hp_{sp}} \leq b_{sp} P^{n,b}_{hp^{max}_{sp}} \tag{5.23}$$

$$b_{sp} + b_{dhw} \leq 1 \tag{5.24}$$

$$P^{n,b,t}_{hp_{tot}} = P^{n,b,t}_{hp_{sp}} + P^{n,b,t}_{hp_{dhw}} \tag{5.25}$$

In (5.22) - (5.24), the binary variables $b_{sp}$, $b_{dhw}$ are introduced to enforce that the HP power consumption for DHW $P^{n,b,t}_{hp_{dhw}}$ and for space heating/cooling $P^{n,b,t}_{hp_{sp}}$ cannot occur simultaneously, where $P^{n,b}_{hp^{max}_{dhw}}$ and $P^{n,b}_{hp^{max}_{sp}}$ the respective maximum

power limits. Additionally, (5.25) dictates that the total HP power consumption $P^{n,b,t}_{hp_{tot}}$ is always the consumption for the space heating/cooling and DHW.

$$c^{n,b,t}_{p_{hp}} = 7.90471e^{-0.024(T^{n,b,t}_{ret}-T^{t}_{a})} = 7.90471e^{c^{n,b,t}_{exp}} : \\ c^{n,b,t}_{exp} = -0.024(T^{n,b,t}_{ret} - T^{t}_{a}) \tag{5.26}$$

$$T^{n,b,t}_{ret} = T^{sp/dhw}_{sup} - Q^{n,b,t}_{hp_{sp/dhw}}/(\dot{m}_{wat}C_{wat}) \tag{5.27}$$

Equation (5.26) dictates the original model of the HP's COP $c_{p_{hp}}$, which depends on the ambient temperature and the dynamic HP's return water temperature $T^{n,b,t}_{ret}$. Due to the non-linearity of (5.26), the exponential part is defined as $c^{n,b,t}_{exp}$, and a piecewise linear (PWL) approximation has been utilized for the COP modeling. Moreover, the HP's return water temperature is modeled in (5.27), where $\dot{m}_{wat}$: the flow water rate and $T_{sup}$ the supply water temperature, which is set at 35°, 50°, and 18° for floor-heating, DHW, and floor-cooling, respectively.

$$Q^{n,b,t}_{hp_{sp/dhw}} = P^{n,b,t}_{hp_{sp/dhw}} c^{n,b,t}_{p_{hp}} : \\ 0 \leq Q^{n,b,t}_{hp_{sp/dhw}} \leq Q^{n,b}_{hp^{max}_{sp/dhw}} \tag{5.28}$$

$$P^{n,b,t}_{pv_{dev}} = P^{n,b,t}_{pv_{max}} - P^{n,b,t}_{pv} : 0 \leq P^{n,b,t}_{pv} \leq P^{n,b,t}_{pv_{max}} \tag{5.29}$$

$$T^{n,b,t}_{dev} = \max(T^{n,b,t}_{sp} - T^{n,b}_{high}, T^{n,b}_{low} - T^{n,b,t}_{sp}, 0) : \\ T^{n,b}_{min} \leq T^{n,b,t} \leq T^{n,b}_{max} \tag{5.30}$$

Consequently, (5.28) dictates the relation between the HP power consumption for space heating/cooling and DHW with the COP and their respective heating output amounts limited to the HP heating capacity $Q^{n,b}_{hp^{max}_{sp/dhw}}$. These equations are the only non-linear equations of the power control model that make the problem MIQP. The instantaneous PV curtailment amount $P_{pv_{dev}}$ is dictated in (5.29) where $P_{pv_{max}}$ & $P_{pv}$ the PV generation (calculated by (3.20)-(3.26)) and used PV power, respectively. The temperature deviation $T_{dev}$ is defined in (5.30) as the temperature difference from the nearest desired temperature interval limit $T^{n,b}_{low}$ or $T^{n,b}_{high}$. The desired temperature interval $[T^{n,b}_{low}, T^{n,b}_{high}]$ has been set at [21°, 23°], while for the needs of the model, the maximum temperature interval $[T^{n,b}_{min}, T^{n,b}_{max}]$ has been set at [17°, 27°]. The variables $P_{pv_{dev}}$ and $T_{dev}$ are used in the objective function with cost penalties (such as with EV charging) to ensure PV max self-consumption and thermal comfort, respectively. Equation (5.30) is a non-linear constraint and cannot be integrated as is in the power control. It is well known that a min or max equation can be linearized by applying the big-M method. Dividing (5.30) into two max functions and applying the big-M method twice, 3 new support decision

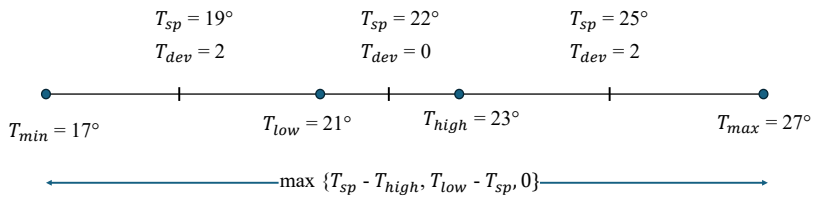


Figure 5.4: Intuitive explanation of $T_{dev}$ by (5.30).

variable series $y_{T_{dev}}, z_{T_{dev}}, c_{T_{dev}}$ and 2 M variables $M_1$ & $M_2$ are introduced and the linearization of (5.30) is realized by (5.31) - (5.37). Figure 5.4 depicts an intuitive explanation of (5.30), while Table 5.3 summarizes the parameters of this section.

$$y^{n,b,t}_{T_{dev}} \geq T^{n,b,t}_{sp} - T^{n,b}_{high} \tag{5.31}$$

$$y^{n,b,t}_{T_{dev}} \geq T^{n,b}_{low} - T^{n,b,t}_{sp} \tag{5.32}$$

$$y^{n,b,t}_{T_{dev}} \leq T^{n,b,t}_{sp} - T^{n,b}_{high} + M_1 z^{n,b,t}_{T_{dev}} \tag{5.33}$$

$$y^{n,b,t}_{T_{dev}} \leq T^{n,b}_{low} - T^{n,b,t}_{sp} + M_1(1 - z^{n,b,t}_{T_{dev}}) \tag{5.34}$$

$$T^{n,b,t}_{dev} \geq y^{n,b,t}_{T_{dev}} \tag{5.35}$$

$$T^{n,b,t}_{dev} \leq M_2 c^{n,b,t}_{T_{dev}} \tag{5.36}$$

$$T^{n,b,t}_{dev} \leq y^{n,b,t}_{T_{dev}} + M_2(1 - c^{n,b,t}_{T_{dev}}) \tag{5.37}$$

### 5.4.3. Node Constraints

The node power balance is dictated in (5.38), which defines that the difference between the dynamic node imported $P^{n,t}_{im}$ and exported $P^{n,t}_{ex}$ power is the total EV/BESS charging power, HP power consumption, and building load demand $P^{n,b,t}_{l}$ minus the total PV rooftop power and EV/BESS discharging power. The parameters $h^{n,j}_{ch}, h^{n}_{bes}$ constitute the EV charger and BESS efficiencies, set at $0.95$ and $0.98$ respectively. The EV charger efficiency also comprises the EV battery losses and the BESS efficiency, and the power converter losses. The losses due to power conversion for BESS operation are lower than the respective of EV (dis)charging due to the lower needed conversion stages; power conversion for EV (dis)charging

needs an additional isolation stage. Finally, (5.39) & (5.40) dictate that all the node composite power is always lower than the input and output node capacity limits, $G^n_{in}$ and $G^n_{out}$, respectively, and force the node not to import and export power simultaneously.

$$P^{n,t}_{im} - P^{n,t}_{ex} = \sum_{j=1}^{J}\left(\frac{P^{n,j,t}_{ch}}{h^{n,j}_{ch}} - P^{n,j,t}_{dis}h^{n,j}_{ch}\right) + \frac{P^{n,bes,t}_{ch}}{h^{n}_{bes}} - P^{n,bes,t}_{dis}h^{n}_{bes} + \sum_{b=1}^{B}\left(P^{n,b,t}_{hp_{tot}} + P^{n,b,t}_{l} - P^{n,b,t}_{pv}\right) \forall t \in T \tag{5.38}$$

$$P^{n,t}_{im} = \sum_{j=1}^{J}\left(\frac{P^{n,j,t}_{ch}}{h^{n,j}_{ch}} - P^{n,j,t}_{dis}h^{n,j}_{ch}\right) + \frac{P^{n,bes,t}_{ch}}{h^{n}_{bes}} - P^{n,bes,t}_{dis}h^{n}_{bes} + \sum_{b=1}^{B}\left(P^{n,b,t}_{hp_{tot}} + P^{n,b,t}_{l} - P^{n,b,t}_{pv}\right) \le G^{n}_{in} \ \forall t \in T \tag{5.39}$$

$$P^{n,t}_{ex} = \sum_{b=1}^{B}\left(P^{n,b,t}_{pv} - P^{n,b,t}_{hp_{tot}} - P^{n,b,t}_{l}\right) + P^{n,bes,t}_{dis}h^{n}_{bes} - \frac{P^{n,bes,t}_{ch}}{h^{n}_{bes}} - \sum_{j=1}^{J}\left(\frac{P^{n,j,t}_{ch}}{h^{n,j}_{ch}} - P^{n,j,t}_{dis}h^{n,j}_{ch}\right) \le G^{n}_{out} \ \forall t \in T \tag{5.40}$$

### 5.4.4. Battery Degradation

The PCS performs energy arbitrage, aiming for higher cost savings; however, the higher utilization of the available assets can have a notable impact on component degradation. This is especially the case for the battery degradation of the EVs and the BESS, for which it has already been seen that a high number of cycles can significantly reduce the lifetime of the batteries. Thus, since the PCS utilizes V2G and a higher number of equivalent cycles of the BESS to take advantage of the daily price deviations to reduce the total power control cost, it is important that the additional battery degradation cost is taken into consideration during the power scheduling of the PCS. As a result, it can be shown whether the degradation cost is comparable enough to the total cost, to alter the PCS decision making depending on the grid size.

#### Non-linear model

$$Q_{cal} = k_{cal}e^{-\frac{E^{cal}_a}{R}\left(\frac{1}{T}-\frac{1}{T^r}\right)}e^{\frac{\alpha F}{R}\frac{U^r_a - U_a}{T^r}} + k_0)\sqrt{t} \tag{5.41}$$

$$Q_{cy,1} = k_{cy,1}e^{-\frac{E_{a,cy1}}{R}\left(\frac{1}{T}-\frac{1}{T^r}\right)}\sqrt{q_{tot}} \tag{5.42}$$

$$Q_{cy,2} = k_{cy,2}e^{-\frac{E_{a,cy2}}{R}\left(\frac{1}{T}-\frac{1}{T^r}\right)}e^{\beta\frac{I_{ch}-I^r_{ch}}{B_c}}\sqrt{q_{ch}} \tag{5.43}$$

The original battery degradation model dictated by (5.41)-(5.43) has been developed for an LFP cell, designed for stationary applications in [200], where the reader is referred for further information. More specifically, (5.41) models the calendar battery aging $Q_{cal}$ that depends mainly on the operating temperature $T$, SOC via the anode potential $U_a$, and time $t$, where $T^r$ is the rated temperature (25°), $U_a^r$ is the anode potential at the rated SOC ($SOC^r = 50\%$), and $k_{cal}$ is the respective coefficient. The cyclic aging is dictated by (5.42)-(5.43), where $I_{ch/dis}^{r,cell}$ the rated cell charging and discharging current; two equations are used for cyclic aging because different aging mechanisms $Q_{cy,1}, Q_{cy,2}$ are energized during charging and discharging, where $k_{cy,1}, k_{cy,2}$ are the respective coefficients. More in particular, (5.42) depends on temperature and total throughput $q_{tot}$; thus, it is activated during both charging and discharging. On the contrary, (5.43) depends on temperature, charging throughput $q_{ch}$, and current $I_{ch}$; thus, it is activated only during charging. All variables in (5.41)-(5.43) refer to the battery cell, where $E_a, R, B_c$ denote the activation energy, internal resistance, and cell capacity, respectively, and $\alpha, \beta$ are constants. Finally, Table 5.4 summarizes the degradation parameters.

### Model Linearization

The original model cannot be integrated into the MIQP problem as is because it is highly non-linear and comprises multiplication of many exponential and square-root terms. Therefore, it has been linearized by transforming it to its equivalent on the logarithmic scale.

$$\bar{Q_{cal}}(25°, SOC = 50\%) = k_{cal}(1 + k_0)\sqrt{t = 1day} \tag{5.44}$$

$$ln(Q_{cy,1}) = ln(k_{cy,1}) + 0.5ln(q_{tot}^{cell}) \tag{5.45}$$

$$ln(Q_{cy,2}) = (ln(k_{cy,2}) - \frac{\beta I_{ch}^{r,cell}}{B_c}) + \frac{\beta}{B_c} I_{ch}^{cell} + 0.5ln(q_{ch}^{cell}) \tag{5.46}$$

$$\begin{aligned} &y = ln(x)\text{: monotonous continuous} \\ a_0 = a_1 * a_2 * a_n \leftrightarrow\ &ln(a_0) = ln(a_1) + ln(a_2) + ln(a_n) \\ &ln(a^b) = bln(a) \end{aligned} \tag{5.47}$$

Equations (5.44)-(5.46) represent the linearization of the degradation model (5.41)-(5.43). Concerning the calendar aging and (5.41), the duration of the simulation is fixed at one day, the BESS SOC is maintained at 50% at the beginning and end of the day, and a thermal management system is assumed to keep the operation temperature at 25°. Hence, a mean calendar capacity loss is used for the day, and (5.41) is transformed to (5.44). Moreover, assuming again a maintained temperature at 25°and using the logarithmic properties, (5.42) & (5.43) are transformed to their equivalents in the logarithmic scale (5.45) & (5.46), respectively, using the logarithmic properties in (5.47).

### Integration into the MIQP model

Equation (5.48) correlates the EV and BESS charging and discharging currents with the cell charging and discharging currents of the respective assets $I_{ch}^{n,cell-j/bes,t}$ and $I_{dis}^{n,cell-j/bes,t}$, which are rated at $I_{ch/dis}^{r,cell} = 3A$ [200]. Furthermore, the total cell current $I_{tot}^{n,cell-j/bes,t}$ is dictated in (5.49).

$$I_{ch/dis}^{n,cell-j/bes,t} = (I_{ch/dis}^{n,j/bes,t}/I_{max}^{n,j/bes})I_{ch/dis}^{r,cell} \quad \forall t \in T \tag{5.48}$$

$$I_{tot}^{n,cell-j/bes,t} = I_{ch}^{n,cell-j/bes,t} + I_{dis}^{n,cell-j/bes,t} \quad \forall t \in T \tag{5.49}$$

Moreover, (5.50) models the EV and BESS total and charging cell throughput dynamics $q_{tot,ch}^{n,cell-j/bes,t}$, which are needed for the calculation of $ln(q_{tot,ch})^{cell-j/bes}$ in (5.45) & (5.46) with the use of the parameter $\lambda = 10^{-7}$ to avoid infinity at zero current. Additionally, (5.51) dictates the limits of the cell total and charging current, and throughput.

$$q_{ch/tot}^{n,cell-j/bes,t} = I_{ch/tot}^{n,cell-j/bes,t}\Delta t + \lambda \quad \forall t \in T \tag{5.50}$$

$$\begin{aligned} 0 \leq I_{ch}^{n,cell-j/bes,t}, I_{tot}^{n,cell-j/bes,t} \leq 3 \quad \forall n,\ t \in T \\ 0 \leq q_{ch}^{n,cell-j/bes,t}, q_{tot}^{n,cell-j/bes,t} = 3\Delta t \quad \forall n,\ t \in T \end{aligned} \tag{5.51}$$

The variables $q_{ch}$ and $q_{tot}$ are transformed to their equivalent $ln(q_{ch})$ and $ln(q_{tot})$, respectively, using PWL approximations of the function $y = ln(x)$, while $ln(Q_{cy,1})$ and $ln(Q_{cy,2})$ are similarly transformed to their equivalent $Q_{cy,1}$ and $Q_{cy,2}$, using the function $x = e^y$. The resulting degradation variables $Q_{cal}$, $Q_{cy,1}$ and $Q_{cy,2}$ constitute capacity loss percentages. Hence, assuming all cells degrade uniformly, the EVs' and BESS battery capacities are needed to calculate the total battery capacity loss. In this regard, (5.52) represents the degradation objective $\min B_{Q_{tot}}^{n}$, which minimizes the total BESS/EV cyclic aging with the addition of the mean BESS/EVs' calendar aging $\bar{Q_{cal}}$. Finally, the total BESS/EV battery aging is calculated post-optimization with the original model (5.41)-(5.43) for verification purposes.

$$\begin{aligned} \min B_{Qtot}^{n} = \min \Delta t(\sum_{t=1}^{T}(Q_{cy,1}^{n,bes,t} + Q_{cy,2}^{n,bes,t})B_r^{n,bes} + \\ \sum_{j=1}^{J}(Q_{cy,1}^{n,j,t} + Q_{cy,2}^{n,j,t})B_r^{n,j}) + \bar{Q_{cal}^{n,bes}}B_r^{n,bes} + \sum_{j=1}^{J}\bar{Q_{cal}^{n,j}}B_r^{n,j} \end{aligned} \tag{5.52}$$

The utilized empirical degradation model considers various degradation factors such as temperature, time, C-rate, and throughput. However, it fails to consider the effects of SOC and DOD, especially for cyclic aging. Therefore, there is an accuracy loss for cycling during very high SOCs, and DODs. Therefore, the following measures have been considered:

1) Stationary BESS: The SOC is directly limited to deviate within the interval [10%, 90%] so that the battery is never completely depleted or charged.

2) EVs: Firstly, the EVs are allowed to participate in the power control only after their SOC reaches 20%. Secondly, due to the CC-CV region, the EVs actively perform energy arbitrage when they are being charged in the CC region. When $SOC > 90\%$, the EVs stop being consecutively charged and discharged due to the low power levels, and afterwards are charged uncontrollably until departure.

### 5.4.5. Objective Function

Finally, the power control objective function for every node $n$ is dictated in (5.53). The PCS is a multi-objective MIQP model that has translated all objectives into a total cost aimed to be minimized. In this regard, all penalty costs are chosen to be much higher than the energy price to attach great importance to the customers' comfort (see Tables 5.2 and 5.3). The total cost comprises:

a) For energy arbitrage: The minimum exchange grid power cost where $P_{im}, C_{buy}$ and $P_{ex}, C_{sell}$ are the imported and exported power and related costs.

b) For PV max self-consumption: The total PV curtailment cost, where $C_{pv_{pen}}$ is the related penalty.

c) For thermal comfort maintenance: The total thermal discomfort cost, where $C_{hp_{pen}}$ is the related penalty and $O^{t,n,b} \in [0, 1]$ is the dynamic building occupancy. The meaning of $O^{t,n,b}$ is that there is no penalty for the EMS if the building temperature is out of the desired range, but the building is not occupied.

d) For charging comfort maintenance: The total EV unfinished charging cost, where $C_{pv_{pen}}$ is the related penalty.

e) For battery degradation mitigation: The total battery degradation cost, where $C_Q^n$ is the degradation cost of 150€/kWh [201]. The placement of (5.52) inside (5.53) directly mitigates battery degradation. In this work, the weights of the different objectives have been adjusted in association with the respective costs. However, placing a higher weight would give a higher importance to battery degradation minimization and hence, directly decrease it through the objective function.

$$\begin{aligned} \min C_n = \Delta t\Big(\sum_{t=1}^{T}\big(P_{im}^{n,t}C_{buy}^{t} - P_{ex}^{n,t}C_{sell}^{t}\big)\Big) \\ + \sum_{t=1}^{T}\sum_{b=1}^{B}\big(P_{pv_{dev}}^{n,b,t}C_{pv_{pen}}^{n,b}\big) + \sum_{t=1}^{T}\sum_{b=1}^{B}\big(T_{dev}^{n,b,t}C_{hp_{pen}}^{n,b}O^{t,n,b}\big) \\ + \sum_{j=1}^{J}E_g^{n,j}C_{ev_{pen}}^{n,j} + B_{Qtot}^{n}C_Q^n \end{aligned} \tag{5.53}$$

### 5.4.6. Optimization Overview

Overall, the optimization problem can be presented in the following standard form (5.54), where the constraints that make the MIP problem MIQP have been marked

with red color. All power control parameters used in Section 5.4 for the modeling of EV/BESS, buildings, and battery degradation are summarized in Tables 5.2, 5.3, and 5.4, respectively.

The main modeling novelty of this chapter is the development and testing of the linearized physics-guided semi-empirical highly non-linear battery degradation model. Moreover, the developed multi-objective function and the simultaneous optimization of all the objectives (EV charging, thermal comfort maintenance, PV max self-consumption, energy arbitrage, battery degradation minimization) are the second main novelty. The main challenge has been maintaining a low accuracy error due to approximations of several non-linearities while keeping the computational time reasonable, even for large grid scenarios.

$$
\begin{aligned}
& minf(x) : f = (5.53)\ s.t. \\
& x = [P_{im}^{n,t}, P_{ex}^{n,t}, P_{pv_{dev}}^{n,t}, T_{dev}^{n,b,t}, E_{g}^{n,j}, B_{Q_{tot}}^{n}]\ \forall n, b, t \in T \\
& h_i(x) = 0 : h_i \in [(5.1), (5.3), (5.4), (5.5), (5.7), (5.8), (5.12), (5.14), \\
& (5.15), (5.16), (5.17), (5.18), (5.19), (5.20), (5.21), (5.25), (5.26), \\
& (5.27), (5.28), (5.29), (5.38), (5.44), (5.45), (5.46), (5.48), (5.49), \\
& (5.50), (5.52)] \\
& g_j(x) \leq 0 : g_j \in [(5.2), (5.4), (5.6), (5.7), (5.8), (5.9), (5.10), (5.11), \\
& (5.13), (5.22), (5.23), (5.24), (5.28), (5.31 - 5.37), (5.39), (5.40), \\
& (5.51)]
\end{aligned}
\tag{5.54}
$$

Table 5.2: BESS and EV Parameters of the Power Control Model.

| Par. | Explanation | Value |
|---|---|---|
| $C_{ev_{pen}}^{n,j}$ | EV Charg. Penalty | 10€/(1%SOC) |
| $h_{ch}^{n,j}$ | EV Charg. Efficiency | 0.95 |
| $h_{bes}^{n}$ | BESS efficiency | 0.98 |
| $P_{ch/dis_{max}}^{n,j}$ | Max EV Dis/Charg. Power | $\min(P_{ev_r}^{n,j}, 22kW)$ |
| $P_{ch/dis_{max}}^{n,bes}$ | Max BESS (dis)charging Power | $0.5C$ |
| $B_{init}^{n,bes}$ | BESS Initial Capacity | $0.5B_{r}^{n,bes}$ |
| $V^{n,t}$ | Node Voltage | 230V |
| $\Phi^{n,j/bes}$ | Number of Phases | 3 |
| $I_{ch/dis_{max}}^{n,j}$ | Max EV Dis/Charg. Current | $\min(I_{ev_r}^{n,j}, 32A)$ |
| $S_{low/high}^{n,bes}$ | Min-Max BESS SOC | $10\% - 90\%$ |
| $V_{nom}$ | Nominal Node Voltage | 230V |
| $\mu_{min/max}^{bes}$ | Min-Max BESS Capacity Thresholds | 0.95, 1.05 |

Table 5.3: Building Parameters of the Power Control Model.

| Par. | Explanation | Value |
|---|---|---|
| $C^{n,b}_{hp_{pen}}$ | Discomfort Penalty | 10€/(°C $\Delta t$) |
| $C^{n,b}_{pv_{pen}}$ | PV Curtail. Penalty | 10€/(kW $\Delta t$) |
| $C_b$ | Build. Thermal Capacity | $4.755 kWh/K$ |
| $V_b$ | Build. Volume | $585 m^3$ |
| $C_{air}$ | Air Thermal Capacity | $0.279 Wh/kgK$ |
| $\rho_{air}$ | Air Density | $1.225 kg/m^3$ |
| $C_{wat}$ | Water Thermal Capacity | $1.16 kWh/kgK$ |
| $\rho_{wat}$ | Water Density | $993 kg/m^3$ |
| $r_b$ | Air Change Rate | $0.3 h^{-1}$ |
| $T^{n,b}_{min/max}$ | Build. Min/Max Temp. | 17°& 27° |
| $T^{n,b}_{low/high}$ | Low/High Comfort Temp. | 21°& 23° |
| $M1, M2$ | Big-M Parameters | 10 |
| $T_{sup}$ | HP Supply Temp.: space heating, cooling & dhw | 35°, 18°& 50° |
| $T^{n,b}_{sp/dhw_{init}}$ | Initial space/DHW Temp. | 22° |
| $T^{des}_{dhw}$ | Desired DHW Temp. | 50° |
| $N_p$ | People per build. | 4 |
| $R_{tank}, H_{tank}$ | Tank Radius & Height | 0.23m & 1.3m |
| $V_{tank}$ | Tank Volume | 215l |
| $U_{tank}$ | Tank Conductivity | $5.98 W/Km^2$ |
| $\dot{m}_{wat}$ | HP water flow rate | $0.8 kg/s$ |
| $V_{w_p}$ | Water Volume/person | $65 l$ |

Table 5.4: Battery Degradation Parameters of the Power Control Model.

| Par. | Explanation | Value |
|---|---|---|
| $k_{cal}$ | Calendar coefficient in (5.44) | $3.694 * 10^{-4}$ |
| $k_0$ | Constant in (5.44) | 0.142 |
| $k_{cy,1}$ | Cyclic coefficient in (5.45) | $1.456 * 10^{-4} Ah^{-0.5}$ |
| $k_{cy,2}$ | Cyclic coefficient in (5.46) | $4.009 * 10^{-4} Ah^{-0.5}$ |
| $\beta$ | Constant in (5.46) | 2.64h |
| $B_c$ | Cell capacity | 3Ah |
| $I^{r,cell}_{ch/dis}$ | Rated Cell Current | 3A |
| $C^n_Q$ | Degradation Cost | $150€/kWh$ |
| $\lambda$ | Constant in (5.50) | $10^{-7}$ |

## 5.5. Case Studies & Scenarios

The PCS model has been applied to several case studies, which can mainly be categorized into: a) with and without BESS use to compare the flexibility of flexible loads and BESS for energy arbitrage, b) Summer and Winter seasons to quantify the related seasonal effect and c) with and without battery degradation to show the degradation influence on the decision-making of the EMS and the total cost. Moreover, two grid size scenarios have been utilized (a small 3-node and a large 13-node grid) to show the grid size level effect.

### 5.5.1. Small (3-node) & Large (13-node) LV Grids

The small grid scenario consists of 3 nodes from different areas (residential, commercial, and mixed). It has been assumed that the three nodes are connected with different radial feeders to the main grid. Each node comprises a 50kWh-rated BESS unit of 0.5C max C-rate, while Figure 5.5 depicts the number of buildings and chargers per node. As explained in Chapter 3, buildings in residential areas, e.g. HHs, are occupied longer during the day (00:00-08:00, 14:00-00:00) compared to commercial buildings such as offices and stores that are mostly occupied during the day (09:00-21:00). Moreover, home chargers at residential areas are characterized by a lower frequency of incoming EV fleets which remain parked for longer times and arrive with lower SOCs compared to public and semi-public chargers. Furthermore, EVs consume approximately a 30% higher amount of energy due to cabin heating during Winter, while building heating consumes a 50% higher amount of energy than building cooling during Summer because of a higher temperature difference with ambient temperature (hence, lower COPs). Finally, the input and output node capacity limits, $G^n_{in}$ and $G^n_{out}$ respectively, are set at 400kW. This scenario is formulated to provide insights into the effect of the grid type on the power control objectives and characteristics during different seasons, e.g., total cost, imported/exported power, BESS, and V2G energy amounts.

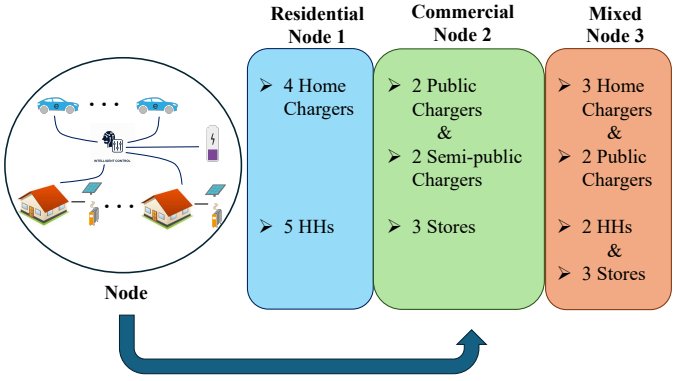


Figure 5.5: Node concept & characteristics of the small grid scenario.

The large grid scenario depicted in Figure 5.6 constitutes a real urban grid in the Netherlands and is one of the two urban grids presented in Chapter 3. Each one of the 13 load locations, hereby called nodes, comprises several loads (buildings) equipped with PVs, HPs, and EV chargers. It is assumed that each node is optimized distributionally in parallel with the use of an aggregator and appropriate power set limits according to the number of loads. Table 5.5 summarizes the number of LCTs at every node. Moreover, a BESS is installed at every node, whose capacity is set at 10kWh per building/charger. Finally, the input and output node capacity limits, $G^n_{in}$ and $G^n_{out}$ respectively, are set at 3.785MW for the large grid example. This scenario is formulated to first show the effect of the investigated grid size on the power control results and validate the insights provided by the small grid scenario. Secondly, it proves the scalability and modifiability of the developed PCS model.

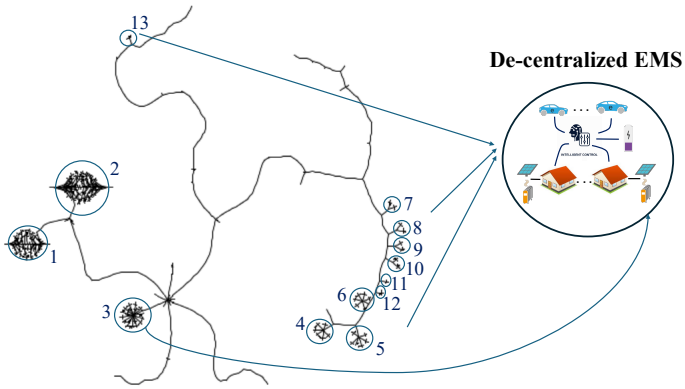


Figure 5.6: Distributional EMS of the large grid scenario with the use of aggregators.

Table 5.5: Node Characteristics of the Large Grid Scenario.

| Nodes | Buildings (PVs, HPs) | Chargers | BESS Capacity [kWh] |
|---|---|---|---|
| 1 | 32 | 32 | 320 |
| 2 | 44 | 44 | 440 |
| 3 | 18 | 18 | 180 |
| 4, 5, 6 | 6 | 6 | 60 |
| 7, 8, 9, 10 | 2 | 2 | 20 |
| 11, 12, 13 | 1 | 1 | 10 |

### 5.5.2. Data Input

The data input used in this chapter regarding the residential and commercial load consumption profiles, EV driving pattern PDFs, EV pool, PV and HP modules, and weather data are the same as in Section 3.3.1. Moreover, day-ahead market (DAM) energy price profiles have been acquired by the Dutch ENTSO-E platform [134], and a Sony US26650FTC1 LIB iron phosphate/graphite cell of $3.2V$ and $3Ah$ nominal voltage and capacity, designed for stationary applications, is derived by [200].

To incorporate a level of uncertainty, LCT profiles have been randomly selected from the respective pools generated with the use of MCS in Chapter 3 (Sections 3.3.2-3.3.5); namely: a) 600 random EV fleet profiles for Home, Semi-public, and Public chargers, b) 200 residential and commercial building occupancy profiles with random occupancy changes, and c) 180 Summer and Winter PV generation profiles with random PV module orientations. Afterwards, the selected LCT profiles have been randomly distributed to the buildings and EV chargers of the nodes of the utilized grid scenarios.

### 5.5.3. Overall Case Studies

Table 5.6 summarizes the case studies of this chapter with their respective simulation times. Cases 1-6 are devoted to the small grid scenario, and Cases 7-12 to the large grid scenario. Cases 1, 3, and 5 investigate the power control of flexible loads, flexible loads + BESS, and flexible loads + BESS + degradation for Winter, while Cases 2, 4, and 6 investigate the related comparisons during Summer. Accordingly, the same applies to the large grid scenario in Cases 7-12. Overall, the case studies described above aim to quantify and reflect on the effect of the following influencing factors on power control characteristics (control cost, grid power exchange amount, V2G energy use, BESS energy use, power flows scheduling, etc):

1) Flexibility of loads and BESS: Stationary BESS and flexible loads, such as EVs and HPs, can both offer flexibility for energy arbitrage. While the BESS is expected to be capable of the highest flexibility because it is not prone to uncertainties, the contribution of flexible loads can be proven comparable in large grids.

2) Grid-size and grid-type effect: Different grid types, such as residential and commercial, can highly influence the power control decision-making due to different characteristics of buildings and EV fleets. Additionally, a larger grid that comprises a higher number of present flexible loads can be proven to be more flexible, also without the use of a BESS.

3) Seasonal effect: Different seasons can have a significant impact on the consumption and power levels of the flexible loads as well as on the PV generation. Thus, it is important to encapsulate the yearly seasonal variations in the investigation of the power control performance.

4) Battery degradation effect: Constant battery charging and discharging can highly increase the steepness of the capacity fading and induce further costs. Therefore, especially in large grids, accumulated degradation costs can become significant and alter the energy arbitrage decision-making.

Table 5.6: Case Studies and Scenarios of the Power Control.

| Cases | Flexibility | Season | Scenario | Degr. | Time |
|---|---|---|---|---|---|
| 1 | Loads | Winter | Small Grid | No | 38’ |
| 2 | Loads | Summer | Small Grid | No | 37’ |
| 3 | Loads & BESS | Winter | Small Grid | No | 41’ |
| 4 | Loads & BESS | Summer | Small Grid | No | 41’ |
| 5 | Loads & BESS | Winter | Small Grid | Yes | 1h & 2’ |
| 6 | Loads & BESS | Summer | Small Grid | Yes | 59’ |
| 7 | Loads | Winter | Large Grid | No | 7h & 50’ |
| 8 | Loads | Summer | Large Grid | No | 7h & 45’ |
| 9 | Loads & BESS | Winter | Large Grid | No | 8h & 5’ |
| 10 | Loads & BESS | Summer | Large Grid | No | 7h & 55’ |
| 11 | Loads & BESS | Winter | Large Grid | Yes | 10h & 3’ |
| 12 | Loads & BESS | Summer | Large Grid | Yes | 9h & 57’ |

### 5.5.4. Simulation Setup & Utilized Software

The simulation timestep has been set to 5 minutes to show in detail the power flow decision-making of the PCS with a reasonable computational time. Moreover, the simulation duration was set to 1 day for both Winter and Summer seasons. Concerning the utilized software, the model was developed in a Python 3.9 environment and was solved with Gurobi 11 solver due to its powerful capabilities in solving MIP problems. Finally, the simulations were performed with an Intel (R) 11th Gen Core(TM) i7-3.00GHz processor with 16GB installed RAM.

### 5.5.5. Limitations

The main limitations of this chapter are: Firstly, the uncertainties considered are the building occupation and the EV driving patterns. However, there are multiple other uncertainties in PCS, such as PV generation, load demand, etc., which should also be managed on Level 2 using the re-optimization of RHO. Secondly, daily simulations were performed due to computational time. The selection of a weekly simulation, which would be the closest to the average of the season, would provide more insights, such as intra-week effects. Thirdly, modeling non-linearities (e.g., CC-CV, COPs) has been integrated with PWL functions in the MIQP problem, while charging efficiencies, which are power-dependent, have been considered steady. Their consideration of the use of a non-linear solver is proposed for future work to address the level of accuracy decrease. Moreover, while the empirical battery degradation model accounts for most degradation mechanisms (time, C-rate, temperature, throughput, etc.), it does not consider the effects of high SOC and DOD on cyclic aging. Finally, all loads at each location of the large grid are aggregated and optimized together as a node, neglecting the effect of the distribution lines between them due to their much shorter length compared to the other lines of the grid. The consideration of the power losses on these lines is also proposed for future work, while an initial attempt has also been made in Chapter 7.

## 5.6. Results

The results of the two grid scenarios for Level 1, derived by the publication [29], are presented below. Apart from some numerical differences due to the forecast error corrections, the insights of the chapter remain similar for Level 2.

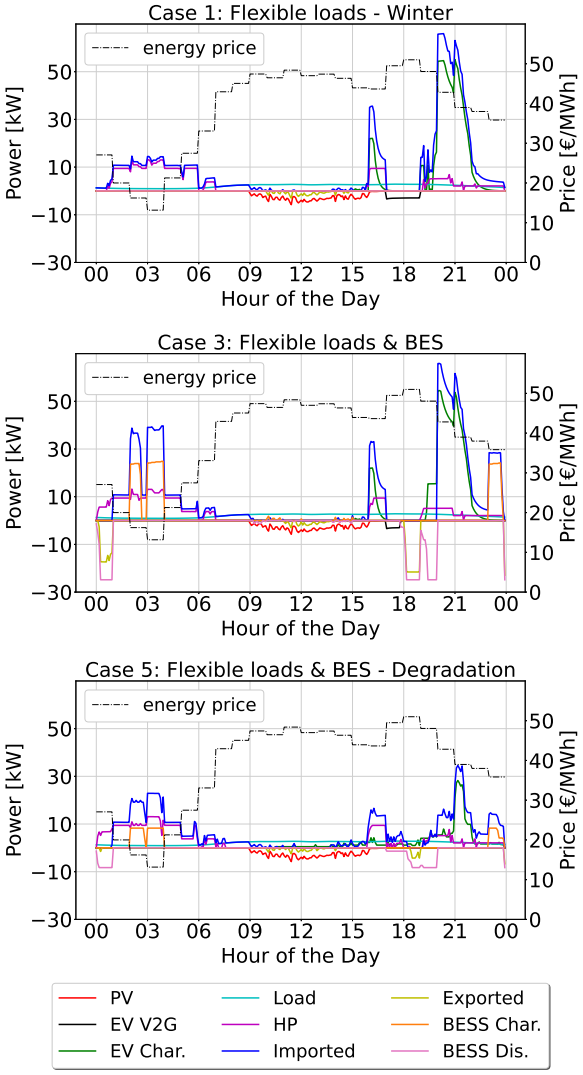


Figure 5.7: Power Flow of Node 3 for Winter Cases 1, 3 & 5.

### 5.6.1. Small Grid Scenario

#### Power Control without BESS

The power flows of Node 3 for Winter Cases 1,3, 5, and Summer Cases 2, 4 are depicted with the daily energy prices in Figures 5.7 and 5.8, respectively. In Case 1 (Figure 5.7), grid power is imported during low energy prices [00:00-07:00] for building and DHW heating, while during [07:00- 09:00], power is imported only for base load cover. Moreover, the highest energy price peak during [17:00-19:00] is avoided, and EVs are charged during the periods [16:00-17:00] and [19:00-00:00]. Additionally, V2G energy is utilized during the highest price peak to cover the base load demand. Finally, PV generation covers the load and is mostly exported because it coincides with the high energy prices [09:00-16:00]. On the contrary, in Case 2 (Figure 5.8), the higher and prolonged Summer PV generation is initially exported during the increasing energy prices of [05:00-10:00] and is consequently used until 19:00 for EV charging, load cover, building cooling, etc. Similarly, the high energy price peak of [19:00-20:00] is mostly avoided, while V2G energy is not preferred due to the availability of PV generation, which causes lower power losses.

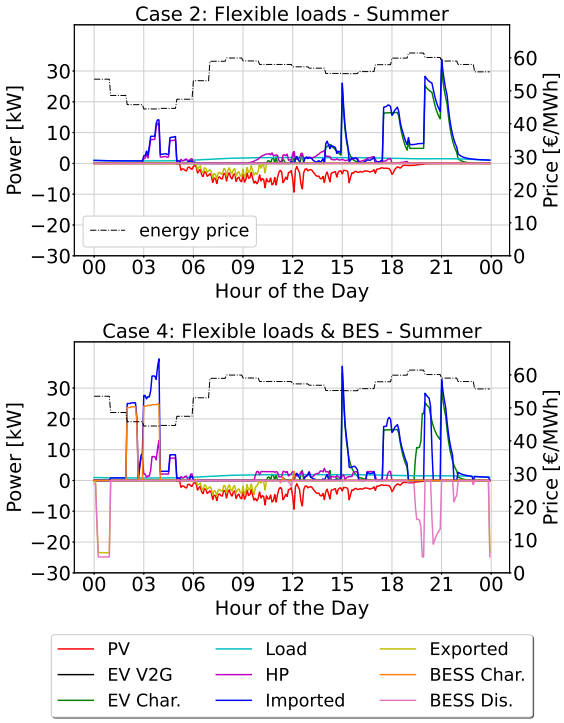


Figure 5.8: Power Flow of Node 3 with & without BESS for Summer (Cases 2 & 4).

### Power Control with BESS

In Figure 5.7, PV generation use, EV charging, and HP operation remain similar for Cases 1 and 3. BESS is mostly charged with grid power during the lowest energy prices of [02:00-04:00], is discharged back to the grid during the highest prices of [18:00-19:00], while it is also used for EV charging and base load cover during [19:00-20:00]. Additionally, the V2G energy use during the high energy prices is considerably decreased compared to Case 1, and BESS use is preferred due to the lower power losses. Similarly, in Cases 2, 4 of Figure 5.8, the control of PV generation and flexible loads behaves the same as in Cases 1 and 3. However, while BESS is mainly charged again during the low prices of [02:00, 04:00], it is discharged for EV charging during the high energy prices of [19:00, 21:00]. Hence, BESS is used more for the flexibility of the node in Case 4, because most revenues are ensured by the PV generation. On the contrary, BESS is used in Case 3 mostly for revenues and cost compensation to compensate for the high imported grid energy due to the low PV availability.

For a closer look at the LCT control, Figure 5.9 depicts the behavior of EV charging, BESS use, and HP heating for Case 3 at Node 3. Figure 5.9 a) shows the coming EV fleets at the 5 chargers of the node. This is depicted by showing the SOCs of the EVs from their arrival time until their departure, and when there is no parked EV, the SOC is zero. Most EV charging for the EVs that stay until the end of the day is performed after 19:00, when the energy prices start to decrease. Moreover, Figure 5.9 b) shows that the EV at Charger 1 provides V2G energy during the high energy peak of [17:00, 18:00] and is charged until its departure SOC after

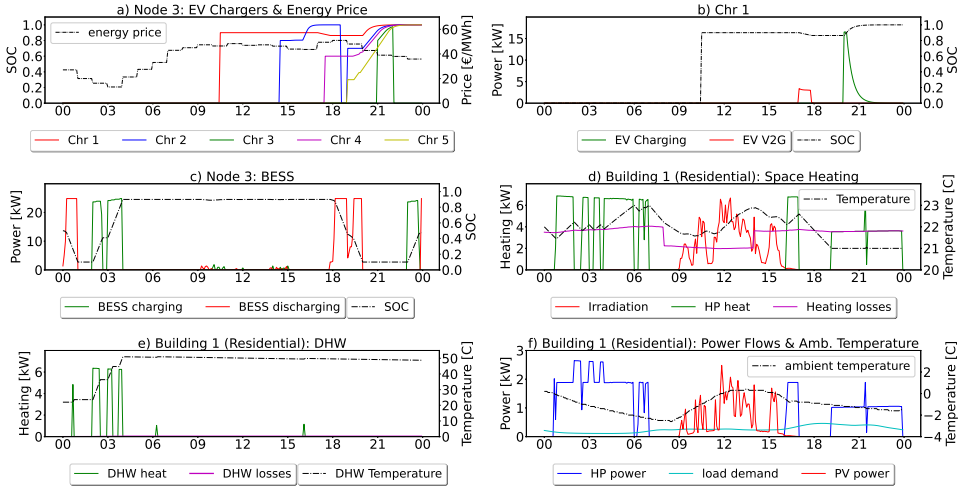


Figure 5.9: Behavior of EV charging (first row), BESS use (second row), and HP heating (third row) for Node 3 in Case 3.

20:00. Figure 5.9 c) shows the charging and discharging power of the BESS as well as the BESS SOC. Additionally, the space heating and DHW of Building 1 of Node 3 are shown in Figs. 5.9 d) and e), respectively. Figure 5.9 d) depicts all heating gains from irradiation and HP heating, and heating losses, while it shows how the building temperature is always maintained within the desired interval [21°, 23°]. Similarly, Figure 5.9 e) shows the DHW heating and the tank temperature that reaches 50°at 07:00 in the morning. Finally, Figure 5.9 f) summarizes the power flows of Building 1 for HP consumption, PV rooftop generation, and load demand.

### Power Control with Battery Degradation

Regarding Case 5 in Figure 5.7, the BESS charging and discharging periods remain similar with and without consideration of battery degradation cost; however, the power levels are notably decreased. Moreover, the discharged BESS energy is more utilized for building heating and EV charging than for power exportation to the grid for revenues. Hence, the BESS use is highly decreased and is preferred only for the basic needs of the node (EV charging and building heating without penalty costs) during the high energy price peaks of [17:00, 20:00]. Additionally, V2G energy is not used due to the combined high round-trip power losses and additional degradation costs. Finally, Table 5.7 summarizes the daily capacity fading in (Wh) and the yearly extrapolation in (%) for the BESS for all nodes and Cases 3-6, showing the effectiveness of the degradation optimization model. For example, while BESS capacity fading is approximately 2.5% in Case 3, it drops to 1.8% in Case 5.

### Power Control Cost & Grid Power Exchange Summary

Figure 5.10a depicts in the upper plot the total imported and exported energy and in the lower plot the total cost (energy cost and degradation cost) of the 3 nodes. Winter cases 1, 3, and 5 have always had higher costs than their respective Summer cases 2, 4, and 6 (up to 60%) because of the higher amount of imported power, as discussed in Section 5.5. For example, Node 1 imported 240kWh and 110kWh in Cases 1 and 2, respectively, (118% increase). Moreover, using a higher PV generation in Summer reduces the total cost, either with direct use or with grid exportation for revenues. Overall, Cases 1-2 export the least amount of energy for all nodes, since they are the least flexible (no BESS). Furthermore, BESS use addition decreases the cost for most nodes by a factor up to 16% (Node 3 in Case 3

Table 5.7: BESS Capacity Fading for Nodes 1-3: Cases 3-5 & Cases 4-6

| | **Capacity Fading** | | | | | | | |
|---|---|---|---|---|---|---|---|---|
| | **Case 3** | | **Case 5** | | **Case 4** | | **Case 6** | |
| **Nodes** | Daily (Wh) | Yearly (%) | Daily (Wh) | Yearly (%) | Daily (Wh) | Yearly (%) | Daily (Wh) | Yearly (%) |
| Node 1 | 3.49 | 2.54 | 2.35 | 1.72 | 2.88 | 2.1 | 1.71 | 1.24 |
| Node 2 | 3.66 | 2.68 | 2.47 | 1.8 | 2.72 | 1.98 | 1.34 | 0.98 |
| Node 3 | 3.41 | 2.48 | 2.4 | 1.76 | 2.29 | 1.76 | 1.16 | 0.84 |

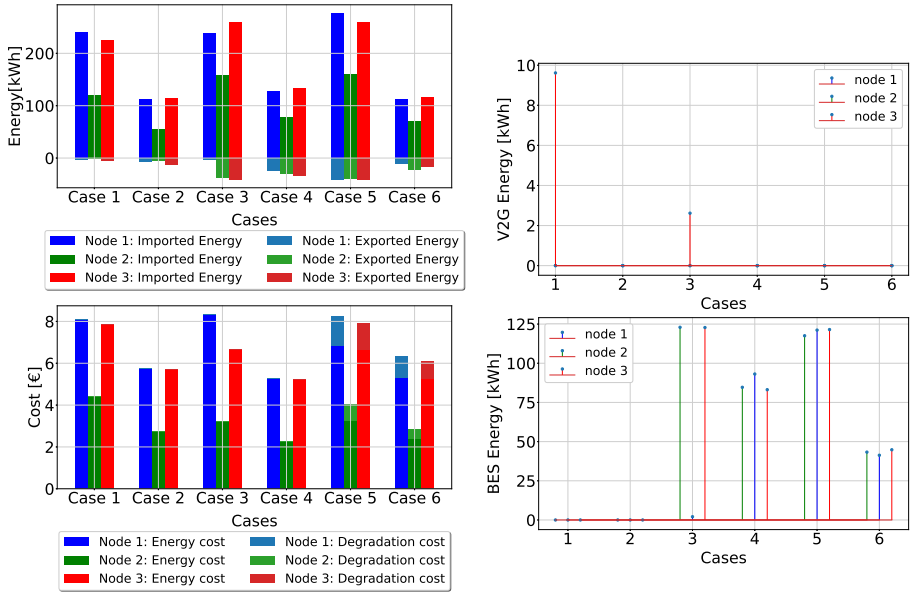


(a) Daily Energy and Degradation Cost (lower) and Grid Energy Exchange (upper).

(b) BESS energy use (lower) and V2G energy use (upper).

Figure 5.10: Power Control Metrics for Nodes 1-3 and Cases 1-6.

compared to Case 1), while the amounts of imported and exported grid power are also increased for all nodes when Cases 3 and 4 are compared to Cases 1 and 2, respectively. Additionally, in battery degradation Cases 5 and 6, the total cost always increases for all nodes when comparing them with their respective Cases 3 and 4. While the energy cost can be lower (e.g., Node 1 in Case 5 compared to Case 3) due to lower grid power exchange to avoid higher degradation, when the degradation cost is summed up, the total cost results are always equal to or higher.

The node type also strongly impacts the exchanged grid power and total cost. The commercial node (Node 2) is generally characterized by a lower cost in all cases. This is because, as explained, commercial buildings (e.g., stores and offices) are occupied less during the day than residential buildings, and EVs are parked for a lower parking time in public chargers and request a lower amount of energy. Hence, the needed imported grid energy is considerably lower (by 30% to 50%) for the commercial node. For that reason, there is also more power window in the feeder to export BESS energy and PV generation for revenues in commercial nodes, and hence, Node 2 exports considerably more power when BESS is introduced, almost comparable to Node 3, which is the most flexible node. Hence, highly flexible nodes or nodes that occupy less of the power capacity can use their BESS capacity more for revenues. Finally, the degradation cost is always higher for Nodes 1 and 3 because they comprise home chargers where EVs request higher energy amounts.

### BESS Energy & V2G Energy Use Summary

Moreover, the type of the node and the various effects considered, such as the seasonal and degradation effects, influence the amount of V2G and BESS use. Regarding the use of BESS and V2G, Figure 5.10b depicts the total V2G energy used (upper plot) and the total BESS energy used (lower plot) per node and case. V2G is used only in Winter Cases 1 and 3, because PV generation is available for a shorter time. For example, V2G energy is generally used during high energy price peaks. During the Winter price peaks of [17:00-20:00], there is no more available PV generation. Moreover, concerning all other cases, BESS use is always preferred over V2G due to the higher BESS efficiency and lower power losses. In this regard, Figure 5.11, derived from the publication [27], depicts the increase in V2G energy use for the three nodes if the EV charging efficiency is increased from the current 0.95 to the future 0.97 or the ideal 0.99. As can be seen, the current round-trip power losses constitute a great limitation to V2G energy use, which can be potentially changed with future improvements. Consequently, higher charging efficiencies will lead to lower required grid energy. However, nodes with low flexibility (Node 2) are still less likely to use V2G. For more information about the PCS performance with and without V2G, and the related impact of seasonal and grid type variations, the reader is referred to [27].

In Cases 5 and 6, where there is additional degradation cost combined with the power losses, V2G energy use becomes inefficient even during Winter. Finally, V2G energy is more likely to be used in Node 3 (the mixed node), which has the highest flexibility, comprising both residential and commercial buildings, and home and (semi-)public chargers. Regarding BESS energy use, as already discussed, Winter (Cases 3 and 5) favors using BESS for charging and discharging power to the grid for revenues for most of the nodes. On the contrary, the available PV

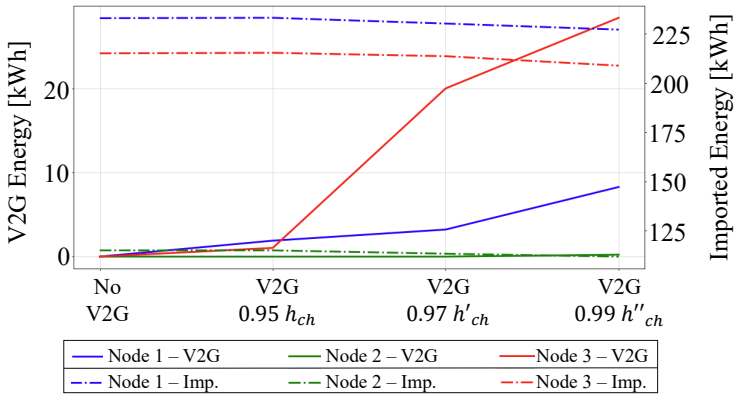


Figure 5.11: Comparison of V2G and grid energy use for Nodes 1-3 with different EV charging efficiencies [27].

generation is preferred during Summer for power exportation, and the BESS is mostly used for the needs of the node instead. Finally, the consideration of battery degradation decreases the use of BESS, especially during Summer, due to the additional degradation cost.

### 5.6.2. Large Grid Scenario

#### Flexible Loads and BESS

Regarding the large grid scenario, Figure 5.12 shows, firstly, in the two lower plots, the power flows of Node 2 for Cases 9 and 10 (BESS cases during Winter and Summer). Node 2 has been chosen for the power flow analysis since it constitutes the node with the highest number of loads. Some of the previous observations from the small grid scenario can also be seen here. For example, during Winter, most building heating and EV charging are performed during the low energy price periods; hence, in the morning before 08:00 and in the evening after 19:00. Moreover, during Summer, most PV generation is exported during the high energy prices until 09:00, while after 09:00 it is mostly used for the needs of the node, e.g. building cooling. However, in contrast with the small grid, less PV generation is exported to the main grid for revenues during Winter, while a considerable amount is used for building heating and EV charging. Hence, in large grids, which comprise many loads (buildings and chargers), PV self-consumption is increased, and grid power exportation is decreased. This is because when a high number of loads are constantly present at a grid, more power is consistently needed during the day, and available PV power will be firstly utilized for their consumption.

Regarding BESS use, BESS is hardly used in Node 2 during both Winter and Summer. This can be explained intuitively as follows. The BESS is constrained to have a similar SOC at the beginning and the end of the day. Hence, the amount with which it is charged during the day (e.g., during the low energy price periods) needs to be discharged during the high energy price periods. However, if during the high energy price periods, there is needed power demand for the loads and the BESS capacity is not enough to cover them, then the node needs to import grid power and cannot discharge the BESS energy to the main grid for revenues. Therefore, the high amount of loads in a large grid also decreases the use of BESS, because it is preferred to use the low energy price time periods to import power for the needs of the node rather than use them to discharge the BESS to the grid for revenues. This is also validated in the upper plot of Figure 5.12, which shows the respective power flows for Node 6 (only 6 buildings and 6 EV chargers), where BESS is considerably more utilized. Hence, it is concluded that the need for BESS is decreased when the grid size is increased.

#### Power Control Cost Comparison

The daily energy cost for all nodes 1-13 and cases 7-12 is shown in Figure 5.13. As in the small grid scenario, the influence of the seasonal effect on the cost is considered the most important since, for most nodes, Summer cases are characterized by a lower total cost. Moreover, the total node cost always results in

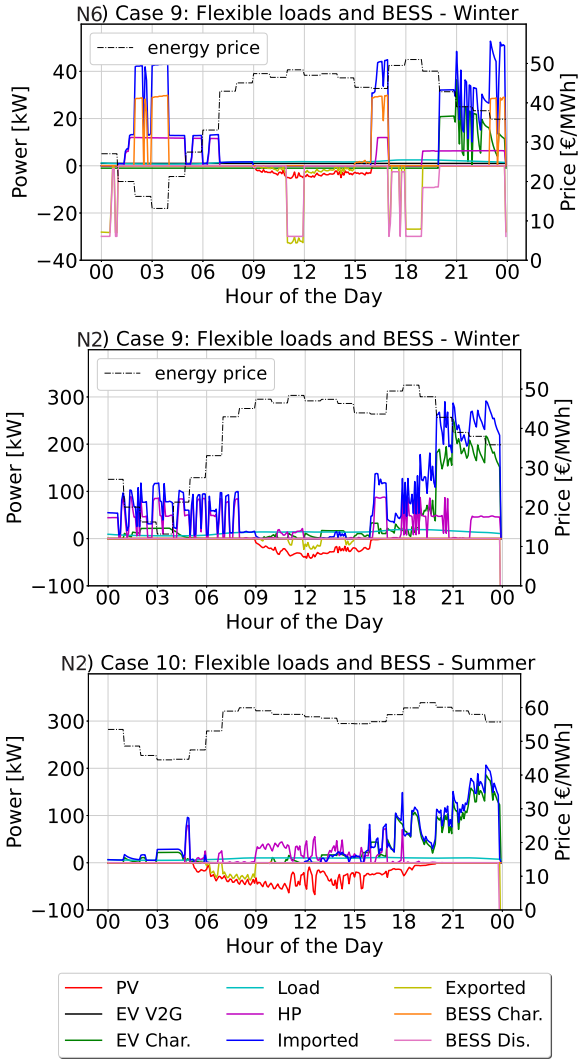


Figure 5.12: Power Flows of Node 6 (6 buildings/chargers) for Case 9 and Node 2 (44 buildings/chargers) for Cases 9 & 10.

equal or lower values when the BESS is used, and as a consequence, Cases 9 and 10 are always less costly than their respective Cases 7 and 8. Moreover, Cases 8 and 10, the Summer BESS cases without degradation, show the lowest total cost for almost every node. Furthermore, using BESS also closes the gap with the other cases, thus reducing the cost difference between cases with other characteristics

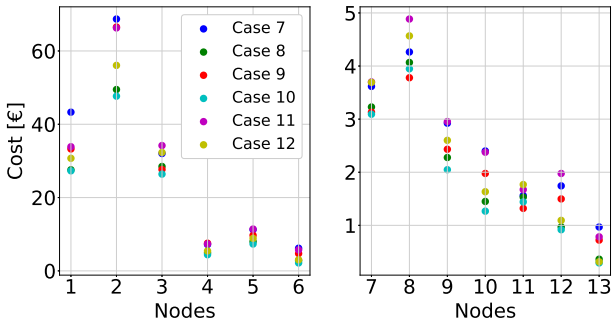


Figure 5.13: Daily Energy Cost for Nodes 1-13 and Cases 7-12.

and influencing factors. Finally, battery degradation also affects the total cost, with Cases 9 and 10 always resulting in a lower cost than their respective Cases 11 and 12. However, in some nodes, such as Nodes 1 and 2, the contribution of the BESS for cost decrease is higher than the impact of degradation; hence, Case 7 results as the most costly case for these nodes. Nevertheless, in most of the nodes, the degradation cost is more significant, and Case 11 is the most costly case. In a limited number of nodes, the degradation cost influence on the total cost is also stronger than the seasonal effect, with Case 12 surpassing Case 9 or 7, such as in Nodes 9 and 8, respectively.

### V2G Energy Comparison

Figure 5.14 depicts on the left the total V2G energy used in the grid for all cases, while the node V2G energy used is shown for the big-level nodes (1, 2, 3) and medium-level nodes (4, 5, 6) with two heatmaps on the right. As explained, V2G is more likely to be used during Winter (Cases 7, 9, 11) due to lower PV availability, reaching up to 100kWh for Case 7. Moreover, introducing BESS in Cases 9-12 decreases the use of V2G since BESS is preferred due to lower power losses. Furthermore, considering battery degradation decreases V2G use further (Cases 11-12). Cases 7 and 9 are characterized by the highest V2G use, also in the heatmaps. Comparing Figure 5.14 with Figure 5.10b, where V2G was only used in Case 1 and slightly in Case 3, V2G is used in all cases for the large grid and is never zero. This is because a grid of a larger size is more favorable for V2G energy use. The heatmaps also show that, excluding Node 6, larger Nodes 1-3 with a higher amount of loads have more flexibility to use V2G in all cases.

### Grid Power Exchange Comparison

Finally, Table 5.8 summarizes the amounts of imported (Imp.) and exported (Exp.) energy for all the Nodes 1-6 and Cases 7-12. The imported energy greatly increases for the Winter cases (150% higher for Node 1 in Case 7 than in Case 8), while the

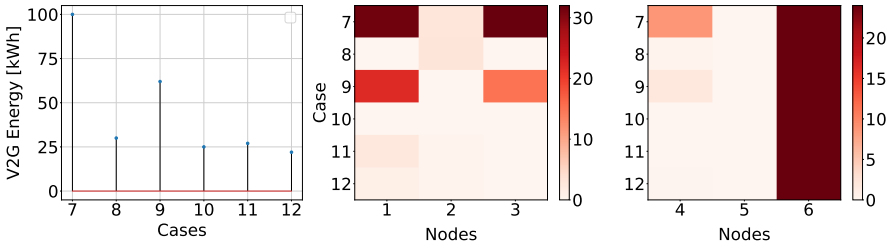


Figure 5.14: Total V2G Energy (left) & Node V2G Energy for Nodes 1-3 (center) and Nodes 4-6 (right) for Cases 7-12.

Table 5.8: Imported Energy (Imp.) & Exported Energy (Exp.) for all Nodes 1-13 and Cases 7-12.

| | Case 7 | | Case 8 | | Case 9 | | Case 10 | | Case 11 | | Case 12 | |
|---|---|---|---|---|---|---|---|---|---|---|---|---|
| N. | Imp. [kWh] | Exp. [kWh] | Imp. [kWh] | Exp. [kWh] | Imp. [kWh] | Exp. [kWh] | Imp. [kWh] | Exp. [kWh] | Imp. [kWh] | Exp. [kWh] | Imp. [kWh] | Exp. [kWh] |
| 1 | 1203.99 | 46.7 | 524.48 | 46.28 | 1647.39 | 487.7 | 527.44 | 55.11 | 927.19 | 73.7 | 644.7 | 180.48 |
| 2 | 1897.15 | 26.7 | 938.6 | 71.28 | 1864.21 | 43.83 | 924.09 | 88.44 | 2073.25 | 277.12 | 1066.84 | 210.47 |
| 3 | 889.28 | 13.2 | 517.47 | 27.09 | 1125.8 | 249.24 | 589.39 | 101.56 | 1017.74 | 151.74 | 583.02 | 100.1 |
| 4 | 244.9 | 17.04 | 111.27 | 20.25 | 248.73 | 20.25 | 152.72 | 60.5 | 294.73 | 68.99 | 131.49 | 44.06 |
| 5 | 304.86 | 9.39 | 154.09 | 17.82 | 371.7 | 76.31 | 178.61 | 42.51 | 331.28 | 44.11 | 166.68 | 32.58 |
| 6 | 194.19 | 10.68 | 68.3 | 20.17 | 281.48 | 98.01 | 101.29 | 54.42 | 255.71 | 71.63 | 66.34 | 22.53 |

use of BESS increases imported and exported amounts at most nodes (Cases 9 and 10 compared to Cases 7 and 8) to use its flexibility for revenues. Moreover, the exported energy amounts are increased for all nodes in Summer Case 8 compared to Winter Case 7 due to the higher PV generation (e.g. 270% for node 3). Finally, comparing the degradation cases 11 and 12 with their respective cases 9 and 10, the consideration of degradation decreases the imported and exported energy amounts for the smaller nodes; however, this is not always the case for Nodes 1-3. Therefore, in larger-size nodes with a larger available BESS capacity, the power control might prefer to use its BESS capacity for revenues to compensate for the degradation cost rather than decrease the BESS equivalent cycle (when degradation is considered).

## 5.7. Discussion and Validation

### 5.7.1. Summary of Findings

The most important findings of this chapter can be summarized as follows:

- Available PV generation or stored BESS energy decrease the likelihood of V2G use, especially in smaller grids. Moreover, the higher round-trip EV charging losses and additional degradation costs also negatively influence the V2G usability, leaving space for V2G use in special periods, such as high

energy price peaks. Finally, nodes with low flexibility, such as the commercial nodes, are also less capable of using V2G.

- As the size of the grid increases, the use of BESS decreases due to the use of the energy price variations to directly import cheap grid energy for load consumption or export PV generation for revenues. This is due to the vast number of loads always present in the control horizon. For the same reason, PV self-consumption and the likelihood of V2G use increase with the grid size.
- The seasonal and grid type effects strongly influence the power control cost and the use of BESS. The lower load consumption during Summer and of commercial buildings/chargers directly decreases the total power control cost. Moreover, commercial nodes leave a higher power window, due to lower exchanged grid power levels, for BESS use. On the contrary, the higher available PV power during Summer is preferred over stored BESS energy.
- As a result of the above, the Winter case, comprising BESS and considering degradation, is defined as the most costly case. On the contrary, the Summer case, comprising BESS without considering degradation, is defined as the least costly case.
- In smaller grids, the degradation costs, although they decrease the BESS power levels, are low enough to affect the decision-making of the PCS. However, in larger grids, accumulated degradation costs can have a significant impact on the scheduling decisions, such as prompting a high exploitation of the BESS capacity for revenues to compensate for the additional induced costs by degradation.

### 5.7.2. Comparison with existing power control works

#### MPC power control works

MPC works use the concept of the moving horizon for their control strategies. MPC models, such as this work, handle uncertainties, triggering re-optimizations of the receding control horizon upon realization of uncertain events. A similar adaptive MPC strategy was developed in the PV-EV-BESS control work in [195], where the new predicted model states are adapted at every re-optimization according to the new user preferences using a Kalman filter-based estimator. However, the modeling of various charging details, such as the CC-CV regions of the capacity degradation, was not included. MPC models that also incorporate HPs and building heating can be found in the building EMS of [179], while EVs were also added in [194]. In [194], re-optimizations are triggered at every timestep, where the new user preferences and forecast data are fed to the mode; consequently, the control horizon moves a period $T$ forward. While re-optimizations at every timestep provide the highest protection against uncertainties, it can become very computationally expensive if the control horizon is too long or the selected timestep is too low. The MPC models in [179], [194], and [178] remained MILP because they considered a steady COP; thus, the rated HP COP, the average COP over the horizon, and an approximation

of the ideal COP, respectively. In this chapter, all cases were re-simulated with average COPS and MILP formulation (3.4 and 6 for Winter and Summer), finding an accuracy error increase up to 10% and a computational time decrease up to 15%. On the contrary, while a variable temperature-dependent COP was considered in the building-level MPC PV-HP-TESS control work in [202], the HP was ON-OFF and could deliver only zero or rated heating output. In this chapter, the variable COP, dictated in (5.26), makes (5.28) quadratic, and the PCS model MIQP. Hence, the model accuracy is increased at the expense of computational burden.

#### Multi-objective power control works

There are multiple ways to solve optimization problems with multiple objectives. Rule-based strategies can be developed that adjust with rules the priority of the objectives according to the dynamic state of the problem (e.g., temperature, SOC, PV generation, load in [192]). However, these rule-based logics can become extremely complex with multiple rules and cannot find the absolute global optima. Nash bargaining models, such as in [196], construct different subproblems for every objective and search for Pareto optimal solutions via iterative methods; however, they can become computationally heavy with more than two objectives. Integrating all objectives (e.g., cost, thermal comfort, emissions, etc.) with different weights in the objective, such as in [191], eliminates the computational expense of the previous methods and has the advantage of easy modification of the priority of the objectives (adjusts priorities deliberately); however, they depend on the proper weight selection. Finally, translating all objectives into one in the objective function, such as in [20], [203], and this chapter's work, transforms the problem into a single simple optimization. All objectives, such as thermal discomfort, EV charging discomfort, PV curtailment minimization, and battery degradation minimization, were translated into cost, which was added to the total power control cost to be optimized. This method can be considered as a subcategory of the multi-objective methods with weight utilization. However, it has the limitation that the objective priority depends on the resulting cost and is hardly altered.

### 5.7.3. Validation

#### Power control model

The power control model has been validated against a rule-based uncontrolled benchmark model based on the work in Chapter 3, and the MPC EV SC model in [203]. The three models have been fed with the same examples and characteristics of buildings, HPs, PVs, and EV fleets, and the same energy prices for a fair comparison. The benchmark model has been created with the uncontrolled building heating model, which operates the HPs only according to the desired building temperature interval [21°, 23°], and with the uncontrolled EV charging model, which charges the EV fleets with rated power as soon as they arrive (Chapter 3). It maximizes PV self-consumption according to the rule logic:

1) When the PV generation is higher than the total load, all the load is covered by the PV generation, and the rest of the PV power is exported to the main grid for

revenues and cost reduction.

2) When the total load is higher than the PV generation, all PV generation is used for its cover, and the rest is covered by imported grid power.

Concerning the benchmark model, this comparison is used to show and validate the performance of the power control model concerning the reduction of the total cost and the needed grid limits against the uncontrolled case of the LCT operation (without energy arbitrage). Concerning the EV SC model in [203], this comparison validates the PCS performance against existing control works. The EV fleets are charged again by performing energy arbitrage, utilizing firstly PV self-consumption and secondly imported grid power. The PCS of this chapter comprises the extra features of building heating, V2G use, and BESS use. Hence, the PCS model needs more imported grid energy since it comprises more capabilities. Thus, the specific cost metric $C_{sp}$ in (5.55), which is the ratio of the total cost $C$ divided by the difference between the total imported and exported power and is measured in $€/kWh$, has been used for a fair cost comparison:

$$C_{sp} = \frac{C}{\sum_{t=1}^{T}(P_{im}^{t} - P_{ex}^{t})} \tag{5.55}$$

In Figure 5.15, the power flows of the uncontrolled, EV SC, and this chapter's power control models are depicted. As seen, the low energy prices during [00:00,

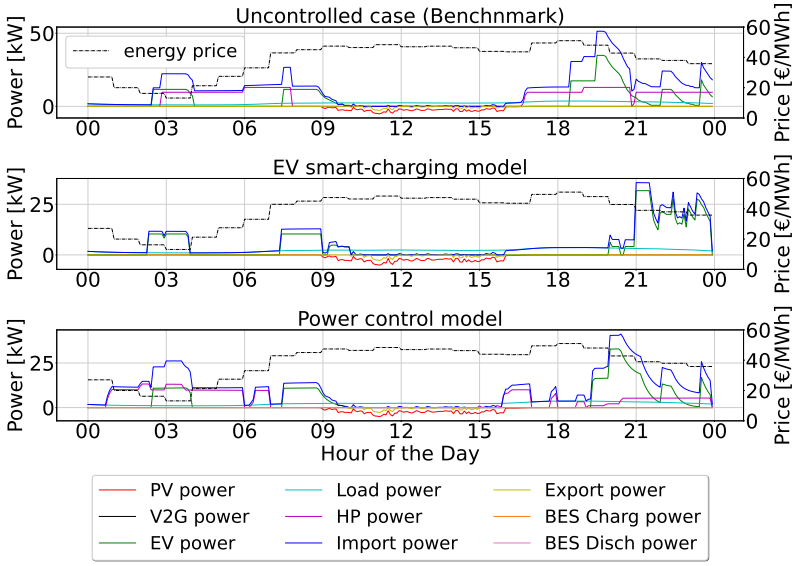


Figure 5.15: Comparison of power flows for the benchmark, EV SC [203], and power control models: Node 1 - Winter.

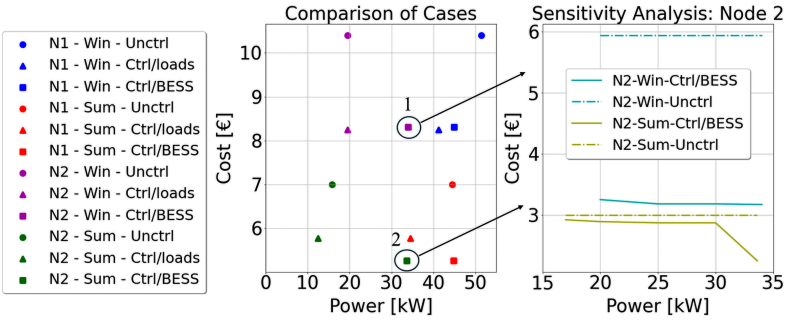


Figure 5.16: Total cost and maximum used power comparison between power control and benchmark models (Unctrl) for Nodes N1-3 (left plot) & Sensitivity analysis of power limits for the two specific cases (right plot).

Table 5.9: Comparison of specific cost (€/kW) for EV SC ([203]) and power control models for Nodes: N1 & N2, Winter - Summer.

| **Models** | **Winter** | | **Summer** | |
|---|---|---|---|---|
| | **N1** | **N2** | **N1** | **N2** |
| **Model in [203]** | 3.05 | 3.24 | 4.59 | 4.76 |
| **Ctrl: No BESS** | 2.9: -4.83% | 3.07: -5.25% | 4.62: +0.74% | 4.49: -5.81% |
| **Ctrl: BESS** | 2.95: -3.09% | 2.25: -30.6% | 4.24: -7.56% | 3.81: -20.11% |

06:00] are not taken advantage of in the uncontrolled model as they are in the power control model. Moreover, the EVs arrive during the energy price peak during [18:00, 20:00] and start charging immediately without avoiding the price peak, in contrast with the power control model. Finally, the power scheduling of the EV SC and PCS models is similar except for the addition of building heating.

Moreover, Figure 5.16 depicts the comparison of Nodes 1 and 2 for Winter and Summer between the uncontrolled model and the PCS model with and without BESS use concerning total cost and maximum needed power capacity (left plot). It can be seen that for all cases the cost is lower for the PCS model, while, in most of them, a lower power capacity is also needed. For example, Node 1 during Winter needs 10.8 € and 51kW maximum power capacity in the uncontrolled model, while it needs 8.3 € and 42kW maximum capacity in the PCS model. In two cases, for Node 2 during Summer and Winter, a higher power capacity was needed for the PCS model using BESS: 32kW and 33kW compared to 16kW and 20kW for the

uncontrolled, respectively. Hence, a sensitivity analysis was realized for the power limits of these cases (right plot), proving that the PCS model cost remains always lower when the same power limits are used. Finally, Table 5.9 summarizes the cost comparison of this chapter's PCS and the EV SC models. The cost is highly reduced, especially when a BESS is used, reaching up to 30.6% reduction. Without the use of BESS, the specific cost of this work's PCS model is slightly lower (up to 5.81%), which is due to the capability of V2G use.

### Battery degradation model

Validation of the original battery degradation model using experimental data has already been realized in [200] under various tests, that lasted for up to 114 days, such as storage, CC cycle, CC-CV cycle, and application-based dynamic current profile tests (real-world PV-residential BESS application). A capacity loss error below 1% of the original capacity was found, while the maximum relative error was below 21%, proving its high accuracy.

For the validation of the linearized model, the real battery degradation has been calculated post-optimization and compared with the linear battery degradation results. Figure 5.17 depicts the real and linear cyclic degradation mechanisms (Qcyc 1 and Qcyc 2) and the total degradation (Qcyc total) for the BESS of Node 1 (upper plot). Moreover, the simultaneous BESS SOC and charging and discharging currents are depicted in the lower plot. The accuracy of the developed linearized degradation model has been proven using the root-mean-squared error (RMSE) values, which are calculated for the comparison of the real and linear total cyclic degradation as follows:

- Node 1: $RMSE = 1.9856 * 10^{-6}$
- Node 2: $RMSE = 1.8346 * 10^{-6}$
- Node 3: $RMSE = 2.0652 * 10^{-6}$

Table 5.10: Further validation of linearized battery degradation model.

| | **Models** | | | | | |
|---|---|---|---|---|---|---|
| | **Model [200]** | | | **Model [204]** | | |
| **Conditions** | **Calendar** | **Cyclic** | **Total** | **Calendar** | **Cyclic** | **Total** |
| Condition 1 | 1.78% | 0.67% | 2.44% | 1.35% | 0.45% | 1.8% |
| Condition 2 | 1.52% | 0.79% | 2.32% | 1.29% | 0.51% | 1.8% |
| Condition 3 | 3.11% | 0.74% | 3.85% | 1.75% | 0.49% | 2.23% |
| Condition 4 | 1.95% | 0.76% | 2.71% | 1.38% | 0.48% | 1.86% |
| Condition 5 | 5.32% | 1.96% | 7.28% | 10.48% | 1.5% | 11.98% |
| Condition 6 | 7.27% | 2.15% | 9.42% | 11.31% | 1.7% | 13% |
| Condition 7 | 4.55% | 2.36% | 6.91% | 10.06% | 1.69% | 11.75% |
| Condition 8 | 9.26% | 2.24% | 11.5% | 12.1% | 1.64% | 13.73% |
| Condition 9 | 5.82% | 2.15% | 7.97% | 10.68% | 1.61% | 12.29% |

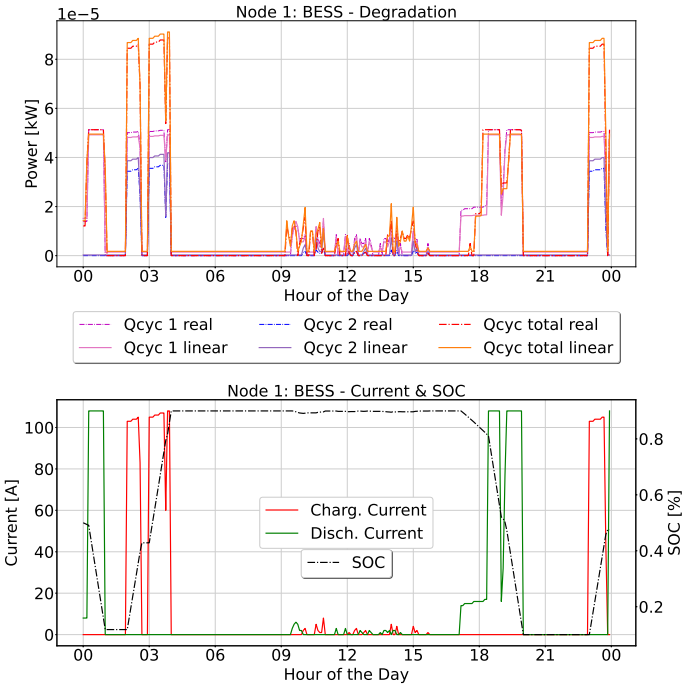


Figure 5.17: Real/linearized cyclic degradation mechanisms in and post optimization (upper). Charging/discharging Current/SOC (lower)

Finally, the model's accuracy has been validated with the models in [200] and [204] under 9 conditions, and the results are summarized in Table 5.10 showing an accuracy error < 3% in most cases and no higher than 14%. The conditions are described below:

1) Simulation Time (ST): 1 year (y), Battery's year of life (YoL) 1$^{st}$, Min aging.
2) ST: 1y, YoL: ST, Min aging and avg SOC.
3) ST: 1y, YoL: ST, Min aging and throughput (TP).
4) ST: 1y, YoL: ST, Min aging, avg SOC, and TP.
5) ST: 9y, YoL: 1$^{st}$, Min aging.
6) ST: 9y, YoL: 10$^{th}$, Min aging.
7) ST: 9y, YoL: ST, Min aging and avg SOC.
8) ST: 9y, YoL: ST, Min aging and TP.
9) ST: 9y, YoL: ST, Min aging, avg SOC, and TP.

### Bi-level Power Control Formulation

Finally, Figure 5.18 demonstrates the effectiveness of the bi-level formulation under both normal conditions and ancillary services provision. The RT schedule of Node 3

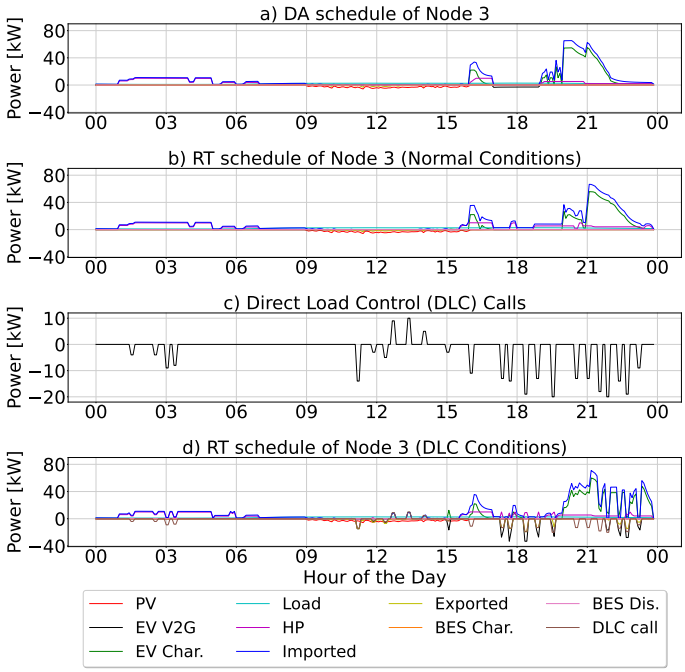


Figure 5.18: Example of both DA and RT power control schedules under normal and DLC conditions.

in Figure 5.18b) deviates very little from the DA schedule in Figure 5.18a) under normal conditions. For example, it is the same until noon, and it deviates in the afternoon when buildings are reoccupied, and EVs arrive at the chargers to correct the forecast errors. Additionally, Figure 5.18d) depicts the modified RT schedule of Node 3 if the PCS participates in ancillary services, such as DLC. The RT schedule under DLC conditions increases or decreases the consumption of the DA schedule in Figure 5.18a) according to DLC calls by the operator shown in Figure 5.18c). A higher focus on the PCS performance for ancillary services provision, such as DLC, will be given in Chapter 7.

## 5.8. Conclusions & Future Work

In this chapter, a two-level MIQP power control model is developed for the DA and RT scheduling of PVs, EVs, HPs, and BESS for energy arbitrage respecting the grid limits. The power control has been tested with and without BESS use under various conditions (seasons, grid types and sizes, and battery degradation). An important finding is that while V2G is less used than the BESS in small grids due to

higher power losses, especially when degradation is considered, opposite trends are observed in larger grids with a vast amount of loads. Hence, the importance of BESS decreases as the grid size increases, while the V2G use is more likely to increase. Due to the multiple loads, a higher PV self-consumption is also observed in larger grids. Moreover, the grid type also has a notable impact on the power control results since commercial grids are characterized by a lower cost due to much less needed grid power and use less V2G due to lower flexibility. On the contrary, due to the higher power window, they are capable of using more BESS energy for revenues. Moreover, the strong influence of the seasonal effect was also seen, with a much lower control cost observed during Summer, while the available PV generation also decreased the BESS and V2G use, Finally, another important finding is that while degradation costs are much lower than the power control costs in smaller grids, affecting only the BESS power levels, they become more important in larger grids and can significantly alter the energy arbitrage decisions. Finally, the PCS model has been compared and validated against other benchmark and control models, showing cost reductions of up to 5.81% and 30.6%, without and with BESS use, respectively.

In future work, considering more uncertainties (PV generation, weather data, load demand) is proposed to qualify the uncertainty management of the RT scheduling level. Moreover, weekly or seasonal simulations are proposed to capture the intra-week effects and strengthen the findings about season comparison. Finally, the dependence of the charger efficiencies on the power levels should be studied, which is expected to have a notable impact on the optimization decision-making.

# 6

# Power Control of LCTs and Ancillary Services Provision: Part 1

*Summary*

As explained in Chapter 2, PCSs can exploit the flexibility of LCTs and BESS not only for energy arbitrage, but also for ancillary services provision. This chapter enhances the PCS of PVs, EVs, HPs, and BESS developed in the previous chapter to provide aFRR reserves, simultaneously with the previous objectives (energy arbitrage, PV self-consumption increase, customers' thermal and charging comfort maintenance, etc.). The contribution of the BESS and the flexible loads to the PCS is evaluated under various conditions, such as different seasons, types (residential, commercial, and mixed), small and large grid size levels, and energy/reserve prices. Validating against the PCS of publication [27] (Chapter 5), designed solely for energy arbitrage, the findings demonstrate the potential for consistently 100% increased cost savings when the PCS participates in the reserve market, especially when the flexible loads and BESS cooperate and interchangeably distribute the various responsibilities. These benefits become even more important in our years with the high increase in energy prices, but also with the much higher reserve prices; hence, higher potential for ancillary services provision. While the always present BESS is able to contribute more to ancillary services provision compared to the uncertain nature of the EV fleets, the contribution of EVs increased to a notable 38.5% compared to the BESS at grids or nodes of larger size. Finally, mixed nodes that comprise both residential-commercial buildings and home-public chargers have a higher potential for ancillary services provision due to higher flexibility, demonstrating a 5x and 12x higher potential compared to residential and commercial nodes, respectively.

*Outline*

The chapter is categorized as follows: The motivation and contributions are summarized in Section 6.1. Section 6.2 comprises the concept of this chapter's PCS, explaining the use of the two levels for simultaneous energy arbitrage and ancillary services provision. In continuation, Section 6.3 comprises the modeling of the PCS categorized to the modeling of the EVs and BESS, buildings, imbalance market, node constraints, and the objective function, while Section 6.4 integrates the utilized case studies and scenarios. The results for two investigated grid scenarios concerning the analysis of power flows, cost, and provided reserve energy, and this chapter's discussion are summarized in Section 6.5. Finally, Section 6.6 concludes the chapter.

This chapter is based on:

S. Warmerdam, N. Damianakis and G. R. C. Mouli. 'Power Control of PV Generation, Flexible Loads, and Battery Energy Storage for Frequency Reserves Provision'. In: *Sustainable Energy, Grids and Networks* (2025). Under Review

## 6.1. Motivation & Contributions

The developed PCSs in the reviewed studies in Chapter 5 did not take into account the contribution and the revenues that can be gained in PCSs when they also participate in the balancing market to provide frequency regulation, such as FCR and aFRR reserves.

The cooperation of PVs with ESS with DR incentive programs for prosumer participation in FCR provision has been explored in [205] and [206], while [207] also accounted for aFRR. Their collective objective was to achieve maximum operational cost reduction, taking advantage of the revenues from the FCR provisions, which succeeded in all the investigated DR programs. However, the studies did not consider the contribution of flexible loads, such as EVs and HPs. EVs were incorporated with PVs and BESS in the component sizing and power optimization study of [20], aiming for simultaneous cost and FCR provision optimization while accounting for component degradation. Moreover, the authors in [208] conducted a sizing and power optimization analysis utilizing an HESS and aiming for PV self-consumption maximization and optimal cost via participation in the FCR market. However, the benefits of the synergy with HPs were not taken into consideration. On the contrary, the authors in [209] showed that the control of HPs together with ESS, RESs, and EVs in DR programs can greatly enhance the EMS flexibility for energy arbitrage and ancillary services provision. However, the work in [209] investigated only the cooperative flexibility of the assets and did not proceed to comparisons regarding their individual contribution. Moreover, all of the studies in this section focused on primary frequency regulation (FCR) and not on secondary (aFRR).

PVs can be effectively combined with BESS, such as in [210], where the economic potential for PV self-consumption maximization and participation in the reserve market for FRR provision was highlighted. This synergy for energy arbitrage and FRR provision also significantly reduced the annual electricity costs for an HEMS in [211], which reached up to 14.5% (electricity and heating) when HPs were added in [212]. The synergy of PVs and HPs in a residential area in [213] also reduced the surplus grid energy by up to 52.6% simultaneously with the total electricity cost, while their use for combined participation in energy and reserve markets was studied in [214]. Additionally, the BESS participation in multiple energy markets (FCR, aFRR, mFRRda) was studied in [215], [118], [216], aiming to quantify the potential of stacked revenue. In [215], SOC supervision and regulation were studied via a local controller to avoid the provision of scheduled power beyond the battery's SOC limits. It was found that while the battery is protected, aFRR and FCR power output throttling may result in market penalties due to the deviation from scheduled ancillary power and should be avoided at all times. However, each study showed a significant increase in revenue, indicating the BESS potential to operate in multiple energy markets. However, the study in [118] did not consider RES and smart loads integration, while the authors in [118] and [216] only included the effect of PV generation in their studies.

As can be observed in Table 6.1, multiple grid-level power control works in the literature have explored the integration of RESs with flexible loads and/or ESS to provide flexibility for cost benefits, ancillary services provision, or other objectives

Table 6.1: Summary of Characteristics & Contributions of Grid-level Cost-oriented Power Control Studies.

| Studies | RES | HPs | EVs | V2G | ESS | Ancillary Services | ESS vs RES/ Flexible loads | Seasonal/ Meteorological effect | Energy price/ Reserve price effect | Grid-type effect | Grid-size effect |
|---|---|---|---|---|---|---|---|---|---|---|---|
| [156] | ✓(PVs) | | | | ✓(BESS) | | | | | | |
| [160] | ✓(PVs) | | | | ✓(BESS) | | | ✓ | | | |
| [157] | ✓(PVs) | | | | ✓(BESS) | | | ✓ | ✓ | | |
| [117] | ✓(PVs) | | | | ✓(BESS) | | | ✓ | ✓ | | |
| [164] | ✓ | | ✓ | ✓ | ✓ | | ✓ | | | | |
| [165] | ✓(PVs) | | ✓ | ✓ | ✓(BESS) | | | | | | ✓ |
| [185] | ✓(PVs) | ✓ | | | ✓(BESS) | | | ✓ | ✓ | | |
| [197] | ✓(PVs) | ✓ | ✓ | ✓ | ✓ | | ✓ | ✓ | | | ✓ |
| [118] | | | | | ✓(BESS) | ✓(aFRR) | | ✓ | | | |
| [206] | ✓(PVs) | | | | ✓ | ✓ | | | ✓ | | |
| [155] | ✓(PVs) | | | | ✓(BESS) | ✓ | | ✓ | ✓ | | |
| [205] | ✓(PVs) | | | | ✓(BESS) | ✓ | | | ✓ | ✓ | ✓ |
| [215] | ✓(PVs) | | | | ✓(BESS) | ✓(aFRR) | ✓ | | | | |
| [216] | ✓(PVs) | | | | ✓(BESS) | ✓(aFRR) | ✓ | ✓ | ✓ | | |
| [207] | ✓(PVs) | | | | ✓(BESS) | ✓(aFRR) | | ✓ | ✓ | | |
| [209] | ✓ | ✓ | ✓ | | ✓ | ✓ | | ✓ | | | |
| [190] | ✓(PVs) | | ✓ | ✓ | ✓(BESS) | ✓ | | | ✓ | | |
| [20] | ✓(PVs) | | ✓ | ✓ | ✓(BESS) | ✓ | | ✓ | | | |
| **Ch.6** | ✓(PVs) | ✓ | ✓ | ✓ | ✓(BESS) | ✓(aFRR) | ✓ | ✓ | ✓ | ✓ | |

in PCSs. However, a multi-objective PCS that integrates PVs, HPs, EVs with V2G capabilities, and BESS and aims to optimize the energy arbitrage cost and revenues by ancillary services provision while respecting the customers' comfort and grid limits is still missing from the literature. Moreover, according to the author's knowledge, the potential of ancillary services provision (such as aFRR) by BESS and flexible loads such as V2G-capable EVs has not yet been investigated and compared under different influencing factors, such as seasons, grid types, grid sizes, and energy prices in the existing literature.

Hence, the contributions of this chapter can be summarized as follows.

- Develops a bi-level MILP power control model that encompasses and optimizes PV generation, EVs, HPs, and BESS for energy arbitrage and aFRR reserves provision, achieving maximum cost savings while respecting grid power limits and ensuring customers' charging and thermal comfort.
- Investigates and compares the performance of EVs and BESS concerning energy arbitrage and aFRR provision, modeling in detail the imbalance market and accounting for multiple influencing factors, namely different grid types, seasons, and energy prices.
- Applies the developed power control model in two different grid size scenarios, a small (3-node) grid and a large (13-node) grid, demonstrating the scalability of the model and validating the performance of EVs and BESS on aFRR provision at a real grid level.

This chapter can provide DSOs with valuable insights into the individual and cooperative potential of BESS and EV chargers to establish a more flexible and frequency-balanced power grid through effective participation in the imbalance market, considering also various uncertain influencing factors.

## 6.2. Power Control Concept

The PCS of this chapter is an extension of the PCS of Chapter 5, enhancing it to offer and provide aFRR reserves in the wholesale market; hence, the concept remains similar: The PCS comprises a number of entities that constitute aggregated EV chargers and buildings (here and onwards called nodes) and controls them distributionally. It also remains bilevel for DA and RT scheduling and is formulated as an MILP problem. Level 1, apart from the functionalities explained in Chapter 5, provides the estimated energy scheduling and offers aFRR reserves to the wholesale market using a single (one-shot) optimization. Similarly, Level 2, using RHO, corrects the accuracy errors between the actual and predicted data with re-optimizations, providing uncertainty management, and deploys the called amount of aFRR reserves that have been accepted in the wholesale imbalance market. The description of the functionalities of the two power control levels for this chapter and their use for participation in the aFRR market is depicted in Figure 6.1.

## 6.3. Power Control Modeling

This section comprises the modeling of the bi-level power control of this chapter and is categorized into the EV and BESS, building, imbalance market, node constraints, and the objective function. The utilized indices $n, j, bes, t, T, ch, dis, init, fr, u, d, \Delta t$ represent the node, charger, BESS, time instant, optimization horizon, charging, and discharging, initial, aFRR, up, down, and the timestep equal to $5'$ respectively. Equations or sections that are the same as in the methodology section 5.4 are referred to in the previous chapter. The aFRR modeling is based on the work in [18].

### 6.3.1. EV & BESS Constraints

In this section, the EV and BESS modeling for this chapter is described. It must be noted that the variables written in bold letters with a "*" constitute the variables that are transferred as parameters from the DA Level 1 to the RT Level 2. Moreover, the

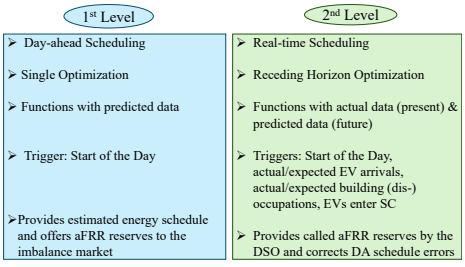


(a) Functionalities of Levels 1 and 2 of the PCS model.

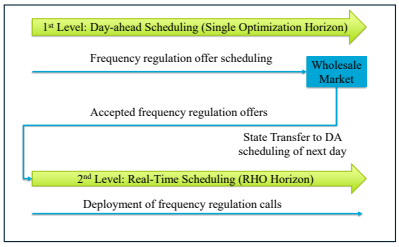


(b) Use of Levels 1 and 2 for participation in the imbalance market.

Figure 6.1: Description of the PCS concept for Chapter 6.

equations in red-colored parentheses with a "*" are only integrated into Level 1.

$$\begin{aligned} P_{ch/dis}^{n,j/bes,t} &= \Phi^{n,j} I_{ch/dis}^{n,j/bes,t} V^{n,t} \quad \forall t \in T \\ \mathbf{P_{fr_u/fr_d}^{n,j/bes,t^*}} &= \Phi^{n,j} I_{fr_u/fr_d}^{n,j/bes,t} V^{n,t} \quad \forall t \in T \end{aligned} \tag{6.1}$$

$$\begin{aligned} B^{n,j/bes,t} &= B_{init}^{n,j/bes} + \Delta t \sum_{t_{init}}^{t} (P_{ch}^{n,j/bes,t} - P_{dis}^{n,j/bes,t}) \\ &+ \Delta t \sum_{t_{init}}^{t} (\mathbf{P_{fr_d}^{n,j/bes,t^*}} h_{ch/bes}^{n,j} - \frac{\mathbf{P_{fr_u}^{n,j/bes,t^*}}}{h_{ch/bes}^{n,j}}) \quad \forall t \in T \end{aligned} \tag{6.2}$$

$$S^{n,j/bes,t} = \frac{B^{n,j/bes,t}}{B_r^{n,j/bes}} \quad \forall t \in T \tag{6.3}$$

Equations in (6.1) model the EV and BESS charging, discharging, up aFRR, and down aFRR powers $P_{ch/dis/fr_u/fr_d}^{n,j,t}$ & $P_{ch/dis/fr_u/fr_d}^{n,bes,t}$, where $I_{ch/dis/fr_u/fr_d}^{n,j,t}$ the up aFRR/down aFRR currents, $\Phi^{n,j} = 3$ and $V^{n,t} = 230V$ as in Chapter 5, and limits are defined in (5.2). Moreover, (6.2) & (6.3) dictate the battery capacity $B$ and SOC $S$ dynamics of the EVs and the BESS which now depend on the sum of the charging, discharging, and aFRR power amounts from $t_{init}$ (equal to the arrival time $T_a^{n,j}$ for EVs). The BESS SOC is also limited here between [0%,90%] by (5.4), which is especially important for aFRR provision to ensure that the battery is never depleted or overcharged. Similarly, the EV batteries are protected below 20% with no participation in power control and above 90% by the CV region. It must be noted that charging and discharging powers are measured at the EVs and BESS while aFRR powers are measured at the connection point with the main grid, and hence, they are integrated with the (dis)charging efficiency $h_{ch}^{n,j}$, $h_{bes}^{n}$ which comprise the power losses of both the charger and the EV battery management system.

$$\begin{aligned} P_{ch}^{n,j/bes,t} + \mathbf{P_{fr_d}^{n,j/bes,t^*}} h_{ch/bes}^{n,j} \leq (\frac{S^{n,j/bes,t}}{k} + \frac{\alpha k - \beta}{\alpha k}) P_{ch_{max}}^{n,j/bes} : \\ \alpha = 10, \beta = 9, k = 16 \; \forall t \in T \end{aligned} \tag{6.4}$$

$$\begin{aligned} I_{ch}^{n,j/bes,t} + I_{fr_d}^{n,j/bes,t} h_{ch/bes}^{n,j} &\leq I_{cv_{max,ch}}^{n,j/bes,t} \quad \forall t \in T \\ I_{cv_{max,ch}}^{n,j/bes,t} &= -\gamma I_r^{n,j/bes,t} S^{n,j/bes,t} + \gamma I_r^{n,j/bes,t} \end{aligned} \tag{6.5}$$

$$\begin{aligned} I_{dis}^{n,j/bes,t} + \frac{I_{fr_u}^{n,j/bes,t}}{h_{ch/bes}^{n,j}} &\leq I_{cv_{max,dis}}^{n,j/bes,t} \quad \forall t \in T \\ I_{cv_{max,dis}}^{n,j/bes,t} &= \gamma I_r^{n,j/bes,t} S^{n,j/bes,t} \end{aligned} \tag{6.6}$$

Equations (6.4) - (6.6) dictate the CC-CV EV/BESS charging and discharging regions, which are similar to (5.6) - (5.8) of Chapter 5 with the addition of the up- and down-aFRR powers/currents.

$$\left(b_{fr_u}^{n,j/bes,t} + b_{fr_d}^{n,j/bes,t} \leq 1 \quad \forall t \in T\right)^* \tag{6.7}$$

$$\mathbf{b}_{\mathbf{fr_u}}^{\mathbf{n,j/bes,t}^*} + b_{ch}^{n,j/bes,t} \leq 1 \quad \forall t \in T \tag{6.8}$$

$$\mathbf{b}_{\mathbf{fr_d}}^{\mathbf{n,j/bes,t}^*} + b_{dis}^{n,j/bes,t} \leq 1 \quad \forall t \in T \tag{6.9}$$

$$\left(P_{fr_u}^{n,j/bes,t} \leq b_{fr_u}^{n,j/bes,t} P_{dis_{max}}^{n,j/bes} \quad \forall t \in T\right)^* \tag{6.10}$$

$$\left(P_{fr_d}^{n,j/bes,t} \leq b_{fr_d}^{n,j/bes,t} P_{ch_{max}}^{n,j/bes} \quad \forall t \in T\right)^* \tag{6.11}$$

Such as in (5.9) - (5.11), where charging and discharging powers are separated with binary variables, two more binaries $b_{fr_d}, b_{fr_u}$ and (6.7) - (6.11) are added to separate $P_{ch}, P_{dis}, P_{fr_d}, P_{fr_u}$ which enforce that only the pairs $P_{ch}, P_{fr_d}$ and $P_{dis}, P_{fr_u}$ can occur simultaneously for both EVs and BESS.

$$I_{ch/dis}^{n,j,t}, I_{fr_u/fr_d}^{n,j,t}, b_{ch/dis}^{n,j,t}, \left(b_{fr_u/fr_d}^{n,j,t}\right)^* = 0 \quad \forall t \notin [T_a^{n,j}, T_d^{n,j}] \tag{6.12}$$

Finally, (6.12) sets the EV charging, discharging, up aFRR, and down aFRR currents $I_{ch}, I_{dis}, I_{fr_u}, I_{fr_d}$ and binary variables to zero outside of the EV parking time $[T_a^{n,j}, T_d^{n,j}]$ (used instead of (5.5)). Equation (5.12) of Chapter 5 calculates the EV unfinished charging gap $E_g^{n,j}$ for the objective function, while (5.13) ensures that the BESS initial and final SOCs remain at similar levels.

### 6.3.2. Building Constraints

The constraints that dictate the operation of the LCTs in the buildings, such as PVs and HPs, are the same (5.14) - (5.37) as in Section 5.4.2, with the difference that a steady COP has been assumed in this chapter. Hence (5.26) and (5.27) are omitted, and HP COPs have been replaced with the average values 3.5 and 6, for Winter and Summer, respectively, transforming (5.28) into a linear constraint. Therefore, the computational time has been reduced, transforming the problem into MILP, to compensate for the addition of the extra aFRR reserves provision functionality. Moreover, with the use of the seasonal average COP values, the accuracy has been slightly affected.

### 6.3.3. Imbalance Market Constraints

This section describes some further constraints that dictate the imbalance market norms and the participation of the PCS; hence, the bidding and scheduling of aFRR reserves to the market in DA and their deployment in RT when called by the TSO. The indices $park, da, rt, a, d, isp$ denote the parking time, day-ahead, real-time, arrival, departure, and imbalance settlement period, respectively.

### Day-ahead (Level 1)

$$\begin{aligned} \text{if } \Delta T^{n,j}_{park-da} = [T^{n,j}_{a-da} : T^{n,j}_{d-da}] \rightarrow \\ \Delta T^{n,j}_{park-rt} = [T^{n,j}_{a-rt} : T^{n,j}_{d-rt}] \text{ where:} \\ T^{n,j}_{a-rt} = T^{n,j}_{a-da} + \delta \quad \& \quad T^{n,j}_{d-rt} = T^{d,j}_{a-da} + \delta : \\ -K \leq \delta \leq K \ \ \& \ \ K = 15' \end{aligned} \tag{6.13}$$

To account for the uncertainty considered in the arrival and departure times of the EV fleets, (6.13) dictates that the real-time EV parking time $\Delta T^{n,j}_{park-rt}$ in Level 2 deviates from the estimated parking time in day-ahead $\Delta T^{n,j}_{park-da}$ by a time difference $\delta$ of maximum $K = 15'$ considered in both the arrival and departure times $T^{n,j}_{a} : T^{n,j}_{d}$, respectively. This is because the parking time uncertainty needs to be considered in the aFRR bidding from EVs in DA; hence, the EVs are only allowed to offer aFRR during the parking time $[T^{n,j}_{a-da} + |K|, T^{n,j}_{d-da} - |K|]$ to ensure that the EV will be present to deploy the called reserves in RT.

$$\begin{aligned} b^{n,bes,t}_{fr_{u/d}} = b^{isp}_{up/down} \ \forall isp \in T \\ b^{n,j,t}_{fr_{u/d}} = b^{isp}_{up/down} \ \forall isp \in \Delta T^{n,j}_{park-rt} \ \& \ ISP = 15 \\ \text{where : } \ l_{isp} = \frac{ISP = 15'}{\Delta t = 5'} \end{aligned} \tag{6.14}$$

$$\begin{aligned} b^{isp}_{up} = 1 \Rightarrow P^{n,j/bes,t}_{fr_u} = P^{n,j/bes,t+1}_{fr_u}, \ \forall isp^{j/bes} \\ b^{isp}_{down} = 1 \Rightarrow P^{n,j/bes,t}_{fr_d} = P^{n,j/bes,t+1}_{fr_d}, \ \forall isp^{j/bes} \end{aligned} \tag{6.15}$$

Moreover, (6.14) - (6.15) enforce that the aFRR bidding of the power control model respects the norms of the wholesale reserve market. The time horizon $T$ of the power control is divided into consecutive ISPs that end for $15'$, the number of which is defined by $T//l_{isp}$. The PCS model acting as a BSP is obligated to offer the same amount of up or down aFRR reserves for 15 consecutive minutes (the whole ISP) according to the rules of the aFRR market. Hence, up and down binary variables, $b^{isp}_{up}$, $b^{isp}_{down}$ respectively, are introduced for all the ISP blocks which are equal to the up and down aFRR binary variables, $b^{n,j/bes,t}_{fr_u}$, $b^{n,j/bes,t}_{fr_d}$ for the BESS and EVs. Concerning the BESS, this is enforced for the whole horizon $T$, while for the EVs, it is enforced for the estimated minimum parking time in real-time $\Delta T^{n,j}_{park-rt}$. Equation (6.14) ensures, with the use of the binaries, that the bidding remains the same for the whole ISP, while (6.15) dictates that for every timestep t in the ISP, the scheduled EV/BESS up and down aFRR power must be the same as the scheduled amounts at the consecutive timestep $t + 1$ in the same ISP. In simpler terms, this ensures that the power remains constant over the bidding interval determined by the ISP, according to market rules set by the TSO.

### Real-time (Level 2)

$$
\begin{aligned}
P_r\left(P^{n,j/bes,t}_{fr_u-rt} = P^{n,j/bes,t}_{fr_u-da}\right) &= \alpha_{up} \\
P_r\left(P^{n,j/bes,t}_{fr_d-rt} = P^{n,j/bes,t}_{fr_d-da}\right) &= \alpha_{down} \\
P_r\left(P^{n,j/bes,t}_{fr_u-rt} = 0 \mid P^{n,j/bes,t}_{fr_u-da}\right) &= 1-\alpha_{up} \\
P_r\left(P^{n,j/bes,t}_{fr_d-rt} = 0 \mid P^{n,j/bes,t}_{fr_d-da}\right) &= 1-\alpha_{down}
\end{aligned}
\tag{6.16}
$$

Where:

- $\alpha_{up}$ and $\alpha_{down}$ are the probabilities that the DA offered up and down aFRR reserves to the market (Level 1) remain equal to the called up and down aFRR reserves from the TSO in RT, respectively (Level 2).

- $1-\alpha_{up}$ and $1-\alpha_{down}$ are the probabilities that the called up and down aFRR reserves in real-time are zero. In this work, as explained below, only these two possibilities are considered.

Finally, 4 different variables are transferred from Level 1 to Level 2: the up and down binary variables $b^{n,j/bes,t}_{fr_{u/d}}$ and the up and down aFRR powers $P^{n,j/bes,t}_{fr_{u/d}}$. The binary variables are transferred as is; however, the scheduled power amounts $P^{n,j/bes,t}_{fr_{u/d}-da}$ deviate from the deployed $P^{n,j/bes,t}_{fr_{u/d}-rt}$ due to acceptance and deployment rates. In this work, it has been assumed that all offered aFRR reserves are accepted as a whole in the wholesale market, because the PCS is allowed to participate with zero bids in the market since the aFRR reserves come from RESs. Thus, the bidding of the power control model is always below the market-clearing price (see Section 2.6.2). However, when aFRR power is called by the TSO during a certain ISP, it is not uniform throughout the full delivery period. For example, an upward power request from the TSO can be positive during the first ten minutes of an ISP and zero during the last five. Therefore, aFRR deployment rates for upward and downward power requests are introduced, denoted as $\alpha_{up}$ and $\alpha_{down}$. These rates represent the chance that scheduled aFRR power is actually called during a timestep in the simulation. By using these rates, a more realistic version of the potential voluntary aFRR earnings is approached. Calculated from 2023 Tennet aFRR data [217], the average upward and downward activation percentage per ISP is 71% and 41%, respectively. These rates are integrated into the power control model with the use of (6.16).

## 6.3.4. Node Constraints

The node constraints, which constitute the node power balance, and the grid input and output power limits for the PCS of this chapter are included here. All the node constraints apply for $\forall t \in T$.

$$P_{im}^{n,t} - P_{ex}^{n,t} = \sum_{j=1}^{J}\left(\frac{P_{ch}^{n,j,t}}{h_{ch}^{n,j}} - P_{dis}^{n,j,t} h_{ch}^{n,j}\right) + \frac{P_{ch}^{n,bes,t}}{h_{bes}^{n}} - P_{dis}^{n,bes,t} h_{bes}^{n} + \sum_{b=1}^{B}\left(P_{hp}^{n,b,t} + P_{l}^{n,b,t} - P_{pv}^{n,b,t}\right),\ \forall t \in T \tag{6.17}$$

$$\sum_{j=1}^{J}\left(\frac{P_{ch}^{n,j,t}}{h_{ch}^{n,j}} - P_{dis}^{n,j,t} h_{ch}^{n,j}\right) + \frac{P_{ch}^{n,bes,t}}{h_{bes}^{n}} - P_{dis}^{n,bes,t} h_{bes}^{n} + \sum_{b=1}^{B}\left(P_{hp}^{n,b,t} + P_{l}^{n,b,t} - P_{pv}^{n,b,t}\right) + \sum_{j=1}^{J}\mathbf{P_{fr_d}^{n,j,t^*}} + \mathbf{P_{fr_d}^{n,bes,t^*}} - \sum_{j=1}^{J}\mathbf{P_{fr_u}^{n,j,t^*}} - \mathbf{P_{fr_u}^{n,bes,t^*}} \leq G_{in}^{n},\ \forall t \in T \tag{6.18}$$

$$\sum_{j=1}^{J}\left(P_{dis}^{n,j,t} h_{ch}^{n,j} - \frac{P_{ch}^{n,j,t}}{h_{ch}^{n,j}}\right) - \frac{P_{ch}^{n,bes,t}}{h_{bes}^{n}} + P_{dis}^{n,bes,t} h_{bes}^{n} - \sum_{b=1}^{B}\left(P_{hp}^{n,b,t} + P_{l}^{n,b,t} - P_{pv}^{n,b,t}\right) - \sum_{j=1}^{J}\mathbf{P_{fr_d}^{n,j,t^*}} - \mathbf{P_{fr_d}^{n,bes,t}} + \sum_{j=1}^{J}\mathbf{P_{fr_u}^{n,j,t^*}} + \mathbf{P_{fr_u}^{n,bes,t^*}} \leq G_{out}^{n},\ \forall t \in T \tag{6.19}$$

Equation (6.17) is the node power balance, similar to (5.38) in Chapter 5. Moreover, similar to (5.39) and (5.40), (6.18) and (6.19) enforce that the composite input and output powers comply with the respeective grid limits, with the addition of the total EV/BESS down- and up-aFRR power with opposite signs in (6.18) and (6.19). The up and down aFRR powers are only integrated into the input and output grid limit equations and not in the power balance. This is because, for example, if down aFRR was contained in (6.17), the node would buy imported power to cover the down aFRR, which is provided as an ancillary service to the main grid for revenues. Hence, aFRR reserves are only integrated into the grid limit equations to reduce the input and output limits for the optimization of the rest of the PCS power flows, which must always respect the power balance.

### 6.3.5. Objective Function

Equation (6.20) is the objective function of this chapter's PCS, which is again a multi-objective problem, whose objectives have been translated into a total cost $C_n$ aimed to be minimized.

a) The first three and the last term remain similar as in (5.53) to ensure energy arbitrage, maximum PV self-consumption, building thermal and EV charging comforts, as explained in the previous chapter.

b) The fourth term is responsible for the maximum earnings from aFRR provision from the EV fleets and BESS, where $C_{up}$ and $C_{down}$ are the reserve prices of up and down regulation in the imbalance market, respectively. It must be noted that in the aFRR market, the BSPs are remunerated for both what they offer in DA and what they deliver in RT, in contrast with FCR, where they are remunerated only for what they offer; hence, for the available capacity. However, this term is only integrated into the objective function of Level 1 during the scheduling of the offered aFRR reserves and not into Level 2. This is because the PCS seeks to maximize its earnings during the DA scheduling, offering the highest reserves, while the called reserves in RT are only controlled by the TSO.

$$\begin{aligned} \min C_n = \Delta t(\sum_{t=1}^{T}(P_{im}^{n,t}C_{buy}^{t} - P_{ex}^{n,t}C_{sell}^{t}) \\ + \sum_{t=1}^{T}\sum_{b=1}^{B}(P_{pv_{dev}}^{n,b,t}C_{pv_{pen}}^{n,b}) + \sum_{t=1}^{T}\sum_{b=1}^{B}(T_{dev}^{n,b,t}C_{hp_{pen}}^{n,b}O^{t,n,b}) \\ \Big( + \sum_{t=1}^{T}(\sum_{j=1}^{J}(P_{fr_d}^{n,j,t}) + P_{fr_d}^{n,bes,t})C_{down}^{t} \\ - \sum_{t=1}^{T}(\sum_{j=1}^{J}(P_{fr_u}^{n,j,t}) + P_{fr_u}^{n,bes,t})C_{up}^{t}))\Big)^{*} \\ + \sum_{j=1}^{J}E_{g}^{n,j}C_{ev_{pen}}^{n,j} \end{aligned} \tag{6.20}$$

Finally, as explained above, some of the newly added equations in this chapter are not used on both levels. Figure 6.2 depicts the equations of Level 1 that are used, not used, and modified in Level 2, and the variables that are transferred as parameters between the two levels. The parameters used in this chapter for the modeling of the LCTs and buildings are the same as in Chapter 5, summarized in Tables 5.2 and 5.3.

## 6.4. Data Input, Case Studies & Limitations

### 6.4.1. Data Input & Simulation Setup

Concerning the simulation setup, daily simulations were again performed in a Python 3.9 environment using the Gurobi 11 solver and a simulation timestep of 5′ for an appropriate trade-off between accurate decision-making and computational time. Although a 5-minute timestep is unable to capture transient effects, it is in a position to show the power control behavior concerning PV and BESS utilization,

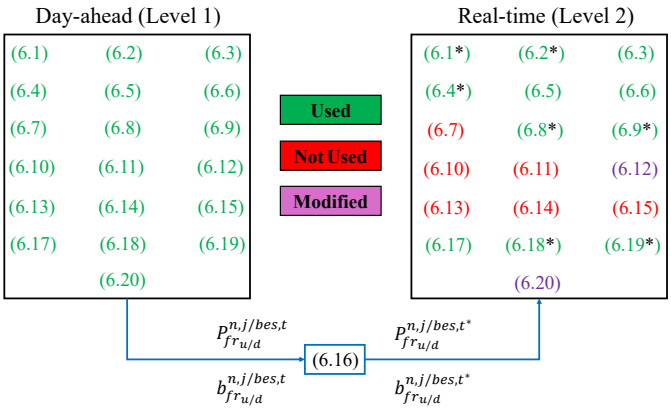


Figure 6.2: Integrated equations and transferred variables of PCS Levels 1 & 2 in Section 6.3.

EV charging, HP heating, and participation in the aFRR market. The utilized data concerning load and LCT profiles and LCT modules are the same as those explained in Section 5.5.2, while the small and large grids used for the PCS of Chapter 5 have also been used in this chapter for the testing of the PCS (see Section 5.5.1). Finally, more DAM energy and reserve price profiles from three different years (2018, 2019, and 2023) have been acquired from the Dutch ENTSO-E platform to also investigate the influence of the price uncertainty on the PCS of this chapter.

## 6.4.2. Case Studies & Scenarios

### Case Studies

Five case studies are conducted to investigate and compare the individual and cooperative contribution of flexible loads and BESS to energy arbitrage and aFRR provision. Each case study explores a unique aspect of the PCS in order to quantify the capabilities of each asset that is integrated. Constraints are adjusted in each

Table 6.2: Technologies and Applications of each Case Study.

| **Case** | Loads & V2G | BESS | EV: aFRR | BESS: aFRR |
|---|---|---|---|---|
| Case 1 | ✓ | | | |
| Case 2 | ✓ | ✓ | | |
| Case 3 | ✓ | ✓ | ✓ | |
| Case 4 | ✓ | ✓ | | ✓ |
| Case 5 | ✓ | ✓ | ✓ | ✓ |

study, treating each aFRR asset as a stand-alone facility. The overall goal is to minimize grid costs, maximize revenues from aFRR provision, while simultaneously minimizing PV curtailment, and ensuring EV owners' and buildings' charging and thermal comfort, respectively. An overview of the LCTs and applications active in each case is given in Table 6.2, while the case studies are explained as follows:

- Case 1: This baseline case lacks BESS and aFRR services, and comprises only PVs, HPs, EVs, and V2G. This case is included to, firstly, show the performance of flexible loads in energy arbitrage, and secondly, to serve as validation for this chapter's PCS and Cases 2-5 against the PCS of publication [27] (Chapter 5). It must be noted that, in this chapter, V2G denotes the power flow from the EV to the node, hence it constitutes the EV discharging for the flexibility of the node and not for aFRR provision to the main grid.
- Case 2: The BESS is added to this case to show the contribution of BESS and its synergy with flexible loads for energy arbitrage. The provision of aFRR reserves by both EVs and BESS is excluded in this case.
- Case 3: In this case, aFRR provision by EVs is added to show the contribution of EVs to power control revenues by ancillary services provision while simultaneously performing energy arbitrage.
- Case 4: In this case, aFRR services are provided only by the BESS to show the contribution of BESS to power control revenues by ancillary services provision while simultaneously performing energy arbitrage.
- Case 5: Finally, flexible loads and BESS are all included in this case to show their synergy for energy arbitrage and aFRR provision.

### Scenarios

The five case studies are investigated for the following three sets of scenarios:

a) One Winter and one Summer day: This set of scenarios is utilized to quantify the seasonal effect and the effect of the weather conditions on the contribution of the different LCTs concerning energy arbitrage (grid power exchange and total power control cost) and aFRR provision (total up and down aFRR power delivered and respective power control revenues).

b) Energy and Reserve Price profiles from three different years: 2018, 2020, and 2023. These scenarios aim to investigate the energy and reserve price effect on energy arbitrage and aFRR provision. Grid frequency balance is becoming increasingly important in recent years, and the deviations in energy and reserve prices are more prominent in 2023 than they were in 2018, leading to a higher need for aFRR reserves.

c) The small (3-node) grid and the large (13-node) grid scenarios of Chapter 5 to address, firstly, the influence of the various grid types and the behavior of the occupancy and charging profiles in different buildings and chargers, respectively, on the grid power exchange, delivered aFRR power, and total power

control costs and revenues. Secondly, the effect of different grid size levels, especially on aFRR provision, is investigated, providing simultaneously proof of the scalability and expandability of the PCS model to a real grid size level. The specifications of the two grids (buildings, EV chargers, BESS capacities) have already been summarized in Section 5.5.1 (see Figures 5.5, 5.6, and Table 5.5), while $G^{n}_{in/out} = 400kW$ & $3.785MW$ remain the power limits of the two grids.

### 6.4.3. Limitations

Such as in Chapters 3, 4, and 5, uncertainty between the two levels has only been inserted for buildings' occupancy and EV driving patterns, whereas a lot of uncertainty sources (building types, LCT modules, price uncertainty, etc.) have been neglected. For example, the study uses DA prices for power optimization and assumes perfect imbalance price forecasts, missing real-time price dynamics. Additionally, it has been assumed that the aFRR bid is always accepted as a whole in the reserve market and called for deployment in real-time. Real-world scenarios involve partial activations and a minimum bid size of 1 MW. Furthermore, battery degradation has not been incorporated in this chapter, which highly affects cost reduction and revenue. Finally, the HP COPs are considered constant and equal to the average 3.5 and 6 for Winter and Summer, respectively, to reduce computational burden, while ramping rates are considered instant due to the 5' simulation step.

## 6.5. Results & Discussion

This section comprises the results and analysis of the two grid scenarios. Subsections 6.5.1-6.5.3 are devoted to the small grid scenario concerning power flows, energy, cost, and aFRR provision analysis, respectively, while subsection 6.5.4 comprises the large grid scenario results. Finally, subsection 6.5.5 comprises the discussion, which summarizes the most important findings of the work.

### 6.5.1. Power Flow Analysis

#### Energy and Reserve Prices

In Figure 6.3, the utilized Winter and Summer energy price profiles (Row 1) and aFRR price profiles (Rows 2-4) for 2018, 2020, and 2023 are depicted. Energy and up-aFRR prices are always positive or zero. In this regard, the PCS always pays for buying grid energy and is remunerated for offering up-aFRR reserves. On the contrary, down-aFRR prices can be positive and negative. Negative down-aFRR prices mean that the PCS is remunerated for offering down-aFRR reserves, while it pays the TSO when the prices are positive. Bidding during positive down-aFRR prices has meaning for generators when these prices are lower than their marginal cost; hence, they have cost savings for not producing. Since the aFRR provision assets are BESS and EVs, this is out of the scope of this work, and the PCS is allowed to bid only during negative down-aFRR prices (this can also be seen in (6.20) where a positive sign is used for down-aFRR reserves bidding).

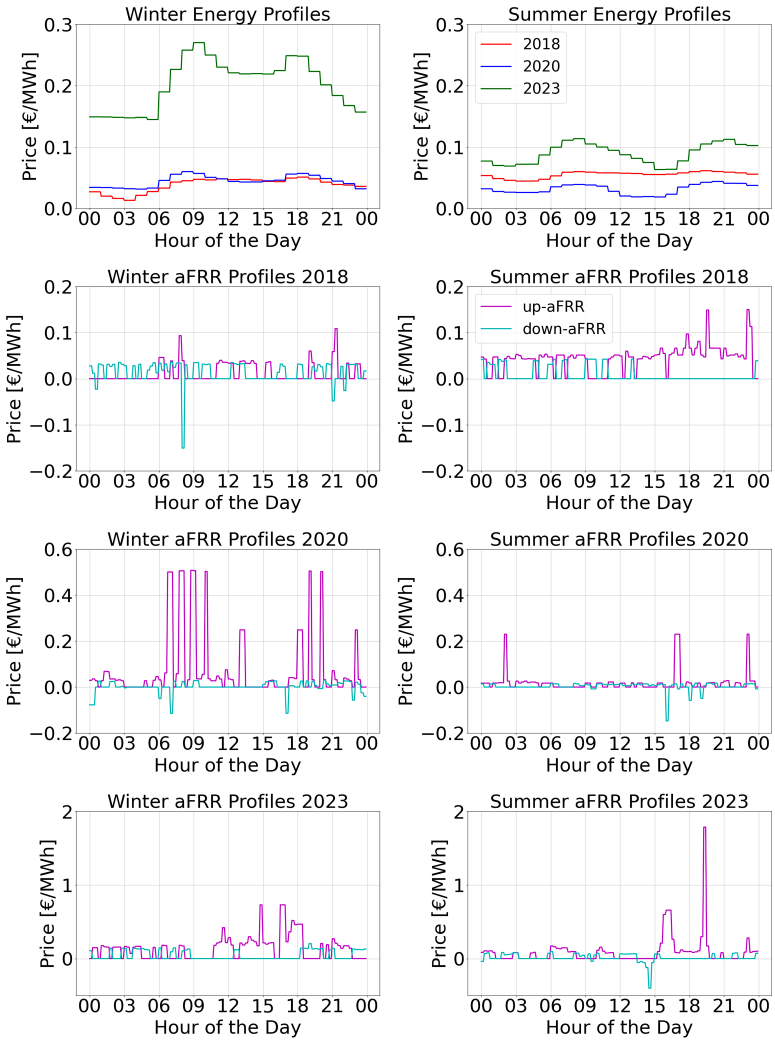


Figure 6.3: Energy (Row 1) and aFRR price profiles (Rows 2-4) for Winter and Summer seasons, years: 2018, 2020, 2023.

As it can be observed, the energy prices are highly increased in 2023, which can reach up to 5.5x times higher during Winter compared to 2018 and 2020. Concerning the aFRR price profiles of the considered days, it can be seen that for all years, especially during Winter, the up-aFRR prices are higher in absolute terms than the negative down-aFRR prices during the largest part of the day. Therefore, the PCS benefits more by providing up-aFRR reserves, hence by decreasing their consumption, especially in recent years 2020 and 2023 due to the abrupt load increase that is supplied by the main grid. Providing down-aFRR reserves, by

increasing consumption, is less frequently beneficial, which can be seen by the longer periods of positive and zero down-aFRR prices. On some of the considered days, like Winter 2023, downward imbalance prices never fall below zero, preventing any downward aFRR power delivery. Finally, Figure 6.3 shows how the aFRR prices are increased in years 2020 and 2023 compared to 2018, showing a higher need for frequency regulation. This illustrates how aFRR power provision is heavily tied to imbalance price fluctuations.

### Energy Arbitrage

Figure 6.4 summarizes some power flow examples to provide insights concerning the PCS performance. The synergy of flexible loads and BESS for energy arbitrage without aFRR provision (Case 2) in Node 3 is depicted in Figure 6.4a for the Winter and Summer of 2023 together with the daily energy price profiles. Concerning Winter, grid power is imported for building heating, BESS and EV charging mostly during the low energy prices; before 06:00 in the morning and after 20:00 in the evening. Most PV power is exported because it is generated during the high energy prices of [06:00, 15:00]. Additionally, the high energy price period of [17:00, 20:00] is avoided, and grid power is not imported. In contrast, V2G and BESS energy is used instead for base load cover, building heating, and EV charging. Concerning Summer, similar observations can be made. For example, the low energy price period of [15:00, 17:00] is utilized for EV and BESS charging, while the BESS is discharged instead of grid power use for EV charging during the energy price peaks of [19:00, 22:00]. Moreover, the PV generation is also here exported for revenues. However, BESS energy is used for the HPs, which are operated here for building cooling during the day [09:00, 16:00]. Furthermore, V2G is less used due to the higher and more prolonged available PV generation, which is preferred due to the round-trip losses of V2G use. This was also observed in Chapter 5.

### aFRR Provision from EVs and BESS individually

The behavior of the power flows of Node 3 during aFRR provision by EVs (Case 3) and the BESS (Case 4) is compared in Figure 6.4b for Winter 2023. Taking into account the up- and down-aFRR prices of Winter 2023 in Figure 6.3, the high up-aFRR prices of [10:00, 18:00] are greatly taken advantage of in both seasons. Additionally, the BESS exploits also the up-aFRR prices of the early morning in Case 4, which cannot occur in Case 3 due to the absence of EVs. Comparing Figure 6.4b with Figure 6.4a, it can be observed that V2G use is highly decreased in Case 3 because EVs are utilized for aFRR reserves provision during the period of [15:00, 18:00]. Instead, the BESS is discharged during this period (e.g., for building heating) and a higher amount of grid energy is imported after 20:00 for EV re-charging. On the contrary, regarding Case 4, V2G use is highly increased compared to Case 2 for use for the flexibility of the node and endures for a longer time period (16:00-20:00), because the BESS is used for aFRR provision. Therefore, it can be seen how the BESS and the EVs are interchangeably utilized for both energy arbitrage and ancillary services provision.

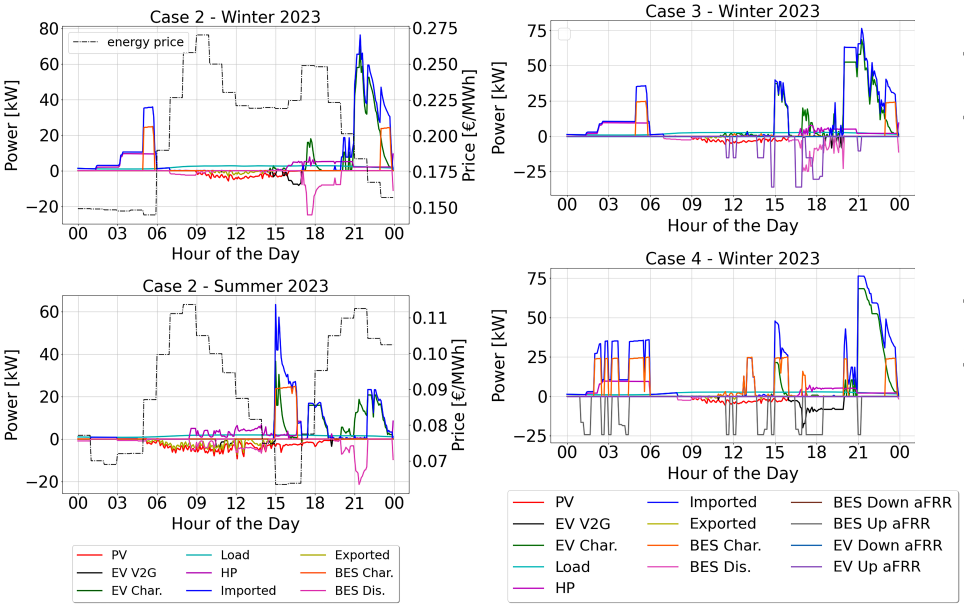


(a) Energy arbitrage with flexible loads and BESS (Case 2) during Winter and Summer (Node 3 - 2023).

(b) Energy arbitrage and aFRR provision by EVs (Case 3) and BESS (Case 4) during Winter (Node 3 -2023).

Figure 6.4: Power Flows of small grid scenario for Cases 2-4.

### aFRR Provision from EVs and BESS combined

Finally, Figure 6.5 depicts the energy arbitrage and aFRR provision by the EVs and the BESS combined (Case 5) for the Winter and Summer of 2023. Figure 6.5b is added so that the up- and down-aFRR power flows are isolated for better clarity. Comparing Figure 6.5a with Figure 6.4b, it can be seen that both the EVs and the BESS combine their capabilities to provide up-aFRR simultaneously during the same time periods as before. Moreover, concerning the Summer season, down-aFRR reserves are offered by both assets in the afternoon, exploiting the negative down-aFRR prices at 09:30 and 14:30 (see Figure 6.3); consumption increase calls by the TSO are expected during Summer afternoons in recent years due to the high renewable generation (e.g., PVs) that burdens the power grid. On the contrary, no down-aFRR reserves are delivered during Winter 2023 due to the absence of negative down-aFRR prices.

## 6.5.2. Energy and Cost Analysis

In this section, the use of grid energy and the total cost of the five investigated cases are compared. In Figure 6.6, the imported and exported energy amounts for Cases 1, 2, and 5 during the Winter and Summer of the three years are depicted. Starting with Case 1, a higher amount of grid energy is imported for all nodes

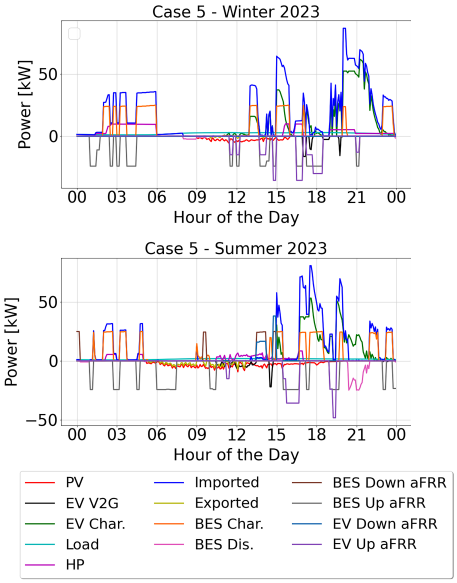


(a) Energy arbitrage and aFRR provision by both flexible loads and BESS (Case 5) during Winter and Summer (Node 3 -2023).

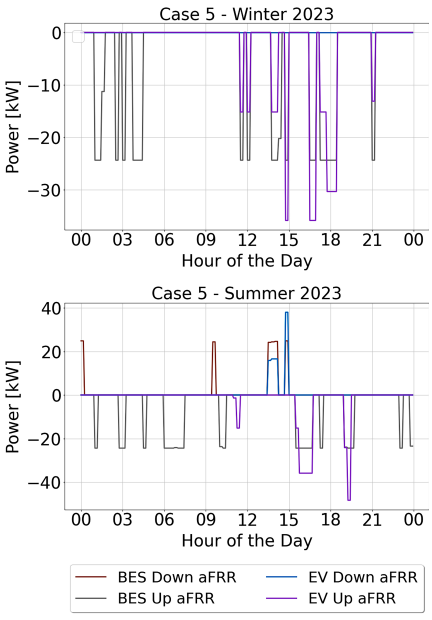


(b) Isolation of aFRR power flows from EVs and BESS in Figure 6.5a.

Figure 6.5: Power Flows of small grid scenario for Case 5.

during Winter (approximately 100% increase). This is, firstly, because a 30% higher consumption is needed for EV charging due to cabin heating, and secondly, building heating consumes more energy than building cooling due to the higher temperature difference with the ambient temperature (Chapter 3). Moreover, commercial nodes (Node 2) import, on average, 50% lower energy during both Winter and Summer seasons compared to residential nodes (Node 1) because commercial buildings are less occupied than residential buildings, and EVs arrive with lower SOC at home chargers than at public chargers. Finally, a higher amount of exported energy is seen for all nodes during Summer due to the higher PV generation.

Regarding Case 2 and BESS use, a slight but notable increase in both imported and exported energy can be seen for all nodes during Summer. The use of BESS for the flexibility of the node (EV charging and building cooling) enables higher exportation of PV generation for revenues, Moreover, a higher increase can be seen in years 2020 and 2023 for all nodes due to the higher variation of the energy prices profiles (see Figure 6.3) which is beneficial for the use of BESS for energy arbitrage and lower power control cost. A similar observation can also be made for Case 1, where the energy arbitrage is performed only by the flexible loads. However, the difference between Cases 1 and 2 remains very low because the loads need the same grid energy amount, and the BESS initial and final SOCs are similar.

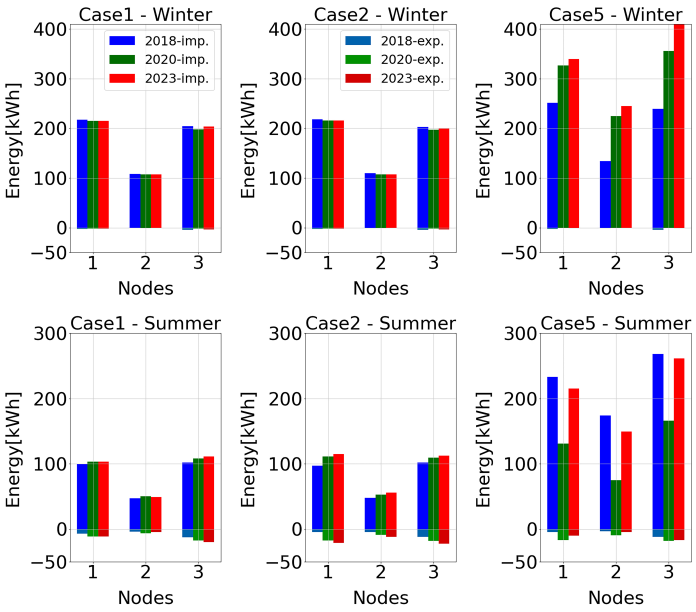


Figure 6.6: Imported and exported grid energy comparison during Winter (upper row) and Summer (lower row) for Nodes 1-3, years 2018-2023, and Cases 1,2, 5.

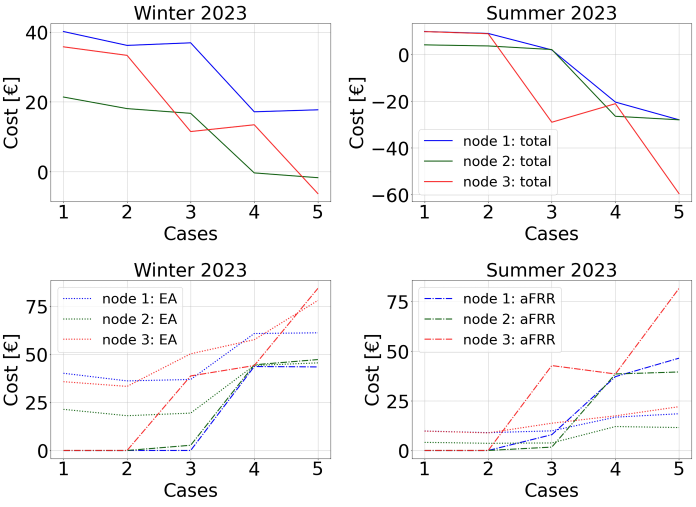


Figure 6.7: Energy arbitrage (EA) cost, aFRR revenues, and total cost comparison for Nodes 1-3, Cases 1-5 during Winter and Summer 2023: Validation against publication [27] (Case 1).

Finally, Case 5 is characterized by the highest increase in imported grid energy for all years and nodes. Node 3 is the most affected node, showing a 100% and 150% for Winter and Summer, respectively, during 2023. Therefore, as will be seen in the next section is the node that provides the highest amount of aFRR reserves due to its highest flexibility since it comprises both residential-commercial buildings and home-public chargers. Moreover, concerning the comparison between the different years, the year 2023 is characterized by the highest increase in grid energy; hence, the highest provision of aFRR reserves due to the higher reserve prices and duration of need for aFRR reserves (Figure 6.3). For the same reason, 2020 is more beneficial than 2018 for Winter, while the opposite applies for Summer.

Figures 6.7 and 6.8 summarize this chapter's cost analysis and serve also as validation of this chapter's Cases 2-5 compared to Case 1 of publication [27]. Figure 6.7 shows in the first row the total cost for Nodes 1-3, Cases 1-5 during Winter and Summer 2023, which is equal to the energy arbitrage (EA) cost minus the aFRR revenues. While a slight decrease is seen from Case 1 to Case 2, the highest cost decrease is shown for the aFRR provision cases, especially for Case 5, which exploits both assets (EVs and the BESS), and for Node 3. Especially for the Summer season, the costs for all nodes result in negative numbers (-60€ for Node 3 in Case 5), which means that the PCS is actually remunerated and not charged for the power control operation. Furthermore, as already explained, the ancillary services provision is mostly beneficial for Node 3 due to its highest flexibility because of the variety of EV fleets. Node 3 (mixed node) is characterized by longer connection times and more simultaneously connected EVs. The number of connected EVs directly influences their ability to participate in the aFRR market, as it determines the available battery storage capacity and aFRR power potential. For the same reason, Node 3 is the only node that has the highest cost decrease during both seasons in Case 3 (aFRR provision by EVs) than in Case 4 (aFRR provision by the BESS), since the BESSs are all 50kWh-rated for all three nodes. Finally, the increase in aFRR revenues but also in the EA cost, which is justified since a higher grid energy amount is imported, can be seen in the second row of Figure 6.7.

To strengthen our observations about the total cost of the investigated cases, Figure 6.8 summarizes the cost reduction achieved in Cases 2-5 compared to Case 1 (power control only with flexible loads) for Winter (first row) and Summer (second row) for all the investigated nodes and years. It can be seen that Case 5 always offers the highest cost reduction, which is almost always above 40% in 2018, and 100% in the recent years 2020 and 2023, while it reaches up to 900% and 800% for Node 2 during Winter 2020 and Summer 2023, respectively. On the contrary, Case 2 (the use of BESS without aFRR provision) offers, in most nodes and scenarios, the least cost reduction. Furthermore, the use of BESS for aFRR provision (Case 4) is more beneficial than the use of EVs (Case 3) except for some scenarios for Node 3, such as Winter and Summer 2023. This is expected because the BESS is present and is capable of offering reserves during the whole simulation period, in contrast with the EV fleets. Moreover, Node 2 shows the highest cost reduction for all cases and scenarios, which is justified by the fact that the power control cost of Node 2 is already the least compared to the other two nodes in Case 1; hence, the

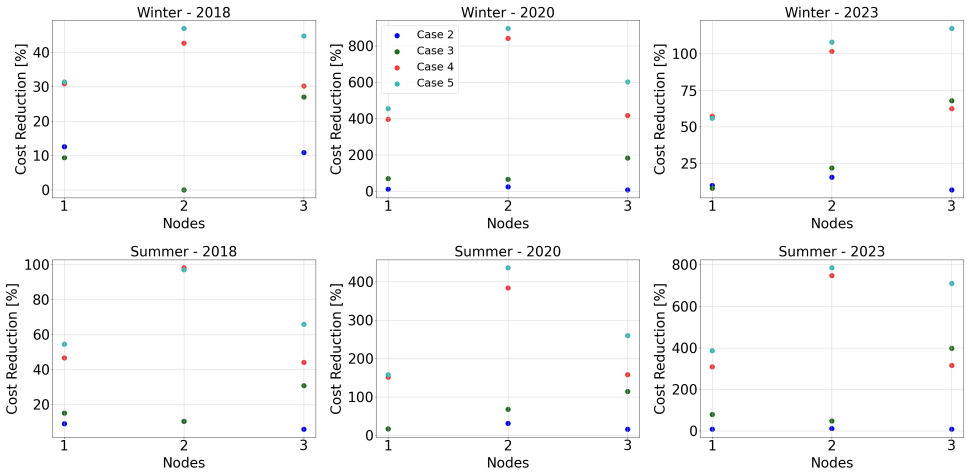


Figure 6.8: Summary of cost reduction by BESS utilization and aFRR provision during Winter (upper row) and Summer (lower row) for Nodes 1-3, years 2018-2023, and Cases 2-5: Validation against publication [27] (Case 1).

additional aFRR revenues are most significant compared to the already EA cost.

Finally, it can be seen that in recent years, the potential of cost reduction by offering ancillary services is further increasing. For example, the cost reduction in Summer 2020 and Summer 2023 reaches up to 4x and 8x times compared to Summer 2018. The only exception constitutes the transition from Winter 2020 to Winter 2023 because the aFRR price levels of the two years are comparable, while the energy price levels of 2023 reach up to 4.5x times higher than the respective levels of 2020. Hence, Case 1 of Winter 2023 is characterized by a much higher cost than Case 1 of Winter 2020. However, while it might seem that the cost reduction due to ancillary services provision is lower during the Winters of recent years, according to the author's opinion, it is evident that the participation in such services is becoming increasingly important due to the much higher energy prices.

### 6.5.3. aFRR Provision Analysis

In this section, the provided energy for up- and down-aFRR reserves for the investigated cases and scenarios is summarized to strengthen the insights of the previous sections. Figure 6.9 depicts the respective results for all nodes during Winter and Summer 2023. The up-aFRR reserves are depicted on the positive y-axis, while the down-aFRR reserves are on the negative side. The first main observation is that the provided up-aFRR reserves are vastly higher than the respective down reserves and can reach up to 400% higher (200kWh compared to 50kWh: Node 3 - Summer 2023). As seen in Figure 6.3, especially during the considered Winter days, only up reserves are provided, due to the beneficial up-aFRR price profiles, while there is a lack of negative down-aFRR prices for

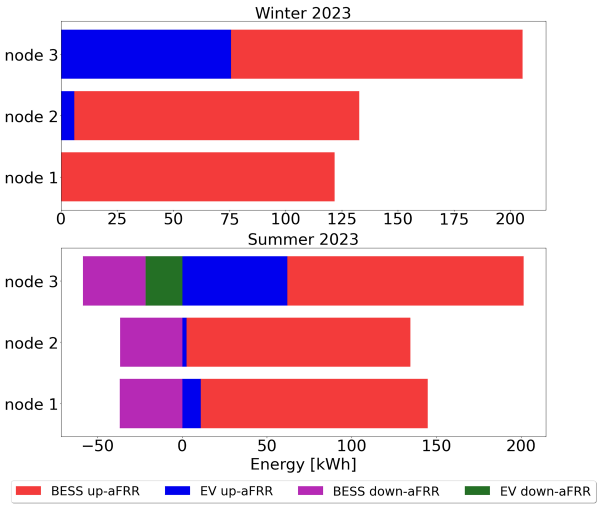


Figure 6.9: Upward and downward aFRR provision by EVs and BESS during Winter and Summer for Nodes 1-3, Case 5, year: 2023.

downward aFRR capacity scheduling. This is expected in Winter, when the TSO most often needs up-regulation due to the high load consumption. Furthermore, as explained before, the BESS provides more up- and down-aFRR energy than the EVs since it is always present, while EVs arrive and depart following specific patterns and must maintain a minimum departure state of charge to ensure user comfort. For example, 40kWh and 140kWh of down and up reserves are provided by the BESS compared to 25kWh and 60kWh by EVs in Node 3 during Summer 2023. It is also noticed that the BESS provides the same aFRR energy at all nodes during each season, which is rational since all BESSs are 50kWh-rated and start and end with the same SOC (50% considered in this work). Finally, it can also be seen here that Node 3 has the capability of providing the highest amount of up- and down-aFRR energy by EVs due to its variety of EV fleets; 60kWh of up-aFRR energy compared to 5kWh and 12kWh of Nodes 2 and 1, respectively, during Summer 2023.

Finally, Figure 6.10 summarizes all up- (first row) and down-aFRR reserves (second row) provision for all nodes, cases, seasons, and years, where W and S denote Winter and Summer, respectively. The highest provided upward and downward aFRR capacities are 200kWh and 60kWh, respectively, for Node 3 in the year 2023. Regarding upward capacity, Cases 4 and 5 provide the highest aFRR amount, especially during the Winters of 2020 and 2023, while Node 3 consistently provides more capacity than the other two nodes for all years and cases. Moreover, comparing the seasons, while more up-regulation was delivered during Winter than Summer in 2020 (expected due to the high grid load consumption in Winter), a high increase can also be seen during Summer in 2023. Finally, comparing the years, the higher need, and hence, higher potential for participation of the PCS in the

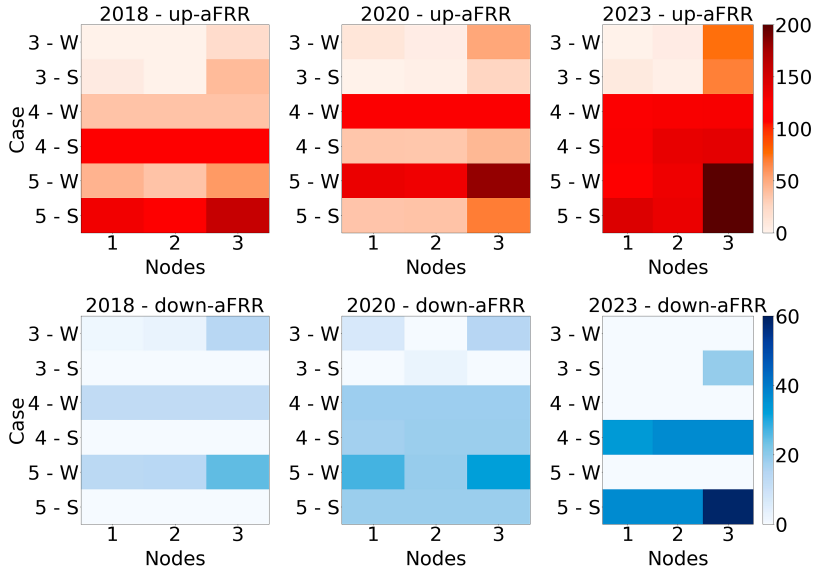


Figure 6.10: Summary of upward (upper row) and downward (lower row) provided aFRR energy (kWh) during Winter (W) and Summer (S), Nodes: 1-3, Cases 3-5, years: 2018, 2020, 2023.

imbalance market is evident in recent years.

Regarding downward capacity, the superiority of Cases 4 and 5, and Node 3 can also be seen here. Moreover, observing the Winter cases of the years 2018-2023, the scheduling and provision of downward aFRR capacity keeps decreasing as the year increases. On the contrary, an increasing trend can be seen during the Summer throughout the years. This is also expected due to the general grid load consumption increase during Winter and RES generation during Summer; hence, the TSO needs less downward regulation during Winter and more during Summer in recent years. However, the downward amount compared to the upward amount remains considerably lower. This is because, firstly, the TSO needs increasingly more upward regulation during the Winter (both in magnitude and duration). Secondly, as explained, upward regulation can also increase during Summer in the most recent years, such as 2023, in different time periods than the downward, due to the use of LCTs, e.g., EV charging during the evening. All of these trends can also be seen in Figure 6.3. However, it must be noted that since the simulations of this work are daily, the insights regarding the comparison of the seasons should not be generalized unless a seasonal analysis is performed.

### 6.5.4. Large Grid Scenario Results

The grid-level example is simulated for Cases 1, 2, 4, and 5; however, only for the Winter season and year 2020, due to long computational times ($> 12$ hours). The

Table 6.3: Cost and Cost Reduction of Cases 2, 4, and 5 compared to Case 1 for the Large Grid Scenario.

| Case | Total Grid Cost (€) | Percentage Difference |
|---|---|---|
| Case 1 | € 213.52 | - |
| Case 2 | € 201.65 | -5.56% |
| Case 4 | -€ 38.32 | -117.95% |
| Case 5 | -€ 890.33 | -516.98% |

simulations show consistent results compared to the small grid example regarding the cost savings and the related synergy of the LCTs acting as aFRR provision assets. Table 6.3 shows the total grid costs summed over all nodes. Similar to the small grid scenario results, Case 4 is the first case to show high profits (118% savings) compared to Case 1 due to revenue generated by aFRR participation. In addition, Case 5 shows the highest savings (517%) due to the presence of both EVs and BESS to participate in the aFRR market. The cost savings of Cases 4 and 5 in the small grid scenario for Winter 2020 are 810% and 900%, respectively. While the cost savings (in percentage) of the large grid scenario for Cases 4 and 5 are lower than the respective savings of the small grid scenario due to the larger size of the grid (a larger grid has already a much higher power control cost from Case 1), the importance of the synergy of the EVs and the BESS for aFRR provision in a PCS is also shown here in this grid scenario.

Figure 6.11 illustrates consistent scaling between aFRR provision and node size (node size decreases with numbering), where downward energy is again indicated in the negative direction. Similar to the small grid scenario simulation, more upward than downward power is delivered due to the already explained higher potential;

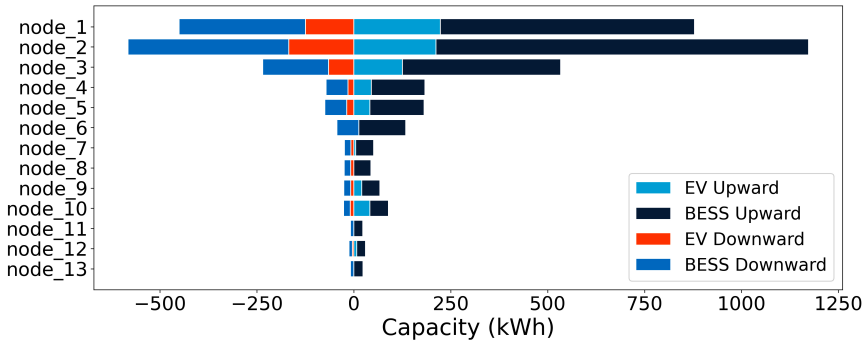


Figure 6.11: Total BESS and EV up- and down-aFRR provided energy for Nodes 1-13 for Case 5 (Winter 2020).

1150kWh up-aFRR provided energy compared to 600kWh down-aFRR energy for Node 2. Moreover, it can be seen that the size of the node has a considerable effect on both the magnitude of aFRR provision by EVs and the BESS individually, as expected, but also concerning the comparison between them. For example, EVs provide negligible aFRR energy at the very small Nodes 11-13. However, the up- and down-aFRR provided energy by EVs already constitute 19% of the respective energy amounts provided by the BESS for the average-size Node 5. Additionally, the percentage is even higher for the large nodes, such as Node 1 and Node 3; for example, the provided down-aFRR energy by EVs constitutes 28,6% of the energy provided by the BESS (100kWh compared to 350kWh) while the respective percentage for up-aFRR reserves is 38.5% (250kWh compared to 650kWh). Hence, it is proven that in larger nodes (or grids) that comprise a vast number of loads, the contribution of loads to ancillary services provision increases and can become comparable to a stationary BESS, even if the BESS capacity increases.

In Figure 6.12, we see a similar pattern for all nodes in the average cost of imported energy (total energy arbitrage cost per imported grid energy in $€/kWh$ as in the small grid scenario results (Figure 6.7). Case 2 exhibits the lowest imported energy cost since the addition of the BESS increases the flexibility of every node compared to Case 1 to perform energy arbitrage for higher revenues, exploiting the low and high energy price peaks of the energy price profiles. In contrast, incorporating aFRR provision in Cases 4 and 5 results in a significant increase in the average cost of imported energy compared to Case 1. This rise is due to the BESS charging at higher day-ahead prices, to subsequently discharge as upward aFRR power or the opposite for the provision of the downward aFRR power. Therefore, these additional costs are compensated by the revenue generated from providing aFRR services, as it was seen for the small grid scenario in Figure 6.7.

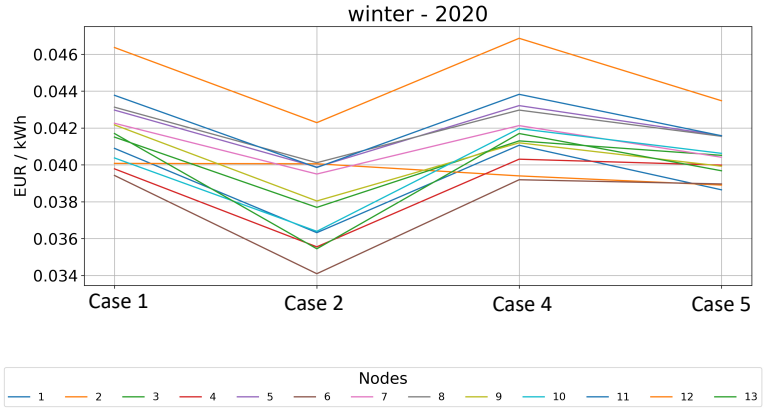


Figure 6.12: Average energy arbitrage cost per imported grid kWh for Cases 1, 2, 4, and 5 in the large grid scenario nodes (Winter - 2020).

### 6.5.5. Discussion of Results

Taking everything into consideration, this chapter compared the individual and combined contribution of flexible loads and BESS to energy arbitrage and aFRR provision, accounting for various influencing factors, such as different seasons, energy and reserve price profiles, grid types, and sizes. The most important findings of the chapter can be summarized as follows:

1) BESSs are generally capable of offering and providing more upward and downward aFRR reserves than EVs due to the lower connection time, EV driving patterns uncertainty, and requested charging energy. However, it was shown that in larger grids or larger nodes that comprise a higher amount of EV chargers and incoming EV fleets, the provided upward and downward reserve amounts are highly increased and can become comparable to the respective amounts provided by the BESS.

2) As expected, the greatest earnings are achieved when both BESS and EVs participate in energy arbitrage and aFRR provision. This is justified not only by the fact that both assets participate in the imbalance market and provide regulation reserves, but also because one asset (e.g., EVs) can take responsibility for energy arbitrage, such as building heating during low energy prices, while the other (e.g., the BESS) provides aFRR reserves to the TSO, and vice versa.

3) Mixed nodes that integrate both residential-commercial buildings and home-public chargers are consistently capable of delivering the majority of aFRR energy while simultaneously performing energy arbitrage. This is because of their higher flexibility due to the variety of flexible loads, such as those of the incoming EV fleets, resulting in a higher duration of EV connectivity during the day, more simultaneously connected EVs, etc.

4) As seen in Chapter 5, V2G is less utilized when there is available PV generation (e.g., Summer season) or a BESS due to higher round-trip power losses that usually overcome the earnings from energy arbitrage. Hence, V2G use is left for activities only in extreme cases, such as building heating during energy price peaks when no PV generation is available. However, when a PCS enables reserve market participation in its power control, the use of V2G for energy arbitrage is less dependent on seasonal effects or the presence of other assets. For example, V2G might be used for the flexibility of the nodes when the BESS is used for aFRR provision, since the power losses are compensated by the additional earnings.

5) Upward aFRR reserves are increasingly needed for the power grid in recent years, especially during Winter, and PCSs that can integrate participation in the imbalance market can be greatly contributive and achieve high cost savings. On the contrary, downward aFRR reserves are less needed than upward, possibly due to the higher use of LCTs. Nevertheless, a notable increase is seen during the Summer of recent years. However, it must be noted again that this insight is highly dependent on the daily volatility of energy and reserve prices and the interrelations between them, and a seasonal analysis should be performed to strengthen this point.

6) Overall, summarizing the investigated influencing factors, the grid type and the seasonal effect were found to be the most important factors since they highly affect both energy arbitrage and ancillary services provision. Energy and reserve prices

follow since they had a strong effect on the amount of provided ancillary services; however, they were less significant regarding energy arbitrage. Finally, the grid size is characterized as the least important influencing factor since most of the work's insights remained similar in the two grid scenarios.

## 6.6. Conclusions

This chapter has enhanced the bi-level multi-objective PCS of PVs, EVs, HPs, and BESSs, which focused on energy arbitrage in Chapter 5, to participate in the aFRR market while simultaneously respecting the grid limits, the charging and thermal comfort of the customers, and maximizing PV self-consumption. The contribution of the flexible loads and the BESS to the energy arbitrage and aFRR reserves provision has been compared under multiple influencing factors, such as different seasons, grid types and sizes, and energy/reserve prices.

Validating against the PCS of Chapter 5, designed solely for energy arbitrage, the findings demonstrate the potential for consistently 100% increased cost savings, reaching up to 900%, when the PCS participates in the reserve market. Moreover, these numbers can be achieved more effectively when more than one asset provides ancillary services (e.g., EVs and BESS), not only because they can both actively participate in the provision of the services, but also because they can share the other responsibilities. For example, the one asset performs building heating while the other provides aFRR reserves. These benefits become even more important in our years with the high increase in energy prices, but also with the much higher reserve prices; hence, higher potential for ancillary services provision. While the always present BESS is able to contribute more to ancillary services provision compared to the uncertain nature of the EV fleets, the contribution of EVs increased to a notable 38.5% compared to the BESS at grids or nodes of larger size. Finally, mixed nodes that comprise both residential-commercial buildings and home-public chargers have a higher potential in bidding and providing up- and down-aFRR reserves due to higher flexibility. Results demonstrated a 5x and 12x higher potential of mixed nodes compared to residential and commercial nodes, respectively.

Such as in Chapter 5, while the chapter addressed the effects of different seasons and different price profiles, only daily simulations were performed due to the high computational expense. The use of weekly and seasonal simulations is strongly recommended for future work since it would strengthen the insights concerning the season comparison and also show intra-weekly effects. Furthermore, it has been assumed that the aFRR bid is always accepted in the reserve market due to the zero-bid of RES-integrated balance responsible parties and deployed as a whole when called in real-time. The probability of no-acceptance and partial deployment is proposed for future work to further address the uncertainty of the reserve market.

# 7

# Power Control of LCTs and Ancillary Services Provision: Part 2

*Summary*

The PCS of this Ph.D. thesis has been developed to provide energy arbitrage in Chapter 5, while aFRR reserves provision has been added in Chapter 6. In this chapter, the PCS has been improved to perform DLC for congestion management, and provide aFRR reserves while, however, simultaneously optimally allocating BESS capacity in a distribution grid. Results showed that a BESS installation is not economically viable only with energy arbitrage for all investigated years. Even when the PCS is allowed to participate in the reserve market, the addition of gains from aFRR provision in the past (2018) was still not enough to install a BESS; however, it has become increasingly profitable in recent years due to the high energy price variations and both up- and down-aFRR prices. Furthermore, it was shown that a centralized BESS at the closest node to the main grid is the most beneficial solution due to lower power losses. Although the variations of energy and reserve price profiles can influence this decision, it was found that the different flexibilities (e.g., aFRR provision by different assets) do not notably alter it. The importance of BESS for congestion management was also proven, increasing DLC and load shifting success rates always above 90%. In this regard, commercial nodes that are characterized by low flexibility are in the greatest need for a BESS installation if they participate in ancillary services provision. Finally, it was also seen in this chapter that the gradual addition of assets and capabilities, such as V2G or ancillary services provision by different assets, always increased the cost savings.

*Outline*

The chapter is divided as follows: Section 7.1 contains the motivation and contributions of the chapter, while Section 7.2 describes the concepts of the two ancillary service provision studies (Study 1: "Direct load control" and Study 2: "aFRR reserves provision with optimal BESS capacity allocation"). In continuation, Section 7.3 integrates the modeling of this chapter's PCS, focusing on the optimal BESS capacity allocation, the new objective function, and the modeling of the power losses on the distribution lines, which constitutes a new modeling feature. Section 7.4 comprises the data input, case studies, and scenarios of the two studies, while Sections 7.5 and 7.6 are devoted to the results and discussions & validation of the chapter concerning the comparison of the findings with previous works, respectively. Finally, Section 7.7 concludes the chapter.

This chapter is based on:

N. Damianakis, K. Kuresoo and G. R. C. Mouli. 'Battery Storage Integration in Power Systems of PVs, and Flexible Loads for Frequency Reserves Provision and Direct Load Control'. In: *Journal of Energy Storage* (2025). Under Review

## 7.1. Motivation & Contributions

The reviewed power control studies in Chapters 5 and 6 did not incorporate optimal BESS allocation in their investigations. Moreover, they did not study the differences between implicit and explicit DR strategies in PCSs. Both of the above constitute the main features of this chapter's investigation.

### 7.1.1. Optimal BESS allocation

Regarding optimal BESS sizing studies, optimally sized BESS-PV systems were investigated in [218], [219], and [220] for minimization of energy or degradation costs. While the authors in [218] focused on self-consumption maximization, the influence of different price tariffs, PV subsidies, and PV output uncertainty was studied in [219]. Additionally, HPs and EVs were added in the BESS-sizing studies of [221, 222] and [223], respectively. The MPC model in [221] focused on handling future uncertainties such as ambient temperature, solar radiation, occupancy, balancing user comfort, energy efficiency, and cost, while basing their BESS-sizing approach on the daily grid energy injections and water storage capacity. However, the optimal sizing of BESS while exploiting their potential for ancillary services provision was not considered in any of the studies.

Optimal BESS sizing in DGs was studied in [216] for PV maximum self-consumption and provision of stacked reserves, such as voltage regulation, congestion relief, peak shaving, and FCR. EVs were also added in the optimal BESS sizing work [20] for a HEMS showing the contribution to grid reliability and economic feasibility, but only if battery degradation is also taken into account. However, most of the BESS capacity optimization studies consider only optimal sizing and not siting (location) because a vast majority of them are HEMS or BEMS and focus on the perspective of the owners.

Optimal sizing and siting studies, which focus on the DSO perspective, can be found in the PV-integrated grid-level works in [224] with the aim of voltage and utilization control and [225] for minimization of delivered energy and installation costs. Other ancillary services for which an optimally sized and sited BESS can be important in a grid-level EMS are minimizing distribution energy losses [226], quality and reliability increase by the decrease of voltage deviations [227], [228], peak shaving, and frequency regulation [229]. However, all of these studies ignored the effect of the installation investment cost, which was accounted for in [230] for smaller and larger DGs. All of the above sizing and siting BESS studies incorporate only PVs and lack the inclusion of flexible loads (EVs and HPs), which are crucial for optimal ESS operation and size reduction. Especially the presence of EVs in the DG, which can act as small-scale batteries for both energy arbitrage and ancillary services provision, is crucial for the optimal BESS allocation.

Finally, review studies of ESS allocation, focusing on optimal sizing and siting, optimization methods, and broader integration strategies, can be found in the literature, such as [231, 232]. Different characterization methods are used in [233] and [234], with the former including power- and energy-related services, network level, and actor, and the latter including load model, network inclusion,

market inclusion, and objective functions. According to [234], ESS technologies are primarily chosen based on power rating and energy capacity, which are distinct aspects requiring separate sizing considerations.

### 7.1.2. PCS & Implicit/Explicit Demand Response (DR)

The discussed studies until here all fall under the category of implicit DR strategies; thus, utilizing price-based tariffs for cost reduction and ancillary services provision. In general, it was shown that the RTP energy tariff is the most widely used strategy in the most recent studies for HEMS or grid-level EMS. The superiority of RTP was shown against other price tariffs, such as TOU and CPP, for cost savings with the synergy of HPs and TES in smart buildings in [235] and [236].

However, PCS can also be utilized to directly provide various services and objectives via DLC (explicit DR). DLC of HPs was studied in residential building areas with thermostatic load control and direct building temperature decrease in [237] and HP blocking periods in [238] for peak shaving and system sizing reduction, respectively. Additionally, a direct activation of passive building storage for HP discharging on cold days and charging on milder days was investigated in [239]. The application of direct load control programs by the DSO in a Swiss region comprising EVs and HPs was investigated in [240]. However, ESS flexibility was not considered in the study. DLC in synergies of PVs, HPs, and BESS was performed according to field measurement data in [241] for PV max self-consumption, which reached up to 43%. Moreover, the flexibility of PVs, EVs, and HPs was used via DLC in [242] to control frequency variations based on the power balance of the loads, while a TES and a peak power penalty were applied in [202] for direct peak shaving. The authors in [202] compared rule-based (DLC) and MPC techniques considering cost-, carbon-, and flexibility-oriented objectives. On the contrary, DLC (explicit DR) was compared with implicit DR strategies in [243] (RTP) and [244] (TOU, CPP, CT, RTP, etc.), where it was found that DLC is more effective in power peaks reduction since price-based strategies can still crease power peaks during different time periods especially in larger systems. Some works also studied the synergy between the two DR strategies. DLC was combined with TOU in [245] and [246]; dynamic active PV power curtailment combined with TOU under different EV charging scenarios was studied in [245] for power quality increase and while the temporary connection shutdown of a HEMS with the main grid was investigated in [246] for PV self-consumption increase and peak shaving. Finally, the combination of DLC and RTP and categorization of household loads to (non)interruptible and (non)deferrable effectively reduced peak shaving in households in [17].

### 7.1.3. Contributions

The characteristics and contributions of the reviewed power control studies for Chapter 7 (implicit/explicit DR and BESS optimal allocation studies) have been summarized in Table 7.1. In Table 7.1, "Opt. size" and "Opt. site" indicate if the study considers optimal BESS size and location, respectively, while "Inv. cost" indicates the inclusion of BESS investment cost. Moreover, "Anc." and "aFRR" denote the

consideration of ancillary services, and whether aFRR is accounted for in these services. Furthermore, all power control studies can be considered DR studies; Table 7.1 includes only the studies that combine or compare implicit and explicit DR strategies ("Imp DR and Exp DR"), such as price tariff-based strategies and DLC. Finally, "Grid" denotes if the study is grid-level, while "Loads vs ESS" denotes if comparisons between flexible loads and BESS have been performed regarding energy arbitrage and/or ancillary services provision.

Table 7.1: Characteristics & Contributions of Reviewed Power Control Studies.

| Paper | BESS | PVs | EVs | HPs | Opt. size | Opt. site | Inv. cost | Anc. | aFRR | Imp DR and Exp DR | Loads vs BESS | Grid |
|---|---|---|---|---|---|---|---|---|---|---|---|---|
| [116] | | ✓ | ✓ | ✓ | | | | | | | | |
| [247] | | ✓ | ✓ | ✓ | | | | | | | | ✓ |
| [243] | | ✓ | | ✓ | | | | ✓ | | TOU **vs** DLC | | ✓ |
| [244] | ✓ | ✓ | ✓ | ✓ | | | | ✓ | | Price tariffs **vs** DLC | | |
| [245] | ✓ | ✓ | ✓ | | | | | ✓ | | TOU **and** DLC | | ✓ |
| [246] | ✓ | ✓ | | ✓ | | | | ✓ | | TOU **and** DLC | | |
| [17] | | ✓ | ✓ | ✓ | | | | ✓ | | RTP **and** DLC | | |
| [210] | ✓ | ✓ | | | | | | ✓ | | | | |
| [212] | ✓ | ✓ | | ✓ | | | | ✓ | ✓ | | | |
| [211] | ✓ | ✓ | | | | | ✓ | ✓ | ✓ | | | |
| [218] | ✓ | ✓ | | | ✓ | | ✓ | | | | | |
| [219] | ✓ | ✓ | | | ✓ | | ✓ | | | | | |
| [220] | ✓ | ✓ | | | ✓ | | ✓ | | | | | |
| [221] | ✓ | ✓ | | ✓ | ✓ | | | | | | | |
| [222] | ✓ | ✓ | | ✓ | ✓ | | ✓ | | | | | |
| [223] | ✓ | ✓ | ✓ | | ✓ | | ✓ | | | | | |
| [216] | ✓ | ✓ | | | ✓ | | ✓ | ✓ | | | | ✓ |
| [20] | ✓ | ✓ | ✓ | | ✓ | | ✓ | ✓ | | | | |
| [225] | ✓ | ✓ | | | ✓ | ✓ | ✓ | | | | | ✓ |
| [224] | ✓ | ✓ | | | ✓ | ✓ | ✓ | ✓ | | | | ✓ |
| [226] | ✓ | ✓ | | | ✓ | ✓ | | ✓ | | | | ✓ |
| [227] | ✓ | ✓ | | | ✓ | ✓ | | ✓ | | | | ✓ |
| [228] | ✓ | ✓ | | | ✓ | ✓ | | ✓ | | | | ✓ |
| [229] | ✓ | ✓ | | | ✓ | ✓ | | ✓ | | | | ✓ |
| [230] | ✓ | ✓ | | | ✓ | ✓ | ✓ | ✓ | | | | ✓ |
| **Ch.7** | ✓ | ✓ | ✓ | ✓ | ✓ | ✓ | ✓ | ✓ | ✓ | RTP **and** DLC | ✓ | ✓ |

According to Table 7.1, while power control models that integrate PVs, EVs, HPs, and BESS for energy arbitrage or ancillary services provision exist in the literature, very few of them combine the potential of implicit and explicit DR strategies, such as RTP and DLC, respectively. Furthermore, grid-level studies that investigate optimal BESS sizing and siting include only PVs in their investigation and ignore the effect of flexible loads (EVs and HPs) and their synergy with the BESS. Finally, according to the author's knowledge, an existing BESS optimal allocation study that performs energy arbitrage and provides aFRR reserves is still missing from the literature. This chapter develops a PV-EV-HP-BESS power control model for energy arbitrage and ancillary services provision while simultaneously optimally allocating BESS capacities in different DG types. The influence of aFRR reserves provision, distribution line losses, grid type, energy/reserve prices, seasons, and different synergies between flexible loads and BESS on the optimal capacity allocation is also investigated. Furthermore, the chapter studies the potential of RTP and DLC in power systems under the effect of different DG types, seasons, and BESS use. Overall, this chapter's contributions can be summarized as follows:

- Develops an MIQP power control model of PVs, EVs, HPs, and BESS, which participates in the energy market with energy arbitrage and the reserve market with aFRR reserves provision while simultaneously optimally allocating BESS capacity in different distribution grids.
- Investigates the influence of aFRR reserves provision, distribution line losses, grid type, energy/reserve prices, seasons, and the synergy of flexible loads and BESS on the optimal BESS capacity allocation.
- Investigates the potential of implicit (RTP) and explicit (DLC) demand response strategies in power control models of flexible loads, with and without BESS, in different distribution grids and seasons for rural and urban areas.

## 7.2. Power Control System & Ancillary Services Concepts

### 7.2.1. Concept of Power Control System

The fundamental model of the PCS developed in this chapter, its core objectives and level functionalities remain the same: distributional DA and RT optimization of aggregated EV chargers and buildings, aiming for maximum cost savings, minimum PV curtailment, ensuring the charging and thermal comfort of the customers, and respecting the grid limits. As Figure 7.1 depicts, this chapter enhances the PCS to utilize the two levels to provide congestion management (Study 1) and aFRR reserves while optimally allocating the BESS capacity (Study 2).

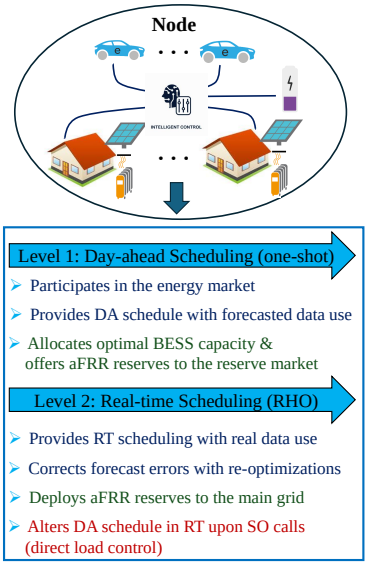


Figure 7.1: Characteristics of the two levels of the bilevel PCS.

### 7.2.2. Concept of Ancillary Services Provision Studies

Study 1 is devoted to DLC, and its concept is depicted in Figure 7.2. DLC is realized in RT (Level 2) and uses the estimated DA schedule of Level 1. The DSO can call two types of DLC, consumption increase (CI) and consumption decrease (CD), which are added as re-optimization triggers in Level 2. If the call is CD, the PCS checks the DA schedule of the node; if the CD amount is lower than the DA imported power at this time period, the RT imported power is reduced by the CD amount; otherwise, the node inverts the grid power exchange and exports the power difference to assist in the total consumption decrease of the DG. The opposite applies in the CI call. Study 1 can be used to assess the congestion management potential of a power control system comprising a number of aggregated assets and, consequently, the level of its flexibility.

Study 2 is devoted to scheduling and deployment of aFRR reserves participating in the wholesale reserve market, while simultaneously optimally allocating BESS capacity at different nodes. The multi-objective optimization of energy arbitrage, aFRR reserves provision, and optimal BESS capacity allocation takes place in

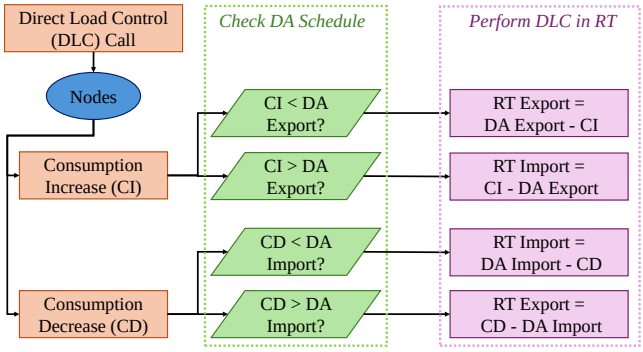


Figure 7.2: Flowchart of the DLC concept in RT (Level 2): Study 1.

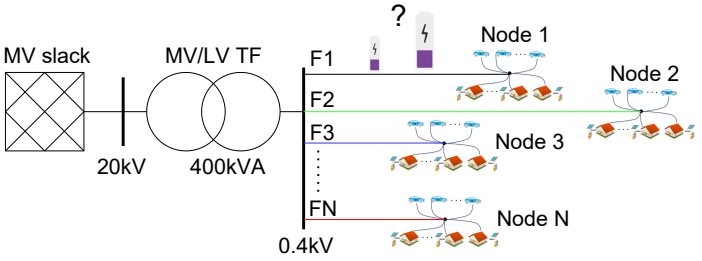


Figure 7.3: Optimal BESS capacity allocation concept at nodes located at different distances from the main grid: Study 2.

the DA level (Level 1) while Level 2 performs energy arbitrage and deploys the scheduled aFRR reserves under uncertainties with the optimally allocated BESS capacities, such as in [210]. Figure 7.3 depicts a grid topology with N nodes that are connected to the main grid with N different feeders on the LV side of a 400kVA MV/LV transformer, and are located at different distances from the main grid. Study 2 can be used in PCS to allocate a total available BESS capacity at different nodes in the grid and investigate the impact of distribution line resistances, PCS objectives, node types (e.g., residential, commercial), etc. It must be noted that the installation and operational costs of the BESS have also been considered in Study 2 since they are crucial for the value and choice of BESS capacity installation in the first place.

## 7.3. Power Control Modeling

This section comprises the methodology of the MIQP power control model for both Studies 1 and 2, which is a continuation of the power control modeling in Chapter 5 and the modeling of aFRR reserves provision in Chapter 6. Sections 7.3.1-7.3.5 include the constraints of the BESS/EV operation, buildings, BESS optimal allocation, aFRR market, and nodes, while the objection function is included in Section 7.3.6. All equations referring to both studies are not marked. Equations that are marked with "$\tilde{()}$" belong only to Study 2, while the "$\hat{()}$" and "$\bar{()}$" marks mean that they are utilized only on Level 1 and Level 2, respectively. Study 1 uses the unmarked equations in Sections 7.3.1, 7.3.2, 7.3.4, 7.3.5, 7.3.6 on both levels. Furthermore, as in Chapter 6, the variables marked in **bold letters** are used as variables on Level 1 of Study 2 and are passed as parameters on Level 2. These variables constitute the offered regulation reserves in the aFRR market day-ahead (uncertain variables), and their deployment upon acceptance in real-time (certain parameters). Finally, in this chapter, the notations: $n, nom, j, bes, \Delta t, ch, dis, fr_u, fr_d, 1s, rho, cv, init, b, sf, ir, amb, air, hp, pv, dev, ins, tp, rt, da, T$ denote the node, nominal, charger, BESS, timestep, charging, discharging, up aFRR, down aFRR, one-shot, RHO, constant voltage, initial, building, surface, irradiation, ambient, air, heat pump, PV, deviation, installation, throughput, real-time, day-ahead, and horizon, respectively. It must be noted that all equations apply for $\forall t \in T$ unless it is stated otherwise.

### 7.3.1. BESS/EV Operational Constraints

Equations regarding the modeling of the charging/discharging/aFRR powers (6.1), battery (6.2), and SOC dynamics (6.3), CC-CV charging/discharging regions (6.4)-(6.6), binary variables used for the separation of powers (5.9) - (5.11) & (6.7) - (6.11), nullification of EV variables outside parking period (6.12), and calculation of EV unfinished charging gap (5.12) remain the same as in Chapters 5 and 6.

Moreover, (7.1) and (7.2) correlate the EV/BESS down-aFRR $P_{fr_d^{fin}}$ and up-aFRR $P_{fr_u^{fin}}$ powers at the point of common coupling (PCC) with the main grid (LV size of the MV/LV transformer) with their respective powers $P_{fr_d}$ and $P_{fr_u}$ at the LCTs,

where $h^{n,j}_{ch/bes}$ the EV/BESS efficiencies and $P_{fr^{los}_{d/u}}$ the respective losses on the distribution lines. The latter are dictated in the quadratic (7.3) and (7.4), which depend on the line resistance $R$ and are integrated into the power control using PWL approximations such as in [225].

$$\left(P^{n,j/bes,t}_{fr^{fin}_{d}} = \mathbf{P^{n,j/bes,t}_{fr_d}}/h^{n,j}_{ch/bes} + P^{n,j,t}_{fr^{los}_{d}}\right) \tag{7.1}$$

$$\left(P^{n,j/bes,t}_{fr^{fin}_{u}} = \mathbf{P^{n,j/bes,t}_{fr_u}} h^{n,j}_{ch/bes} - P^{n,j/bes,t}_{fr^{los}_{u}}\right) \tag{7.2}$$

$$\left(P^{n,j/bes,t}_{fr^{los}_{d}} = \Phi^{n,j}(I^{n,j/bes,t}_{fr_d}/h^{n,j}_{ch/bes})^2 R^n\right) \tag{7.3}$$

$$\left(P^{n,j/bes,t}_{fr^{los}_{u}} = \Phi^{n,j}(I^{n,j/bes,t}_{fr_u} h^{n,j}_{ch/bes})^2 R^n\right) \tag{7.4}$$

Additionally, (7.5) and (7.6) are utilized on Level 2 of Study 2 to ensure that the BESS and EVs have sufficient available capacity to provide both downward and upward regulation for the next ISP respecting the minimum and maximum SOC limits $S_m$ and $S_M$. Specifically, for downward regulation, it is essential that there is adequate space in the EV battery to accommodate additional energy, whereas, for upward regulation, the battery must contain sufficient deliverable stored energy.

$$\left(\left(B^{n,j/bes,t}_{rho} \leq S_M B^{n,j/bes}_{r} - \sum_{t_{init}}^{t} \left(P_{ch} + \mathbf{P_{fr_d}}\right)^{n,j/bes,t} \Delta t\right.\right. \tag{7.5}$$

$$\left.\left. B^{n,j/bes,t}_{rho} \geq S_m B^{n,j/bes}_{r} + \sum_{t_{init}}^{t} \left(P_{dis} + \mathbf{P_{fr_u}}\right)^{n,j/bes,t} \Delta t\right)\right) \tag{7.6}$$

### 7.3.2. Building Constraints

The building constraints used in this chapter remain similar to those used in Section 6.3.2 of Chapter 6; hence, (5.14) - (5.37) as in Section 5.4.2 are used with omission of (5.26) and (5.27). In this chapter, the average Winter and Summer HP COPs 3.5 and 6 are utilized to decrease the computational expense of this chapter's PCS.

### 7.3.3. aFRR Market Constraints

The aFRR market of this chapter is emulated in the same manner as in Section 6.3.3 of Chapter 6; hence integrating (6.13)-(6.16). In this way, the two PCS methods of Chapters 6 and 7 can be cross-validated in Section 7.6.4.

### 7.3.4. BESS Optimal Allocation Constraints

This section comprises the equations for BESS optimal capacity allocation at the grid nodes, which are used on Level 1 of Study 2. The binary variable $b_{ins}$ is introduced to enable capacity allocation at a node or node. Equation (7.7) defines the feasible region of the variable BESS capacity $B_r$ while (7.8) dictates that the total BESS capacity $B^{bes}_{tot}$ is below a predefined value; in this investigation, $B^{bes}_{tot} = B^{n,bes}_{max} = 150kWh$ (the total capacity of the 3 BESS in Chapter 6). The maximum charging and discharging BESS power $P^{bes}_{max}$ is modeled in (7.9), depends on the total BESS capacity $B_r$, and is set at 0.5 C-rate. In addition, the relation between the maximum BESS power $P^{bes}_{max}$ and current $I^{bes}_{max}$ is dictated in (7.10).

$$B^{n,bes}_{min}\mathbf{b^{n,bes}_{ins}} \leq B^{n,bes}_{r} \leq B^{n,bes}_{max}\mathbf{b^{n,bes}_{ins}} \tag{7.7}$$

$$\sum_{n=1}^{3}\left(\mathbf{B^{n,bes}_{r}}\right) \leq B^{bes}_{tot} \tag{7.8}$$

$$P^{n,bes}_{dis_{max}} = P^{n,bes}_{ch_{max}} = \mathbf{P^{n,bes}_{max}} = 0.5B^{n,bes}_{r} \tag{7.9}$$

$$\mathbf{I^{n,bes}_{max}} = \frac{P^{n,bes}_{max}}{\Phi^{n,bes}V_{nom}} \tag{7.10}$$

According to (7.11), the BESS SOC at the start of the simulation $S^{n,bes,t=0}$ can be either $S_{init} = 0.5$ or zero. Moreover, (7.12) - (7.13) combined dictate the instantaneous SOC $S$ and its feasible region $[S_{min}, S_{max}]$, turning it to zero if no BESS capacity is installed at the node. The total BESS discharging throughput $B_{tp_{tot}}$ is modeled in (7.14), depends on the total discharging and up-aFRR power during the horizon $T$ and is limited to the rated BESS capacity in (7.15) (one equivalent cycle per day) to reduce and maintain consistent degradation during all case studies. Finally, (7.16) is used on Level 2 and forces the BESS SOC in RHO to follow with an uncertainty budget of 10% the BESS SOC in DA.

$$S^{n,bes,t=0} = S^{n,bes}_{init}\mathbf{b^{n,bes}_{ins}} \tag{7.11}$$

$$S^{n,bes}_{min} \leq S^{n,bes,t}\mathbf{b^{n,bes}_{ins}} \leq S^{n,bes}_{max} \tag{7.12}$$

$$S^{n,bes}_{min}\mathbf{b^{n,bes}_{ins}} \leq S^{n,bes,t} \leq S^{n,bes}_{max}\mathbf{b^{n,bes}_{ins}} \tag{7.13}$$

$$B^{n,bes}_{tp_{tot}} = \sum_{t=0}^{T}\left(P^{n,bes,t}_{dis} + P^{n,bes,t}_{fr_u}\right)\Delta t \tag{7.14}$$

$$B^{n,bes}_{tp_{tot}} \leq \mathbf{B^{n,bes}_{r}} \tag{7.15}$$

$$\left(0.9S^{n,bes,t}_{1s} \leq S^{n,bes,t}_{rho} \leq 1.1S^{n,bes,t}_{1s}\right) \tag{7.16}$$

### 7.3.5. Node Constraints

The equations, included in this section, describe the function of the nodes (de-centrally in the PCS model) and their communication with the main grid. The node dynamic power balance $P_{bal}^{n,t}$ is dictated in (7.17) and is the sum of all LCT powers inside the node apart from the aFRR powers: charging $P_{ch}^{j,bes}$, discharging $P_{dis}^{j,bes}$, HP $P_{hp}$, base load $P_l$, and PV $P_{pv}$. The respective node current $I^n$ is defined in (7.18), while the total node current $I_{tot}^n$ (that comprises also the currents for aFRR reserves provision) is dictated in (7.19) and limited by the maximum current limit $I_{max}$. To avoid high non-linearities, this chapter has again utilized the nominal voltage $V_{nom} = 230V$ in both studies, assuming very low deviations. To limit the total node current $I_{tot}$, $I_{max}^n$ has been calculated in (7.20) according to the accepted voltage drop tolerance of ± 5% set by the standard IEC 60038 [248].

$$P_{bal}^{n,t} = \sum_{j=1}^{J}\left(\frac{P_{ch}^{n,j,t}}{h_{ch}^{n,j}} - P_{dis}^{n,j,t} h_{ch}^{n,j}\right) + \frac{P_{ch}^{n,bes,t}}{h_{bes}^{n}} - P_{dis}^{n,bes,t} h_{bes}^{n} + \sum_{b=1}^{B}\left(P_{hp}^{n,b,t} + P_{l}^{n,b,t} - P_{pv}^{n,b,t}\right),\ \forall t \in T \tag{7.17}$$

$$I^{n,t} = \frac{P_{bal}^{n,t}}{\Phi^n \cdot V_{nom}} \tag{7.18}$$

$$\left(I_{tot}^{n,t} = I^{n,t} + \frac{I_{fr_d}^{n,bes,t}}{h_{bes}^{n}} - I_{fr_u}^{n,bes,t} h_{bes}^{n} + \sum_{j=1}^{J}\left(\frac{I_{fr_d}^{n,j,t}}{h_{ch}^{n,j}} - I_{fr_u}^{n,j,t} h_{ch}^{n,j}\right),\ -I_{max}^{n} \le I_{tot}^{n,t} \le I_{max}^{n}\right) \tag{7.19}$$

$$\left(I_{max}^{n} = \frac{V_{nom} - V_{nom} 0.05}{R^n}\right) \tag{7.20}$$

The currents $I, I_{tot}$ are defined at the location of the nodes on the distribution lines. The power losses on the lines $P_{los}$ caused by the energy arbitrage current $I$ are dictated and PWL approximated in (7.21), such as for the aFRR power losses in (7.3), (7.4). The power losses have been accounted for in (7.22) to calculate the final imported $P_{im}$ and exported $P_{ex}$ at the PCC with the main grid. As with $P_{ch}$ and $P_{dis}$, binary variables $b_{im}$ and $b_{ex}$ are introduced for imported power and exported power, respectively, so that they are forced not to occur simultaneously as a pair and with up and down regulation, respectively. For Study 2 that provides aFRR reserves, the limits for imported and exported powers must be decreased according to the offered down- and up-aFRR powers in (7.23) and (7.24), respectively.

$$\left(P_{los}^{n,t} = 3 I_{n,t}^2 R^n\right) \tag{7.21}$$

$$P_{im}^{n,t} - P_{ex}^{n,t} = P_{bal}^{n,t} + (P_{los}^{n,t}) \tag{7.22}$$

$$P_{im}^{n,t} + (\mathbf{P}_{\mathbf{fr_d^{fin}}}^{\mathbf{n,bes,t}} + \sum_{j=1}^{J} \mathbf{P}_{\mathbf{fr_d^{fin}}}^{\mathbf{n,j,t}}) \leq G_{in}^{n} \tag{7.23}$$

$$P_{exp}^{n,t} + (\mathbf{P}_{\mathbf{fr_u^{fin}}}^{\mathbf{n,bes,t}} + \sum_{j=1}^{J} \mathbf{P}_{\mathbf{fr_u^{fin}}}^{\mathbf{n,j,t}}) \leq G_{out}^{n} \tag{7.24}$$

### 7.3.6. Objection Function

As in Chapters 5 and 6, the PCS is again a multi-objective problem, which performs energy arbitrage respecting the grid limits, provides ancillary services, and ensures that the PV self-consumption is maximized and that the charging and thermal comfort of the customers are never violated. The optimization objective (7.25) translates all the above objectives into one objective (total cost $C$ minimization) and, hence, becomes a single objective function which is more easily solvable.

$$\begin{aligned}
\min C = \Delta t \sum_{n=1}^{N} \Bigg( & \sum_{t=1}^{T} (P_{im}^{n,t} C_{buy}^{t} - P_{ex}^{n,t} C_{sell}^{t}) \\
& + \sum_{t=1}^{T} \sum_{b=1}^{B} (P_{pv_{dev}}^{n,b,t} C_{pv_{pen}}^{n,b}) + \sum_{t=1}^{T} \sum_{b=1}^{B} (T_{dev}^{n,b,t} C_{hp_{pen}}^{n,b} O^{t,n,b}) \\
& + \sum_{j=1}^{J} E_{g}^{n,j} C_{ev_{pen}}^{n,j} + \Bigg( \left( \frac{\mathbf{B}_{\mathbf{r}}^{\mathbf{n,bes}} C_{cap}^{n,bes,\mathbf{B_r}}}{y_{bes}^{lif} \cdot 365} + \frac{\mathbf{P}_{\mathbf{max}}^{\mathbf{n,bes}} C_{OM}^{n,bes}}{365} \right) \\
& \Big( \Big( + \sum_{t=1}^{T} \Big( \sum_{j=1}^{J} (P_{fr_d^{fin}}^{n,j,t}) + P_{fr_d^{fin}}^{n,bes,t} \Big) C_{down}^{t} \\
& - \sum_{t=1}^{T} \Big( \sum_{j=1}^{J} (P_{fr_u^{fin}}^{n,j,t}) + P_{fr_u^{fin}}^{n,bes,t} \Big) C_{up}^{t} \Big) \Big) \Big)
\end{aligned} \tag{7.25}$$

$$C_{cap}^{n,bes,B_r^{n,bes}} = C_e B_r^{n,bes} + C_p P_{max}^{n,bes} + C_{fix} \tag{7.26}$$

The total cost encompasses the following components:

1) The grid exchange cost minimization for the energy arbitrage, where $C_{buy}$ and $C_{sell}$ the imported power cost and exported power revenue in €/kWh (first term).

2) The PV curtailment - thermal discomfort - EV unfinished charging costs, where $C_{hp_{pen}}, C_{hp_{pen}}, C_{ev_{pen}}$ the respective penalty costs for the customers' satisfaction in €/kW, €/°, and €/kWh (second, third, and fourth terms). Components 1) and 2) are included in both studies and levels.

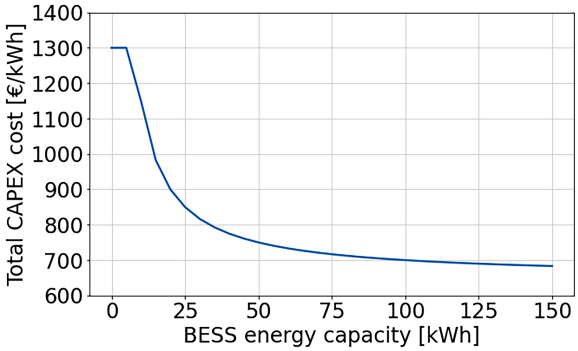


Figure 7.4: BESS Total CAPEX cost as a function of size in kWh.

3) The BESS cost which comprises the capital expenditure (CAPEX) $C_{cap}^{n,bes,B_r}$ and the operational and maintenance (O&M) costs of BESS $C_{OM}^{n,bes}$ normalized to one day, where $y_{bes}^{lif} = 15$ the BESS lifetime in years (fifth term). The BESS CAPEX cost is capacity- and power-dependent plus a fixed installation cost, as dictated in (7.26) and depicted in Figure 7.4 (integrated with PWL approximation), where $C_e, C_p, C_{fix}$ the respective cost factors (Table 7.2) by NREL predictions [249] and German BESS market data [250]. The operational and maintenance (O&M) residential BESS costs are approximately $25€/kW_{ins}$ per year [251]. 3) is important in Study 2 on Level 1, so that the PCS decides if it is beneficial to install BESS at a node.

4) The up- and down-aFRR revenues from EV and BESS, where $C_{down}$ and $C_{up}$ the respective prices in €/kWh (sixth term). 4) is utilized only in Study 2 on Level 1 during the scheduling of the offered aFRR reserves.

For Study 1, the objective function is linear (first four terms); hence, the quadratic equality constraints make the PCS only MIQCP (quadratically-constrained). For Study 2, the objective function becomes quadratic due to the fifth term; hence, the PCS becomes purely MIQP. Finally, Table 7.2 summarizes the BESS parameters used for the PCS of this chapter.

## 7.4. Data Description, Simulation Setup, Case Studies & Scenarios

### 7.4.1. Data input

This investigation uses the small grid scenario as in Chapters 5 and 6 for all case studies and scenarios. Moreover, the same data is used regarding the base load, PVs, HPs, EVs, and weather data. Additionally:

1) LIB specifications summarized in Table 7.2 are derived by multiple battery manufacturers and consistent with ongoing ESS research [218]. The BESS-related costs are derived from multiple sources [249], [250], [251].

Table 7.2: BESS Parameters for the PCS of Chapter 7.

| Parameters | Explanation | Value |
|---|---|---|
| $S_{min}^{n,bes}$ | Min BESS SOC | 10% |
| $S_{max}^{n,bes}$ | Max BESS SOC | 90% |
| $S_{init}^{n,bes}$ | Initial BESS SOC | 0.5 |
| $S_{fin}^{n,bes}$ | Final BESS SOC | 0.4-0.6 |
| $B_{tot}^{bes}$ | Total BESS Capacity | 150kWh |
| $B_{tp_{tot}}^{n,bes}$ | BESS throughput | 1 cycle/day |
| $y_{bes}^{lif}$ | BESS lifetime | 15 years |
| $C_e$ | BESS CAPEX capacity coef. | 400€/kWh |
| $C_p$ | BESS CAPEX power coef. | 500€/kW |
| $C_{fix}$ | BESS fixed installation cost | 5000€ |
| $C_{OM}^{n,bes}$ | BESS OM cost | 25€/kW |

2) Energy and reserve price profiles are derived from the Dutch ENTSO-E platform. The considered DAM price Winter profiles 22.01.18 (same as in Chapter 5), 02.01.23, 09.01.23, and 24.01.23 and Summer profiles 23.07.18 (same as in Chapter 5), 04.07.23, 13.07.23, and 01.08.23 are close to the yearly 3-month average Winter and Summer price profiles, and are depicted in Figure 7.5. The daily price volatility is significantly higher in 2023 compared to 2018; however, the shape of the price profile is similar. The difference between the lowest and highest price hours is over 110 €/MWh for all three winter days in 2023. Concerning the Summer days, the duck curve phenomenon (significantly lower day prices compared to morning and evening peak hours due to the high PV generation) is clearly visible for 2023 prices.

Upward and downward reserve price ranges are depicted in Figure 7.6. On 22.01.18, the imbalance prices for both upward and downward regulation are also in this chapter relatively low compared to the days of 2023. On 09.01.23, there are high upward regulation prices, peaking above 1000 €/MWh, and notable negative downward prices reaching up to -434 €/MWh (high potential also for downward regulation), while on 24.01.21, there are high upward regulation prices with no negative downward prices, indicating a strong incentive for upward regulation. The Summer days, such as 13.07.23, indicate high upward prices (up to 1500 €/MWh) and significant negative downward prices (up to -500 €/MWh), showing a highly volatile market with a high potential for both profitable upward and downward regulation.

3) The heavy rural and heavy urban grids of Chapter 3 are utilized in Study 1, which are acquired by the Dutch DSO Enexis Groep. More specifically, the DLC calls for CI or CD have been developed and fed as input to the PCS in Study 1, according to the T/F and line overloading issues found in these grids during Winter and Summer in Chapter 3.

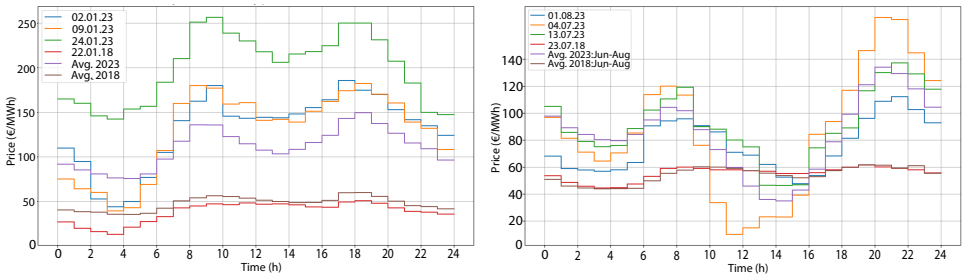


(a) Energy Price Profiles: Winter days

(b) Energy Price Profiles: Summer days

Figure 7.5: DA energy price profiles in the NL for the used days for years 2018 and 2023.

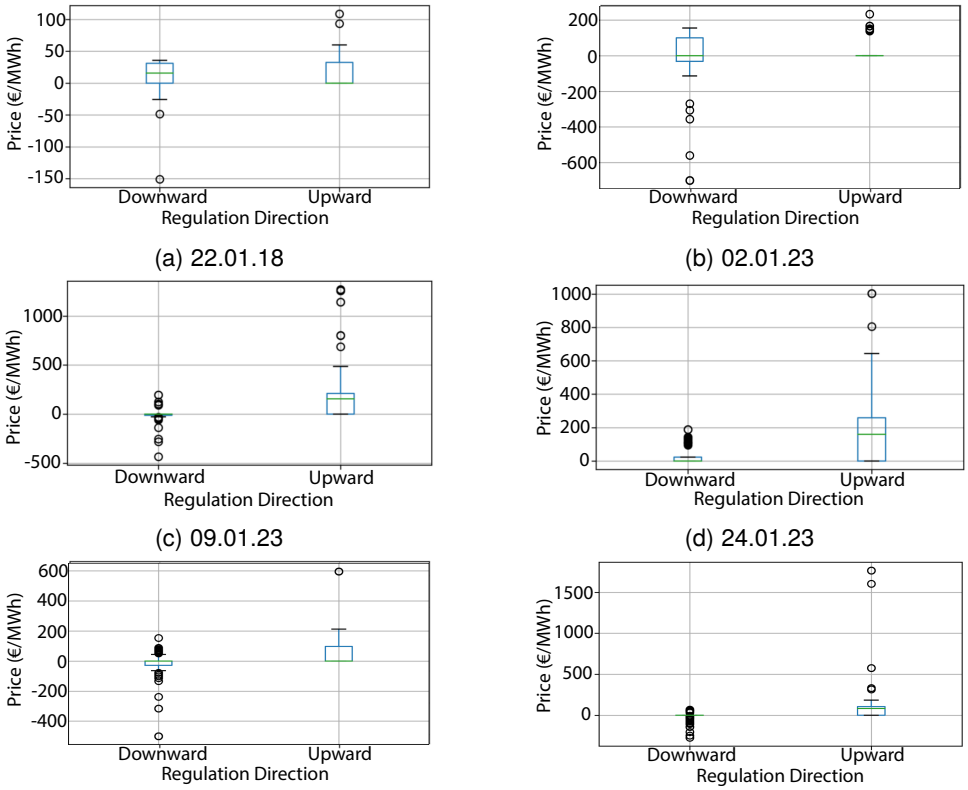


(a) 22.01.18

(b) 02.01.23

(c) 09.01.23

(d) 24.01.23

(e) 04.07.23

(f) 13.07.23

Figure 7.6: Imbalance Settlement Prices in the NL for four Winter and two Summer days.

### 7.4.2. Studies, Cases, and Scenarios

#### Study 1: Direct load control (DLC) with and without BESS use

The cases and scenarios used in Study 1 are summarized in Table 7.3. The DLC calls endure for 10' and depend on the investigated seasons (Winter or Summer) and the grid where the nodes are located, a rural and an urban grid. The response to the DLC calls has been investigated with only load flexibility and with its synergy with BESS use. If they cannot successfully respond to the DLC call, they continue their power scheduling as is. This study analyzes, firstly, the congestion management potential of different node types in different grids and seasons, and secondly, the importance of BESS use at different nodes serving as motivation for Study 2. A 50kWh BESS capacity has been assigned to all nodes.

#### Study 2: aFRR Energy Provision with optimal BESS capacity allocation

The cases and scenarios used in Study 2 are summarized in Table 7.4, which is devoted to the optimal total 150kWh BESS capacity allocation to the three nodes. Case 1 optimally locates the BESS capacity while the nodes perform only energy arbitrage, such as in Study 1. Provision of aFRR reserves by the BESS is added in Case 2, while EVs can also provide in Case 3. Finally, the V2G capability of EVs has been added in Case 4. It must be noted that V2G is denoted as the EV capability to discharge power to assist in the flexibility of the node, such as base load cover, building heating/cooling, etc. The cases have been investigated with three different line distance scenarios between the nodes and the main grid, whose resistance is calculated based on the per-length resistance of the commonly used LV AXPK.4x120 cable [252]. Table 7.5 summarizes the initially investigated resistance scenarios in the upper part (denoted with "1.") and two more scenarios in the lower part ("2." and "3.") used to investigate their influence. Study 2 quantifies, firstly, the discussed effects on the optimal BESS capacity allocation, and secondly, whether BESS use is economical for energy arbitrage and ancillary services provision compared to the installation and operational costs.

Table 7.3: Summary of Case Studies: Study 1 (DLC)

| Cases | Grid Scenario | Season Scenario |
|---|---|---|
| Loads-V2G | Rural | Winter |
| Loads-V2G & BESS | Urban | Summer |

Table 7.4: Summary of Case Studies: Study 2 (aFRR)

| Case | BESS Optim | BESS aFRR | EV V2G | EV aFRR |
|---|---|---|---|---|
| Case 1 | ✓ | | ✓ | |
| Case 2 | ✓ | ✓ | | |
| Case 3 | ✓ | ✓ | | ✓ |
| Case 4 | ✓ | ✓ | ✓ | ✓ |

Table 7.5: Feeder Resistances for 3 different scenarios: Study 2

| Feeder | Length | Resistance | Feeder | Length | Resistance |
|---|---|---|---|---|---|
| 1.F1 | 200 m | 0.06 Ω | | | |
| 1.F2 | 100 m | 0.03 Ω | | | |
| 1.F3 | 150 m | 0.04 Ω | | | |
| 2.F1 | 150 m | 0.04 Ω | 3.F1 | 350 m | 0.1 Ω |
| 2.F2 | 200 m | 0.06 Ω | 3.F2 | 350 m | 0.1 Ω |
| 2.F3 | 100 m | 0.03 Ω | 3.F3 | 350 m | 0.1 Ω |

### 7.4.3. Simulation Setup and Used Software

Firstly, the simulation timestep has again been set at 5 minutes to provide a balance between computational time and accuracy. Secondly, due to the high computational expense of the studies (especially of Study 2), the duration of all simulations has again been set at one day. Four different days from each season have been selected as different price scenarios. Finally, all experiments have been conducted within a Python 3.10 environment, using an Intel 11th-generation processor and the Gurobi 10 solver, which is highly suitable for solving MIP mathematical problems.

### 7.4.4. Limitations

Firstly, as in Chapters 5 and 6, while the chapter incorporates some level of uncertainty (e.g., EV driving patterns and building occupancy patterns), there are other sources of uncertainty that have not been considered. Moreover, the daily average HP COPs (3.5 for Winter and 6 for Summer) have been used and, hence, the influence of COP deviations is ignored, such as in Chapter 6. Concerning the aFRR market, this chapter has assumed that the aFRR bid is always accepted as a whole day-ahead and called for deployment in real-time. In reality, partial activations are possible (same as in Chapter 6). Additionally, while measures against battery degradation have been taken, the BESS capacity fading has not been explicitly calculated. Finally, the grid topology comprises, for simplicity, nodes at separated DFs and optimally allocates the BESS capacity considering only the distance and flexibility of the nodes and their interaction with the main grid. The influence of nodes interacting with each other, e.g., if they were placed on the same DF, is ignored in the study.

## 7.5. Results

### 7.5.1. Study 1: Direct Load Control

Figure 7.7 depicts the 10-minute calls from the DSO for DLC for the rural and urban grid during Winter and Summer. The frequency and time periods of the DLC calls have been created according to the overloading and voltage deviation results that have been found in Chapter 3 and depend on the investigated grid type and season. The magnitude of the DLC calls has been, firstly, qualitatively

categorized as follows: "zero" if transformer/line overloading $< 50\%$, "low" if overloading $< 75\%$, "medium" if overloading $< 100\%$, and "high" if overloading $> 100\%$. Secondly, the final magnitude values of the DLC calls have been created according to the maximum DA grid exchange power. For example, for a node with a maximum of approximately 40-45kW DA grid exchange power: "low" corresponds to a $\Delta P \in [0, 5] kW$, "medium" to a $\Delta P \in [5, 15] kW$, and "high" to a $\Delta P \in [15, 20] kW$.

Comparing Winter and Summer for both rural and urban grids, the time period of consumption increase calls is more limited during Winter (mostly during [11:00, 15:00]) due to the shorter and lower PV generation, while during Summer they can be seen in the time window of [08:00, 18:00]. Moreover, the high consumption of the urban grid decreases the timespan of CI calls even more. On the contrary, consumption decrease calls are mostly seen in the evening after 18:00, especially during the Winter season, due to combined EV charging and building heating. Furthermore, the magnitude and frequency of the CD calls are greater during Winter compared to Summer. Finally, the considered urban grid is located in the Netherlands, which is characterized by heavily overpopulated suburban and urban areas. Hence, overloading of urban grids is frequent during the whole day, especially during Winter, which can be clearly seen in Figure 7.7 b).

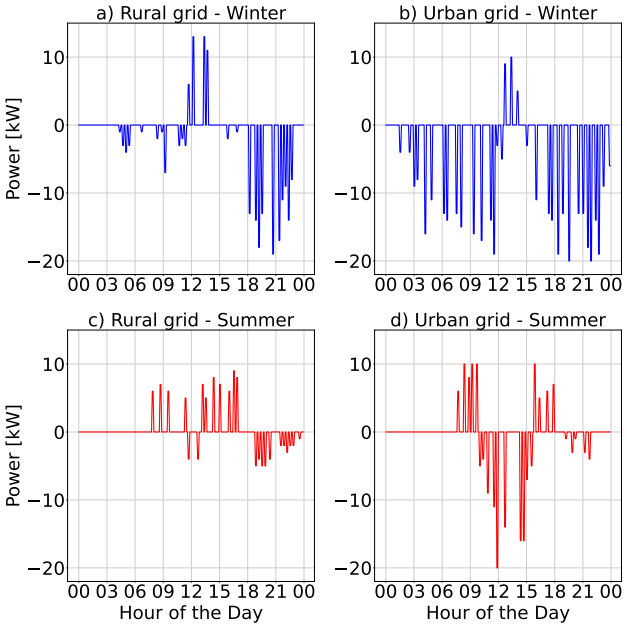


Figure 7.7: DLC calls for rural and urban grids during Winter and Summer.

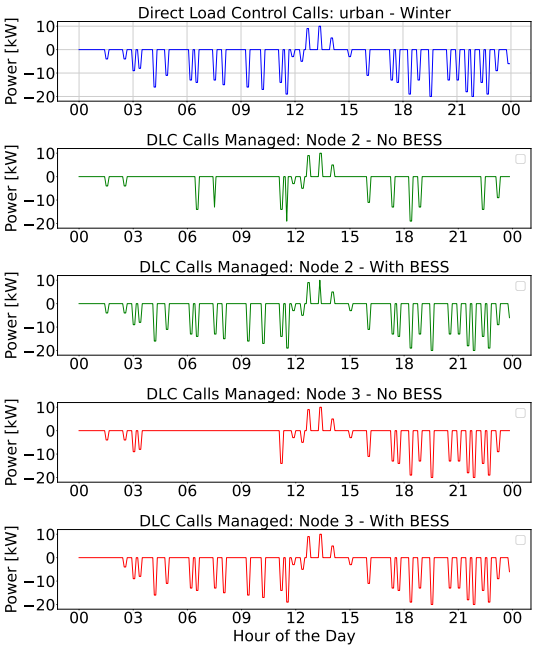


Figure 7.8: DLC response by Nodes 2 & 3 with and without BESS.

The goal is to quantify the success rate of the different nodes in responding to DLC calls, adjusting their DA schedules. In this regard, Figure 7.8 depicts, firstly, the DLC calls in the urban grid during Winter, and the managed DLC calls by Nodes 2 and 3 with and without the use of BESS. Without the use of BESS, the commercial node (Node 2) can adjust its DA schedule for a limited number of DLC calls, since it comprises only commercial buildings and public chargers. On the contrary, the mixed node (Node 3), which comprises a variety of residential/commercial buildings and home/public chargers, is more in a position to achieve successful responses. However, when the BESS is introduced, both nodes are highly successful for DA schedule adjustments, even if the DLC calls are created independently from their DA power scheduling. In addition, Figure 7.9 depicts the DA and RT power schedules of Node 1 for the urban grid during Winter without the use of BESS for the DLC calls to which the node managed to respond. Node 1 successfully responds to the first DLC calls for consumption decrease in the morning before 04:00 and decreases the building heating, and, in continuation, it expands it timely until 06:00 in the morning. Moreover, during the consumption increase calls in the afternoon between [12:00, 15:00], it stops exporting the PV generation and uses the building HPs to increase the consumption, while the PV generation covers the base load. Finally, during the consumption decrease in the evening, it decreases the EV charging during multiple DLC calls, while it even uses V2G power to export power to the main grid. In continuation, EV charging is highly increased after 23:00, when the main grid is less burdened.

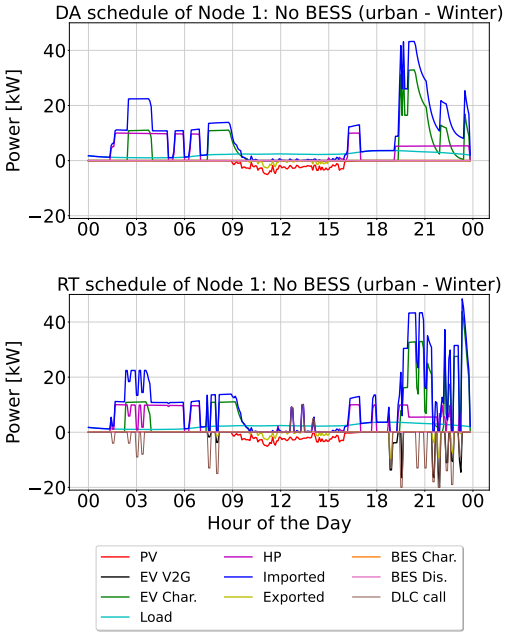


Figure 7.9: Adjustment of the DA schedule of Node 1 in RT for DLC calls management.

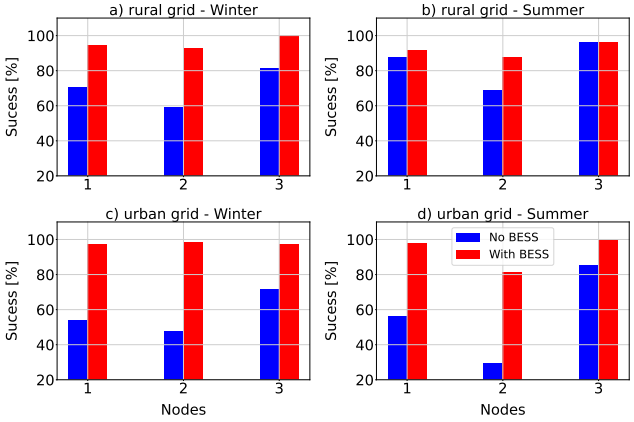


Figure 7.10: Percentage of successful node responses to DLC calls per grid and season.

Finally, Figure 7.10 summarizes the success rate of all three nodes to DLC calls for both grids and seasons with and without BESS use. Node 2, due to its low flexibility, has consistently the lowest success rate, which can go even down to 27%, whereas Node 3 has consistently the highest, which can reach up to 95%. On the contrary, when a BESS is used, the success rate overpasses 90% (in most cases even 95%). The reason the use of BESS doesn't reach 100% is that the C-rate is limited to 0.5 to avoid excess degradation. Thus, this study proves the value of a BESS for simultaneous energy arbitrage and ancillary services provision, such as congestion management, and serves as motivation for Study 2. Furthermore, it can be concluded that commercial nodes (Node 2) with low load flexibility have a higher need for a BESS in their power system. Additionally, the same is concluded for the heavily loaded urban grids, especially during Winter.

### 7.5.2. Study 2: aFRR Energy Provision with optimal BESS allocation

#### BESS Capacity Allocation

The optimal BESS allocation of Cases 1-4 for the investigated Winter and Summer scenarios is depicted in Figures 7.11 and 7.12, respectively. For both Winter and Summer 2018 and Case 1, the PCS decides not to install BESS across all cases. This is because the maximum revenue that can be gained with energy arbitrage is limited. For example, on 04.07.23, this amounts to 25.5€ (150kWh for 0.17€ /kWh), which is lower than the daily BESS cost. This shows effectively that the energy price levels and variations, and the BESS cost play a very important role. Moreover, for both seasons and most cases, most BESS capacity is allocated at Node 2. The preference for Node 2 can be attributed to the fact that it is closer to the main grid, hence it has lower power losses. However, exceptions constitute the

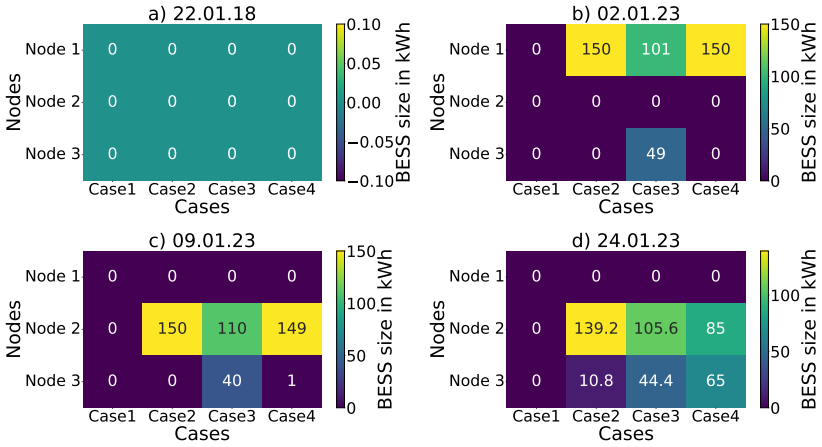


Figure 7.11: Optimal BESS capacity allocation (Winter cases).

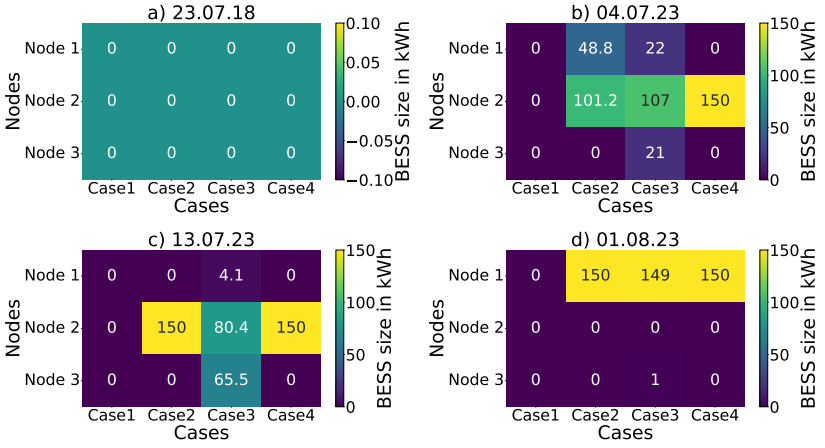


Figure 7.12: Optimal BESS capacity allocation (Summer cases).

Winter day of 02.01.23 and Summer day of 01.08.23, where for all Cases 2-4, all BESS capacity is allocated at Node 1. Regarding these days, the PCS allocates the BESS capacity at the node with the highest resistance, to benefit from additional downward aFRR power from power losses. This is because the imbalance price profiles these specific days provide more opportunities for downward regulation (three times higher than upward regulation during 02.01.23). Hence, the PCS tends to allocate BESS capacity to nodes where the combination of imbalance prices and resistance yields the highest economic benefit. Finally, an interesting insight is that for specific day scenarios, most BESS capacity is allocated at the same node for all Cases 2-4, which shows that the addition or subtraction of a flexibility mode (aFRR by BESS, aFRR by EVs, or V2G capability) plays a less significant role compared to price profiles and node distances from the grid.

### Influence of distribution line resistance on optimal BESS capacity allocation

The previous analysis showed that Node 2 is preferred during both seasons with the initial resistances. For the two other resistance scenarios, the days 09.01.23 and 13.07.23 are chosen for Winter and Summer, depicted in Figures 7.13 and 7.14, respectively, with similar insights. The distance of the nodes from the main grid plays a very important role in the optimal BESS capacity allocation. The lowest resistance is assigned to Node 3 in Figures 7.13a) and 7.14a) results in most BESS capacity allocated at this node. Moreover, this agrees for all Cases 2-4, showing again that the node distance is more important than the utilized assets for ancillary services provision concerning optimal allocated BESS capacity and optimal cost.

However, observing Figures 7.13b) and 7.14b) which belongs to the equal resistance matrix, Node 2 is again preferred for the highest allocated BESS capacity. The reason is that, firstly, (see Section "Provided aFRR Energy"), Node 2 has the

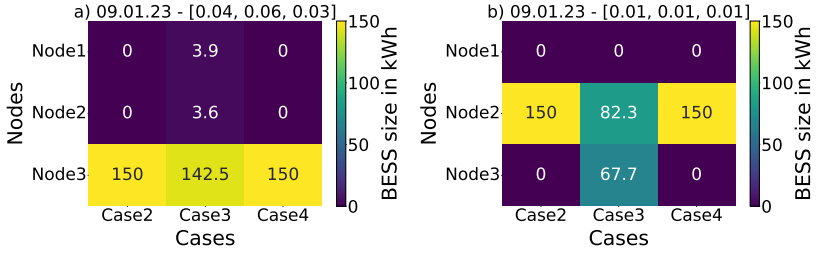


Figure 7.13: Optimal BESS capacity allocation during different line resistances (Winter cases).

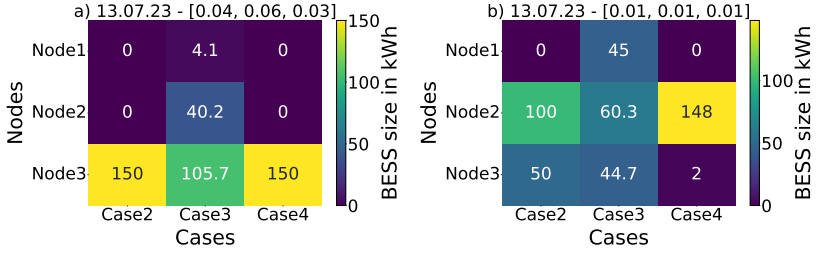


Figure 7.14: Optimal BESS capacity allocation during different line resistances (Summer cases).

lowest peak EV charging load and the base load, which leaves more room for aFRR reserves provision by the BESS when it is allocated. Secondly, Node 2 is the node with the least flexibility due to the less occupied commercial buildings and the shorter parking period of the EVs at the public chargers. Hence, the BESS is needed to increase the revenues from both energy arbitrage and ancillary services provision.

### Optimal Cost

In Figure 7.15, the total grid cost savings for Cases 2-4 compared to Case 1 can be seen for the Winter days. Introducing aFRR service for BESS in Case 2 significantly boosts cost savings; up to 207% (461% for Summer). Additionally, when both BESS and EVs provide aFRR services in Case 3, the cost savings are even higher; up to 281% (573% for Summer). Furthermore, the addition of V2G capability for EVs (Case 4) consistently increases the cost savings slightly but notably compared to Case 3 (290%). This is justified because EVs can firstly, offer a higher amount of both upward and downward reserves, and secondly, they are more flexible to perform energy arbitrage for the node responsibilities while simultaneously, aFRR reserves are offered to the grid (by e.g. the BESS). This observation concerning the synergy of EVs and BESS has also been seen in Chapter 6. Finally, it is shown that

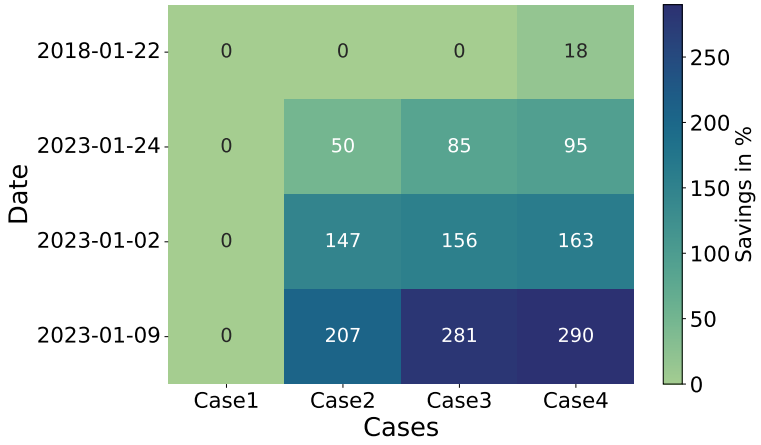


Figure 7.15: Cost savings per case compared to Case 1 (Winter cases).

the BESS profitability is highly dependent on the prices. If the energy and reserve prices are low, the BESS cannot make enough revenue to cover the costs (year 2018). The higher cost savings in 2023 highlight the importance of favorable price conditions for maximizing the benefits of BESS and EV integrations.

### Provided aFRR Energy

The delivered aFRR energy for Cases 2-4 is depicted for two Winter days (02.01.23 and 09.01.23) in Figure 7.16. Comparing the nodes, Node 3 provides the highest balancing energy amount by EVs for all cases and season days. This is justified again by its greater variability in occupied buildings (residential and commercial), and in EV fleets at home and public chargers; thus, a longer duration of EV connectivity. On the contrary, whenever a significant BESS capacity amount is allocated at a node (e.g., at Node 1 for 02.01.23 or Node 2 for 09.01.23), the upward and downward aFRR energy amounts delivered by the BESS are considerably higher compared to the respective amounts delivered by the EVs. This was also expected in this chapter since the BESS, which is stationary and always present, can choose the best time periods for providing regulation, while the EVs, on the contrary, are limited by the time they are connected to the charger.

During the above cases, the synergy of BESS and EVs in aFRR provision, combined with V2G capability, results again in the highest delivered aFRR energy, up to a total of 155kWh upward and 180kWh downward energy during 09.01.23. For example, the total amount of upward regulation energy increases by 23 kWh for 09.01.23 in Case 4 compared to Case 3. While the total delivered regulation reserves by EVs are slightly increased when V2G capability is enabled, the delivered reserves by the BESS are vastly increased. This is because the BESS is in a better position to be involved with ancillary services while the V2G-capable EVs are involved with the node's energy arbitrage. V2G also has a higher influence on the

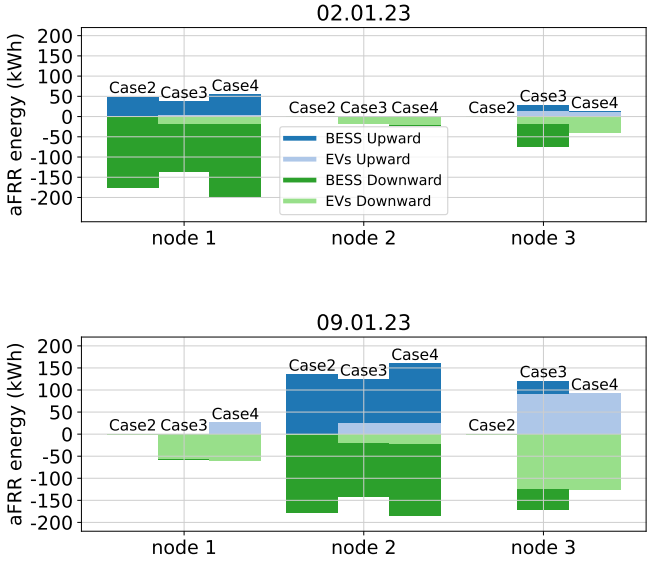


Figure 7.16: Provided aFRR energy during Winter.

upward regulation because the loads and HP need to be supplied with the energy of either PV, BESS, or EVs with V2G during the upward regulation. Additionally, it is usually seen that the delivered upward and downward aFRR energy amounts by the BESS are slightly decreased in Case 3 compared to Case 2; thus, when the EVs are also capable of delivering regulation. However, the cost savings in Case 3 have been consistently higher than in Case 2 for all investigated scenarios. Hence, when both assets are capable of providing regulation, the BESS uses a greater amount of its capacity to increase the revenues from energy arbitrage and maximize the total earnings from both strategies. In any case, when the provided aFRR energy amounts from the BESS and EVs of all nodes are added for each case, Case 4 always provides more aFRR energy than Case 3, and Case 3 from Case 2. This shows the significance of adding all flexibilities together; hence, aFRR provision by BESS, aFRR provision by EVs, and V2G for assistance inside the node.

### Optimal Power Flows

Finally, Figure 7.17 depicts some examples of optimal power flows for the considered cases during both seasons. Three cases were chosen for the analysis of the model's power flows during Winter, which are summarized in Figure 7.17a; a1) Case 1 for Node 3 on 09.01.23 to show the energy arbitrage, a2) Case 2 for Node 2 (where most BESS capacity was allocated) on 09.01.23 for aFRR provision by the

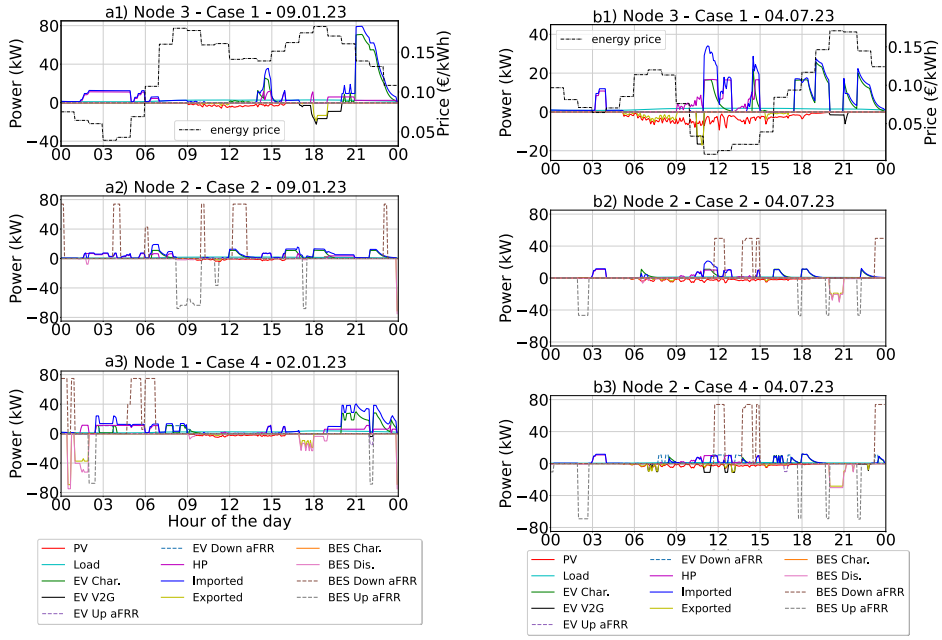


(a) Power Control: Cases 1, 2 & 4 (Winter). (b) Power Control: Cases 1, 2 & 4 (Summer).

Figure 7.17: Optimal Power Flows during Winter and Summer.

BESS, and a3) Case 4 for Node 1 (where most BESS capacity was allocated) on 02.01.23 for the influence of different prices. In Figure 7.17a1), building heating is performed during the low energy prices after midnight (before 06:00 a.m.). During the day, the PV power generated during [09:00 - 16:00] is always first used for base load cover and EV charging and then for revenues by exportation to the grid. Additionally, the power system utilizes the low energy price period after 21:00 for EV charging with higher power. During the high energy price period of [17:00 - 21:00], EV V2G is used both for building heating and revenue exploitation of the energy price variations. Regarding Figure 7.17a2) (Case 2 - Node 2), the BESS provides a higher amount of downward than upward aFRR energy amount. Most upward regulation energy is provided during [08:00 - 10:00] in the morning, when the BESS also discharges to cover the base load, since power cannot be imported at the same time. Moreover, the maximum downward regulation power is higher than the upward, which results from the power losses of the distribution lines. During the downward regulation, the BESS is charged from the grid, meaning that the downward power measured at the substation is the sum of cable power losses and the charging power; the opposite applies in upward regulation. Finally, Figure 7.17a3) depicts the power flows of Node 1 at Case 4 during 02.01.23. Compared to 09.01.23, the prices and the demand for upward regulation are lower; therefore, the provided downward

regulation capacity is even higher. The BESS only exports energy to the grid when the energy prices are higher than the reserve prices, which occurs, for example, during [01:00 - 02:00] and [17:00 - 18:00]. On the contrary, the reserve prices are higher during [02:00 - 02:30]; hence, the BESS schedules upward regulation rather than discharging for power exportation because of the higher revenues. Upward aFRR power can be seen by both assets at 22:00, while V2G is also simultaneously used to cover the base load since grid power cannot be imported.

Furthermore, three cases were chosen for the analysis of the model's power flows during Summer, which are summarized in Figure 7.17b; b1) Case 1 for Node 3 at 04.07.23 to show the energy arbitrage, b2) Case 2 for Node 2 (where most BESS capacity was allocated) at 04.07.23 for aFRR provision by the BESS, and b3) Case 4 for Node 2 (where most BESS capacity was allocated) at 04.07.23 for aFRR provision by the synergy of BESS, EVs, and V2G capability. Regarding Figure 7.17b1), the Summer power levels are significantly lower than the respective Winter levels; for example, the maximum EV charging power is 50% lower at Node 3. This is justified by the lower EV consumption during Summer and the lower needed power for building cooling than heating. It can be observed that the Summer evening energy price peaks during [20:00-22:00] are again mostly avoided. The PV generation is higher and more prolonged (during 05:00-20:00) and hence, it is used not only for exportation for revenues but also assists in EV charging and building cooling after 09:00. V2G is less used due to the high PV generation availability; however, it is still seen when the energy prices are high and there is no PV generation (e.g. during [20:00 - 21:30]. Moreover, regarding the aFRR provision plots Figure 7.17b2-3), the timeline of the power flows concerning both aFRR energy provision and node flexibility remains similar in Cases 2 and 4. Moreover, the regulation by the EVs can also be seen during the day in Figure 7.17b3), which, however, remains in much lower power levels (10kW). The most notable difference is that the power levels of both upward and downward regulation provided by the BESS are highly increased (e.g., from 45kW to 75kW). This can be justified by the use of V2G for the node flexibility (e.g. building cooling at 10:30 or exportation to the grid for revenues at 13:00) and the extra revenues by the contribution of the EVs to the aFRR provision. As explained before, higher BESS power levels and C-rates are correlated with higher degradation costs. The compensation of these costs by the two newly added features in the model at Case 4 can lead to a higher use of the BESS for aFRR provision, and hence, higher revenues gained.

## 7.6. Discussion & Validation

### 7.6.1. DLC

Regarding the DLC potential of different DGs (residential, commercial, etc.), it was seen that commercial grids have the lowest capability for DLC due to their low flexibility when BESS is not installed, as also found in the previous chapters of this Ph.D. thesis. On the contrary, mixed grids that comprise a variety of buildings and EV chargers have a higher success rate of DLC and load shifting that does not drop below 70% even when they are located in urban areas during Winter (the most

demanding scenario for DLC) and a BESS is not installed. These findings are in agreement with the results in [202], where the importance of high EV availability for DLC was also shown. As in [202], the importance of ESS for DLC was also seen here, reaching success rates higher than 90% for most cases. The effectiveness of implicit and explicit DR strategies, such as RTP and DLC, using flexible loads of residential buildings (Node 1) for simultaneous peak shaving and cost reduction is also seen here, such as in [17]; always above 55% even without the BESS. However, in this study, which is the first study to compare the DLC potential of different grid types in different seasons, it was shown that grids with commercial buildings and public chargers are at the highest need for a BESS to combine these two objectives; otherwise, the DLC success rate can drop below 30%.

### 7.6.2. Optimal BESS installation and allocation

Regarding the BESS installation, it was seen that when the BESS investment cost is considered, energy arbitrage (Case 1) is not enough for BESS installation, neither in the past (2018) nor in recent years (2023). Even when the PCS is allowed to participate in the reserve market, the addition of gains from aFRR provision in 2018 was still not enough to install a BESS. If the energy community aims to reduce their energy bills without installing BESS, using EVs for aFRR is more cost-effective than using BESS for energy arbitrage. This comes in agreement with the findings in [216]; a study conducted in 2020. However, with the recent energy and reserve price variations of 2023, the installation of BESS has become cost-effective and will become even more so if the investment costs are further reduced. This was also seen in [229], where the authors concluded that only with participation in ancillary services such as frequency regulation does the BESS installation become economically viable with a reasonable payback period.

Regarding the BESS allocation, it is generally optimal to install the higher BESS capacity at the closest node to the main grid due to the lower power losses, irrespective of the season. That means that the power losses have a higher impact than the flexibility of the node. However, if the node furthest from the substation exhibits higher excess PV production and negative downward imbalance prices occur more frequently, optimal BESS integration could involve allocating more capacity to that node to enhance self-consumption and maximize downward balancing revenue. Nonetheless, the prevalence of favorable upward prices and generally lower power losses highlights the importance of considering both regulation directions. This finding contradicts the findings in [228], where the authors allocated most BESS capacity at nodes further from the main grid. However, in this work, the BESS was also used for the improvement of voltage deviations, which are more severe at nodes at a higher distance from the main grid.

Additionally, the BESS capacity was mostly allocated for every combination of energy and reserve price profiles at one node, which remained the same for Cases 2-4. Hence, a centralized BESS is preferred over smaller distributed BESS in the grid, and only power limits can alter this decision. Moreover, power losses have a higher impact than the used assets for aFRR provision. However, when the

same distance was considered for all three nodes, most of the BESS capacity was allocated at the commercial node (Node 2). This was seen because Node 2 has the lowest flexibility on its own (shorter EV parking periods at public chargers and commercial buildings' occupancy), and hence, the addition of a BESS flexibility is more important. Moreover, the power exchange of Node 2 with the main grid is on much lower levels, leaving more space on the capacity of the distribution lines to use the BESS for aFRR reserves provision. The preference of commercial over residential nodes for higher BESS capacity allocation was also seen in [228]; however, this is the first study that compared different node types independently with different distances from the grid.

### 7.6.3. aFRR provision with the use of different assets

Regarding the provided aFRR energy in the considered cases, the gradual addition of assets and capabilities (aFRR provision by BESS in Case 2, aFRR provision by EVs in Case 3, V2G capability in Case 4) always increased the cost savings compared to Case 1, as expected. The most interesting observation has been that the addition of V2G capability in Case 4 notably decreased the costs and, in many cases, increased the provided frequency regulation, even if the used assets for regulation did not change. This was justified by the fact that EVs were capable of providing flexibility inside the node for other reasons (e.g., base load or building heating), allowing the BESS to be more actively involved with ancillary services. In any case, the sum of provided aFRR energy from all assets and nodes was always higher in Case 4 than in Case 3, and in Case 3 than in Case 2. Finally, the effect of the node type was again seen in the provided aFRR energy; Node 3 showed a higher potential for ancillary services provision than the less flexible Node 2.

### 7.6.4. Validation

This work is based on the approach in Chapter 6, where the optimization of the energy arbitrage and aFRR reserves provision was realized with fixed 50kWh BESS capacities for all three nodes (decentralized method), while here the total 150kWh BESS capacity was simultaneously optimally allocated at the nodes (centralized

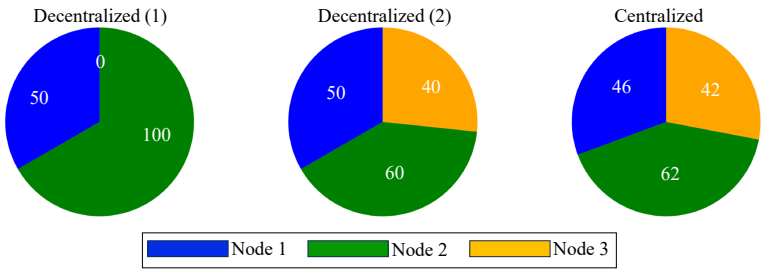


Figure 7.18: Comparison of the methods in Chapters 6 (decentralized) and 7 (centralized) for optimal BESS allocation in Case 1 (sizes in [kWh]).

method). To validate the approach in this chapter, an iterative for-loop with discrete BESS sizes was used to find the global optimal allocation of the total BESS capacity in Chapter 6 and compare the results with this chapter's approach. The for-loop method was simulated with two BESS size step matrices: [0, 50, 100, 150] (Decentralized 1) and [0, 10, 20, 30, 40, 50, 60] (Decentralized 2). The results are depicted in Figure 7.18 for Case 1 and Winter day 24.01.23, finding a deviation of only 0.011% from this chapter's centralized approach, when using a 10kWh step.

Moreover, the power flows of the two approaches are compared in Figure 7.19 for Node 2 and Case 3, finding a negligible difference and a relative error of 0.01%.

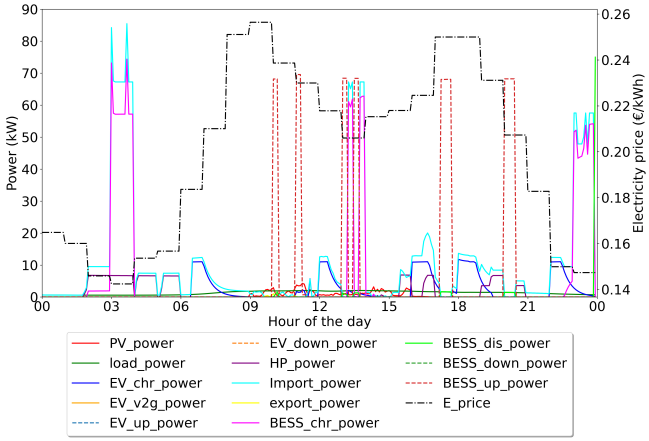


(a) Power flows using the approach in Chapter 7.

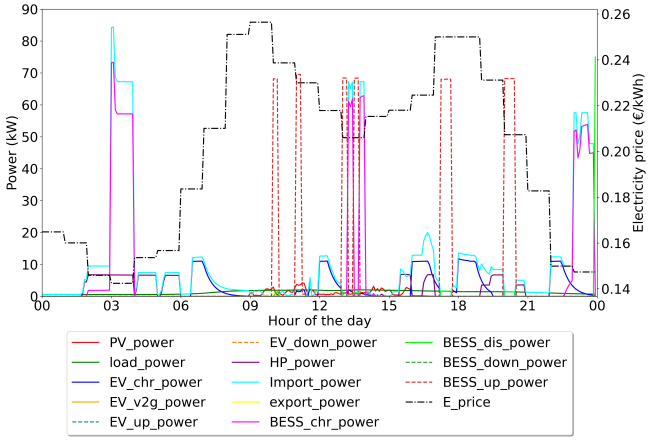


(b) Power flows using the approach in Chapter 6.

Figure 7.19: Comparison of the power flows in Node 2 - Case 3 - 24.01.23.

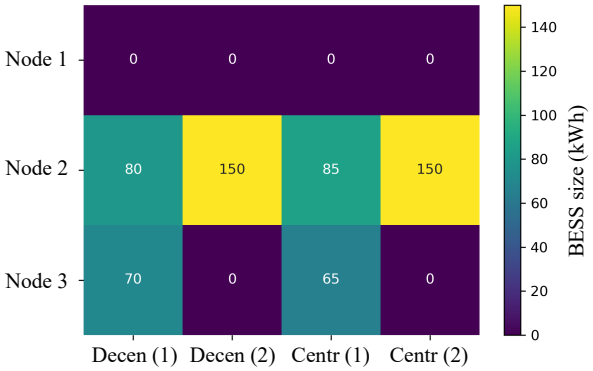


Figure 7.20: Comparison of the methods in Chapters 6 (decentralized) and 7 (centralized) for optimal BESS allocation in Case 5.

Finally, the BESS size step matrices: [0, 20, 50, 70, 80] (Decen 1) and [0, 50, 100, 150] (Decen 2) were used for the optimal BESS allocation with the for-loop in Chapter 6 and the results are shown in Figure 7.20. Similar results can be seen for the approach in this chapter with two different initializations: activation of installation binary at Node 2, allowing the solver to choose the BESS size (Centr 1), and setting the BESS size to 150kWh, allowing the solver to activate the preferred node installation binary (Centr 2).

In conclusion, the two approaches (centralized and decentralized) provide similar results with very small deviation error. Comparing the two methods, this approach can find the global optimum for the entire grid; however, it can have convergence issues if more features or nodes are added, because it becomes a non-convex MIQP. On the contrary, the iterative method based on the approach in Chapter 6 is always a convex MIQP; however, a global optimum can be found only if the step size of the BESS matrix is small enough to cover the entire range of the solution space.

## 7.7. Conclusions

In this chapter, the PCS of PVs, EVs, HPs, and BESS has been enhanced to combine implicit and explicit DR strategies (RTP tariff and DLC) for energy arbitrage and congestion management, and optimally allocate BESS capacity while providing frequency regulation at different node types and different conditions, such as distribution losses, grid type, energy/reserve prices, seasons, and LCT synergies. Results showed that a BESS installation is not economically viable only with energy arbitrage for all investigated years. Even when the PCS is allowed to participate in the reserve market, the addition of gains from aFRR provision in the past (2018) was

still not enough to install a BESS; however, it has become increasingly profitable in recent years due to the high energy price variations and both up- and down-aFRR prices. Furthermore, it was shown that a centralized BESS at the closest node to the main grid is the most beneficial solution due to lower power losses. Although the variations of energy and reserve price profiles can influence this decision, it was found that the different flexibilities (e.g., aFRR provision by different assets) do not notably alter it. The importance of BESS for congestion management was also proven, increasing DLC and load shifting success rates always above 90%. In this regard, commercial nodes that are characterized by low flexibility are in the greatest need for a BESS installation if they participate in ancillary services provision. Finally, it was also seen in this chapter that the gradual addition of assets and capabilities, such as V2G or ancillary services provision by different assets, always increased the cost savings.

For future work, simultaneous battery degradation optimization is proposed, which is especially important for the constant use of batteries for ancillary services. Moreover, the considered grid topology, while suitable for the direct comparison of different node types and distances from the main grid, ignores the effect of the interactions of the nodes of a distribution grid. Finally, as in Chapters 5 and 6, a seasonal or yearly simulation is proposed that can provide more concrete insights about the optimal BESS capacity allocation.

# 8

# Conclusion

As explained in Chapter 1, the goal of this Ph.D. thesis has been the investigation of, firstly, the grid impact of the integration of PVs, EVs, and HPs in future distribution grids and, secondly, of their power control with ESS with the goals of cost and grid impact minimization, and ancillary services provision. To that end, regarding the first goal, this thesis began with reviewing in Chapter 2 all existing knowledge concerning the various grid impact issues induced by different individual and combined integrations of the considered LCTs in different distribution grids. The thesis then proceeded with detailed modeling of PVs, EVs, and HPs, and the development of two bottom-up grid impact assessment studies for balanced and unbalanced integration in Chapters 3 and 4, respectively. Voltage deviations and component overloading in the first study, and voltage unbalance in the second study, were quantified in real-world LV distribution grids under the effect of different seasons, distributional areas, LCT combinations, penetrations, phase connections, and grid integrations.

Regarding the second goal, this thesis began with an introduction to power control systems, ancillary services provision, as well as battery energy storage systems and their degradation mechanisms in Chapter 2. Using the constructed LCT models from the first goal in Chapter 3, the thesis proceeded in developing a two-level RTP-based MIQP power control system model for the day-ahead and real-time scheduling of PV generation, V2G-capable EVs, HPs, and BESS with the goal of energy arbitrage, respecting the customers' comfort and grid limits in Chapter 5. In continuation, the PCS model was enhanced to participate in the reserve market by offering aFRR reserves day-ahead and deploying them in real-time in Chapter 6. Finally, the PCS model was refined, firstly, to simultaneous perform direct load control for congestion management and, secondly, to comprise a BESS capacity allocation method at different nodes of a distribution grid in Chapter 7. The performance of the PCS models on energy arbitrage and ancillary services provision was evaluated under different seasons, grid types (residential, commercial), grid sizes (small and large grid scenarios), battery degradation, energy/reserve prices, and BESS-loads synergies, while the influence of the distribution line losses was considered in the BESS optimal allocation method.

*Q1: What is the grid impact on component overloading and voltage deviations due to the balanced grid integration of uncontrolled electrified mobility, heating, and distributed generation in distribution grids?*

The grid impact of the balanced integration of uncontrolled PV, EV, and HP operation in distribution grids concerning component overloading and voltage deviations depends highly on the adopted LCT combination, penetration level, grid type, and loading, intra-week and seasonal effects, but also on the approach followed for the grid impact assessment.

Winter is considered overall a "heavier" season than Summer in terms of all investigated grid impact issues due to the higher EV consumption during Winter because of cabin heating, and due to the higher HP consumption because of lower COPs. This was seen for all LCT combinations and penetration levels. Moreover, the existing grid loading has a high impact not only on the overall violation but also on the slope of the violations as the LCT penetrations increase. For that reason, the suburban grids in this Ph.D. thesis were found to be the most vulnerable, since Dutch suburban DGs are highly populated, having always overloaded components and voltage violations even from lower than 50% penetration levels for all LCT combinations. Additionally, the combined PV-EV-HP integration has been found, as expected, to be the most hazardous combination, overloading 4/6 DGs from 50% and 5/6 DGs from 80% penetration levels. Furthermore, the more frequent use of HPs for heating/cooling provoked a higher grid impact overall in terms of both violation incidents and magnitude, often reaching higher than 400%, regarding all investigated issues; however, the longer EV charging periods provoked more long-lasting violations which can endure as long as 500'. Moreover, overloading, especially of T/Fs, was the most crucial issue under all conditions regarding both duration and magnitude, reaching up to 800% overloading at 100% PV-EV-HP penetration for the heavy-loaded suburban grid. The significance of the T/F overloading was expected since most LV DGs are fed by an MV/LV transformer, which is burdened with all the grid power exchange.

Additionally, mitigation of grid impact issues can occur during increasing combined EV-PV penetrations (e.g., from 50% to 80%), because EV charging is long-lasting and high-powered, and, especially at semi-public and public chargers, has higher chances of time overlap with PV generation. In contrast, the HPs are less easily temporarily combined with PVs, because the PV generation is at its highest when the (residential) buildings are not occupied. Finally, all the insights above remained similar regardless of the followed approach. However, bottom-up approaches have been found to produce violations of higher magnitude due to the simultaneous operation of the components. On the contrary, top-down approaches can produce violations with longer-term duration because they tend to average the results over time. Therefore, the use of both approaches is recommended in grid impact assessment studies to incorporate both effects and for cross-validation.

*Q2: What is the grid impact on phase unbalance due to the unbalanced grid integration of uncontrolled electrified mobility, heating, and distributed generation in distribution grids?*

The grid impact of the unbalanced integration of uncontrolled PV, EV, and HP operation on voltage unbalance in DGs also depends on several factors. Such factors can be again the LCT combination and consumption interrelations with seasonal and intra-week effects, penetration levels, DG types and loading, as well as the LCT phase connections, grid distribution, and consumption/power levels.

The existing grid loading also plays a vital role here, with the Dutch suburban grids showing VUFs that can reach up to 8% at 100% LCT penetration level. However, the grid topology was found to be as important as the existing loading. In this regard, DGs that comprise a high number of radial feeders are more prone to voltage unbalance due to higher voltage deviations by loads located at the feeders' ends. For example, the light-loaded urban grid showed a 2% VUF compared to the 1% VUF of the heavy-loaded one (same LCT penetration), because the former comprises most of the loads at the end of its radial feeders. The combined integration of PVs, EVs, and HPs was again found to be the most hazardous combination, increasing the VUF of half of the DGs above 2% at a 50% penetration level. Regarding season comparison, in balanced LCT grid integration (RQ1), Winter was always the most hazardous season. In contrast, the LCT combination and the seasonal effect were found to be more interrelated in the unbalanced LCT grid integrations. The HP integration consistently resulted in higher VU than the EV integration in PV-integrated DGs during Winter (due to the single-phase connection of all residential HPs). However, opposite trends were seen in the Summer, where EV integration resulted in higher VU. As seen, in balanced power flows, simultaneous operation of generators and loads would most probably be beneficial for mitigating violations. On the contrary, simultaneous LCT operation can become detrimental to unbalanced power flows if LCTs inject and withdraw power from different phases simultaneously. Hence, the higher PV generation during Summer provoked higher unbalance in PV-EV integration, because PVs and EVs overlap much more than PVs and HPs. Hence, it is concluded that the correlation of the investigated season and LCT combination has the strongest impact on the VU results; in contrast, the LCT grid distribution has a less significant impact, since it did not have a notable impact on the insights above.

Regarding the use of consumption and power levels as mitigation measures, both thermal comfort decrease (consumption-based) and average charging (power-based) decreased the total duration of VU violations in a range between 11% and 25%. The thermal comfort use also notably decreased the VUF magnitude (up to 15%). On the contrary, average charging caused contradictory results. This is because average charging reduces the charging power levels; however, by increasing the EV charging duration and hence, the simultaneity of EV charging with other LCT operations, such as PV generation. Hence, it is recommended that more sophisticated power control strategies (such as phase-changing SC) should be investigated for unbalance mitigation.

*Q3: How can power control of energy storage systems (ESS) and flexible loads, such as electric vehicles (EVs) and heat pumps (HPs), contribute to energy arbitrage without grid violation?*

Energy arbitrage without grid violation can be achieved with a bi-level power control system that exchanges power with the main grid and exploits the flexibility of loads, such as V2G-capable EVs and HPs, with or without the use of BESS. The PCS belongs to the implicit demand response strategies because it uses an RTP energy tariff to cover the customers' charging and thermal needs, and maximize PV self-consumption while aiming for maximum cost savings. The two levels represent the day-ahead and real-time scheduling, the latter of which uses receding horizon optimization to cope with various load uncertainties.

The PCS performance on energy arbitrage is affected by several factors. The seasonal effect is significant due to the PV generation difference, such for the grid energy exchange (50% higher decrease in grid energy for all nodes during Summer) as for the V2G use. V2G use was decreased during the Summer due to high PV power availability. It was further decreased by the use of BESS (up to 75%) due to the higher power losses, and was left for extreme cases, such as periods of high energy price peaks. However, a significant increase was proven with future charging efficiencies. Moreover, the BESS use was also influenced, since available PV generation was also preferred over stored BESS energy (35% decrease during Summer). Moreover, the grid type plays a vital role in all performance metrics. Commercial grids are characterized by lower total cost since they need 30%-50% lower grid energy amount due to shorter buildings' occupancy and EV parking periods. As a consequence, they can use more the BESS due to the higher power window, but less V2G due to lower flexibility. On the contrary, mixed nodes that comprise a variety of buildings (residential, commercial) and chargers (home, public) are always recommended because they can exploit a higher load flexibility for cost savings by V2G and BESS use, effective grid power exchange, etc.

Furthermore, as the size of the grid increases, the importance of BESS decreases due to the use of the energy price variations to directly import cheap grid energy for load consumption or export PV generation for revenues. This is due to the vast number of loads always present in the control horizon. For the same reason, PV self-consumption and the likelihood of V2G use increase with the grid size. Moreover, in smaller grids, the degradation costs, although they decreased the BESS power levels by approximately 40%, were low enough to affect the decision-making of the PCS. However, in larger grids, accumulated degradation costs can have a significant impact on the scheduling decisions, such as prompting a high exploitation of the BESS capacity for revenues to compensate for the additional induced costs by degradation. As a result of the above, the Winter case, comprising BESS and considering degradation, is defined as the most costly case; on the contrary, the Summer case, comprising BESS without considering degradation, is defined as the least costly case (e.g., 70€ compared to 40€ for the same node and case study).

*Q4: While performing energy arbitrage, how can the power of energy storage systems (ESS) and flexible loads, such as electric vehicles (EVs) and heat pumps (HPs), be controlled to provide grid ancillary services?*

Ancillary services can be provided with the PCS of PVs, EVs, HPs, and BESS that is developed in **Q3** for energy arbitrage. Firstly, system-wide aFRR reserves provision is provided without and with BESS optimal capacity allocation at the participating nodes in Chapters 6 and 7, respectively. The first level is used to offer aFRR reserves to the reserve market day-ahead, and the second to deploy them in real-time. Secondly, implicit (RTP) and explicit (DLC) DR strategies are combined to provide local ancillary services (congestion management). The DLC is realized upon DSO calls on the second level using the estimated scheduling of the first level.

The PCS performance on ancillary services provision is affected by several factors. As expected, the maximum cost savings were seen when the PCS used both loads and BESS for aFRR provision, achieving consistently higher than 100% cost reduction compared to solely energy arbitrage (Chapter 6). This was not only because services are provided by all assets, but also because one asset (e.g., EVs) could provide energy arbitrage, such as building heating with V2G, while the BESS provided services to the power grid. This was also seen in Chapter 7 when enabling V2G further increased the cost savings (10%), even if the aFRR provision assets remained the same. Hence, the importance of V2G is highly increased when services are provided despite the limitation of power losses explained in **Q3**.

The always-present BESS is able to contribute more to ancillary services provision compared to the uncertain load nature (e.g., EV fleets); however, the contribution of loads increased to a notable 38.5%, showing that they can become comparable to the BESS at larger grids with a vast amount of loads (Chapter 6). Moreover, while a BESS installation was proven not economically viable only with energy arbitrage when considering the investment cost, the increasing need for ancillary services in recent years has become highly beneficial in this regard, reaching up to 207% with aFRR provision by the BESS alone, and shifting load shifting success rates of DLC always above 90%. Additionally, a centralized BESS closest to the main grid is most often the most beneficial solution due to lower power losses, irrespective of the season or the different node flexibilities (different services provision assets), although price profile variations can have a significant influence (Chapter 7).

Finally, the grid type was again proved to be a highly influential factor as in energy arbitrage in **Q3**. The highly flexible mixed grids that integrate both residential-commercial buildings and home-public chargers were consistently capable of delivering the majority of aFRR energy (at least 25% higher) while simultaneously performing energy arbitrage (Chapter 6). On the contrary, the least flexible commercial grids are in the greatest need for a BESS installation if they participate in ancillary services provision, which was proven in all frequency regulation, DLC, and optimal BESS capacity allocation studies; load shifting capabilities for DLC can drop below 30% without a BESS (Chapter 7).

**OVERALL HIGH-LEVEL CONCLUSIONS**

Overall, this Ph.D. thesis concludes that LCTs can be highly detrimental to the future DGs; however, they can also provide the solution to their own problem if they are co-integrated effectively in PCSs. However, the PCS performance highly depends on the flexibility of the integrated assets. The superiority of mixed grids that could exploit a high load flexibility was seen regarding all performance indicators in this thesis. Moreover, such PCSs are almost always multi-objective. Energy arbitrage has only meaning when the grid limits are not violated. In addition, the results of energy arbitrage can be highly undermined if aspects such as battery degradation are ignored. However, one must keep in mind that the higher the number of objectives, the higher the PCS computational expense. A proper balance between objectives, assumptions, and utilized approach must always be found. Finally, in both impact assessment and power control grid-level studies, many findings are subject to the investigation conditions. The conditions must be set with a multidisciplinary point of view, and care needs to be taken about which findings can be generalized.

**RECOMMENDATIONS FOR FUTURE RESEARCH**

*Regarding the LCT grid impact assessment:* This Ph.D. thesis has considered a level of uncertainty in the development of the LCT models. However, many more sources of uncertainty exist in grid impact studies, such as different building and technology properties, that should also be encapsulated. Moreover, this thesis focused solely on slow AC EV charging, whereas DC fast charging will be highly important in future electric transportation. Furthermore, the use of more real-world rural, suburban, and urban DGs, preferably from different countries, is proposed to ensure the generalization of results. Finally, the use of LCT power and consumption levels for unbalance mitigation had contradictory results. More sophisticated power control strategies (e.g., phase-changing EV chargers) are recommended to conclude about unbalance mitigation without the use of additional assets.

*Regarding the LCT power control systems:* Firstly, as above, considering more uncertainties (PV generation, weather data, load demand, etc.) is proposed to qualify the uncertainty management of the RT scheduling. Secondly, the dependence of charger efficiencies on power levels should also be studied, as this can have a notable impact, especially for V2G use. Thirdly, the Ph.D. thesis performed only daily simulations due to the high computational expense. Weekly or seasonal simulations are strongly recommended to strengthen insights, especially for season comparison and optimal BESS capacity allocation. Finally, while the incorporated battery degradation model addresses several degradation influencing factors, BESS SOC and DOD are not explicitly encapsulated. Concerning the aFRR reserves provision, it has been assumed that the aFRR bid was always accepted in the reserve market due to the zero-bid of BRPs that use RES energy, and was always deployed as a whole when called in RT. The probability of non-acceptance or partial deployment is highly proposed to address the reserve market uncertainty. Moreover, the considered grid topology, while suitable for the comparison of nodes with different characteristics, ignored the node interactions in a distribution grid.

# Bibliography


[1] M. Rüdisüli, S. Teske and U. Elber. 'Impacts of an Increased Substitution of Fossil Energy Carriers with Electricity-Based Technologies on the Swiss Electricity System'. In: *Energies* 12 (June 2019), p. 2399.

[2] R. Oliyide and L. Cipcigan. 'The impacts of electric vehicles and heat pumps load profiles on low voltage distribution networks in Great Britain by 2050'. In: *International Multidisciplinary Research Journal* (Dec. 2021), pp. 30–45.

[3] B. Asare-Bediako, W. Kling and P. Ribeiro. 'Future residential load profiles: Scenario-based analysis of high penetration of heavy loads and distributed generation'. In: *Energy and Buildings* 75 (2014), pp. 228–238. ISSN: 0378-7788.

[4] C. Protopapadaki and D. Saelens. 'Heat pump and PV impact on residential low-voltage distribution grids as a function of building and district properties'. In: *Applied Energy* 192 (2017), pp. 268–281. ISSN: 0306-2619.

[5] E. E. Agency. *Greenhouse Gas Emissions by Source Sector, EU, 2022*. [Accessed: 9 July 2025]. 2023.

[6] R. Gupta, A. Pena-Bello, K. N. Streicher, C. Roduner, Y. Farhat, D. Thöni, M. K. Patel and D. Parra. 'Spatial analysis of distribution grid capacity and costs to enable massive deployment of PV, electric mobility and electric heating'. In: *Applied Energy* 287 (2021), p. 116504. ISSN: 0306-2619.

[7] European Environment Agency. *New registrations of electric vehicles*. [Accessed: 18 January 2024]. 2023.

[8] European Heat Pump Association. *EHPA Market Report 2023 - Executive Summary*. [Accessed: 18 January 2024]. 2023.

[9] SolarPower Europe. *EU Market Outlook for Solar Power 2023–2027*. [Accessed: 18 January 2024]. 2023.

[10] B. Thormann and T. Kienberger. 'Evaluation of Grid Capacities for Integrating Future E-Mobility and Heat Pumps into Low-Voltage Grids'. In: *Energies* 13 (Sept. 2020), p. 5083.

[11] N. Brinkel, M. Gerritsma, T. AlSkaif, I. Lampropoulos, A. van Voorden, H. Fidder and W. van Sark. 'Impact of rapid PV fluctuations on power quality in the low-voltage grid and mitigation strategies using electric vehicles'. In: *International Journal of Electrical Power & Energy Systems* 118 (2020), p. 105741. ISSN: 0142-0615.

[12] A. Navarro-Espinosa and L. F. Ochoa. 'Probabilistic Impact Assessment of Low Carbon Technologies in LV Distribution Systems'. In: *IEEE Transactions on Power Systems* 31.3 (2016), pp. 2192–2203.

[13] T. Antić, T. Capuder and M. Bolfek. 'A Comprehensive Analysis of the Voltage Unbalance Factor in PV and EV Rich Non-Synthetic Low Voltage Distribution Networks'. In: *Energies* 14 (Dec. 2020).

[14] W. Kong, K. Ma and F. Li. 'Probabilistic impact assessment of phase power imbalance in the LV networks with increasing penetrations of low carbon technologies'. In: *Electric Power Systems Research* 202 (2022), p. 107607. ISSN: 0378-7796.

[15] F. Giordano, A. Ciocia, P. D. Leo, A. Mazza, F. Spertino, A. Tenconi and S. Vaschetto. 'Vehicle-to-Home Usage Scenarios for Self-Consumption Improvement of a Residential Prosumer With Photovoltaic Roof'. In: *IEEE Transactions on Industry Applications* 56.3 (2020), pp. 2945–2956.

[16] J. Hu, H. Zhou, Y. Li, P. Hou and G. Yang. 'Multi-time Scale Energy Management Strategy of Aggregator Characterized by Photovoltaic Generation and Electric Vehicles'. In: *Journal of Modern Power Systems and Clean Energy* 8.4 (2020), pp. 727–736.

[17] Z. Chen, Y. Chen, R. He, J. Liu, M. Gao and L. Zhang. 'Multi-objective residential load scheduling approach for demand response in smart grid'. In: *Sustainable Cities and Society* 76 (2022), p. 103530. ISSN: 2210-6707.

[18] N. Damianakis, Y. Yu, G. C. R. Mouli and P. Bauer. 'Frequency Regulation Reserves Provision in EV Smart-Charging'. In: *2023 IEEE Transportation Electrification Conference  Expo (ITEC)*. 2023, pp. 1–6.

[19] S. Huang and Q. Wu. 'Dynamic Tariff-Subsidy Method for PV and V2G Congestion Management in Distribution Networks'. In: *IEEE Transactions on Smart Grid* 10.5 (2019), pp. 5851–5860.

[20] W. Vermeer, G. R. C. Mouli and P. Bauer. 'Optimal Sizing and Control of a PV-EV-BES Charging System Including Primary Frequency Control and Component Degradation'. In: *IEEE Open Journal of the Industrial Electronics Society* 3 (2022), pp. 236–251.

[21] G. Abdelaal, M. I. Gilany, M. Elshahed, H. M. Sharaf and A. El'gharably. 'Integration of Electric Vehicles in Home Energy Management Considering Urgent Charging and Battery Degradation'. In: *IEEE Access* 9 (2021), pp. 47713–47730.

[22] N. Damianakis, G. R. C. Mouli and P. Bauer. 'Grid impact of photovoltaics, electric vehicles and heat pumps on distribution grids — An overview'. In: *Applied Energy* 380 (2025), p. 125000. ISSN: 0306-2619.

[23] P. Lozano Ruiz, N. Damianakis and G. Ram Chandra Mouli. 'Physics-Based and Data-Driven Modeling of Degradation Mechanisms for Lithium-Ion Batteries—A Review'. In: *IEEE Access* 13 (2025), pp. 21164–21189.

[24] N. Damianakis, G. C. R. Mouli and P. Bauer. 'Risk-averse Estimation of Electric Heat Pump Power Consumption'. In: *2023 IEEE 17th International Conference on Compatibility, Power Electronics and Power Engineering (CPE-POWERENG)*. 2023, pp. 1–6.

[25] N. Damianakis, G. R. C. Mouli, P. Bauer and Y. Yu. 'Assessing the grid impact of Electric Vehicles, Heat Pumps & PV generation in Dutch LV distribution grids'. In: *Applied Energy* 352 (2023), p. 121878. ISSN: 0306-2619.

[26] Y. Wesseling, N. Damianakis, G. Ram Chandra Mouli and P. Bauer. 'Grid Impact of Unbalanced Phase Integration of PV Generation, Electrified Mobility, and Heating in LV Distribution Grids'. In: *IEEE Access* 13 (2025), pp. 56887–56907.

[27] N. Damianakis, G. R. C. Mouli, Y. Yu and P. Bauer. 'Coordinated Power Control of PV Generation, Electric Mobility and Electric Heating in Different Grids'. In: *2024 IEEE 10th International Power Electronics and Motion Control Conference (IPEMC2024-ECCE Asia)*. 2024, pp. 2082–2087.

[28] N. Damianakis, Y. Yu, G. R. C. Mouli and P. Bauer. 'Impact of Uncertainties and Price of Robustness in receding-horizon EV Smart-Charging'. In: *2024 IEEE 21st International Power Electronics and Motion Control Conference (PEMC)*. 2024, pp. 1–6.

[29] N. Damianakis, G. R. C. Mouli and P. Bauer. 'Power Control of PV Generation, Electric Mobility, Electric Heating and Battery Energy Storage'. In: *Applied Energy* (2025). Under Review.

[30] S. Warmerdam, N. Damianakis and G. R. C. Mouli. 'Power Control of PV Generation, Flexible Loads, and Battery Energy Storage for Frequency Reserves Provision'. In: *Sustainable Energy, Grids and Networks* (2025). Under Review.

[31] N. Damianakis, K. Kuresoo and G. R. C. Mouli. 'Battery Storage Integration in Power Systems of PVs, and Flexible Loads for Frequency Reserves Provision and Direct Load Control'. In: *Journal of Energy Storage* (2025). Under Review.

[32] J. Liang, Y. ( Qiu and B. Xing. 'Impacts of the co-adoption of electric vehicles and solar panel systems: Empirical evidence of changes in electricity demand and consumer behaviors from household smart meter data'. In: *Energy Economics* 112 (2022), p. 106170. ISSN: 0140-9883.

[33] F. M. Uriarte, A. Toliyat, A. Kwasinski and R. E. Hebner. 'Consumer-data approach to assess the effect of residential grid-tied photovoltaic systems and electric vehicles on distribution transformers'. In: *2014 IEEE 5th International Symposium on Power Electronics for Distributed Generation Systems (PEDG)*. 2014, pp. 1–8.

[34] F. Heymann, J. Silva, V. Miranda, J. Melo, F. J. Soares and A. Padilha-Feltrin. 'Distribution network planning considering technology diffusion dynamics and spatial net-load behavior'. In: *International Journal of Electrical Power Energy Systems* 106 (2019), pp. 254–265. ISSN: 0142-0615.

[35] J. Munkhammar, P. Grahn and J. Widén. 'Quantifying self-consumption of on-site photovoltaic power generation in households with electric vehicle home charging'. In: *Solar Energy* 97 (2013), pp. 208–216. ISSN: 0038-092X.

[36] O. Ceylan, S. Paudyal, S. Dahal and N. R. Karki. 'Assessment of harmonic distortion on distribution feeders with electric vehicles and residential PVs'. In: *2017 7th International Conference on Power Systems (ICPS)*. 2017, pp. 621–626.

[37] P. Rodríguez-Pajarón, A. Bayo and J. Milanović. 'Probabilistic assessment of the impact of electric vehicles and nonlinear loads on power quality in residential networks'. In: *International Journal of Electrical Power  Energy Systems* 129 (July 2021), p. 106807.

[38] S. Mueller, F. Moeller, M. Klatt, J. Meyer and P. Schegner. 'Impact of Large-Scale Integration of E-Mobility and Photovoltaics on Power Quality in Low Voltage Networks'. In: *International ETG Congress 2017*. 2017, pp. 1–6.

[39] Y. Yu, D. Reihs, S. Wagh, A. Shekhar, D. Stahleder, G. R. C. Mouli, F. Lehfuss and P. Bauer. 'Data-Driven Study of Low Voltage Distribution Grid Behaviour With Increasing Electric Vehicle Penetration'. In: *IEEE Access* 10 (2022), pp. 6053–6070.

[40] Y. Gabdullin and B. Azzopardi. 'Impacts of High Penetration of Photovoltaic Integration in Malta'. In: *2018 IEEE 7th World Conference on Photovoltaic Energy Conversion (WCPEC) (A Joint Conference of 45th IEEE PVSC, 28th PVSEC & 34th EU PVSEC)*. 2018, pp. 1398–1401.

[41] R. Luthander, M. Shepero, J. Munkhammar and J. Widén. 'Photovoltaics and opportunistic electric vehicle charging in the power system - a case study on a Swedish distribution grid'. In: *IET Renewable Power Generation* 13 (Feb. 2019).

[42] A. Kotsonias, L. Hadjidemetriou, E. Kyriakides and Y. Ioannou. 'Operation of a Low Voltage Distribution Grid in Cyprus and the Impact of Photovoltaics and Electric Vehicles'. In: *2019 IEEE PES Innovative Smart Grid Technologies Europe (ISGT-Europe)*. 2019, pp. 1–5.

[43] A. A. Raouf Mohamed, R. J. Best, D. John Morrow, A. Cupples and I. Bailie. 'Impact of the deployment of solar photovoltaic and electrical vehicle on the low voltage unbalanced networks and the role of battery energy storage systems'. In: *Journal of Energy Storage* 42 (2021), p. 102975. ISSN: 2352-152X.

[44] F. M. Uriarte and R. E. Hebner. 'Residential Smart Grids: Before and after the appearance of PVs and EVs'. In: *2014 IEEE International Conference on Smart Grid Communications (SmartGridComm)*. 2014, pp. 578–583.

[45] C. Van Someren, M. Visser and H. Slootweg. 'Impacts of electric heat pumps and rooftop solar panels on residential electricity distribution grids'. In: *2021 IEEE PES Innovative Smart Grid Technologies Europe (ISGT Europe)*. 2021, pp. 01–06.

[46] D. J. S. Coumans, M. O. W. Grond and E. J. Coster. 'Impacts of future residential electricity demand and storage systems on 'classic' LV-network design'. In: *2015 IEEE Eindhoven PowerTech*. 2015, pp. 1–6.

[47] A. Angioni, T. Schlösser, F. Ponci and A. Monti. 'Impact of Pseudo-Measurements From New Power Profiles on State Estimation in Low-Voltage Grids'. In: *IEEE Transactions on Instrumentation and Measurement* 65.1 (2016), pp. 70–77.

[48] C. Protopapadaki and D. Saelens. 'Sensitivity of low-voltage grid impact indicators to weather conditions in residential district energy modeling'. In: *2018 Building Performance Analysis Conference and SimBuild*. Sept. 2018.

[49] M. Bilton, C. Nnamdi Ebeanu, M. Woolf, P. Djapic, M. Wilcox and G. Strbac. *Impact of low voltage – connected low carbon technologies on network utilisation*. Imperial College London, 2014.

[50] T. Schlösser, S. Stinner, A. Monti and D. Müller. 'Analyzing the impact of home energy systems on the electrical grid'. In: *2014 Power Systems Computation Conference*. 2014, pp. 1–7.

[51] S. Meunier, C. Protopapadaki, R. Baetens and D. Saelens. 'Impact of residential low-carbon technologies on low-voltage grid reinforcements'. In: *Applied Energy* 297 (2021), p. 117057. ISSN: 0306-2619.

[52] C. Protopapadaki and D.Saelens. 'Towards metamodeling the neighborhood-level grid impact of low-carbon technologies'. In: *Energy and Buildings* 194 (2019), pp. 273–288. ISSN: 0378-7788.

[53] C. Protopapadaki, R. Baetens and D. Saelens. 'Exploring the Impact of Heat Pump-Based Dwelling Design on the Low-Voltage Distribution Grid'. In: *14th Conference of the International Building Performance Simulation Association*. Dec. 2015.

[54] D. Fischer, J. Scherer, A. Flunk, N. Kreifels, K. Byskov-Lindberg and B. Wille-Haussmann. 'Impact of HP, CHP, PV and EVs on households' electric load profiles'. In: *2015 IEEE Eindhoven PowerTech*. 2015, pp. 1–6.

[55] N. Voulis, M. Warnier and F. M. Brazier. 'Understanding spatio-temporal electricity demand at different urban scales: A data-driven approach'. In: *Applied Energy* 230 (2018), pp. 1157–1171. ISSN: 0306-2619.

[56] R. Galvin, S. Quinn, S. Hunt, P. White, D. Murray, V. Tierney, F. O'Donnell and C. Molloy. 'System wide power flow analysis of the Irish distribution network to assess the impact of projected low carbon technology loads and generation including significant increase of electric vehicles connected to the grid'. In: *CIRED Porto Workshop 2022: E-mobility and power distribution systems*. Vol. 2022. 2022, pp. 255–259.

[57] M. J. M. Al Essa and L. M. Cipcigan. 'Integration of renewable resources into Low Voltage grids stochastically'. In: *2016 IEEE International Energy Conference (ENERGYCON)*. 2016, pp. 1–5.

[58] A. Navarro and L. Ochoa. *Deliverable 3.6 "What-if scenario impact studies based on real LV networks*. English. United Kingdom: Electricity North West Limited (ENWL), Sept. 2014.

[59] X. Jiang, E. Corr, B. Stephen and B. G. Stewart. 'Impact of Increased Penetration of Low-Carbon Technologies on Cable Lifetime Estimations'. In: *Electricity* 3.2 (2022), pp. 220–235. ISSN: 2673-4826.

[60] G. Viganò, D. Clerici, C. Michelangeli, D. Moneta, A. Bosisio, A. Morotti, B. Greco and P. Caterina. 'Energy transition through PVs, EVs, and HPs: a case study to assess the impact on the Brescia distribution network'. In: *2021 AEIT International Annual Conference (AEIT)*. 2021, pp. 1–6.

[61] S. Bhattacharyya, M. Wijnand and T. Slangen. 'Estimating the future impact of residential EV loads on low voltage distribution networks'. In: *CIRED Porto Workshop 2022: E-mobility and power distribution systems*. Vol. 2022. 2022, pp. 128–132.

[62] A. Rafi, T. Lee and W. Wu. 'Impact of low-carbon technologies on the power distribution network'. In: *IOP Conference Series: Earth and Environmental Science* 329.1 (Sept. 2019), p. 012055.

[63] B. Thormann and T. Kienberger. 'Estimation of Grid Reinforcement Costs Triggered by Future Grid Customers: Influence of the Quantification Method (Scaling vs. Large-Scale Simulation) and Coincidence Factors (Single vs. Multiple Application)'. In: *Energies* 15.4 (2022). ISSN: 1996-1073.

[64] M. Daraei, A. Avelin and E. Thorin. 'Optimization of a regional energy system including CHP plants and local PV system and hydropower: Scenarios for the County of Västmanland in Sweden'. In: *Journal of Cleaner Production* 230 (May 2019).

[65] A. Weiss, F. Biedenbach and M. Mueller. 'Simulation and analysis of future electric mobility load effects in urban distribution grids'. In: *ETG Congress 2021*. 2021, pp. 1–6.

[66] R. Wardle and P. Davison. *Initial Load and Generation Profiles from CLNR Monitoring Trials*.

[67] T. Veli, B. Simpson and M. Watson. 'Impact of combined low-carbon technologies within a home, the multi-asset demand execution concept'. In: *CIRED - Open Access Proceedings Journal* (2020).

[68] N. MacMackin, L. Miller and R. Carriveau. 'Investigating distribution systems impacts with clustered technology penetration and customer load patterns'. In: *International Journal of Electrical Power  Energy Systems* 128 (2021), p. 106758. ISSN: 0142-0615.

[69] B. Fritz, G. Sampaio and R. J. Bessa. 'Data-driven Assessment of the DER Flexibility Impact on the LV Grid Management'. In: *2023 IEEE Belgrade PowerTech*. 2023, pp. 1–6.

[70] P. van Zoest, E. Veldman, Z. Lukszo and P. Herder. ‘Analysis of future electricity demand and supply in the low voltage distribution grid’. In: *Proceedings of the 11th IEEE International Conference on Networking, Sensing and Control*. 2014, pp. 619–624.

[71] C. Edmunds, S. Galloway, J. Dixon, W. Bukhsh and I. Elders. ‘Hosting capacity assessment of heat pumps and optimised electric vehicle charging on low voltage networks’. In: *Applied Energy* 298 (2021), p. 117093. ISSN: 0306-2619.

[72] R. Reibsch, P. Blechinger and J. Kowal. ‘The importance of battery storage systems in reducing grid issues in sector-coupled and renewable low-voltage grids’. In: *Journal of Energy Storage* 72 (2023), p. 108726. ISSN: 2352-152X.

[73] D. Fischer, A. Surmann and K. B. Lindberg. ‘Impact of emerging technologies on the electricity load profile of residential areas’. In: *Energy and Buildings* 208 (2020), p. 109614. ISSN: 0378-7788.

[74] F. Teske, I. Wittl, F. Funk, A. Fehrle and J. Franke. ‘A Design for an Urban Electricity Market to Reduce the Expansion of the Low Voltage Distribution Grid’. In: *2021 IEEE Electrical Power and Energy Conference (EPEC)*. 2021, pp. 340–346.

[75] A. Coelho, F. Soares, J. Iria and J. P. Lopes. ‘Evaluation of the Economic, Technical, and Environmental Impacts of Multi-Energy System Frameworks in Distribution Networks’. In: *2023 IEEE Belgrade PowerTech*. 2023, pp. 1–6.

[76] A. Alsharif, C. W. Tan, R. Ayop, A. Dobi and K. Y. Lau. ‘A comprehensive review of energy management strategy in Vehicle-to-Grid technology integrated with renewable energy sources’. In: *Sustainable Energy Technologies and Assessments* 47 (2021), p. 101439.

[77] S. Okhuegbe, C. Mwaniki and M. Akorede. ‘Optimal Sizing of Hybrid Energy Systems in a Microgrid: A Review’. In: *2019 Sustainable Research Innovation Conference*. 2019.

[78] T. M. Gur. ‘Review of electrical energy storage technologies, materials and systems: challenges and prospects for large-scale grid storage’. In: *Energy & Environmental Science* 11.10 (2018), pp. 2696–2767.

[79] X. Luo, J. Wang, M. Dooner and J. Clarke. ‘Overview of current development in electrical energy storage technologies and the application potential in power system operation’. In: *Applied energy* 137 (2015), pp. 511–536.

[80] M. C. Argyrou, P. Christodoulides and S. A. Kalogirou. ‘Energy storage for electricity generation and related processes: Technologies appraisal and grid scale applications’. In: *Renewable and Sustainable Energy Reviews* 94 (2018), pp. 804–821. ISSN: 1364-0321.

[81] H. L. Ferreira, R. Garde, G. Fulli, W. Kling and J. P. Lopes. ‘Characterisation of electrical energy storage technologies’. In: *Energy* 53 (2013), pp. 288–298.

[82] M. Killer, M. Farrokhseresht and N. G. Paterakis. ‘Implementation of Large-scale Li-ion Battery Energy Storage Systems within the EMEA Region’. In: *Applied Energy* 260 (2020), p. 114166. ISSN: 0306-2619.

[83] H. A. Behabtu, M. Messagie, T. Coosemans, M. Berecibar, K. A. Fante, A. A. Kebede and J. V. Mierlo. ‘A Review of Energy Storage Technologies’ Application Potentials in Renewable Energy Sources Grid Integration’. In: *Sustainability* 12.24 (2020), p. 10511.

[84] H. Chen, T. Cong, W. Yang, C. Tan, Y. Li and Y. Ding. ‘Progress in electrical energy storage systems: a critical review’. In: *Progress in Natural Science* 19 (Mar. 2009), pp. 291–312. ISSN: 1002-0071.

[85] Z. Šimić, D. Topić, G. Knežević and D. Pelin. ‘Battery energy storage technologies overview’. In: *International journal of electrical and computer engineering systems* 12.1 (2021), pp. 53–65.

[86] B. S. Dunn, H. Kamath and J. M. Tarascon. ‘Electrical Energy Storage for the Grid: A Battery of Choices’. In: *Science* 334 (2011), pp. 928–935.

[87] Y. Miao, P. Hynan, A. Von Jouanne and A. Yokochi. ‘Current Li-ion battery technologies in electric vehicles and opportunities for advancements’. In: *Energies* 12.6 (2019), p. 1074.

[88] Y. Preger, H. M. Barkholtz, A. Fresquez, D. L. Campbell, B. W. Juba, J. Romàn-Kustas, S. R. Ferreira and B. Chalamala. ‘Degradation of commercial lithium-ion cells as a function of chemistry and cycling conditions’. In: *Journal of The Electrochemical Society* 167.12 (2020), p. 120532.

[89] M. Dubarry, N. Qin and P. Brooker. ‘Calendar aging of commercial Li-ion cells of different chemistries – A review’. In: *Current Opinion in Electrochemistry* 9 (2018), pp. 106–113. ISSN: 2451-9103.

[90] MIT Energy Initiative. *Future of Energy Storage*. Accessed: March 13, 2024. Massachusetts Institute of Technology. 2022.

[91] M. Broussely, P. Biensan, F. Bonhomme, P. Blanchard, S. Herreyre, K. Nechev and R. Staniewicz. ‘Main aging mechanisms in Li ion batteries’. In: *Journal of Power Sources* 146.1 (2005). Selected papers pressented at the 12th International Meeting on Lithium Batteries, pp. 90–96. ISSN: 0378-7753.

[92] J. Vetter, P. Novák, M. Wagner, C. Veit, K.-C. Möller, J. Besenhard, M. Winter, M. Wohlfahrt-Mehrens, C. Vogler and A. Hammouche. ‘Ageing mechanisms in lithium-ion batteries’. In: *Journal of Power Sources* 147.1 (2005), pp. 269–281. ISSN: 0378-7753.

[93] X. Han, L. Lu, Y. Zheng, X. Feng, Z. Li, J. Li and M. Ouyang. ‘A review on the key issues of the lithium ion battery degradation among the whole life cycle’. In: *eTransportation* 1 (2019), p. 100005. ISSN: 2590-1168.

[94] A. Barré, B. Deguilhem, S. Grolleau, M. Gérard, F. Suard and D. Riu. ‘A review on lithium-ion battery ageing mechanisms and estimations for automotive applications’. In: *Journal of Power Sources* 241 (2013), pp. 680–689. ISSN: 0378-7753.

[95] J. Wang, J. Purewal, P. Liu, J. Hicks-Garner, S. Soukazian, E. Sherman, A. Sorenson, L. Vu, H. Tataria and M. W. Verbrugge. 'Degradation of lithium ion batteries employing graphite negatives and nickel–cobalt–manganese oxide + spinel manganese oxide positives: Part 1, aging mechanisms and life estimation'. In: *Journal of Power Sources* 269 (2014), pp. 937–948. ISSN: 0378-7753.

[96] X.-G. Yang, Y. Leng, G. Zhang, S. Ge and C.-Y. Wang. 'Modeling of lithium plating induced aging of lithium-ion batteries: Transition from linear to nonlinear aging'. In: *Journal of Power Sources* 360 (2017), pp. 28–40. ISSN: 0378-7753.

[97] S. F. Schuster, T. Bach, E. Fleder, J. Müller, M. Brand, G. Sextl and A. Jossen. 'Nonlinear aging characteristics of lithium-ion cells under different operational conditions'. In: *Journal of Energy Storage* 1 (2015), pp. 44–53. ISSN: 2352-152X.

[98] S. Gantenbein, M. Schönleber, M. Weiss and E. Ivers-Tiffée. 'Capacity Fade in Lithium-Ion Batteries and Cyclic Aging over Various State-of-Charge Ranges'. In: *Sustainability* 11.23 (2019). ISSN: 2071-1050.

[99] M. Simolka, J. .-. Heger, H. Kaess, I. Biswas and K. A. Friedrich. 'Influence of cycling profile, depth of discharge and temperature on commercial LFP/C cell ageing: post-mortem material analysis of structure, morphology and chemical composition'. In: *Journal of Applied Electrochemistry* 50.11 (2020), pp. 1101–1117.

[100] N. Takenaka, A. Bouibes, Y. Yamada, M. Nagaoka and A. Yamada. 'Frontiers in Theoretical Analysis of Solid Electrolyte Interphase Formation Mechanism'. In: *Advanced Materials* 33.37 (2021), p. 2100574.

[101] M. B. Pinson and M. Z. Bazant. 'Theory of SEI Formation in Rechargeable Batteries: Capacity Fade, Accelerated Aging and Lifetime Prediction'. In: *Journal of The Electrochemical Society* 160.2 (Dec. 2012), A243.

[102] Y. Gao, J. Jiang, C. Zhang, W. Zhang, Z. Ma and Y. Jiang. 'Lithium-ion battery aging mechanisms and life model under different charging stresses'. In: *Journal of Power Sources* 356 (2017), pp. 103–114. ISSN: 0378-7753.

[103] L. Su, J. Zhang, C. Wang, Y. Zhang, Z. Li, Y. Song, T. Jin and Z. Ma. 'Identifying main factors of capacity fading in lithium ion cells using orthogonal design of experiments'. In: *Applied Energy* 163 (2016), pp. 201–210. ISSN: 0306-2619.

[104] V. A. Sethuraman, L. J. Hardwick, V. Srinivasan and R. Kostecki. 'Surface structural disordering in graphite upon lithium intercalation/deintercalation'. In: *Journal of Power Sources* 195.11 (2010), pp. 3655–3660. ISSN: 0378-7753.

[105] U. R. Koleti, A. Rajan, C. Tan, S. Moharana, T. Q. Dinh and J. Marco. 'A Study on the Influence of Lithium Plating on Battery Degradation'. In: *Energies* 13.13 (2020). ISSN: 1996-1073.

[106] C. Uhlmann, J. Illig, M. Ender, R. Schuster and E. Ivers-Tiffée. 'In situ detection of lithium metal plating on graphite in experimental cells'. In: *Journal of Power Sources* 279 (2015). 9th International Conference on Lead-Acid Batteries – LABAT 2014, pp. 428–438. ISSN: 0378-7753.

[107] M. Petzl, M. Kasper and M. A. Danzer. 'Lithium plating in a commercial lithium-ion battery – A low-temperature aging study'. In: *Journal of Power Sources* 275 (2015), pp. 799–807. ISSN: 0378-7753.

[108] Q. Liu, C. Du, B. Shen, P. Zuo, X. Cheng, Y. Ma, G. Yin and Y. Gao. 'Understanding undesirable anode lithium plating issues in lithium-ion batteries'. In: *RSC Adv.* 6 (91 2016), pp. 88683–88700.

[109] M. Petzl and M. A. Danzer. 'Nondestructive detection, characterization, and quantification of lithium plating in commercial lithium-ion batteries'. In: *Journal of Power Sources* 254 (2014), pp. 80–87. ISSN: 0378-7753.

[110] S. P. Rangarajan, Y. Barsukov and P. P. Mukherjee. 'Anode potential controlled charging prevents lithium plating'. In: *J. Mater. Chem. A* 8 (26 2020), pp. 13077–13085.

[111] Y. Tian, C. Lin, H. Li, J. Du and R. Xiong. 'Detecting undesired lithium plating on anodes for lithium-ion batteries – A review on the in-situ methods'. In: *Applied Energy* 300 (2021), p. 117386. ISSN: 0306-2619.

[112] G. Zhang, X. Wei, G. Han, H. Dai, J. Zhu, X. Wang, X. Tang and J. Ye. 'Lithium plating on the anode for lithium-ion batteries during long-term low temperature cycling'. In: *Journal of Power Sources* 484 (2021), p. 229312. ISSN: 0378-7753.

[113] D. Ren, K. Smith, D. Guo, X. Han, X. Feng, L. Lu, M. Ouyang and J. Li. 'Investigation of Lithium Plating-Stripping Process in Li-Ion Batteries at Low Temperature Using an Electrochemical Model'. In: *Journal of The Electrochemical Society* 165.10 (July 2018), A2167.

[114] B. Behi, A. Baniasadi, A. Arefi, A. Gorjy, P. Jennings and A. Pivrikas. 'Cost–Benefit Analysis of a Virtual Power Plant Including Solar PV, Flow Battery, Heat Pump, and Demand Management: A Western Australian Case Study'. In: *Energies* 13.10 (2020). ISSN: 1996-1073.

[115] M. Blonsky, P. Munankarmi and S. P. Balamurugan. 'Incorporating Residential Smart Electric Vehicle Charging in Home Energy Management Systems'. In: *2021 IEEE Green Technologies Conference (GreenTech)*. IEEE. 2021.

[116] M. Yousefi, A. Hajizadeh, M. N. Soltani and B. Hredzak. 'Predictive Home Energy Management System With Photovoltaic Array, Heat Pump, and Plug-In Electric Vehicle'. In: *IEEE Transactions on Industrial Informatics* 17.1 (2021), pp. 430–440.

[117] S. Bandyopadhyay, G. R. C. Mouli, Z. Qin, L. R. Elizondo and P. Bauer. 'Techno-Economical Model Based Optimal Sizing of PV-Battery Systems for Microgrids'. In: *IEEE Transactions on Sustainable Energy* 11 (3 2020), pp. 1657–1668.

[118] A. Mohamed, R. Rigo-Mariani, V. Debusschere and L. Pin. 'Stacked revenues for energy storage participating in energy and reserve markets with an optimal frequency regulation modeling'. In: *Applied Energy* 350 (2023), p. 121721. ISSN: 0306-2619.

[119] F. D'Ettorre, M. Banaei, R. Ebrahimy, S. A. Pourmousavi, E. Blomgren, J. Kowalski, Z. Bohdanowicz, B. Łopaciuk-Gonczaryk, C. Biele and H. Madsen. 'Exploiting demand-side flexibility: State-of-the-art, open issues and social perspective'. In: *Renewable and Sustainable Energy Reviews* 165 (2022), p. 112605. ISSN: 1364-0321.

[120] A. Mohammad, R. Zamora and T. T. Lie. 'Transactive Energy Management of PV-Based EV Integrated Parking Lots'. In: *IEEE Systems Journal* 15.4 (2021), pp. 5674–5682.

[121] T. M. Aljohani, A. F. Ebrahim and O. A. Mohammed. 'Dynamic Real-Time Pricing Mechanism for Electric Vehicles Charging Considering Optimal Microgrids Energy Management System'. In: *IEEE Transactions on Industry Applications* 57.5 (2021), pp. 5372–5381.

[122] R. Cheng, W. Cheng, J. Li, Z. Chen, J. Shi, Z. Pan, Y. Wu and T. Yu. 'Stochastic Dynamic Programming-Based Online Algorithm for Energy Management of Integrated Energy Buildings With Electric Vehicles and Flexible Thermal Loads'. In: *IEEE Access* 9 (2021), pp. 58780–58789.

[123] R. Carli, G. Cavone, T. Pippia, B. De Schutter and M. Dotoli. 'Robust Optimal Control for Demand Side Management of Multi-Carrier Microgrids'. In: *IEEE Transactions on Automation Science and Engineering* 19.3 (2022), pp. 1338–1351.

[124] B. Wang, P. Dehghanian and D. Zhao. 'Chance-Constrained Energy Management System for Power Grids With High Proliferation of Renewables and Electric Vehicles'. In: *IEEE Transactions on Smart Grid* 11.3 (2020), pp. 2324–2336.

[125] S. K. Rathor and D. Saxena. 'Energy management system for smart grid: An overview and key issues'. In: *International Journal of Energy Research* 44.6 (2020), pp. 4067–4109.

[126] B. Zhou, W. Li, K. W. Chan, Y. Cao, Y. Kuang, X. Liu and X. Wang. 'Smart home energy management systems: Concept, configurations, and scheduling strategies'. In: *Renewable and Sustainable Energy Reviews* 61 (2016), pp. 30–40.

[127] Netbeheer Nederland. *Wachtlijsten Nemen Toe*. Accessed: 2024-04-22. Feb. 2024.

[128] Tennet. *Market Roles*. Accessed: 2023-08-22. 2023.

[129] Tennet. *Balance Responsible Party (BRP)*. Accessed: 2023-04-22. 2023.

[130] TenneT. *Manual aFRR for BSPs*. Accessed: 2023-07-05. Oct. 2022.

[131] Tennet. *Balancing Service Providers (BSP)*. Accessed: 2023-08-22. 2023.

[132] TenneT. *Onbalansprijssystematiek (Version 6)*. Accessed: 2023-08-29. Mar. 2022.

[133] G. Rancilio, A. Rossi, D. Falabretti, A. Galliani and M. Merlo. 'Ancillary services markets in europe: Evolution and regulatory trade-offs'. In: *Renewable and Sustainable Energy Reviews* 154 (2022), p. 111850.

[134] European Network of Transmission System Operators for Electricity (ENTSO-E). *Objectives of ENTSO-E*. Accessed: 2023-08-22. 2023.

[135] TenneT. *FCR Manual for BSP's*. Accessed: 2023-07-01. Mar. 2022.

[136] TenneT. *Manual / Product Information Incident Reserves for BSPs*. Accessed: 2023-07-05. Feb. 2023.

[137] TenneT. *Dutch ancillary services - TenneT*. Accessed: 2023-12-01. 2023.

[138] L. G. Swan and V. I. Ugursal. 'Modeling of end-use energy consumption in the residential sector: A review of modeling techniques'. In: *Renewable and Sustainable Energy Reviews* 13.8 (2009), pp. 1819–1835. ISSN: 1364-0321.

[139] Y. Li, Z. O'Neill, L. Zhang, J. Chen, P. Im and J. DeGraw. 'Grey-box modeling and application for building energy simulations - A critical review'. In: *Renewable and Sustainable Energy Reviews* 146 (2021), p. 111174. ISSN: 1364-0321.

[140] S. Edelstein. *Here's why EVs don't lose as much range in hot-weather AC use*. 2023.

[141] L. Ferrarini, S. Rastegarpour and L. Caseri. 'Predictive Control-Oriented Models of a Domestic Air-to-Water Heat Pump Under Variable Conditions'. In: *IEEE Robotics and Automation Letters* 5.4 (2020), pp. 5363–5369.

[142] B. Abhinandana, K. Beddiar, Y. Amirat and M. Benbouzid. 'Simplified Building Thermal Model Development and Parameters Evaluation Using a Stochastic Approach'. In: *Energies* 13 (June 2020), pp. 1–23.

[143] S. A. Tabatabaei, W. Van der Ham, M. C. A. Klein and J. Treur. 'A Data Analysis Technique to Estimate the Thermal Characteristics of a House'. In: *Energies* 10.9 (2017). ISSN: 1996-1073.

[144] A. H. Smets, K. Jäger, O. Isabella, R. van Swaaij and M. Zeman. *Solar Energy: The physics and engineering of photovoltaic conversion technologies and systems*. UIT, 2016.

[145] P. Murty. 'Chapter 10 - Power Flow Studies'. In: *Power Systems Analysis (Second Edition)*. Ed. by P. Murty. Second Edition. Boston: Butterworth-Heinemann, 2017, pp. 205–276. ISBN: 978-0-08-101111-9.

[146] Hulsman, L. and Schloser, T. and Koch, M. and Ohl, U. *Electric Vehicle and Heat Pump Hosting Capacity Assessment for a German 25,000-noded Distribution Network*. 21 Wind & Solar Integration Workshop. 12th Oct. 2022.

[147] J. van der Burgt, S. P. Vera, B. Wille-Haussmann, A. N. Andersen and L. H. Tambjerg. 'Grid impact of charging electric vehicles; study cases in Denmark, Germany and The Netherlands'. In: *2015 IEEE Eindhoven PowerTech*. 2015, pp. 1–6.

[148] M. Al Essa. 'Power Quality of Electrical Distribution Systems Considering PVs, EVs and DSM'. In: *Journal of Control, Automation and Electrical Systems* 31 (Sept. 2020), pp. 1–13.

[149] Y. Li and P. A. Crossley. 'Monte Carlo study on impact of electric vehicles and heat pumps on LV feeder voltages'. In: *12th IET International Conference on Developments in Power System Protection (DPSP 2014)*. 2014, pp. 1–6.

[150] C. McGarry, A. Anderson, I. Elders and S. Galloway. 'A Scalable Geospatial Data-Driven Localization Approach for Modeling of Low Voltage Distribution Networks and Low Carbon Technology Impact Assessment'. In: *IEEE Access* 11 (2023), pp. 64567–64585.

[151] P. Pillay and M. Manyahe. 'Definitions of Voltage Unbalance'. In: *IEEE Power Engineering Review* 21.5 (2001), pp. 49–51.

[152] Netherlands. *Electricity Code: Article 7.3c*. Ed. by Overheid.nl. May 2023.

[153] Netherlands. *Electricity Code: Article 2.33*. Ed. by Overheid.nl. May 2023.

[154] G. R. Chandra Mouli, M. Kefayati, R. Baldick and P. Bauer. 'Integrated PV Charging of EV Fleet Based on Energy Prices, V2G, and Offer of Reserves'. In: *IEEE Transactions on Smart Grid* 10.2 (2019), pp. 1313–1325.

[155] J.-T. Liao, Y.-S. Chuang, H.-T. Yang and M.-S. Tsai. 'BESS-Sizing Optimization for Solar PV System Integration in Distribution Grid'. In: *IFAC-PapersOnLine* 51 (28 2018), pp. 85–90.

[156] W. Zhuo and A. V. Savkin. 'Profit Maximizing Control of a Microgrid with Renewable Generation and BESS Based on a Battery Cycle Life Model and Energy Price Forecasting'. In: *Energies* 12 (15 2019), p. 2904.

[157] I. Worighi, T. Geury, M. El Baghdadi, J. Van Mierlo, O. Hegazy and A. Maach. 'Optimal Design of Hybrid PV-Battery System in Residential Buildings: End-User Economics, and PV Penetration'. In: *Applied Sciences* 9 (5 2019), p. 1022.

[158] A. Traore, A. Taylor, M. A. Zohdy and F. Z. Peng. 'Modeling and Simulation of a Hybrid Energy Storage System for Residential Grid-Tied Solar Microgrid Systems'. In: *Journal of Power and Energy Engineering* 05 (05 2017), pp. 28–39.

[159] U. Akram, R. Shah and N. Mithulananthan. 'Hybrid energy storage system for frequency regulation in microgrids with source and load uncertainties'. In: *IET Generation, Transmission  Distribution* 13 (22 2019), pp. 5048–5057.

[160] S. Hajiaghasi, M. M. Hosseini Ahmadi, P. Goleij, A. Salemnia and M. Hamzeh. 'Hybrid energy storage sizing based on discrete Fourier transform and particle swarm optimization for microgrid applications'. In: *International Transactions on Electrical Energy Systems* 31 (12 2021).

[161] S. Lei, Y. He, J. Zhang and K. Deng. ‘Optimal Configuration of Hybrid Energy Storage Capacity in a Microgrid Based on Variational Mode Decomposition’. In: *Energies* 16 (11 2023), p. 4307.

[162] F. Ni, Z. Zheng, Q. Xie, X. Xiao, Y. Zong and C. Huang. ‘Enhancing resilience of DC microgrids with model predictive control based hybrid energy storage system’. In: *International Journal of Electrical Power  Energy Systems* 128 (2021), p. 106738.

[163] A. Sangswang and M. Konghirun. ‘Optimal Strategies in Home Energy Management System Integrating Solar Power, Energy Storage, and Vehicle-to-Grid for Grid Support and Energy Efficiency’. In: *IEEE Transactions on Industry Applications* 56.5 (2020), pp. 5716–5728.

[164] M. P. Fanti, A. M. Mangini, M. Roccotelli and W. Ukovich. ‘Optimal energy management integrating renewable energy, energy storage systems and electric vehicles’. In: *2017 IEEE 14th International Conference on Networking, Sensing and Control (ICNSC)*. 2017.

[165] M. H. K. Tushar, A. W. Zeineddine and C. Assi. ‘Demand-Side Management by Regulating Charging and Discharging of the EV, ESS, and Utilizing Renewable Energy’. In: *IEEE Transactions on Industrial Informatics* 14 (6 2018), pp. 2671–2679.

[166] S. Ali, T. N. Malik and A. Raza. ‘Risk-Averse Home Energy Management System’. In: *IEEE Access* 8 (2020), pp. 91779–91798.

[167] X. Wu, X. Hu, S. Moura, X. Yin and V. Pickert. ‘Stochastic control of smart home energy management with plug-in electric vehicle battery energy storage and photovoltaic array’. In: *Journal of Power Sources* 333 (2016), pp. 203–212. ISSN: 0378-7753.

[168] S. Mateen, A. Haque, V. S. B. Kurukuru and M. A. Khan. ‘Discrete Stochastic Control for Energy Management With Photovoltaic Electric Vehicle Charging Station’. In: *CPSS Transactions on Power Electronics and Applications* 7.2 (2022), pp. 216–225.

[169] A. Kazemtarghi and A. Mallik. ‘A two-stage stochastic programming approach for electric energy procurement of EV charging station integrated with BESS and PV’. In: *Electric Power Systems Research* 232 (2024), p. 110411. ISSN: 0378-7796.

[170] Z. Foroozandeh, S. Ramos, J. Soares and Z. Vale. ‘Goal Programming Approach for Energy Management of Smart Building’. In: *IEEE Access* 10 (2022), pp. 25341–25348.

[171] A. Imran, G. Hafeez, I. Khan, M. Usman, Z. Shafiq, A. B. Qazi, A. Khalid and K.-D. Thoben. ‘Heuristic-Based Programable Controller for Efficient Energy Management Under Renewable Energy Sources and Energy Storage System in Smart Grid’. In: *IEEE Access* 8 (2020), pp. 139587–139608.

[172] M. Roccotelli, A. M. Mangini and M. P. Fanti. ‘Smart District Energy Management With Cooperative Microgrids’. In: *IEEE Access* 10 (2022), pp. 36311–36326.

[173] J.-W. Lee and M.-K. Kim. ‘An Evolutionary Game Theory-Based Optimal Scheduling Strategy for Multiagent Distribution Network Operation Considering Voltage Management’. In: *IEEE Access* 10 (2022), pp. 50227–50241.

[174] A. Çiçek, İ. Şengör, S. Güner, F. Karakuş, A. K. Erenoğlu, O. Erdinç, M. Shafie-Khah and J. P. S. Catalão. ‘Integrated Rail System and EV Parking Lot Operation With Regenerative Braking Energy, Energy Storage System and PV Availability’. In: *IEEE Transactions on Smart Grid* 13.4 (2022), pp. 3049–3058.

[175] S. Rafique, M. J. Hossain, M. S. H. Nizami, U. B. Irshad and S. C. Mukhopadhyay. ‘Energy Management Systems for Residential Buildings With Electric Vehicles and Distributed Energy Resources’. In: *IEEE Access* 9 (2021), pp. 46997–47007.

[176] N. A. El-Taweel, H. Farag, M. F. Shaaban and M. E. AlSharidah. ‘Optimization Model for EV Charging Stations With PV Farm Transactive Energy’. In: *IEEE Transactions on Industrial Informatics* 18.7 (2022), pp. 4608–4621.

[177] A. Zahedmanesh, K. M. Muttaqi and D. Sutanto. ‘A Cooperative Energy Management in a Virtual Energy Hub of an Electric Transportation System Powered by PV Generation and Energy Storage’. In: *IEEE Transactions on Transportation Electrification* 7.3 (2021), pp. 1123–1133.

[178] F. D’Ettorre, P. Conti, E. Schito and D. Testi. ‘Model predictive control of a hybrid heat pump system and impact of the prediction horizon on cost-saving potential and optimal storage capacity’. In: *Applied Thermal Engineering* 148 (2019), pp. 524–535. ISSN: 1359-4311.

[179] R. Gelleschus, M. Böttiger and T. Bocklisch. ‘Optimization-Based Control Concept with Feed-in and Demand Peak Shaving for a PV Battery Heat Pump Heat Storage System’. In: *Energies* 12.11 (2019). ISSN: 1996-1073.

[180] P. Duhirwe Nzivugira, J. Hwang, J. Ngarambe, S. Kim, K. Kim, K. Song and G. Yun. ‘A novel deep learning-based integrated photovoltaic, energy storage system and electric heat pump system: Optimising energy usage and costs’. In: *International Journal of Energy Research* 45 (Jan. 2021).

[181] D. Coppitters, W. De Paepe and F. Contino. ‘Robust design optimization of a photovoltaic-battery-heat pump system with thermal storage under aleatory and epistemic uncertainty’. In: *Energy* 229 (2021), p. 120692. ISSN: 0360-5442.

[182] D. Clift and H. Suehrcke. ‘Control optimization of PV powered electric storage and heat pump water heaters’. In: *Solar Energy* 226 (Sept. 2021), pp. 489–500.

[183] A. L. Facci, V. K. Krastev, G. Falcucci and S. Ubertini. ‘Smart integration of photovoltaic production, heat pump and thermal energy storage in residential applications’. In: *Solar Energy* 192 (2019). Thermal Energy Storage for Solar Applications, pp. 133–143. ISSN: 0038-092X.

[184] J. Vivian, E. Prataviera, F. Cunsolo and M. Pau. ‘Demand Side Management of a pool of air source heat pumps for space heating and domestic hot water production in a residential district’. In: *Energy Conversion and Management* 225 (2020), p. 113457. ISSN: 0196-8904.

[185] T. Wakui, K. Sawada, R. Yokoyama and H. Aki. ‘Predictive management for energy supply networks using photovoltaics, heat pumps, and battery by two-stage stochastic programming and rule-based control’. In: *Energy* 179 (2019), pp. 1302–1319. ISSN: 0360-5442.

[186] S. Eggimann, J. W. Hall and N. Eyre. ‘A high-resolution spatio-temporal energy demand simulation to explore the potential of heating demand side management with large-scale heat pump diffusion’. In: *Applied Energy* 236 (2019), pp. 997–1010. ISSN: 0306-2619.

[187] J. Valinejad, M. Marzband, M. Korkali, Y. Xu and A. S. Al-Sumaiti. ‘Coalition Formation of Microgrids with Distributed Energy Resources and Energy Storage in Energy Market’. In: *Journal of Modern Power Systems and Clean Energy* 8.5 (2020), pp. 906–918.

[188] N. Good and P. Mancarella. ‘Flexibility in Multi-Energy Communities With Electrical and Thermal Storage: A Stochastic, Robust Approach for Multi-Service Demand Response’. In: *IEEE Transactions on Smart Grid* 10.1 (2019), pp. 503–513.

[189] W. Violante, C. A. Cañizares, M. A. Trovato and G. Forte. ‘An Energy Management System for Isolated Microgrids With Thermal Energy Resources’. In: *IEEE Transactions on Smart Grid* 11.4 (2020), pp. 2880–2891.

[190] Q. Yan, B. Zhang and M. Kezunovic. ‘Optimized Operational Cost Reduction for an EV Charging Station Integrated With Battery Energy Storage and PV Generation’. In: *IEEE Transactions on Smart Grid* 10 (2 2019), pp. 2096–2106.

[191] C. L. Athanasiadis, T. A. Papadopoulos, G. C. Kryonidis and D. I. Doukas. ‘A Holistic and Personalized Home Energy Management System With Non-Intrusive Load Monitoring’. In: *IEEE Transactions on Consumer Electronics* 70.4 (2024), pp. 6725–6737.

[192] L. Zhang, G. Feng, K. Huang, Y. Bi, S. Chang and A. Li. ‘Design and optimization for photovoltaic heat pump system integrating thermal energy storage and battery energy storage’. In: *Energy and Buildings* 329 (2025), p. 115277. ISSN: 0378-7788.

[193] W. Vermeer, G. R. Chandra Mouli and P. Bauer. ‘Real-Time Building Smart Charging System Based on PV Forecast and Li-Ion Battery Degradation’. In: *Energies* 13.13 (2020). ISSN: 1996-1073.

[194] M. A. Fotouhi Ghazvini, K. Antoniadou-Plytaria, D. Steen and L. A. Tuan. 'Two-stage demand-side management in energy flexible residential buildings'. In: *The Journal of Engineering* 2024.4 (2024), e12372.

[195] S. Sen and M. Kumar. 'Distributed-MPC Type Optimal EMS for Renewables and EVs Based Grid-Connected Building Integrated Microgrid'. In: *IEEE Transactions on Industry Applications* 60.2 (2024), pp. 2390–2408.

[196] Y. Li, J. Wang and Y. Cao. 'Multi-objective distributed robust cooperative optimization model of multiple integrated energy systems considering uncertainty of renewable energy and participation of electric vehicles'. In: *Sustainable Cities and Society* 104 (2024), p. 105308. ISSN: 2210-6707.

[197] P. Huang, M. Lovati, X. Zhang, C. Bales, S. Hallbeck, A. Becker, H. Bergqvist, J. Hedberg and L. Maturi. 'Transforming a residential building cluster into electricity prosumers in Sweden: Optimal design of a coupled PV-heat pump-thermal storage-electric vehicle system'. In: *Applied Energy* 255 (2019), p. 113864. ISSN: 0306-2619.

[198] G. Stamatellos, O. Zogou and A. Stamatelos. 'Interaction of a House's Rooftop PV System with an Electric Vehicle's Battery Storage and Air Source Heat Pump'. In: *Solar* 2.2 (2022), pp. 186–214.

[199] S. M. Hosseini, R. Carli and M. Dotoli. 'Robust Optimal Energy Management of a Residential Microgrid Under Uncertainties on Demand and Renewable Power Generation'. In: *IEEE Transactions on Automation Science and Engineering* 18.2 (2021), pp. 618–637.

[200] M. Schimpe, M. E. von Kuepach, M. Naumann, H. C. Hesse, K. Smith and A. Jossen. 'Comprehensive Modeling of Temperature-Dependent Degradation Mechanisms in Lithium Iron Phosphate Batteries'. In: *Journal of The Electrochemical Society* 165.2 (Jan. 2018), A181.

[201] *Battery Report*. Tech. rep. Volta Foundation, 2024.

[202] J. Gasser, H. Cai, S. Karagiannopoulos, P. Heer and G. Hug. 'Predictive energy management of residential buildings while self-reporting flexibility envelope'. In: *Applied Energy* 288 (2021), p. 116653. ISSN: 0306-2619.

[203] Y. Yu, L. De Herdt, A. Shekhar, G. R. C. Mouli and P. Bauer. 'EV Smart Charging in Distribution Grids–Experimental Evaluation Using Hardware in the Loop Setup'. In: *IEEE Open Journal of the Industrial Electronics Society* 5 (2024), pp. 13–27.

[204] M. Petit, E. Prada and V. Sauvant-Moynot. 'Development of an empirical aging model for Li-ion batteries and application to assess the impact of Vehicle-to-Grid strategies on battery lifetime'. In: *Applied Energy* 172 (2016), pp. 398–407. ISSN: 0306-2619.

[205] M. H. Imani, M. J. Ghadi, S. Ghavidel and L. Li. 'Demand Response Modeling in Microgrid Operation: a Review and Application for Incentive-Based and Time-Based Programs'. In: *Renewable and Sustainable Energy Reviews* 94 (2018), pp. 486–499.

[206] V. S. Tabar, S. Ghassemzadeh and S. Tohidi. 'Energy management in hybrid microgrid with considering multiple power market and real-time demand response'. In: *Energy* 174 (2019), pp. 10–23.

[207] J. R. Nelson and N. G. Johnson. 'Model predictive control of microgrids for real-time ancillary service market participation'. In: *Applied Energy* 269 (2020), p. 114963.

[208] M. Gomez-Gonzalez, J. C. Hernández, P. G. Vidal and F. Jurado. 'Novel optimization algorithm for the power and energy management and component sizing applied to hybrid storage-based photovoltaic household-prosumers for the provision of complementarity services'. In: *Journal of Power Sources* 482 (2021), p. 228918.

[209] C. Zhou, P. Wang, T. Bao, S. Yao, Y. Tang and P. Yang. 'Flexible load optimal regulation strategy of commercial buildings under the environment of electricity market'. In: *Energy Reports* 9 (2023), pp. 1705–1716.

[210] H. Firoozi, H. Khajeh and H. Laaksonen. 'Optimized operation of local energy community providing frequency restoration reserve'. In: *IEEE Access* 8 (2020), pp. 180558–180575.

[211] G. Litjens, E. Worrell and W. Van Sark. 'Economic benefits of combining self-consumption enhancement with frequency restoration reserves provision by photovoltaic-battery systems'. In: *Applied energy* 223 (2018), pp. 172–187.

[212] G. Angenendt, M. Merten, S. Zurmühlen and D. U. Sauer. 'Evaluation of the effects of frequency restoration reserves market participation with photovoltaic battery energy storage systems and power-to-heat coupling'. In: *Applied Energy* 260 (2020), p. 114186.

[213] T. Dengiz, P. Jochem and W. Fichtner. 'Demand response with heuristic control strategies for modulating heat pumps'. In: *Applied Energy* 238 (2019), pp. 1346–1360. ISSN: 0306-2619.

[214] C. Finck, R. Li and W. Zeiler. 'Optimal control of demand flexibility under real-time pricing for heating systems in buildings: A real-life demonstration'. In: *Applied Energy* 263 (2020), p. 114671. ISSN: 0306-2619.

[215] A. G. Papakonstantinou, G. N. Psarros and S. A. Papathanassiou. 'Frequency regulation in island grids with battery storage participating in automatic generation control'. In: *School of Electrical and Computer Engineering, National Technical University of Athens (NTUA), Greece* (2024).

[216] L. Maeyaert, L. Vandevelde and T. Döring. 'Battery Storage for Ancillary Services in Smart Distribution Grids'. In: *Journal of Energy Storage* 30 (2020), p. 101524. ISSN: 2352-152X.

[217] Tennet TSO. *System Balance and Price Information*. 2023.

[218] U. Mulleriyawage and W. Shen. 'Optimally sizing of battery energy storage capacity by operational optimization of residential PV-Battery systems: An Australian household case study'. In: *Renewable Energy* 160 (2020), pp. 852–864.

[219] L. Zhou, Y. Zhang, X. Lin, C. Li, Z. Cai and P. Yang. 'Optimal sizing of PV and BESS for a smart household considering different price mechanisms'. In: *IEEE access* 6 (2018), pp. 41050–41059.

[220] L. Bhamidi and S. Sivasubramani. 'Optimal sizing of smart home renewable energy resources and battery under prosumer-based energy management'. In: *IEEE Systems Journal* 15.1 (2020), pp. 105–113.

[221] M. Killian, M. Zauner and M. Kozek. 'Comprehensive smart home energy management system using mixed-integer quadratic-programming'. In: *Applied energy* 222 (2018), pp. 662–672.

[222] T. Terlouw, T. AlSkaif, C. Bauer and W. van Sark. 'Optimal energy management in all-electric residential energy systems with heat and electricity storage'. In: *Applied Energy* 254 (2019), p. 113580.

[223] U. Akram, M. Khalid and S. Shafiq. 'An improved optimal sizing methodology for future autonomous residential smart power systems'. In: *IEEE Access* 6 (2018), pp. 5986–6000.

[224] R. Johnson, M. Mayfield and S. Beck. 'Optimal placement, sizing, and dispatch of multiple BES systems on UK low voltage residential networks'. In: *Journal of Energy Storage* 17 (2018), pp. 272–286.

[225] O. D. Melgar Dominguez, M. Pourakbari Kasmaei, M. Lavorato and J. R. S. Mantovani. 'Optimal siting and sizing of renewable energy sources, storage devices, and reactive support devices to obtain a sustainable electrical distribution systems'. In: *Energy Systems* 9 (2018), pp. 529–550.

[226] A. Kumar, N. K. Meena, A. R. Singh, Y. Deng, X. He, R. Bansal and P. Kumar. 'Strategic integration of battery energy storage systems with the provision of distributed ancillary services in active distribution systems'. In: *Applied Energy* 253 (2019), p. 113503.

[227] P. Boonluk, A. Siritaratiwat, P. Fuangfoo and S. Khunkitti. 'Optimal siting and sizing of battery energy storage systems for distribution network of distribution system operators'. In: *Batteries* 6.4 (2020), p. 56.

[228] R. Chedid and A. Sawwas. 'Optimal placement and sizing of photovoltaics and battery storage in distribution networks'. In: *Energy Storage* 1.4 (2019), e46.

[229] N. B. Arias, J. C. López, S. Hashemi, J. F. Franco and M. J. Rider. 'Multi-objective sizing of battery energy storage systems for stackable grid applications'. In: *IEEE Transactions on Smart Grid* 12.3 (2020), pp. 2708–2721.

[230] M. Nick, R. Cherkaoui and M. Paolone. 'Optimal siting and sizing of distributed energy storage systems via alternating direction method of multipliers'. In: *International Journal of Electrical Power & Energy Systems* 72 (2015). The Special Issue for 18th Power Systems Computation Conference., pp. 33–39. ISSN: 0142-0615.

[231] M. Stecca, L. R. Elizondo, T. B. Soeiro and P. Bauer. *Energy storage sizing and location in distribution networks considering overall grid performance*. IEEE, 2020.

[232] B. Yang, J. Wang, Y. Chen, D. Li, C. Zeng, Y. Chen, Z. Guo, H. Shu, X. Zhang, T. Yu *et al.* 'Optimal sizing and placement of energy storage system in power grids: A state-of-the-art one-stop handbook'. In: *Journal of energy storage* 32 (2020), p. 101814.

[233] J. L. Lorente, X. A. Liu, R. Best and D. J. Morrow. 'Energy storage allocation in power networks – A state-of-the-art review'. In: *2018 53rd International Universities Power Engineering Conference (UPEC)*. 2018, pp. 1–6.

[234] M. Zidar, P. S. Georgilakis, N. D. Hatziargyriou, T. Capuder and D. Škrlec. 'Review of energy storage allocation in power distribution networks: applications, methods and future research'. In: *IET Generation, Transmission & Distribution* 10.3 (2016), pp. 645–652.

[235] B. Alimohammadisagvand, J. Jokisalo and K. Sirén. 'Comparison of four rule-based demand response control algorithms in an electrically and heat pump-heated residential building'. In: *Applied Energy* 209 (2018), pp. 167–179. ISSN: 0306-2619.

[236] P. Fitzpatrick, F. D'Ettorre, M. De Rosa, M. Yadack, U. Eicker and D. P. Finn. 'Influence of electricity prices on energy flexibility of integrated hybrid heat pump and thermal storage systems in a residential building'. In: *Energy and Buildings* 223 (2020), p. 110142. ISSN: 0378-7788.

[237] A. Mugnini, F. Polonara and A. Arteconi. 'Energy flexibility in residential buildings clusters'. In: *E3S Web of Conferences* 197 (Jan. 2020), p. 03002.

[238] D. Fischer, T. Wolf, J. Wapler, R. Hollinger and H. Madani. 'Model-based flexibility assessment of a residential heat pump pool'. In: *Energy* 118 (2017), pp. 853–864. ISSN: 0360-5442.

[239] E. Sperber, U. Frey and V. Bertsch. 'Reduced-order models for assessing demand response with heat pumps – Insights from the German energy system'. In: *Energy and Buildings* 223 (2020), p. 110144. ISSN: 0378-7788.

[240] S. Yilmaz, C. Chanez, P. Cuony and M. K. Patel. 'Analysing utility-based direct load control programmes for heat pumps and electric vehicles considering customer segmentation'. In: *Energy Policy* 164 (2022), p. 112900. ISSN: 0301-4215.

[241] S. Baraskar, D. Günther, J. Wapler and M. Lämmle. 'Analysis of the performance and operation of a photovoltaic-battery heat pump system based on field measurement data'. In: *Solar Energy Advances* 4 (2024), p. 100047. ISSN: 2667-1131.

[242] A. Ewais, A. Elnoby, T. Mohamed, M. M. Mahmoud, Y. Qudaih and A. Hassan. 'Adaptive frequency control in smart microgrid using controlled loads supported by real-time implementation'. In: *PLOS ONE* 18 (Apr. 2023).

[243] J. Clauß, S. Stinner, I. Sartori and L. Georges. 'Predictive rule-based control to activate the energy flexibility of Norwegian residential buildings: Case of an air-source heat pump and direct electric heating'. In: *Applied Energy* 237 (2019), pp. 500–518. ISSN: 0306-2619.

[244] C. Winzer and P. Ludwig. 'Optimal Design of Dynamic Grid Tariffs'. In: *SSRN* (2022).

[245] A. Demirci, S. Mirza Tercan, E. E. E. Ahmed, U. Cali and I. Nakir. 'A Novel Electric Vehicle Charging Management With Dynamic Active Power Curtailment Framework for PV-Rich Prosumers'. In: *IEEE Access* 12 (2024), pp. 120239–120249.

[246] K. Tamashiro, T. Alharbi, A. Mikhaylov, A. M. Hemeida, N. Krishnan, M. E. Lotfy and T. Senjyu. 'Investigation of Home Energy Management with Advanced Direct Load Control and Optimal Scheduling of Controllable Loads'. In: *Energies* 14.21 (2021). ISSN: 1996-1073.

[247] C. Srithapon and D. Månsson. 'Optimal Electric Vehicle Charging using Real-Time Coordinated and Decentralized Cooperating Heat Pump in Community Grids'. In: *2022 IEEE PES Innovative Smart Grid Technologies Conference Europe (ISGT-Europe)*. IEEE. 2022, pp. 1–6.

[248] International Electrotechnical Commission. *IEC 60038: IEC standard voltages*. Technical report. International Electrotechnical Commission, 2009.

[249] National Renewable Energy Laboratory. *Annual Technology Baseline*. Accessed on: Accessed: April 16, 2024. 2023.

[250] J. Figgener, C. Hecht, D. Haberschusz, J. Bors, K. G. Spreuer, K.-P. Kairies, P. Stenzel and D. U. Sauer. 'The development of battery storage systems in Germany: A market review (status 2023)'. In: *arXiv preprint arXiv:2203.06762* (2023).

[251] G. He, R. Ciez, P. Moutis, S. Kar and J. F. Whitacre. 'The economic end of life of electrochemical energy storage'. In: *Applied energy* 273 (2020), p. 115151.

[252] AS Draka Keila Cables. *Product Datasheet for Draka Joukaabel AXPK 4G120*. Accessed: 26 April 2024.

[253] I. Diab, N. Damianakis, G. R. Chandra-Mouli and P. Bauer. 'A shared PV system for transportation and residential loads to reduce curtailment and the need for storage systems'. In: *Applied Energy* 353 (2024), p. 122131. ISSN: 0306-2619.

[254] A. M. Agudin, N. Damianakis, G. R. C. Mouli and P. Bauer. 'Leveraging Location-Unconstrained Vehicle to Grid to Reduce Energy Community Costs'. In: *IEEE Transactions on Transportation Electrification* (2025). Under Review.

# Acknowledgements

Coming to the end of this Ph.D. dissertation, I want to acknowledge all the support I received. Because, as I stated in Proposition 6, success should not be only measured by the point we reach, but also by the recognition of the tools we possessed during the process and the individuals who provided us with these tools.

First of all, I would like to thank the members of this committee for joining me in this Ph.D. defense. Especially, I would like to thank my promotor Prof. Bauer and copromotor Dr.ir. G.R.C. Mouli for all their advice and guidance these past 4 years, and together with the NEON project, for giving me the opportunity to work on this Ph.D. topic and do my part for the technical advance of my field. Moreover, not only was I welcomed and guided from the very beginning by the older Ph.D. colleagues of our group, such as Sachin and Ibrahim, but significant help also came from the younger ones, such as Dario and Alvaro. I hope I reciprocated as well as I could. Special thanks to Robin! who has always been 24/7 in the office, keeping me company when I work from there (rumors say he never leaves nor does he come again!).

Secondly, I would like to thank my family both for their financial support and the inspiration they have been to me. I have been one of the few lucky ones who had the luxury to be supported financially during all their BSc and MSc years until the age of 28. In contrast, I have witnessed so many students struggling to balance studies and part-time jobs for the necessary income. Moreover, both my parents and my sister decided to take the difficult road from early on to pursue their life goals, something that has always been inspiring to me. You see, most of my family are already respected scientists, so I guess I had to achieve something of similar importance to stand proudly beside them.

Thirdly, my recognition goes to the people whom I call my second family, because although we are not blood-related, they have stood up for me like brothers and sisters all these years along the way. A lot of times, I heard Ph.D. colleagues consider quitting under the psychological pressure of the workload and uncertainty of success. I never considered that once, and the reason is these people whose respect and admiration are priceless to me. Names do not matter, since they already know who they are, but if I had to give some indicative names, these names would be Semina, Mpampis, Dimitris, Antonis, Ilias, Maximos, Pantelis, Kostas, Panagiotis (plural), Nikos (plural)$^2$, etc. These people do not have a Ph.D.; some of them did not even study at a university. But their help was proven many times as valuable as academic advice, even if this help was just a late-night discussion at times when work pressure and personal life problems were overwhelming me. And for this, they will always have my deepest gratitude.

Continuing from this point, I would also like to address my thanks to the people

who have doubted me ever since my high school years and those who gave me a hard time knowingly during this Ph.D. journey. Their words and actions have been a great motivation for me along the way, proving to me now that I can achieve what I am set out to do, no matter what happens in my personal life, if the right people stand beside me.

Last but not least, this Ph.D. thesis is dedicated to my recently passed away beloved dog and best friend, Ares, my duties to whom I bestowed upon others during the last 4 years to pursue my goals. But, unlike power systems, time goes beyond the grasp of our control, and now, it seems I am left with none of it to go back and make it up to him for the moments we lost. I had been told several times in the past that "everything comes at a cost", and now I know what that really means.

P.S. Big thanks and appreciation to my friend Panajot Sinjari for the design of this Ph.D. thesis cover, for which I had absolutely zero hope of designing by myself.

...οι ταπεινοί να δικαιωθούν
και οι πεινασμένοι να φάνε."

# Curriculum Vitæ

## Nikolaos Damianakis

18-12-1993 Born in Athens, Greece.

## Education

2005–2011 High School
4th High School, Glyfada, Athens

2011–2018 Joint BSc & MSc Degree in Electrical & Computer Engineering
National Technical University of Athens, Athens, Greece

2019–2021 MSc Degree in Electrical Power Engineering
Delft University of Technology, Delft, Netherlands

2021–2025 Ph.D. Electric Power Management Systems
Delft University of Technology, Delft, Netherlands

*Thesis:* Grid Impact & Power Control of Low-Carbon Technologies in Future Distribution Grids

*Promotor:* Prof. dr. P. Bauer

## Work Experience

1/2018–6/2018 Vacuum technology & Gas sensing applications
National Hellenic Research Foundation, Athens, Greece
Project: Repair and Service of ArF UV laser & Thin-film development techniques
Supervisor: Prof. dr. M. Kompitsas

9/2020–12/2020 Short-circuit Protection of DAB Converter
Heliox B.V., Hardware Department, Best, Netherlands
Project: An off-board charger with HF SiC devices
Supervisor: H.d. Groot

## Awards

2011 Grant for highest score in University's Final Exams

# List of Publications

## 1. Publications Related to the Thesis

### 1.1. Journal Publications


7. N. Damianakis, G. R. C. Mouli and P. Bauer. 'Grid impact of photovoltaics, electric vehicles and heat pumps on distribution grids — An overview'. In: *Applied Energy* 380 (2025), p. 125000. ISSN: 0306-2619

6. P. Lozano Ruiz, N. Damianakis and G. Ram Chandra Mouli. 'Physics-Based and Data-Driven Modeling of Degradation Mechanisms for Lithium-Ion Batteries—A Review'. In: *IEEE Access* 13 (2025), pp. 21164–21189

5. N. Damianakis, G. R. C. Mouli, P. Bauer and Y. Yu. 'Assessing the grid impact of Electric Vehicles, Heat Pumps & PV generation in Dutch LV distribution grids'. In: *Applied Energy* 352 (2023), p. 121878. ISSN: 0306-2619

4. Y. Wesseling, N. Damianakis, G. Ram Chandra Mouli and P. Bauer. 'Grid Impact of Unbalanced Phase Integration of PV Generation, Electrified Mobility, and Heating in LV Distribution Grids'. In: *IEEE Access* 13 (2025), pp. 56887–56907

3. N. Damianakis, G. R. C. Mouli and P. Bauer. 'Power Control of PV Generation, Electric Mobility, Electric Heating and Battery Energy Storage'. In: *Applied Energy* (2025). Under Review

2. S. Warmerdam, N. Damianakis and G. R. C. Mouli. 'Power Control of PV Generation, Flexible Loads, and Battery Energy Storage for Frequency Reserves Provision'. In: *Sustainable Energy, Grids and Networks* (2025). Under Review

1. N. Damianakis, K. Kuresoo and G. R. C. Mouli. 'Battery Storage Integration in Power Systems of PVs, and Flexible Loads for Frequency Reserves Provision and Direct Load Control'. In: *Journal of Energy Storage* (2025). Under Review


### 1.2. Conference Publications


3. N. Damianakis, G. C. R. Mouli and P. Bauer. 'Risk-averse Estimation of Electric Heat Pump Power Consumption'. In: *2023 IEEE 17th International Conference on Compatibility, Power Electronics and Power Engineering (CPE-POWERENG)*. 2023, pp. 1–6

2. N. Damianakis, G. R. C. Mouli, Y. Yu and P. Bauer. 'Coordinated Power Control of PV Generation, Electric Mobility and Electric Heating in Different Grids'. In: *2024 IEEE 10th International Power Electronics and Motion Control Conference (IPEMC2024-ECCE Asia)*. 2024, pp. 2082–2087

1. N. Damianakis, Y. Yu, G. R. C. Mouli and P. Bauer. 'Impact of Uncertainties and Price of Robustness in receding-horizon EV Smart-Charging'. In: *2024 IEEE 21st International Power Electronics and Motion Control Conference (PEMC)*. 2024, pp. 1–6

# 2. Publications Collaborative Projects

## 2.1. Journal Publications

2. I. Diab, N. Damianakis, G. R. Chandra-Mouli and P. Bauer. 'A shared PV system for transportation and residential loads to reduce curtailment and the need for storage systems'. In: *Applied Energy* 353 (2024), p. 122131. ISSN: 0306-2619

1. A. M. Agudin, N. Damianakis, G. R. C. Mouli and P. Bauer. 'Leveraging Location-Unconstrained Vehicle to Grid to Reduce Energy Community Costs'. In: *IEEE Transactions on Transportation Electrification* (2025). Under Review

## 2.2. Conference Publications

1. N. Damianakis, Y. Yu, G. C. R. Mouli and P. Bauer. 'Frequency Regulation Reserves Provision in EV Smart-Charging'. In: *2023 IEEE Transportation Electrification Conference  Expo (ITEC)*. 2023, pp. 1–6

# Propositions

accompanying the dissertation

## Grid Impact & Power Control of Low-Carbon Technologies in Future Distribution Grids

converting the problem to its solution

by

**Nikolaos DAMIANAKIS**

1. Low-Carbon technologies are the two sides of the same coin; they represent the greatest danger of modern power grids as well as their solution **(this thesis)**.

2. The flexibility provided by a power management system is bound to the flexibility of the customers it comprises. No matter how sophisticated it is, its effectiveness is limited if the customers have similar requirements **(this thesis)**.

3. Power management systems are inherently multi-objective. The lower the number of their objectives, the higher the number of assumptions their performance depends on **(this thesis)**.

4. Technical ideas and innovations in grid-level system studies depend more than anything else on the investigated conditions, such as grid sizes, grid locations, adoption rates of technologies, etc. **(this thesis)**. My findings regarding batteries and electric vehicles belong to the trash can if my friends in Greece are not convinced that buying an EV does not reduce their masculinity.

5. Research is more like art than a 9-5 office job. Ideas are born with zooming out and not with zooming in.

6. Society always tends to measure a person's success depending on the point they have reached. On the contrary, the point from which they started, the tools they possessed during the process, and the level of acknowledgment to the people who provided them with these tools are equally important (if not more).

7. The greatest merit of democracy is the ability of everyone's opinion to be heard. So is its greatest imperfection.

8. Everyone seems to have certain opinions about whether something is right or wrong. However, the terms “right” and “wrong” can only be meaningful after the respective set of rules is defined and apply only according to this set; the same goes for the terms "good" and "bad".

9. "What actually is" is in the end as important as "what is communicated". Intentions eventually lose their value if an effective way of transmitting them fails to be found.

10. The value of an idea does not depend only on its innovation but also on its practicality. Big ideas are meaningless if the framework for which they are intended is not ready to accommodate them; and I am not talking only about power management systems.

These propositions are regarded as opposable and defendable, and have been approved as such by the promotor Prof.dr.ir Pavol Bauer and the copromotor Dr.ir. Gautham Ram Chandra Mouli.

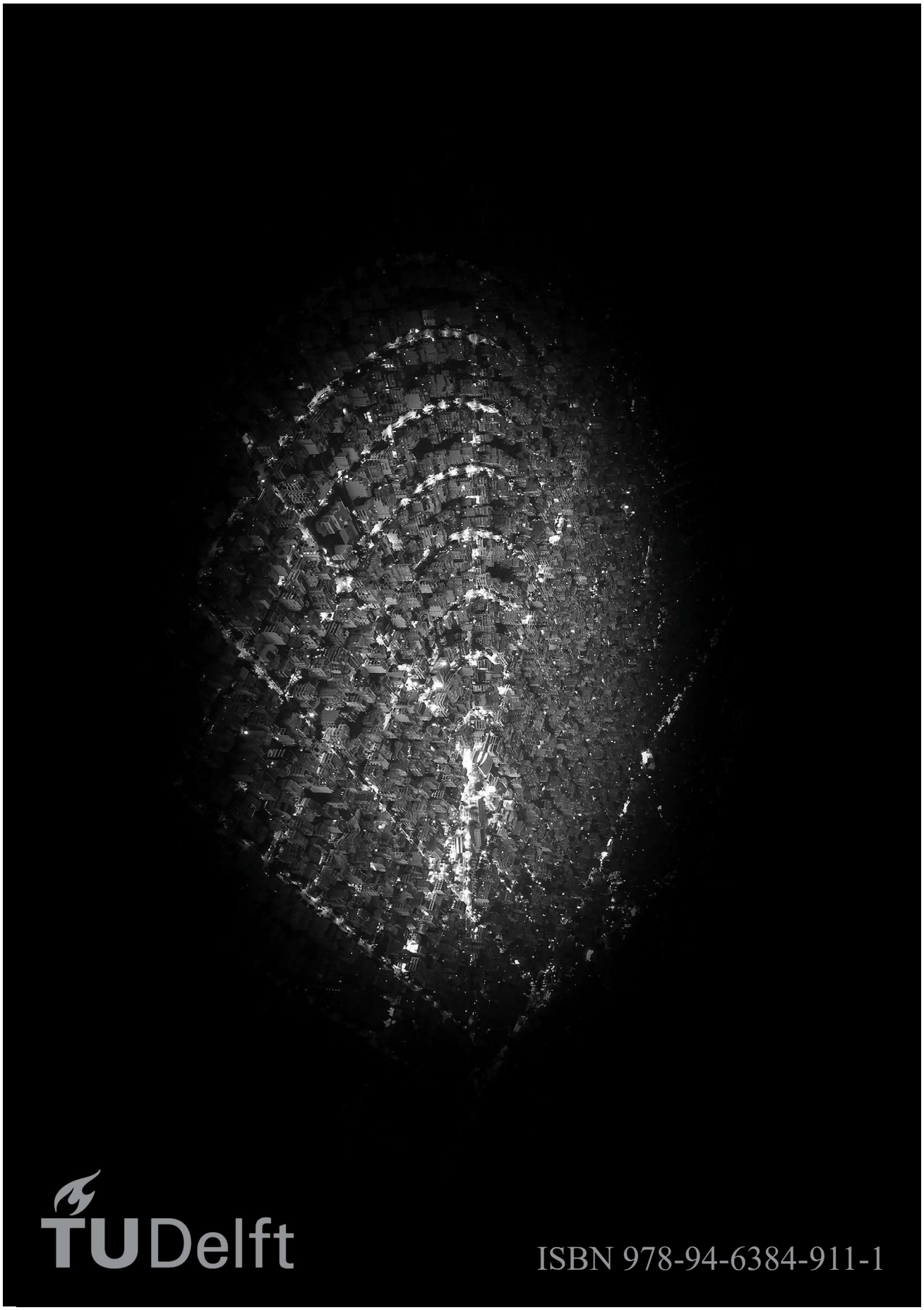

TU Delft

ISBN 978-94-6384-911-1